Intracellular Drug Delivery: A Route to More Selective and Effective Treatments for Disease

Quynh Nhu Mai

B. Pharm. Sci. (Hons)

A thesis submitted for the degree of Doctor of Philosophy at Monash University in 2018

Drug Discovery Biology

Monash Institute of Pharmaceutical Sciences

Faculty of Pharmacy and Pharmaceutical Sciences

Monash University

Copyright notice

© Quynh Nhu Mai (2018). Except as provided in the Copyright Act 1968, this thesis may not be reproduced in any form without the written permission of the author.

I certify that I have made all reasonable efforts to secure copyright permissions for third party content included in this thesis and have not knowingly added copyright content to my work without the owner's permission.

Table of contents

Abstract

The Neurokinin 1 receptor (NK_1R) is a G protein-coupled receptor (GPCR) and member of the tachykinin family expressed in the central nervous system, immune cells, gastrointestinal tract and vascular endothelia. It is associated with neurogenic inflammation, gastrointestinal function and nociceptive transmission. Stimulation of NK_1R by the endogenous agonist, substance P, initiates $G\alpha_q$-mediated signalling, receptor phosphorylation and β-arrestin recruitment to initiate clathrin-dynamin mediated endocytosis. Internalised NK_1R has a spatially and temporally dynamic signalling profile which has been demonstrated to underlie pathophysiological outcomes distinct from the plasma membrane. Therefore, endosomal NK_1R populations may be considered a therapeutically distinct target. This thesis explores this concept, through the characterisation of NK_1R signalling from endosomes, and the development of two novel drug delivery systems: 1) Lipid-conjugation to anchor soluble molecules into membranes and enhance their targeting; 2) pH-sensitive nanoparticles were used as a non-covalent method of packaging NK_1R antagonists for targeted endosomal drug delivery.

We investigated the inhibitory potential for lipid-conjugation of Spantide I, a first generation NK_1R antagonist (Spantide-Cholestanol). Assessment of the endosomal signalling pathways of NK_1R suggested that Spantide-Cholestanol inhibited endosomal signalling with greater potency. We propose a mechanism whereby lipid-conjugation provides sustained association with membranes and can be directed to endosomes to improve inhibition of internalised NK_1R signalling.

Fluorescence correlation spectroscopy and localisation of a lipid-conjugated fluorescent probe (Cy5-Cholestanol) suggested that there was enrichment in endosomes, and at the plasma membrane. Further investigation of this plasma membrane-associated ligand population revealed that Spantide-Cholestanol has inhibitory effects on receptor trafficking and some plasma membrane-delimited signalling events. Therefore, while Spantide-Cholestanol effectively inhibits endosomally localised NK_1R signalling, it also has the potential to bind and modulate plasma membrane localised NK_1R.

An alternative approach for endosomal drug delivery is the non-covalent loading of NK_1R antagonists into pH-sensitive, block copolymer nanoparticles (NPs). The nanoparticle core contained a pH responsive monomer which at acidic pH below the pK_a resulted in the

protonation of the monomers, triggering repulsion and drug release. This pH is known to be achieved in the acidic endosome environment and therefore may be appropriate for endosome-selective drug release. However, cationic NPs reportedly reduce cell viability. To address this issue, we incorporated diethylene glycol (DEG) into block copolymer to shield the cell from toxicity induced by the charged monomeric subunits at endosomal pH. We observed a DEG-dependent increase in cell health, and internalisation of NPs into Rab5-positive endosomes, to demonstrate that these pH responsive nanoparticles may offer a suitable approach for selective delivery drugs into endosomes.

The key findings in this thesis emphasise the importance of considering receptor trafficking/localisation in the entire receptor signalling profile. We have observed that lipidation increases drug localisation in endosomes, significantly improving drug potency to inhibit endosomal signalling. However, some of the drug remains at the plasma membrane and can antagonise the population of membrane-localised NK_1R. This suggests that nanodelivery of drugs to endosomes may be a more selective therapeutic strategy. Overall, the efficient and selective delivery of drugs to compartmentalised receptor populations will have important implications for drug discovery programs.

Declaration

This thesis contains no material which has been accepted for the award of any other degree or diploma at any university or equivalent institution and that, to the best of my knowledge and belief, this thesis contains no material previously published or written by another person, except where due reference is made in the text of the thesis.

Chapter 2 includes an unpublished manuscript prepared for publication titled, "Lipidation improves antagonist potency and the inhibition of NK1R signalling in endosomes." For this manuscript, I contributed to 70% of the work, including planning, designing and performing a majority of the experiments. I also analysed the data, prepared the figures, and wrote, drafted, and revised the manuscript. Co-authors and their contributions to the manuscript are as follows: T.Q., B.G., L.A., and J.C. synthesised tripartite probes (4%); P.S. and JRS performed in vivo experiments (2%); H.R.Y. designed and performed BRET experiments (1%); M.C. conceived the studies (1%); S.J.B. and S.J.H conceived the FCS studies (1%); N.W.B. conceived the studies (5%); M.L.H conceived the studies, designed experiments and drafted the manuscript (8%); N.A.V conceived the studies, designed experiments and drafted the manuscript (8%).

Chapter 4 includes an unpublished manuscript prepared for publication titled, "Incorporation of Di(Ethylene Glycol) Methyl Ether Methacrylate (DEGMA) to Reduce Polycation-Dependent Cytotoxicity of pH-Sensitive Nanoparticles." For this manuscript, I contributed to 60% of the work, including planning, designing and performing a majority of the experiments. I also analysed the data, prepared the figures, and wrote, drafted, and revised the manuscript. Co-authors and their contributions to the manuscript are as follows: N.M.V performed Alamar Blue experiments (10%); N.T. conceived, designed and validated the nanoparticles (5%); P.R.G. contributed to the nanoparticle design (1%); A.H.T.D contributed

to the nanoparticle design and preliminary experiments (2%); J.F.Q. conceived the studies (2%); M.R.W. conceived the studies, designed and synthesised the nanoparticles (5%); N.W.B. conceived the studies (2%); N.A.V. conceived the studies and designed experiments (8%); T.P.D. conceived the studies (4%).

This thesis includes one original paper published in a peer reviewed journal. The core theme of the thesis is “Intracellular Drug Delivery: A Route to More Selective and Effective Treatments for Disease”. The ideas, development and writing up of all the papers in the thesis were the principal responsibility of myself, the student, working within the Drug Discovery Biology theme of the Monash Institute of Pharmaceutical Sciences, under the supervision of Dr Nicholas A. Veldhuis, Prof. Christopher J.H. Porter, and Prof. Nigel Bunnett.

The inclusion of co-authors reflects the fact that the work came from active collaboration between researchers and acknowledges input into team-based research.

In the case of Chapter 2, my contribution to the work involved the following:

Thesis chapter	Publication title	Status	Nature and extent (%) of student's contribution	Co-author name(s) Nature and % of Co-author's contribution*	Co-author(s), Monash Student Y/N
2	-Neurokinin 1 receptor signaling in endosomes mediates sustained nociception and is a viable therapeutic target for prolonged pain relief	Published	15% Planned and designed experiments. Performed subcellular trafficking of tripartite probes, internalisation experiments, and kinetic drug uptake experiments. Analysed experiments. Revised the manuscript.	D.D.J. analysed NK_1R trafficking (15%); T.L performed *in vivo* experiments (10%); M.L.H. performed FRET (10%); N.A.V. studied trafficking and FRET (12%); W.L.I. performed electrophysiology (5%); D.P.P. performed microscopy (2%); T.Q., L.A., N.B. and J.C. synthesised probes (5%); C.K.H. analysed transcription (1%); M.J.S. , B.G. and J.S.S. designed probes (1%); A.M. and P.J.R. designed and synthesised inhibitors of endocytosis (1%); V.E. designed and prepared cationic liposomes (1%); R.N. and S.M. and P.G. conceived, measured and analysed neuropeptide release from spinal cord (1%); G.A.H. and M.J.C. conceived the studies (1%); C.J.H.P. conceived and designed the studies to use tripartite probes to therapeutically target endosomal receptors (5%); M.C. conceived, designed, and completed all BRET analyses of subcellular NK_1R trafficking and G protein activation (5%) ; and N.W.B. conceived the studies, designed experiments, interpreted the results, and wrote the manuscript (10%).	Y

Student Signature: 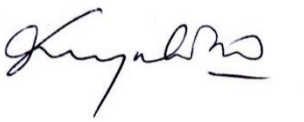 Date: 05/06/2018

The undersigned hereby certify that the above declaration correctly reflects the nature and extent of the student's and co-authors' contributions to this work. In instances where I am not the responsible author I have consulted with the responsible author to agree on the respective contributions of the authors.

Main supervisor signature:  Date: 05/06/2018

Acknowledgements

Firstly, I would like to thank my supervisors Dr. Nicholas Veldhuis, Prof. Christopher Porter, and Prof. Nigel Bunnett for their guidance and support throughout my PhD. Their positivity, enthusiasm and encouragement has kept me motivated and excited about my current work and for the opportunities to come. In particular, I would like to thank Nik for guiding me through my PhD research and helping me navigate through the maze of office politics. I am grateful for your support, endless patience and steady supply of pep talks and jokes. Your friendship has made every minor victory a little sweeter, and every defeat a little less painful.

I would like to thank my supervisors in Nottingham, Prof. Stephen Hill and Dr. Stephen Briddon for their guidance and support, and the Cell Signalling Research family for welcoming me into the group and making my studies abroad productive and enjoyable.

In addition, I would like to express my sincerest thanks to Dr. Michelle Halls, Dr. Michael Whittaker, Dr. Meritxell Canals, Cameron Nowell, Dr. Nghia Truong, Chris Lumb, and Daisy Albanese for their invaluable advice, help in the lab and in lab meetings.

I would like to acknowledge my panel members, Dr. Michelle Halls and Prof. Thomas Davis for the insight and guidance that they have provided throughout my candidature.

I would also like to thank my peers from the Integrated Neurogenic Mechanisms lab for their support, discussions and advice. To my friends and colleagues at MIPS and in the Cell Signalling Group, especially Dr. Pradeep Rajasekhar, Dr. Ee Von Moo, Dr. Bo Yun, Dr. Stefan Tomlins, Dr. Kathy Sengmany, Dr. Sheng Yu Ang, Kon Matis, Alastair Keen, Dr. Strawberry Chris, Chris Siwek, Arisbel Batista Gondin, Saori Mukaida, Birgit Caspar, Dr. Mark Soave, Dr. Laura Kilpatrick, and Nickolaj Groenewoud, thank you for the friendship, endless laughs and for the much-needed distractions.

To Mum, Dad, Quyen, Kev, Kim and Will, thank you for your emotional support, believing in me and encouraging me. Your late-night karaoke sessions, fast food runs, and meme supply have given me breaks from my PhD and kept me sane.

Lastly, I would like to thank caffeine and alcohol for their constant comfort and companionship through this crazy roller coaster ride.

List of Abbreviations

AC	adenylate cyclase
ADAM	a disintegrin and metalloproteinase
ANOVA	analysis of variance
AP2	adaptor protein 2
APP	Amyloid precursor protein
ATP	adenosine triphosphate
AUC	area under the curve
βArr	beta arrestin
BRET	bioluminescence resonance energy transfer
cAMP	cyclic adenosine monophosphate
CAN	acetonitrile
CKAR	C kinase activity reporter
CLIC	clathrin-independent carriers
CLR	Calcitonin receptor-like receptor
CNS	central nervous system
Cy5-Chol	Cyanine 5-PEG-Cholestanol
Cy5-EE	Cyanine-5-PEG-ethyl ester
DAG	diacylglycerol
DMEM	Dulbecco's modified Eagle's medium
ECL	extracellular loop
ECM	extracellular matrix
EDTA	ethylenediaminetetraacetic acid
EGFR	epidermal growth factor receptor
EKAR	extracellular signal-regulated kinase activity reporter
Epac	exchange protein directly activated by cAMP
ERK1/2	extracellular signal-regulated kinase 1 & 2
FBS	foetal bovine serum
FRET	fluorescence resonance energy transfer
GDP	guanosine diphosphate
GEEC	GPI-AP enriched early endosomal compartment
GPCR	G protein-coupled receptor
Grb2	growth factor receptor bound 2
GRK	G protein receptor kinase
GTP	guanosine triphosphate

HBSS	Hanks' Balanced Salt Solution
HEK	human embryonic kidney
HPLC	high performance liquid chromatography
IP3	inositol triphosphate
JNK	c-Jun N-terminal kinase
LX	leuokotriene
MAPK	mitogen-activated protein kinase
MLC	myosin regulatory light chain
MVB	multivesicular bodies
NK_1R	neurokinin 1 receptor
NKA	neurokinin A
NKB	neurokinin B
NMR	nuclear magnetic resonance
PBS	phosphate buffered saline
PG	prostaglandin
PI	propidium iodide
PI3K	phosphoinositol-3 kinase
PIP_2	phosphatidylinositol 4,5-bisphosphate
PKA	protein kinase A
PKC	protein kinase C
PLA_2	Phospholipase A_2
PLC	phospholipase C
PTHR	parathyroid hormone receptor type 1
ROCK	Rho-associated coiled-coil kinase
SP	Substance P
TAMRA	Tetramethylrhodamine
TM	transmembrane

Chapter 1

General Introduction

1.1 Compartmentalised signalling of G protein-coupled Receptors

1.1.1 G Protein-Coupled Receptors

G protein-coupled receptors (GPCRs) constitute more than 800 genes in the human genome and are the largest group of mammalian membrane proteins (Fredriksson *et al.*, 2003, Fredriksson *et al.*, 2005). Extracellular ligands such as hormones, lipids, neurotransmitters and small molecules bind to GPCRs to activate the receptor. Subsequently, diverse intracellular signalling events are initiated to elicit a cellular and physiological response (Pierce *et al.*, 2002). Seven-pass transmembrane proteins (Figure 1.1), GPCRs, can be subdivided into 5 classes based on the conserved sequence and structure: rhodopsin (family A), secretin (family B), glutamate (family C), frizzled/taste2, and adhesion receptor families (Fredriksson *et al.*, 2003, Lagerström *et al.*, 2008). The importance of GPCRs is highlighted by the 40% of market therapeutic drugs targeted to GPCRs (Tyndall *et al.*, 2005). The rhodopsin-like receptors are the largest GPCR family, representing 80% of human GPCRs which is reflected in the drug market with the largest number of receptors targeted clinically (Tyndall *et al.*, 2005).

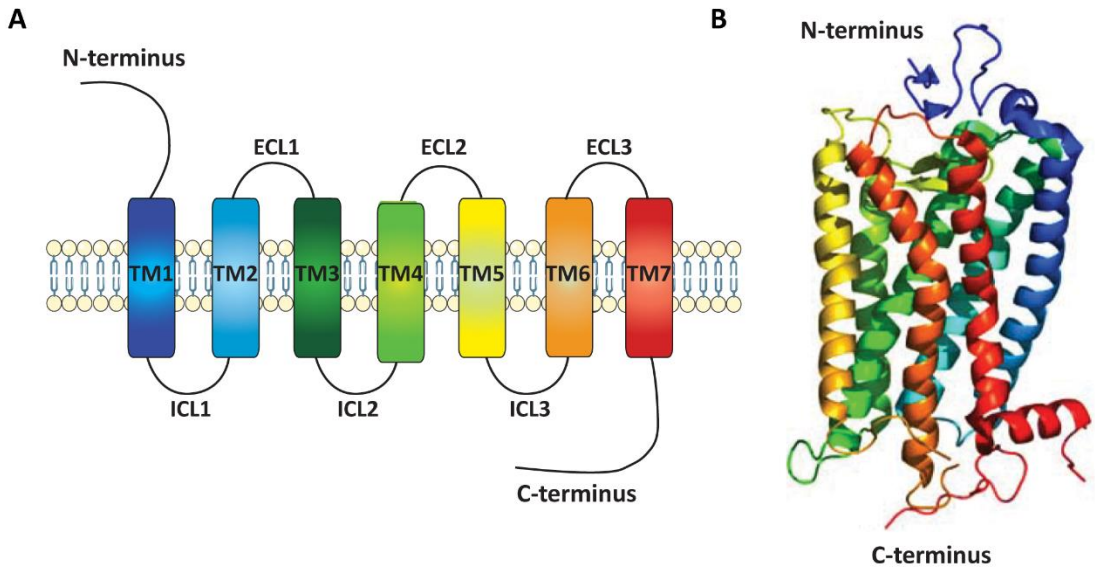

Figure 1.1. A, Schematic diagram of a seven-transmembrane receptor showing the transmembrane domains (TM), extracellular loops (ECL) and intracellular loops (ICL). **B,** A ribbon diagram of the crystal structure of bovine Rhodopsin (pdb f88). Adapted from Tyndall *et. al, 2005***.**

1.1.2 GPCR signalling transduction, desensitisation and recycling

Signal transduction is an important biological process in which receptors detect extracellular stimuli and initiate an intracellular response. G protein-coupled receptors mediate a wide range of signalling events including responses to hormones and neurotransmitters (Ji *et al.,* 1998, Rosenbaum *et al.,* 2009). Upon agonist binding, GPCRs undergo a conformational change to recruit the heterotrimeric complex, Gα and Gβγ. The α-subunit is activated, releasing the guanidine diphosphate (GDP) in exchange for guanidine triphosphate (GTP), leading to the dissociation of the heterotrimeric complex from the receptor. The heterotrimeric complex subsequently dissociates into the α-subunit and the βγ-complex, which modulate several distinct cellular signalling pathways (Bourne *et al.,* 1991, Neer 1995). The respective subunits activate or inhibit downstream effectors such as phospholipases and adenylate cyclase or regulate ion channels (Neer 1995, Hamm 1998, Rosenbaum *et al.,* 2009). After the activation of the α-subunit, the GTP is hydrolysed to return the subunit to the inactive state and reassociate with the βγ-dimer. Activated GPCRs can also recruit G protein-coupled receptor kinases (GRK1-7), which phosphorylate and desensitise the receptor by preventing further coupling of G-proteins. For many GPCRs, phosphorylation of the receptor increases the affinity of β-arrestin (β-arr) for the receptor (Krupnick *et al.,* 1998, Pitcher *et al.,* 1998). β-Arr is an adaptor protein that recruits important intracellular trafficking proteins such as adaptor protein 2 (AP2) and clathrin, to form a clathrin coated pit and to initiate the endosomal uptake of cargo, such as an GPCRs, into an endosomal

vesicle (Figure 1.2) (Goodman Jr *et al.*, 1996, Claing *et al.*, 2002). This process also requires a large GTPase protein known as dynamin, which forms a coil around the vesicle neck, to mediate vesicle budding and scission from the plasma membrane (Sweitzer *et al.*, 1998, Hinshaw 2000, Doherty *et al.*, 2009).

The canonical GPCR model suggests that GPCR internalisation decreases the number of receptors available at the plasma membrane to bind extracellular ligands and limits access to plasma membrane effectors and thus attenuates signalling (Oakley *et al.*, 1999, Claing *et al.*, 2002). Further, internalised GPCRs can be redistributed through the endosomal network to be recycled to the plasma membrane by recycling endosomes or be translocated through the lysosomal pathway for degradation (Figure 1.2) (Trejo *et al.*, 1999, Shenoy *et al.*, 2001, Di Guglielmo *et al.*, 2003).

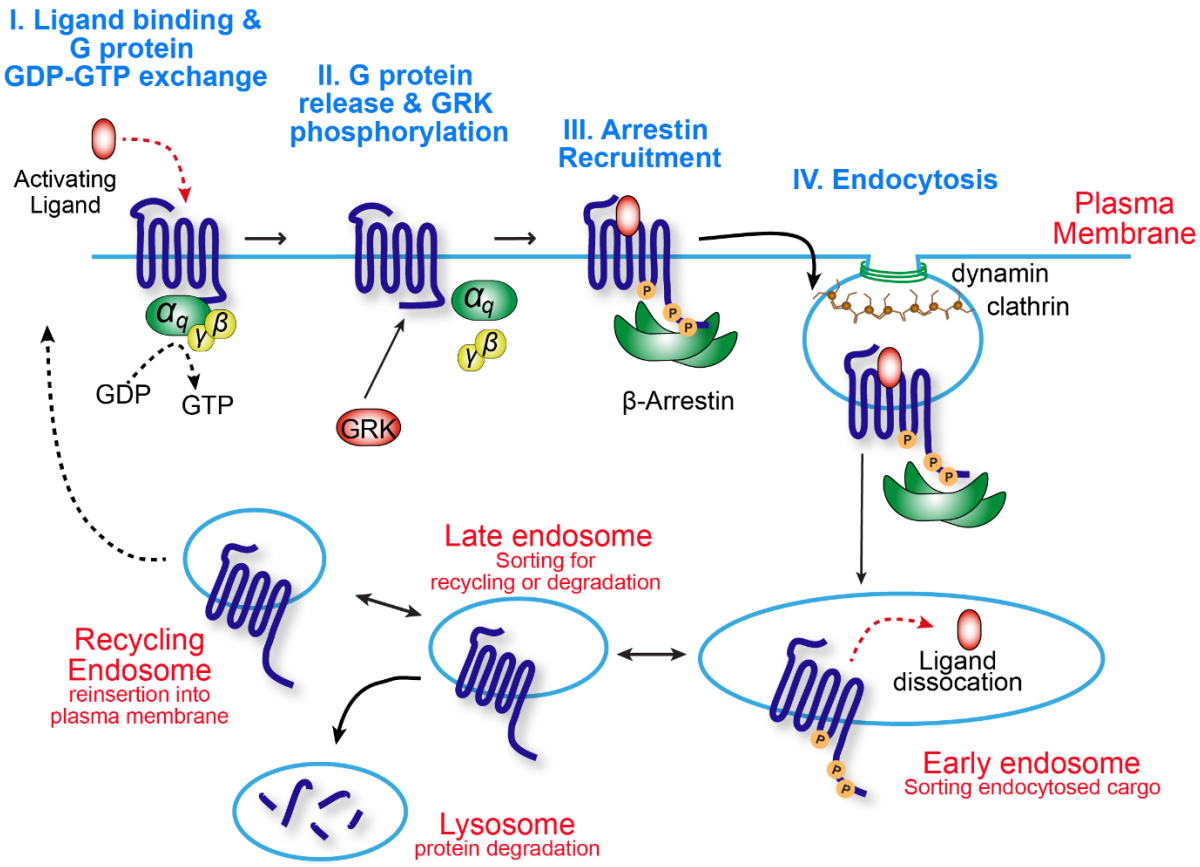

Figure 1.2. Canonical GPCR activation and trafficking pathways. An extracellular ligand mediates a conformational change in the GPCR, leading G-protein stimulation and release, GRK phosphorylation, arrestin recruitment and clathrin/dynamin-mediated endocytosis into early endosomes. Ligand degradation and sorting in late endosomes results in two GPCRs fates: degradation in lysosomes or translocation to recycling endosomes to be trafficked to the plasma membrane.

1.1.3 Compartmentalised GPCR signalling from Endosomes

In the canonical signalling dogma, GPCRs are activated by extracellular ligands to signal from the plasma membrane and subsequent βArr-mediated receptor internalisation is terminates receptor signalling by either dismantling GPCR signalling complexes before recycling receptor cargo back to the cell surface or by permanently downregulating GPCR via lysosomal degradation. However, with the advancement of new tools to study GPCRs, additional mechanisms of GPCR signalling have been identified leading to a shift in this GPCR signalling paradigm. Endosomes, endoplasmic reticulum, nuclei and Golgi have been revealed as spatially and temporally distinct platforms for GPCRs to regulate second messengers and mediate unique physiological processes.

The endosomal microenvironment contains small volumes, favouring ligand-receptor binding and slow endosomal sorting to promote long residence times of active receptors. βArr first emerged as a pleiotropic scaffolding protein when it was revealed that βArr 1 interacts with the non-receptor tyrosine kinase (Luttrell 1999). Further studies of βArr have identified numerous binding partners, some of which include extracellular signal regulated kinase (ERK1/2), phosphatidylinositol-3 kinase (PI3K), rapidly accelerated fibrosarcoma kinase (Raf), c-Jun N-

terminal kinase 3 (Jnk3), Ca^{2+}/calmodulin kinase II (CaMKII) and exchange protein directly activated by cAMP 1 (Epac 1) (Daaka *et al.,* 1998, Tohgo *et al.,* 2002, Povsic *et al.,* 2003, Song *et al.,* 2009, DeFea 2011). These binding partners may also include the direct or downstream activation of transcription factors. βArr-dependent endosomal signalling has since been shown to mediate intracellular signalling of numerous receptors such as the neurotensin 1 receptor and proteinase activated receptor 2 (DeFea *et al.,* 2000, Law *et al.,* 2012). With the development of nanobody based biosensors such as nanobody 37, which detects the active conformation of $G\alpha_s$ and nanobody 80, which binds the active conformation of the β_2 adrenergic receptor, the spatial and temporal profiles of these proteins have been probed (Irannejad *et al.,* 2013). This has led to the detection of agonist-dependent β_2 adrenergic receptor activation and subsequently, the detection of recruitment and activation of $G\alpha_s$ at the plasma membrane and in endosomes (Irannejad *et al.,* 2013). This suggests that GPCR signalling may also be mediated by G-proteins in the endosome after βArr-dependent internalisation. βArr-dependent receptor internalisation into endosomes provides a physical platform for the recruitment of binding partners to generate large signalling complexes or signalosomes.

Another way in which signalling of receptors from endosomes are distinguished from plasma membrane-delimited signals is by the duration of receptor signalling. This has previously been investigated with the parathyroid hormone receptor type 1 (PTHR). The activation of the receptor by the PTHR agonists, $PTHrP_{1\text{-}36}$ (plasma membrane-restricted) and $PTH_{1\text{-}34}$ (internalising) initiated two distinct cAMP signalling profiles (Figure 1.3). Both agonists elicited maximal cAMP responses (Ferrandon *et al.,* 2009). A transient cAMP signal was recorded using the non-internalising agonist and a persistent response was recorded when the PTHR was stimulated with the internalising agonist (Ferrandon *et al.,* 2009). These data indicated that the

sustained cAMP signal originated from endosomal compartments. Further investigation using a dominant negative form of dynamin to block internalisation of the receptor by PTH_{1-34} elicited a transient cAMP response, which supported the hypothesis of different temporal signalling profiles being initiated by temporally distinct sites (Ferrandon *et al.*, 2009). The spatial and temporally distinct signalling of receptors have also been investigated using compartment-specific biosensors. Förster resonance energy transfer (FRET) biosensors for ERK1/2 localised to the cytoplasm and nucleus were used to measure plasma membrane and endosomal delimited signalling of the calcitonin gene-related receptor (Calcitonin receptor-like receptor; CLR) respectively (Yarwood *et al.*, 2017). This was also further investigated using the dynamin inhibitor, Dyngo 4a and a dominant negative dynamin, Dynamin K44E to confirm the location of CLR signalling (Yarwood *et al.*, 2017).

Together, the roles of βArr and endocytosis in GPCR signalling revealed diverse functions beyond the signal termination, internalisation, desensitisation, and downregulation. Endosomes can provide a unique platform for GPCR-scaffold protein complexes which generate signals that are spatially and temporally distinct from the plasma membrane.

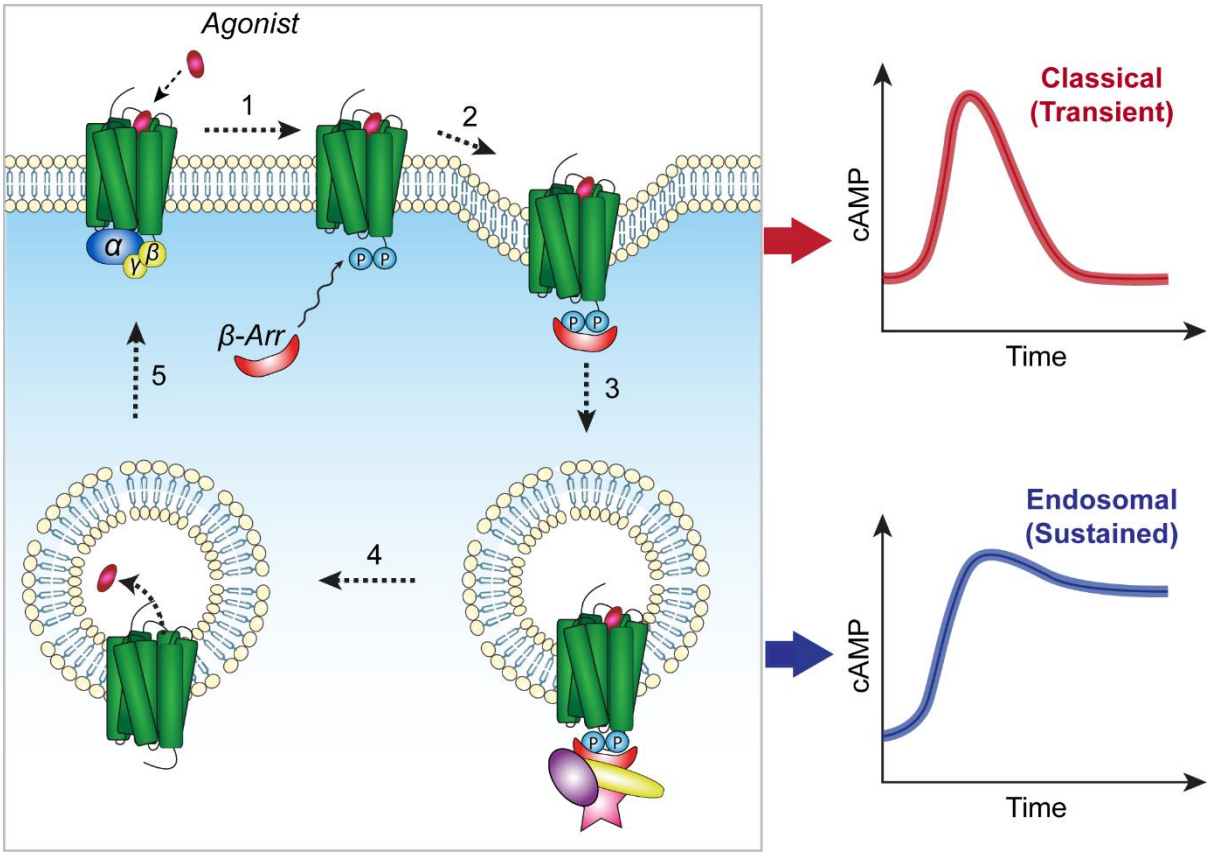

Figure 1.3. Classical and endosomal (sustained) signalling of GPCRs using PTHR as a model 1) Agonist activation of the receptor and the recruitment of the heterotrimeric complex. 2) Phosphorylation of the receptor by GRKs and subsequent binding of β-Arr. 3) β-Arr initiates clathrin and dynamin-mediated endocytosis of the receptor. The receptor- β-Arr complex interacts with binding partners to mediate endosomal signalling. 4) The agonist is removed from the binding pocket. 5) The receptor is recycled to the plasma membrane for activation. *Adapted from Pavlos and Friedman, 2017.*

1.1.4 Physiological implications of compartmentalised signalling

The identification of endosomes as receptor signalling platforms has led to research efforts to determine the effect of endosomally-derived signalling on physiology and disease. Multiple

studies have been conducted, revealing the relationship between endocytosis and neurodegenerative disorders, cancer, and pain (Simons *et al.,* 2000, Nixon 2005, Mellman *et al.,* 2013, Yarwood *et al.,* 2017). Cancer cells, for example, commonly have dysfunctional signalling caused by genetic changes to receptors such as integrins and receptor tyrosine kinases (Wiley *et al.,* 2001, Caswell *et al.,* 2009). Expression of mutant p53, which has been implicated in many cancers, can enhance the recycling of cell surface receptors, including integrins (Muller *et al.,* 2009). Disruption to the trafficking of integrin receptors has been identified as a contributing factors in cancer. A mechanism of dysfunctional trafficking exhibited in cancers is the upregulation of the Rab-family of small GTPases which regulate endosomal maturation and sorting (Porther *et al.,* 2015). The upregulation of Rab proteins associated with early endosomes and recycling such as Rab25 and Rab35 have been shown to promote receptor recycling (Caswell *et al.,* 2009, Johnson *et al.,* 2015, Porther *et al.,* 2015). Dynamin 1 which is involved in vesicular fission has also been implicated in cancer and is up-regulated in lung tumour cell lines (Schmid 2017).

With the emerging roles of endosomal platforms in receptor signalling and disease, the effect of internalising, or "location biased" drugs on different phenotypes are have been explored. For the regulation of the PTHR, the comparison of the agonists $PTHrP_{1\text{-}36}$ (non-internalising) and $PTH_{1\text{-}34}$ (internalising) on serum calcium, plasma 1,25-dihydroxyvitamin D, and fractional calcium were measured in healthy human volunteers (Horwitz *et al.,* 2003). Both peptides had similar effects on the serum calcium and fractional calcium. Interestingly, the $PTH_{1\text{-}34}$ was also more effective in the renal production of 1,25-dihydroxyvitamin D (Horwitz *et al.,* 2003). These data indicated that the internalising $PTH_{1\text{-}34}$ peptide and intracellular signalling of PTHR is responsible for renal production of 1,25-dihydroxyvitamin D.

Similarly, permeable and impermeable clinical antagonists of the β_1 adrenergic receptor (β_1AR) have also been studied in the context of compartmentalised signalling. The application of an impermeable antagonist prior to a permeable agonist resulted in the inhibition of cell surface-dependent cAMP production. In contrast, the permeable antagonist attenuated β_1AR signalling from the cell surface and the Golgi (Irannejad *et al.,* 2017). Clinically, the permeable antagonist reduces the heart rate and the force of contractions, whereas the impermeable antagonist only reduces heart rate (Seipel *et al.,* 1993, Holubarsch *et al.,* 1995). These observations demonstrated that the cell surface signalling of the receptor regulates the heart rate, whereas the Golgi localised receptor plays a role in regulating the force of contractions.

Overall, the effect of distinct receptor signalling platforms can be translated into physiological effects, creating new targets for drug design. Therefore, studying current and new clinical drugs in the context of endosomal signalling may provide valuable insight into the specific physiological outcome of targeting receptors in different platforms.

1.2 Tachykinins and the Neurokinin receptor family

The tachykinins are a family of peptides involved in nociception, cancer and inflammation (Bowden *et al.,* 1994, Hökfelt *et al.,* 2001, Mayordomo *et al.,* 2012, Muñoz *et al.,* 2014). The first discovered member of the tachykinin family, substance P (SP), is an undecapeptide associated with multiple physiological roles including pain transmission, microvascular permeability and gastrointestinal regulation of motility, secretion, and inflammation (Gaddum 1931, Lu *et al.,* 1997, Nichols *et al.,* 1999, Shimizu *et al.,* 2008). Many other neuropeptides, neurokinins, hemokinins and endokinins have since been identified in the tachykinin family peptides, of which the most potent mammalian tachykinins are SP, neurokinin A (NKA), and neurokinin B (NKB) (Steinhoff

et al., 2014). The tachykinins are derived from three *Tac* genes. *Tac1* encodes for SP and NKA and *Tac3* encodes for NKB. The tachykinins have conserved sequences that are required for the activation of tachykinin receptors (Phe-X-Gly-Leu-Met-NH_2) (Almeida *et al.,* 2004). The tachykinin receptors are GPCRs and are classed as family A rhodopsin-like receptors (Steinhoff *et al.,* 2014). There are three receptors that bind tachykinin peptides, known as neurokinin receptors (NK_1R, NK_2R, and NK_3R). The different affinities of tachykinins peptides for each receptor have been reported and investigated in detail (Steinhoff *et al.,* 2014). The amino terminal sequence of the tachykinins impart specificity for the receptors (Figure 1.4). For the NK_1R, SP has the greatest affinity, followed by NKA and NKB (Regoli *et al.,* 1994, Pennefather *et al.,* 2004). At the NK_2R, NKA has the greatest affinity (Pennefather *et al.,* 2004). Lastly, NKB has the greatest affinity at the NK_3R, followed by NKA and SP (Pennefather *et al.,* 2004). The most commonly studied of the tachykinin receptors is NK_1R (SP receptor).

A

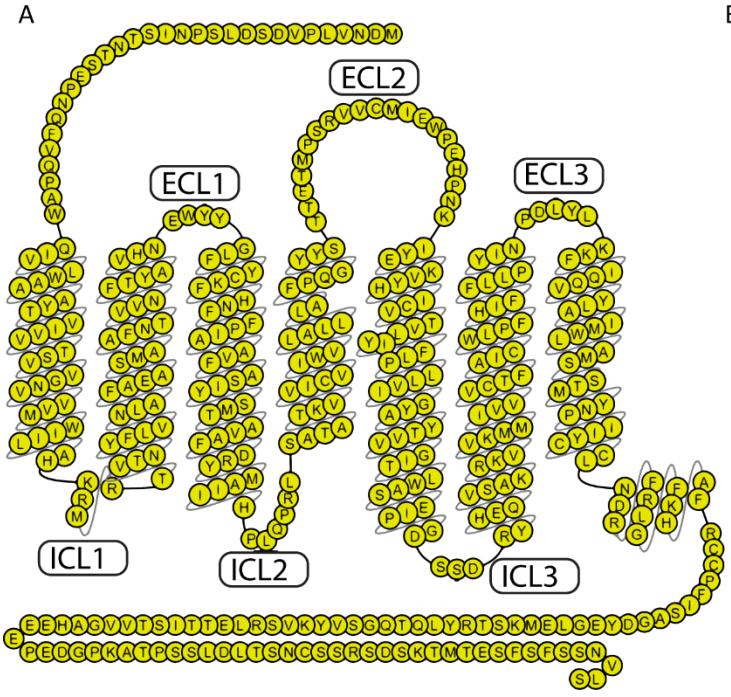

B

	Amino acid sequence
SP	RPKPQQFFGLM-NH_2
NKA	HKTDSFVGLM-NH_2
NKB	DMHDFFVGLM-NH_2

Decreasing affinity

Figure 1.4. A, Neurokinin 1 receptor snake diagram. **B,** Common NK_1R agonists amino acid sequences. Underlining denotes the conserved sequences necessary for receptor activation (Phe-X-Gly-Leu-Met-NH_2).

1.2.1 Neurokinin 1 receptor structure

The NK_1R is encoded in the *TACR1* gene and has been cloned from multiple mammalian species, all of which lead to expression of a protein 407 amino acids in length (Yokota *et al.,* 1989, Gerard *et al.,* 1991, Hershey *et al.,* 1991, Takeda *et al.,* 1991, Sundelin *et al.,* 1992). An additional splice variant of the receptor has also been identified, and compared to the full-length NK_1R, it has been identified as a truncated protein, lacking 96 residues of the C-terminus (truncation at residue 311). The rat NK_1R has 94.5% homology to the human receptor has been extensively studied to understand important motifs (e.g. conserved glycosylation sites) and arrestin interactions at the N and C-terminal tails (Yokota *et al.,* 1989, Almeida *et al.,* 2004). These studies have demonstrated that the N-terminal sequence is required for high affinity binding with SP insertion into the hydrophobic binding pocket (transmembrane II and VII), while the C-terminal sequence determines the G-protein specificity of the receptor (Fong *et al.,* 1992, Fong *et al.,* 1992, Huang *et al.,* 1994). Further, the carboxyl tail and the third intracellular loop also determine interactions with βArrs (Schmidlin *et al.,* 2003, Lai *et al.,* 2008).

1.2.2 Signal transduction of the NK_1R

SP-mediated activation of NK_1R couples to the pertussis toxin-insensitive $G\alpha_q$ protein, leading to the activation of phospholipase C isoforms (e.g. PLCβ) (Torrens *et al.,* 1989, Khawaja *et al.,* 1996). As summarised in Figure 1.5, PLC cleaves phosphatidylinositol 4, 5-bisphosphate to produce

diacylglycerol (DAG), which activates protein kinase C (PKC) and enhances the production of inositol 1, 4, 5-triphosphate (IP3), to stimulate IP_3 receptors and mobilise calcium (Ca^{2+}) from intracellular stores (Quartara *et al.*, 1997, Sorkin *et al.*, 2009, Pelayo *et al.*, 2014, Steinhoff *et al.*, 2014) (Nakajima *et al.*, 1992). PKC activity at the plasma membrane can also promote transactivation of epidermal growth factor receptor (EGFR) to stimulate extracellular signal-regulated kinase (ERK) (Jensen *et al.*, 2014). The stimulation of the NK_1R also leads to the activation of AC generating cAMP (Nakajima *et al.*, 1992). The mechanism by which the NK_1R mediates AC has been associated with the $G\alpha_q$-mediated activation of the Ca^{2+}-dependent PKC pathway (Jensen *et al.*, 2017).

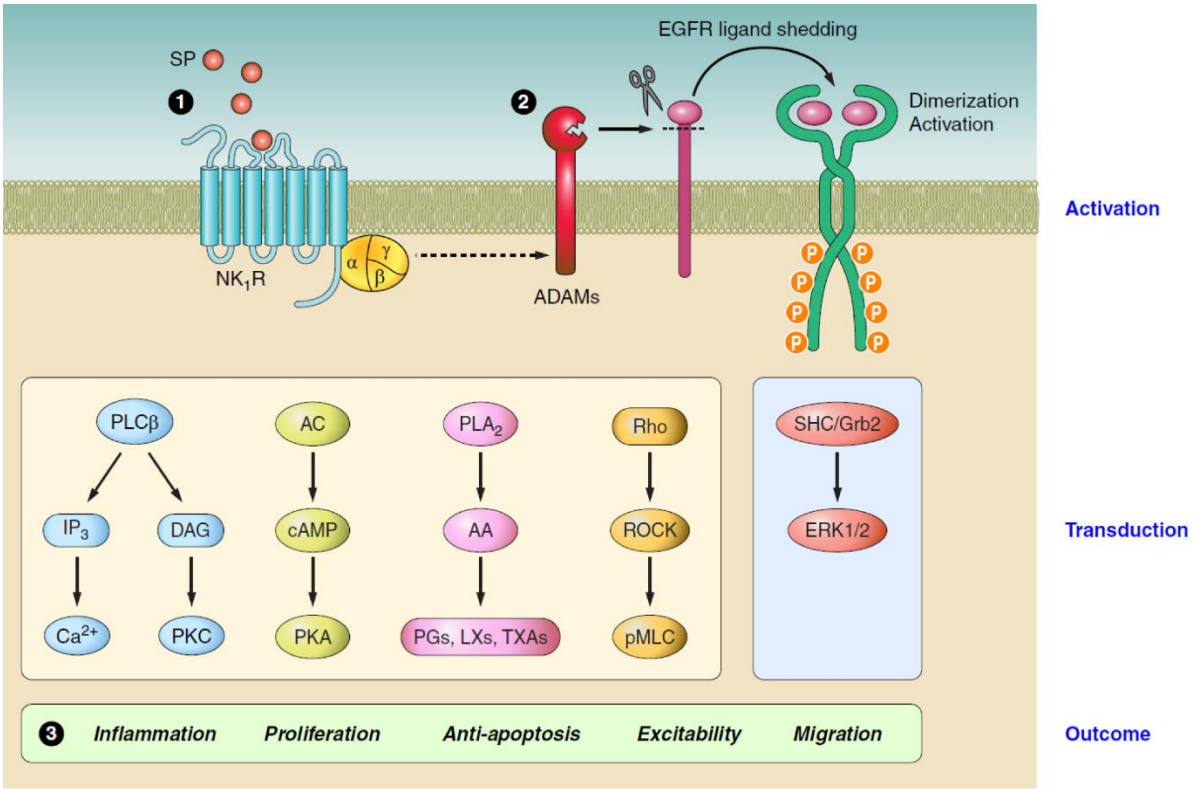

Figure 1.5. Neurokinin 1 receptor activation, signal transduction and physiological outcome. 1) The neurokinin 1 receptor (NK_1R) is activated by substance P (SP). NK_1R recruits the

heterotrimeric G-proteins and initiates plasma membrane-delimited signalling to activate phospholipase Cβ (PLCβ); inositol 1, 4, 5-triphosphate (IP3); intracellular calcium (Ca^{2+}); diacylglycerol (DAG); protein kinase C (PKC); adenylate cyclase (AC); cyclic AMP (cAMP); protein kinase A (PKA); Phospholipase A_2 (PLA_2); prostaglandins (PGs); leuokotrienes (LXs); thromboxane A_2 (TXA); Rho; Rho-associated coiled-coil kinase (ROCK); and myosin regulatory light chain (MLC). 2) The NK_1R activates a disintegrin and metalloproteinase (ADAM) cleaves epidermal growth factor receptor agonist to activate the receptor (EGFR). EGFR activation and phosphorylation leads to the ERK1/2 via a SHC and growth factor receptor bound 2 (Grb2) complex. 3) The physiological consequences of pathways in the NK_1R signalling repertoire. *Adapted from Steinhoff et. al., 2014.*

Phospholipase A_2 is also activated in response to NK_1R activation, leading to the production of arachidonic acids and precursors to inflammatory mediators including prostaglandins, leukotrienes and thromboxane (Katsube *et al.,* 2001). Concomitantly, the activation of NK_1R leads to Rho/Rho-associated coiled-coil kinase (ROCK)-dependent plasma membrane blebbing to form cell-derived vesicles or exosomes, as a mechanism for intercellular communication that is not well understood (Meshki *et al.,* 2009, Chen *et al.,* 2012). The signal transduction can be terminated at the plasma membrane by the depletion of the agonist due to the enzymatic degradation of SP by the membrane-bound neutral endopeptidase, neprilysin (Roosterman *et al.,* 2007, Cattaruzza *et al.,* 2009). In addition, as summarised in Figure 1.6, the agonist-bound receptor can be phosphorylated by GRKs to promote the recruitment of βArr 1/2 to the receptor and terminate plasma membrane-delimited signalling by initiating the internalisation

of the receptor by clathrin-dynamin mediated endocytosis (Mantyh *et al.,* 1995, Barak *et al.,* 1999, McConalogue *et al.,* 1999).

Following receptor internalisation, the SP-NK_1R-βArr signalling complex stimulates pathways that are distinct from plasma membrane-delimited events, including cytosolic cAMP, cytosolic PKC activity and the recruitment of Src and MEKK to activate nuclear ERK, independently of EGFR, in multi-protein scaffolding complexes (signalosomes) (DeFea *et al.,* 2000, Jafri *et al.,* 2006, Cottrell *et al.,* 2009, Murphy *et al.,* 2009, Jensen *et al.,* 2014). FRET biosensors localised in the cytosol and in the nucleus have been used to measure increases and decreases in activated ERK. Using this tool, cytosolic ERK signals were revealed to originate from plasma membrane signalling of the receptor, while the nuclear ERK was dependent on internalisation, these data support previous studies investigating βArr dependent signalling (DeFea *et al.,* 2000, Jafri *et al.,* 2006). Interestingly, the treatment of $G\alpha_q$ (UBO-QIC) and PKC (GF109203X) inhibitors in NK_1R expressing cells attenuated both plasma membrane and nuclear ERK signalling while an EGFR inhibitor (AG14718) attenuated the plasma membrane delimited only, having no significant effect on the endosomal ERK signal (Jensen *et al.,* 2014).

Termination of the endosomal signal, receptor recycling and resensitisation can be initiated by the removal of SP from the NK_1R binding pocket, leading to the disassembly of the signalosome. Previous studies demonstrated that endosomal acidification was required for the recycling and resensitisation of the receptor, to promote the removal of SP from the receptor binding pocket. SP-NK_1R interactions are highly pH-dependent, and a neprilysin related zinc-metalloendopeptidase known as endothelin converting enzyme 1 (ECE1) requires acidic pH for the proteolytic cleavage and deactivation of SP (Roosterman *et al.,* 2007, Cattaruzza *et al.,* 2009, Cottrell *et al.,* 2009, Jensen *et al.,* 2014).

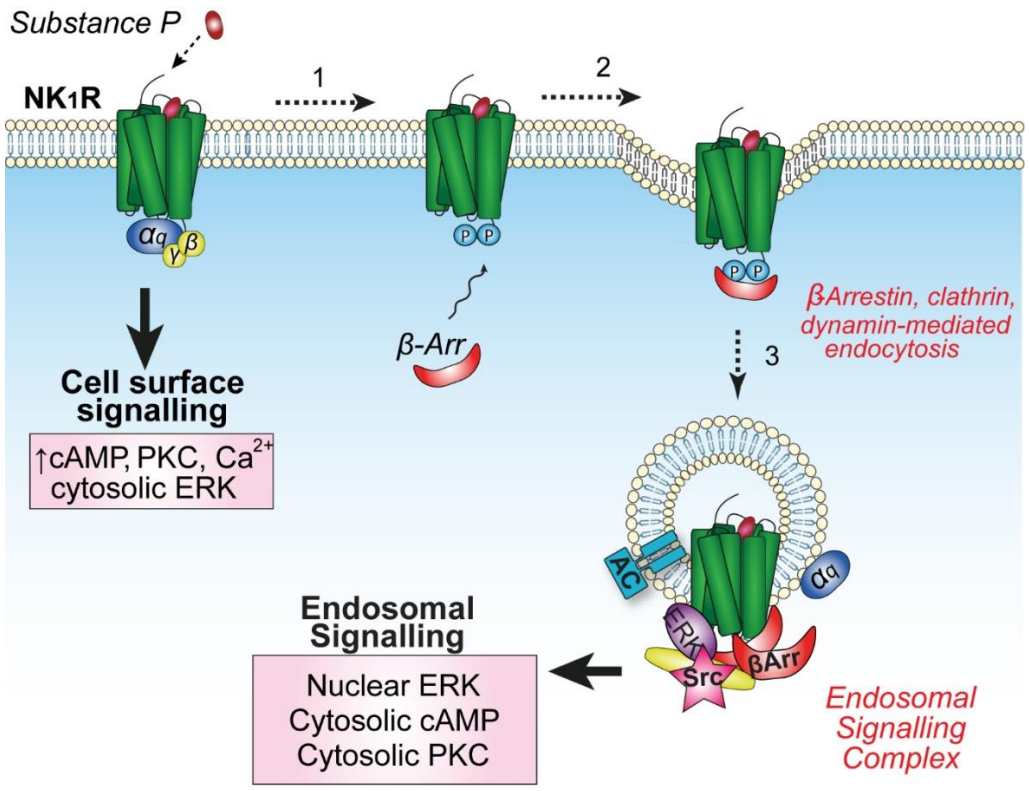

Figure 1.6. Compartmentalised signalling of NK_1R. 1) Activation of the NK_1R by SP initiates plasma membrane delimited signalling. 2) Receptor phosphorylation leads to the recruitment of βArr, the subsequent recruitment of clathrin coated pits. 3) The receptor is internalised by clathrin-dynamin mediated endocytosis. Within the endosome, the NK_1R can have a unique subset of signalling distinct from the plasma membrane.

1.2.3 NK_1R expression, distribution and associated pathophysiology

Substance P is expressed in the central nervous system and in peripheral tissues. In adult rats and humans, SP is expressed in and released from central projections of nociceptors in the dorsal horn and from various regions in the brain including: the medulla, the amygdala, the hypothalamus, the

ventral striatum, the dorsal striatum, the raphe nuclei, the substantia nigra, the nuclei of the pontine tegmentum, and the medial habenular nucleus (Cooper *et al.,* 1981, Harlan *et al.,* 1989, Marchand *et al.,* 1991, Chawla *et al.,* 1997, Uhlén *et al.,* 2015). SP is expressed in enteric neurons of the myenteric plexus and submucosal plexus, as well as the extrinsic primary afferent fibres of the gut (Shimizu *et al.,* 2008). SP has also been detected in peripheral sites including glandular cells, the respiratory tract, the urogenital system, skin, and lymphoid organs (Candenas *et al.,* 2005, Uhlén *et al.,* 2015, Mashaghi *et al.,* 2016, Szallasi *et al.,* 2017, Kaczyńska *et al.,* 2018). The NK_1R has a similar distribution profile throughout the CNS and peripheral tissues. The expression and distribution of NK_1R have been extensively studied and while much is known about tachykinin signalling, new roles continue to be revealed. The following describes the central nervous system and the gastrointestinal system as two key examples of characterised physiological studies, to illustrate the importance of NK_1R and other neurokinin receptors in disease, and therefore demonstrate the importance of developing potent-selective drugs to target conditions where NK_1R cell signalling is a key contributor to disease etiology and ongoing pathology.

1.2.4 Central nervous system

The NK_1R is widely expressed in the CNS and has been localised in mammalian models including the guinea pig and rats, where high levels of expression were detected in the striatum, nucleus accumbens, the lateral nucleus of the hypothalamus, hippocampus, habenula, the interpeduncular nucleus (Maeno *et al.,* 1993, Otsuka *et al.,* 1993, Yoshifumi *et al.,* 1994, Lai *et al.,* 2008). In the brain stem, NK_1R was expressed in the nucleus of the tractus solitarius, the raphe nuclei and the medulla oblongata (Otsuka *et al.,* 1993). In the spinal cord, NK_1R has also been well characterised and shown by fluorescence confocal microscopy to undergo receptor internalisation in neurons

within laminae I and II, following and the application of SP peptide or excitatory postsynaptic potential (Marvizón *et al.,* 1997, Marvizón *et al.,* 1999).

The NK_1R signalling in the CNS is an important mechanism for central pain transmission and inflammation. When noxious stimuli excite primary sensory nerves in the periphery (e.g. innervating skin or viscera), this promotes simultaneous release of SP in peripheral tissues and the dorsal horn of the spinal cord, where sensory neurons synapse with second-order neurons of the CNS (Mantyh *et al.,* 1995). In the periphery, SP activation of NK_1R on endothelial cells and epithelial cells to cause plasma extravasation, granulocyte infiltration and cytokine release (Greeno *et al.,* 1993, Bowden *et al.,* 1994, Bai *et al.,* 1995, Renzi *et al.,* 2000). In the spinal cord, NK_1R stimulation leads to neuronal excitation and central pain transmission. SP stimulation of the NK_1R achieves these physiological outcomes via Gαq dependent signalling followed by rapid internalisation and recycling of the receptor in the spinal cord (Mantyh *et al.,* 1989, Mantyh *et al.,* 1995, Mantyh *et al.,* 1995, Pelayo *et al.,* 2011) and in vasculature (Greeno *et al.,* 1993). Importantly, this has been observed in clinically relevant settings. For example, patients with chronic visceral pain conditions, a reduction in NK_1R availability in regions of the brain associated with nociception was measured (Bergström *et al.,* 2004, Jarcho *et al.,* 2013).

1.2.5 Gastrointestinal system

The distribution of NK_1R in the gastrointestinal tract has been investigated using autoradiography, immunohistochemistry and fluorescent ligand binding (Mantyh *et al.,* 1989, Boutaghou-Cherid *et al.,* 2006). The expression of NK_1R has previously been identified, localised and pharmacologically studied in mammalian gastrointestinal tracts of rats, guinea pigs, murines and humans (Grady *et al.,* 1996, Lavin *et al.,* 1998, Lomax *et al.,* 1998, Vannucchi *et al.,* 1999,

Salmhofer *et al.,* 2001, Boutaghou-Cherid *et al.,* 2006, Chen *et al.,* 2007). NK_1R has been localised to extrinsic enteric neurons and nerve fibres from the dorsal root ganglia and vagal ganglia which receive sensory information from the gut and have been implicated in neurogenic inflammation (Baron *et al.,* 1983, Grady *et al.,* 1996, Harrison *et al.,* 2001). Activation of NK_1R, as well as NK_3R contribute to slow excitatory transmission in enteric neurons (Johnson *et al.,* 2004). NK_2R localised in intrinsic enteric neurons innervate smooth muscle and NK_1R is distributed in interstitial cells of Cajal (ICC) (Lavin *et al.,* 1998, Shimizu *et al.,* 2008). SP-dependent activation of NK_1R leads to the modulation of ion channels on the ICC to mediate the coordination of rhythmic contractions in the gut, to modulate gut motility (Lavin *et al.,* 1998, M. *et al.,* 2004, Maria-Simonetta 2006, Kim *et al.,* 2012). Fluid secretion, which facilitates propulsion, is mediated by the activation of neurokinin receptors on epithelial cells, enteric neurones or immune relate cells including lymphocytes (Boutaghou-Cherid *et al.,* 2006). In addition to the role of neurokinin receptors in the modulation of neurotransmission, motility, fluid secretion and motility of the intestine, NK_1R has also been extensively studied as an inflammatory mediator in the gut (M. *et al.,* 2004, Koon *et al.,* 2006, Maria-Simonetta 2006). NK_1R is expressed on lymphocytes of the lamina propria and on macrophages in the intestine (Castagliuolo *et al.,* 1997, Maggi 1997, Goode *et al.,* 2000). Therefore, the dysregulation or dysfunction of NK_1R and tachykinins can underlie many inflammatory bowel diseases such as Crohn's disease and ulcerative colitis (Neunlist *et al.,* 2003, J. *et al.,* 2007). Clostridium difficile-dependent production of toxin A results in inflammation, has been demonstrated to induce pseudomembranous colitis. Further histological examination detected an upregulation of NK_1R in the blood vessels and lymphoid structure in the intestine (Mantyh *et al.,* 1996). Similar results were observed in Crohn's disease and ulcerative colitis, in which NK_1R expression was upregulated in arterioles, venules

and in lymph nodules (Mantyh *et al.,* 1988). The contribution of NK_1R to inflammatory bowel disease was supported in NK_1R knockout studies in which clostridium difficile did not induce secretory and inflammatory mechanisms, or toxin A induced epithelial damage in the intestine (Castagliuolo *et al.,* 1998). Similar results were also achieved using an NK_1R antagonist which reduced toxin A-dependent histological and physiological damage of the colon.

1.3 Drug Delivery

1.3.1 Targeted drug delivery

Traditionally, many areas of drug delivery have focused on techniques to increase solubility and permeability as a means of increasing drug absorption and systemic exposure (Allen *et al.,* 2004). However, the non-selective increase in systemic drug concentrations can lead to off target toxicity since drug exposure is increased in both target and non-target sites. A solution to this is to increase tissue specificity, thereby concentrating a drug to target tissues, cell types or organs. In order to achieve this, many formulation and delivery approaches have been explored, including the use of surface functionalised nanoparticles, liposomes, and dendrimers (Maurer *et al.,* 2001). Currently, these approaches have focussed on drug targeting at a systemic level and show significant promise in drug targeting to specific organs. Due to the complexity and limited understanding of the chemical-biological interface where these drug targeting strategies are applied, less effort has been directed towards refining drug targeting strategies to subcellular target sites, to achieve highly selective targeting to specific intracellular locations such as organellar compartments (Allen *et al.,* 2004, Stone *et al.,* 2009).

1.3.2 Intracellular Drug Delivery

Viruses can deliver genes into host cells for replication in an efficient manner. Synthetic drug delivery design aims to mimic viral delivery efficiency, increasing specificity and subsequently decreasing off target drug effects (Allen *et al.,* 2004, Petros *et al.,* 2010). Advancements in nanotechnology and cell biology have been informative in the development of surface functionalised nanoparticles for targeted delivery as well as stimuli responsive nanoparticles (Benns *et al.,* 2000, Duncan 2003, Johnston *et al.,* 2006, Ganta *et al.,* 2008, Zhou *et al.,* 2011, Mura *et al.,* 2013). Subcellular regions contain distinct microenvironments and can be utilised as stimuli for cargo release mechanisms, which may include the reduction of covalent bonds (Meng *et al.,* 2009), pH (Ganta *et al.,* 2008, Gao *et al.,* 2010, Zhou *et al.,* 2011), enzymatic cleavage and temperature (Bae *et al.,* 1987, Nakayama *et al.,* 2006).

Lipid-tethered drugs have recently been explored as an alternative delivery method for improved cellular drug uptake and intracellular targeting by anchoring a drug to the cell membrane (Rajendran *et al.,* 2008, Rajendran *et al.,* 2010, Rajendran *et al.,* 2012). Lipid-tethered drugs are expected to more avidly associate with the plasma membrane and subcellular compartments and may direct the movement of a drug through the endosomal trafficking pathway. In addition, this may also increase the potency of an agonist or antagonist, by increasing its local concentration (Saftig *et al.,* 2009, Sorkin *et al.,* 2009). This concept was initially investigated for targeting inhibitors to β secretase, as a potential treatment option for Alzheimer's disease. The secretase is an enzyme that cleaves amyloid precursor protein (APP) and catalyses the formation of β-amyloid. β-amyloid is an insoluble peptide that aggregates in the brain resulting in the plaques which are associated with the development of Alzheimer's disease symptoms (Vassar *et al.,* 1999, Yan *et al.,* 1999, Luo *et al.,* 2001). β-secretase resides on the plasma membrane; however, it only cleaves

APP at an acidic pH in the endosome (Vassar *et al.,* 1999, Yan *et al.,* 1999). Lipidation of the otherwise soluble inhibitor of β-secretase results in an increased accumulation of the inhibitor within endosomes (Rajendran *et al.,* 2008). Importantly, this accumulation translated to an 80% decrease in β-secretase cleavage of APP relative to a vehicle treatment (Rajendran *et al.,* 2008). Comparatively, a PEG-linked inhibitor without a lipid-anchor present showed limited activity (Rajendran *et al.,* 2008, Schieb *et al.,* 2010). Lipidation was therefore shown to target drugs into endosomal compartments. This has led to significant improvements in the therapeutic potential of drugs to target receptors, enzymes and proteins within endosomes, which may have implications in pathophysiology (Rajendran *et al.,* 2008, Folk *et al.,* 2012, Linning *et al.,* 2012).

1.3.3 Drug internalisation via Endocytic pathways

Endocytosis is one of the many dynamic processes that mediate the uptake of drugs from the extracellular matrix into the cell and is responsible for sorting, recycling and degrading both peptidic and synthetic drugs (Gruenberg 2001, Kobayashi *et al.,* 2001, Gruenberg 2003, Murphy *et al.,* 2009). Drug uptake mediated by endosomal processes can occur constitutively, for example through bulk fluid uptake via macropinocytosis or phagocytosis, or can be ligand triggered, for example via ligand-receptor binding (Doherty *et al.,* 2009, Zhang *et al.,* 2015).

Ligand-mediated uptake can occur through the well characterised clathrin-dependent pathway or via clathrin-independent pathways including caveolar, Rho A-dependent, and clathrin-independent carriers/GPI-AP (CLIC/GEEC) endocytosis (Johannes et al., 2015). The primary vesicles internalised through these pathways can undergo homotypic fusion or fuse with sorting/early endosomes (Parton *et al.,* 2013, Di Fiore *et al.,* 2014, Irannejad *et al.,* 2014, Mayor *et al.,* 2014). Molecules can then be sorted and translocated via recycling endosomes back to the

plasma membrane, towards lysosomes for degradation, or towards the trans-Golgi network (Huotari *et al.*, 2011, Elkin *et al.*, 2016).

1.3.4 Lipid composition of the plasma membrane

The plasma membrane has a diverse and heterogenous composition of lipids that can interact with membrane-bound proteins (van Meer 2005, Lu *et al.,* 2018). The lipids in the plasma membrane have previously been separated into detergent-soluble and detergent-resistant fractions (Yu *et al.,* 1973). Further research of the lipid compositions have led to the identification of glycosphingolipids, cholesterol and saturated phospholipids comprising the detergent-resistant fraction (Amigo *et al.*, 1999, van Meer 2005, Van Meer *et al.*, 2008). Previously, these detergent-resistant lipids were hypothesised to form rigid and organised lipid raft microdomains. However, with the development of more sensitive techniques with greater resolution, these lipids have been observed to have transient, energetically favourable interactions (Simons *et al.,* 2004, Lu *et al.,* 2018). The depletion of sterols using methyl-β-cyclodextrin resulted in altered signal transduction as well as protein trafficking (Simons *et al.*, 2000). Cholesterol has been implicated as an allosteric regulator of signalling and may also play a role in the organisation of signalling molecules through adaptor and scaffolding proteins such as the post-synaptic density 95, disc large 1, and zonular occludens 1 (PDZ) proteins (Sheng *et al.,* 2012, Song *et al.,* 2014). The depletion of cholesterol by methyl-β-cyclodextrin resulted in the loss of caveolae and the formation of unstable or aborted clathrin coated pits which were recovered with the replenishment of cholesterol (Sinha *et al.*, 2011, Kim *et al.,* 2017). These observations indicated that the enrichment of cholesterol in caveolae and clathrin coated pits are required for stable vesicle formation and subsequent internalisation.

1.3.5 Endosomal acidification

Endosomes are highly-regulated dynamic tubule-vesicular networks that exchange membranes and protein cargo throughout the cell to regulate most cell processes. Each endosomal subtype is closely related but occupy distinct intracellular regions and favour distinct cargo due to differences in protein composition and pH (Doherty *et al.,* 2009, Huotari *et al.,* 2011). Complex, membrane-associated proton pumps, V-ATPases, regulate the luminal pH of endosomal compartments. V-ATPases increase positive ions within the lumen and hence acidify vesicles (Beyenbach *et al.,* 2006, Marshansky *et al.,* 2008). Distribution of V-ATPase concentrations on different endosomal membranes account for the asymmetry in pH between early endosomes, late endosomes, and lysosomes (Beyenbach *et al.,* 2006, Marshansky *et al.,* 2008, Huotari *et al.,* 2011). Furthermore, asymmetric pH environments provide another means by which molecules that are endocytosed can be sorted and trafficked, due to its influence on interactions with respective targets (Huotari *et al.,* 2011). For example, acidification of endosomes can promote ligand protonation to provide favourable conditions for hydrolytic reactions and the binding or release of ligands by receptors and enzymes. The metallopeptidase, endothelin converting enzyme 1 and the protease, β-secretase are just some examples that highlight the importance of distinct pH environments. Both proteases are membrane bound; however, they only exist in an active conformation when they are in the acidic environment of an endosome (Roosterman *et al.,* 2007, Rajendran *et al.,* 2008). During endosomal maturation, endosomal compartments are acidified to a pH of 6.1-6.8 in early endosomes, 6.0-4.8 in late endosomes and approximately 4.5 in lysosomes (Figure 1.7). These differences provide distinct pH environments between each endosomal compartment and other intracellular organelles (Mellman *et al.,* 1986, Doherty *et al.,* 2009, Huotari *et al.,* 2011)

1.3.6 Endosomal protein composition

The plasma membrane and endosomal compartments have unique compositions of regulatory proteins for sorting. The Ras-like proteins in the brain (Rab) family consist of 61 members and comprise the largest subfamily of small GTPases of the Ras family (Pereira-Leal *et al.,* 2001). Rab proteins are localised across the entire endosomal network for the regulation of vesicle budding, endosomal tethering, fusion and motility (Zerial *et al.,* 2001, Huotari *et al.,* 2011). The spatial separation and localisation of the Rab proteins correlate with their functions (Zerial *et al.,* 2001). For example, the Rab22 protein localised in early endosomes is associated with membrane and protein trafficking to recycling endosomes (Mohrmann *et al.,* 1999, Kauppi *et al.,* 2002). Given the distinct localisation of the Rab proteins, they are commonly used as fluorescent fusion proteins and have been useful tools for the identification of endosomal compartments.

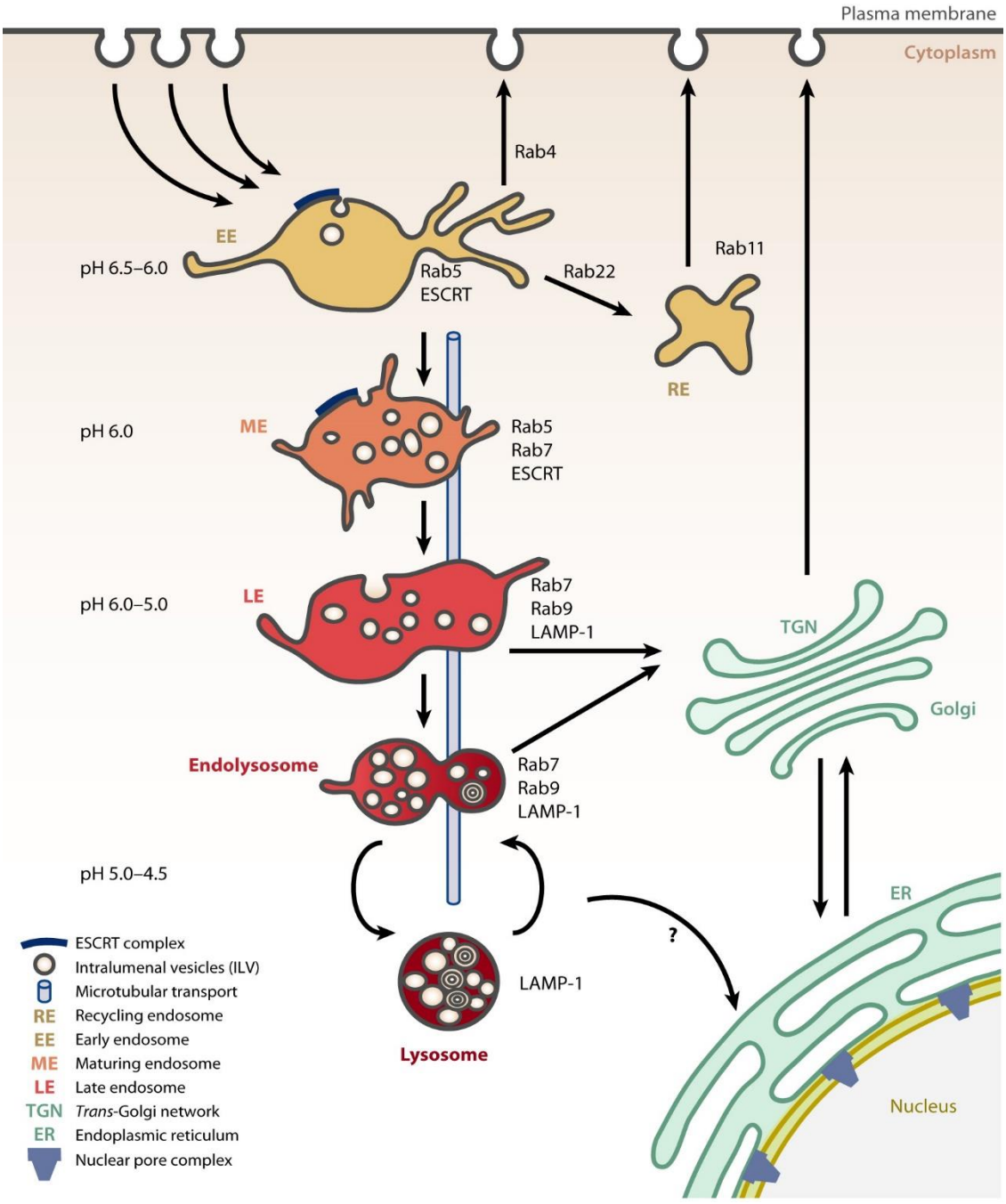

Figure 1.7. Endosomal maturation. Internalised vesicles are incorporated into early endosomes (EE). Endosomal sorting can direct molecules and proteins towards the recycling endosome (RE) or towards the degradative pathway via maturing endosomes (ME), late endosomes (LE), endolysosome to the lysosome. Sorted products may also be translocated from the LE or

endolysosomes to the transgolgi network (TGN) to be shuffled to the endoplasmic reticulum (ER) or plasma membrane for recycling *(Mercer et al., 2010). Adapted from Mercer et. al., 2010.*

1.4 Drug molecule design

To direct a drug into the endosomal network by associating it with a membrane, the overall construct must consist of three main components: a water-soluble drug, a linker and a lipid. The construct is a simple concept, however, there are many factors to consider in the construct design to ensure the drugs are delivered to the correct intracellular compartment, as well as retaining, or optimising the potency of the drug.

1.4.1 Lipid modifications to peptidic drugs

Membrane associated proteins account for 25-40% of proteins in the cell membrane. These associations with cellular membranes are attributed to either proteinaceous or lipid-anchors that partition into the phospholipid bilayer (Levental *et al.,* 2010). Typically, for a protein to partition into the hydrophobic environment of the plasma membrane, protein anchors are required that comprise of α-helices or β-sheets where the hydrophobic chains of the amino acids face outwards (Lodish *et al.,* 1995, Levental *et al.,* 2010). It has been hypothesised that transient, but distinct distributions of lipids are involved in the promotion of signalling and protein interactions by dictating the spatial organisation of membrane bound proteins (Simons *et al.,* 1997, Simons *et al.,* 2000, Simons *et al.,* 2000, Allen *et al.,* 2007). An example of the spatial organisation of lipids is during endocytosis, in which caveolae and clathrin-coated pits have a high density of cholesterol which has supports lipid packing to allow for pit formation (Sinha *et al.,* 2011, Kim *et al.,* 2017). Selectivity of transfer of lipids into different regions of the plasma membrane can be used to

influence the partitioning of peptides into specific regions of the plasma membrane and to direct peptides to different endosomal fates (Levental *et al.,* 2010, Lingwood *et al.,* 2010).

The lipid moiety increases the affinity of the drug for the plasma membrane (Rajendran *et al.,* 2008, Rajendran *et al.,* 2012). The lipid embeds into the lipid bilayer of the plasma membrane and therefore can be internalised by endocytic processes. Cholestanol, a sterol, is expected to be enriched in membranes forming clathrin coated pits and caveolae, thereby increasing the likelihood of endocytic uptake (Levental *et al.,* 2010, Rajendran *et al.,* 2012). Linning *et al.* explored the effect of lipid variations on the potency of an inhibitor GL189 to target the membrane-bound β-secretase, which is localised in lipid rafts (Linning *et al.,* 2012). Calculated EC50 values from concentration response data for dihydrocholesterol and cholesterol, lipid raft anchors, were 0.74 nM and 0.39 nM respectively (Schieb *et al.,* 2010, Linning *et al.,* 2012). Long chained lipid alcohols, myristyl (C14) and lignoceryl (C24) were significantly less potent than the sterol anchors, with calculated values of 177.01 nM 7.66 nM respectively (Linning *et al.,* 2012). The changes in potency of the inhibitor from different membrane anchors emphasise the potential of targeting by lipid-conjugation and the importance of selecting an appropriate anchor.

1.4.2 Drug substitution position

The main objective of this strategy is to deliver the drug without compromising its activity. Therefore, the linker should be conjugated at a position on the drug that will not interfere with drug-target binding. The importance of linker substitution location was examined by Linning *et al*. who demonstrated the importance of this concept by testing three lipidated molecules that varied only in the linker substitution position on the drug molecule, a β-secretase inhibitor (Linning *et al.,* 2012). Of the three variants of the β-secretase inhibitor construct, two of the constructs

increased the potency of the drug; one of which increased the potency by ≈9 fold from EC50= 863 nM to EC50= 9.7 nM. In contrast, the last variant of the inhibitor rendered the molecule inactive (Linning *et al.*, 2012).

1.4.3 Linker selection

For a given drug, the linker and the lipid are structural determinants of utility and can be optimised to target specific substructures. The linker essentially tethers the drug and lipid components together. It has previously been hypothesised that optimising the chain length should improve the proximity of the drug and the target (Miriam *et al.*, 2011, Folk *et al.*, 2012). Rajendran *et al.* demonstrated the necessity of the PEG linker in a study by directly conjugating the β-secretase inhibitor to cholestanol for comparison with a cholestanol tethered inhibitor via an 89 Å PEG chain. β-secretase is responsible for the cleavage of APP into sAPPβ fragments and changes in sAPPβ produced were attributed to inhibition by the drug construct (Rajendran *et al.*, 2008). The results showed that the β-secretase inhibitor directly conjugated to the cholestanol was inactive relative to a vehicle control. Comparatively, the inhibitor tethered to the cholestanol via an 89 Å PEG chain elicited a decrease in sAPPβ by 80% (Rajendran *et al.*, 2008). However, more recent investigations of variations in linker types and lengths between 26 and 96 Å has indicated no significant correlation between linker properties and response to a the β-secretase inhibitor (Schieb *et al.*, 2010). Therefore, findings in previous studies of the role of the linker suggests that the linker is a necessary structural component of a lipid-conjugated drug, however, the function of the construct is tolerable to variation in linker length and type (Rajendran *et al.*, 2008, Schieb *et al.*, 2010).

1.5 Scope of thesis

NK_1R is widely expressed in mammals and is a key contributor to many important physiological functions including wound healing, gut motility and pain transmission. However, the dysregulation of NK_1R signalling and distribution has been demonstrated to contribute to disease etiology and ongoing pathology. Currently, there are high affinity, potent and selective NK_1R antagonists available. However, many antagonists have been unsuccessful clinically, possibly due to the distribution of NK_1R into endosomes, lack of species selectivity, lack of efficacy for unknown reasons or due to unwanted side effects profiles (Steinhoff *et al.*, 2014). This hypothesis is supported by cell-based experiments which indicate that the NK_1R can continue to signal endosomally, leading to sustained ERK signalling (Cottrell *et al.*, 2009, Cattaruzza *et al.*, 2013, Jensen *et al.*, 2014). Further, positron emission tomography of [^{18}F]SPA-RQ in the brains of patients suffering two forms of chronic pain demonstrated a reduction in the density of NK_1R which may be due to constitutive activation and internalisation (Jarcho *et al.*, 2013). Although the physiological effects of intracellular signalling of the NK_1R remain unknown, the lack of drugs available for chronic pain and inflammatory diseases may be due to limited access to the internalised receptor. Therefore, it is important to design drugs and delivery methods to enhance the delivery of NK_1R antagonists to endosomal compartments for treating chronic pain diseases. Methods for targeting drugs to specific tissues and organs are well established and can improve drug uptake at the site of action. However, the therapeutic potential of using delivery devices to target drugs to specific subcellular compartments has not been explored. Therefore, the focus of this thesis was to investigate and characterise lipid conjugation and pH-dependent nanoparticles as endosomal drug delivery strategies to improve cellular uptake, promote distinct patterns of intracellular localisation and ultimately improve drug action.

In **chapter 2**, blocking the internalisation of NK_1R attenuated the intracellular signalling in cell lines, prompting an investigation into the role of NK_1R internalisation in the signalling of primary DRG and nociception *in vivo*. The internalisation of NK_1R was determined as a necessary cellular mechanism for sustained nociception. Here, we also characterise lipid-conjugate drugs and demonstrate the improved localisation, distribution, affinity and potency of Spantide I in cell lines, primary DRGs and in mouse models.

To characterise lipid-conjugated compounds in the context of their biophysical and molecular dynamic properties, in **chapter 3**, FCS was used to determine the concentration and diffusion of the probes. Experiments in solution revealed that the lipid-conjugated, and a lipid-free control probe non-specifically bind to reduce measured concentrations. Although the addition of FBS prevented non-specific binding, not all the lipid-conjugate probe concentrations were recovered. Together with the data from chapter 2, these FCS results suggest that despite the lower concentration of the lipid-conjugated NK_1R antagonist in solution, the probe can still access the NK_1R and inhibit NK_1R intracellular signalling.

Given the localisation of lipid-conjugated probes in multiple intracellular locations, including the plasma membrane, the use of pH responsive nanoparticle as endosomal drug carriers was investigated in **chapter 4**. However, many polymeric pH-responsive nanoparticles have been demonstrated to induce polycation-dependent cytotoxicity. Therefore, in this thesis a protective diethylene glycol monomer has been investigated and identified which prevents cytotoxicity to demonstrate that these pH responsive nanoparticles may offer a suitable approach for selective delivery drugs into endosomes.

Chapter 2

Investigating lipid-conjugation as a tool for delivering drugs to internalised Neurokinin 1 Receptors

In this chapter, the signalling and translocation of the NK_1R is explored in depth to elucidate the complete signalling repertoire. The spatial and temporal profile has been studied in the context of cell lines, primary tissue, and isolated primary cells. To understand the physiological consequences of intracellular NK_1R signalling, behavioural studies were performed in mice. This chapter also explores the use of lipid-conjugation to promote the delivery of a soluble NK_1R antagonist to endosomes to inhibit intracellular NK_1R signalling and subsequent physiological effects. The chapter has been divided into two parts. Part I, consists of a published paper titled, "Neurokinin 1 receptor signaling in endosomes mediates sustained nociception and is a viable therapeutic target for prolonged pain relief," which focuses on the intracellular signalling cascade of the NK_1R and the physiological consequences of compartmentalised signalling. In this paper lipid-conjugation was demonstrated as an approach to targeting drugs toward endosomes to inhibit intracellular NK_1R signalling. In Part II, the focus is on the characterisation of lipid-conjugated probes to extend the study in Part I and allow for a more comprehensive understanding of lipid-conjugation as a drug delivery tool. This includes the characterisation of the drug binding, activity, and distribution properties at the plasma membrane and in a range of organelles. To investigate the effect of lipid-conjugation on endocytosis and drug kinetics, two different administration protocols were applied. Together, the two parts of this chapter provide a comprehensive understanding of intracellular NK_1R signalling and lipid-dependent drug delivery.

Part I: Neurokinin 1 receptor signalling in endosomes mediates sustained nociception and is a viable therapeutic target for prolonged pain relief

Dane D. Jensen*, TinaMarie Lieu*, Michelle L. Halls*, Nicholas A. Veldhuis, Wendy L. Imlach, Quynh N. Mai, Daniel P. Poole, Tim Quach, Luigi Aurelio, Joshua Conner, Carmen Klein Herenbrink, Nicholas Barlow, Jamie S. Simpson, Martin J. Scanlon, Bimbil Graham, Adam McCluskey, Phillip J. Robinson, Virginie Escriou, Romina Nassini, Serena Materazzi, Pierangelo Geppetti, Gareth A. Hicks, Macdonald J. Christie, Christopher J. H. Porter, Meritxell Canals, Nigel W. Bunnett

Science Translational Medicine **2017**, **9**, eaal3447

PAIN

2017 © The Authors, some rights reserved; exclusive licensee American Association for the Advancement of Science.

Neurokinin 1 receptor signaling in endosomes mediates sustained nociception and is a viable therapeutic target for prolonged pain relief

Dane D. Jensen,[1,2]* TinaMarie Lieu,[1,2]* Michelle L. Halls,[1]* Nicholas A. Veldhuis,[1,2] Wendy L. Imlach,[3] Quynh N. Mai,[1,2] Daniel P. Poole,[1,2] Tim Quach,[1,2] Luigi Aurelio,[1,2] Joshua Conner,[1,2] Carmen Klein Herenbrink,[1,2] Nicholas Barlow,[1] Jamie S. Simpson,[1] Martin J. Scanlon,[1] Bimbil Graham,[1] Adam McCluskey,[4] Phillip J. Robinson,[5] Virginie Escriou,[6] Romina Nassini,[7] Serena Materazzi,[7] Pierangelo Geppetti,[7] Gareth A. Hicks,[8] Macdonald J. Christie,[3] Christopher J. H. Porter,[1,2†] Meritxell Canals,[1,2†] Nigel W. Bunnett[1,2,9,10†]

Typically considered to be cell surface sensors of extracellular signals, heterotrimeric GTP-binding protein (G protein)–coupled receptors (GPCRs) control many pathophysiological processes and are the target of 30% of therapeutic drugs. Activated receptors redistribute to endosomes, but researchers have yet to explore whether endosomal receptors generate signals that control complex processes in vivo and are viable therapeutic targets. We report that the substance P (SP) neurokinin 1 receptor (NK_1R) signals from endosomes to induce sustained excitation of spinal neurons and pain transmission and that specific antagonism of the NK_1R in endosomes with membrane-anchored drug conjugates provides more effective and sustained pain relief than conventional plasma membrane–targeted antagonists. Pharmacological and genetic disruption of clathrin, dynamin, and β-arrestin blocked SP-induced NK_1R endocytosis and prevented SP-stimulated activation of cytosolic protein kinase C and nuclear extracellular signal–regulated kinase, as well as transcription. Endocytosis inhibitors prevented sustained SP-induced excitation of neurons in spinal cord slices in vitro and attenuated nociception in vivo. When conjugated to cholestanol to promote endosomal targeting, NK_1R antagonists selectively inhibited endosomal signaling and sustained neuronal excitation. Cholestanol conjugation amplified and prolonged the antinociceptive actions of NK_1R antagonists. These results reveal a critical role for endosomal signaling of the NK_1R in the complex pathophysiology of pain and demonstrate the use of endosomally targeted GPCR antagonists.

INTRODUCTION

Whereas acute pain allows avoidance of injury and is essential for survival, chronic pain accompanies disease (for example, inflammatory diseases and neuropathies) and therapy (for example, chemotherapy), afflicts 20% of individuals at some point of their lives, and is a major cause of suffering (*1*). The mechanisms that underlie the transition between acute (physiological) and chronic (pathological) pain and that sustain chronic pain are unknown. Current therapies for chronic pain are often ineffective or produce unacceptable side effects. The opioid epidemic, a leading cause of medication-induced death, highlights the need for improved pain therapy (*2*).

With almost 1000 members in humans, heterotrimeric GTP-binding protein (G protein)–coupled receptors (GPCRs) are the largest receptor family, participate in most physiological and pathophysiological processes, are the target of ~30% of therapeutic drugs (*3*), and control all steps of pain transmission (*1*, *4*). GPCRs at the peripheral terminals of primary sensory neurons detect ligands from inflamed and injured tissues, and GPCRs control the activity of second-order spinal neurons that transmit pain signals centrally. Although GPCRs are a major therapeutic target for chronic pain, most GPCR-targeted drugs for pain have failed in clinical trials, often for unknown reasons (*4*, *5*).

GPCRs are conventionally viewed as cell surface receptors that detect extracellular ligands and couple to G proteins, which trigger plasma membrane–delimited signaling events (second messenger formation, growth factor receptor transactivation, and ion channel regulation). Activated GPCRs associate with β-arrestins (βARRs), which uncouple receptors from G proteins and terminate plasma membrane signaling. βARRs also couple receptors to clathrin and adaptor protein-2 and convey receptors and ligands to endosomes (*6*). Once considered merely a conduit for GPCR trafficking, endosomes are a vital site of signaling (*4*, *7*, *8*). βARRs recruit GPCRs and mitogen-activated protein kinases to endosomes and thereby mediate endosomal GPCR signaling (*9*, *10*). Some GPCRs in endosomes activate $G\alpha_s$ G proteins, suggesting endosomal cyclic adenosine monophosphate (cAMP)–dependent signaling (*11*, *12*). GPCR/G protein/βARR complexes also contribute to sustained signaling by internalized receptors (*13*). Although a growing number of GPCRs can signal from endosomes, the mechanisms and outcomes of endosomal signaling are incompletely understood, and its relevance to complex pathophysiological processes in vivo is unexplored. Drug discovery programs aim to identify ligands for

[1]Monash Institute of Pharmaceutical Sciences, Monash University, Parkville, Victoria 3052, Australia. [2]Australia Research Council Centre of Excellence in Convergent Bio-Nano Science and Technology, Monash University, Parkville, Victoria 3052, Australia. [3]Discipline of Pharmacology, University of Sydney, New South Wales 2006, Australia. [4]School of Environmental and Life Sciences, University of Newcastle, New South Wales 2308, Australia. [5]Children's Medical Research Institute, University of Sydney, New South Wales 2145, Australia. [6]Unité de Technologies Chimiques et Biologiques pour la Sante, CNRS UMR8258, INSERM U1022, Université Paris Descartes, Chimie ParisTech, 75006 Paris, France. [7]Department of Health Sciences, Clinical Pharmacology Unit, University of Florence, 6-50139 Florence, Italy. [8]Takeda Pharmaceuticals, Boston, MA 02139, USA. [9]Department of Pharmacology and Therapeutics, University of Melbourne, Victoria 3010, Australia. [10]Departments of Surgery and Pharmacology, Columbia University College of Physicians and Surgeons, Columbia University, 21 Audubon Avenue, Room 209, New York City, NY 10032, USA.
*These authors contributed equally to this work.
†Corresponding author. Email: nb2733@cumc.columbia.edu (N.W.B.); chris.porter@monash.edu (C.J.H.P.); meri.canals@monash.edu (M.C.)

Downloaded from http://stm.sciencemag.org/ by guest on June 19, 2017

cell surface GPCRs, and whether endosomal GPCRs are a therapeutic target remains to be determined.

We examined the contribution of endocytosis of the neurokinin 1 receptor (NK_1R) to substance P (SP)–mediated nociception. Painful stimuli release SP from the central projections of primary sensory neurons in the dorsal horn of the spinal cord, where SP induces endocytosis of the NK_1R in second-order neurons, which integrate nociceptive signals (*5*, *14*). The NK_1R may also be internalized in pain-sensing regions of the brain of patients with chronic pain (*5*, *15*). We hypothesized that endosomal signaling is a critical but unappreciated contributor to pain transmission and that targeting NK_1R antagonists to sites of endosomal signaling might provide an effective route to pain relief. Thus, the clinical failure of conventional NK_1R antagonists for the treatment of chronic pain and other chronic conditions associated with NK_1R endocytosis (*5*) might relate to their inability to target and antagonize the NK_1R within multiprotein signalosomes of acidified endosomes.

RESULTS

Clathrin, dynamin, and βARRs mediate NK_1R endocytosis

To quantify NK_1R endocytosis, we used bioluminescence resonance energy transfer (BRET) to assess NK_1R proximity to βARRs and resident proteins of plasma membranes (KRAS) and early endosomal membranes (RAB5A) in human embryonic kidney (HEK) 293 cells (fig. S1A). SP (1 or 10 nM) increased NK_1R–RLUC8/βARR1/2–yellow fluorescent protein (YFP) BRET (fig. S1, B and C), which is consistent with βARR-mediated NK_1R endocytosis (*16*). SP decreased NK_1R-RLUC8/KRAS-Venus BRET and concomitantly increased NK_1R-RLUC8/RAB5A-Venus BRET (fig. S1, D to G), indicating NK_1R endocytosis. The dynamin inhibitor Dyngo-4a (Dy4) (*17*), the clathrin inhibitor Pitstop-2 (PS2) (*18*), and a dominant-negative version of dynamin (K44E) (*19*) inhibited NK_1R endocytosis, whereas inactive analogs (Dy4 inact and PS2 inact) and wild-type (WT) dynamin had no effect. Dynamin K44E increased the NK_1R-RLUC8/βARR1/2-YFP BRET, suggesting that dynamin-dependent translocation of the NK_1R/βARR from the plasma membrane to endosomes initiates NK_1R/βARR dissociation (fig. S1H). Dy4 and PS2 also inhibited endocytosis of fluorescent Alexa Fluor 568–SP in HEK-NK_1R cells, causing retention in punctate structures (fig. S1I). These structures may represent ligand/receptor clusters in invaginated pits in cells treated with Dy4 or at the plasma membrane in cells treated with PS2. Thus, βARRs, clathrin, and dynamin mediate SP-induced NK_1R endocytosis.

NK_1R endocytosis mediates SP signaling in subcellular compartments

To study the link between GPCR endocytosis and signaling in subcellular compartments with high spatiotemporal fidelity, we expressed, in HEK293 cells, the NK_1R and fluorescence resonance energy transfer (FRET) biosensors for cytosolic (CytoEKAR) or nuclear (NucEKAR) extracellular signal–regulated kinase (ERK) activity, plasma membrane (pmCKAR) or cytosolic (CytoCKAR) protein kinase C (PKC) activity, and plasma membrane (pmEpac2) or cytosolic (CytoEpac2) cAMP (fig. S2A) (*20*). SP (1 nM) induced a gradual and sustained activation of nuclear ERK (Fig. 1, A to C) and a rapid and sustained activation of cytosolic PKC (Fig. 1, D to F) and cAMP (Fig. 1, G to I). SP rapidly and transiently activated cytosolic ERK (fig. S2, B and C), did not affect plasma membrane PKC (fig. S2, D and E), and increased plasma membrane cAMP (fig. S2, F and G). Inhibitors of clathrin (PS2) and dynamin (Dy4) abolished SP stimulation of nuclear ERK (Fig. 1, A to C), cytosolic PKC (Fig. 1, D to F), and cytosolic cAMP (Fig. 1, G to I), indicating a requirement for endocytosis. In contrast, PS2 and Dy4 did not affect SP activation of cytosolic ERK (fig. S2, B and C) or plasma membrane cAMP (fig. S2, F and G), which do not require endocytosis, but amplified plasma membrane PKC activity (fig. S2, D and E). Expression of dynamin K44E, but not dynamin WT, prevented SP stimulation of nuclear ERK (Fig. 1, J to L). Dynamin K44E did not prevent SP stimulation of cytosolic ERK but caused the response to become sustained when compared to dynamin WT (fig. S2, H to J). Knockdown of dynamin-1 and clathrin heavy chain with small interfering RNA (siRNA) (fig. S2, K and L) prevented SP activation of nuclear ERK (Fig. 1, M and N).

Transcription is a major endpoint of GPCR signaling, including activation of nuclear ERK. The β_2-adrenergic receptor signals from endosomes to regulate transcription (*21*). To investigate the contribution of NK_1R endocytosis to SP-stimulated transcription, we expressed in HEK-NK_1R cells a reporter encoding secreted alkaline phosphatase (SEAP) under control of the serum response element (SRE) transcription factor. SP (10 nM) stimulated SRE-SEAP secretion after 4 and 24 hours, indicating stimulated transcription (Fig. 1O). Dynamin K44E abolished SP-stimulated transcription at both times. Dynamin K44E reduced the efficacy but not the potency of SP-induced transcription, measured after 24 hours (fig. S2M). Thus, NK_1R endocytosis is required for SP stimulation of transcription.

We have previously shown that βARRs mediate NK_1R endosomal signaling and nuclear ERK activation (*9*, *22*, *23*). To examine the contribution of G proteins to endosomal NK_1R signaling, we used BRET to study SP-induced trafficking of $G\alpha_q$ subunits to early endosomes containing RAB5A. SP (0.1 to 10 nM) decreased NK_1R-RLUC8/KRAS-Venus and increased NK_1R-RLUC8/RAB5A-Venus BRET, demonstrating endocytosis, and decreased $G\alpha_q$-RLUC8/$G\gamma_2$-Venus BRET, consistent with G protein activation (Fig. 2, A to C, and fig. S3, A to C). SP increased $G\alpha_q$-RLUC8/RAB5A-Venus BRET, which indicates $G\alpha_q$ translocation to early endosomes that contain the internalized NK_1R (Fig. 2D and fig. S3D). In SP-stimulated cells, NK_1R-immunoreactivity (IR) and $G\alpha_q$-IR colocalized with early endosomal antigen 1 (EEA1)–IR (Fig. 2, E and F); IR was detected using immunofluorescence and super-resolution microscopy.

The $G\alpha_q$ inhibitor UBO-QIC prevented SP activation of nuclear ERK (Fig. 2G and fig. S3E), which also depends on βARRs and PKC but not on epidermal growth factor receptor transactivation (*9*, *22*, *23*). UBO-QIC, the phospholipase C (PLC) inhibitor U73122, and the Ca^{2+} chelator EGTA prevented activation of cytosolic PKC (Fig. 2H and fig. S3F), which is consistent with a $G\alpha_q$, PLC, and Ca^{2+}-dependent PKC pathway. UBO-QIC, the PKC inhibitor GF109203X, and EGTA, but not the $G\alpha_s$ inhibitor NF449, prevented SP generation of cytosolic cAMP (Fig. 2I and fig. S3G), supporting a role for $G\alpha_q$-mediated activation of Ca^{2+}-dependent PKC in the generation of cAMP. UBO-QIC did not affect NK_1R endocytosis (fig. S3H). In addition to inhibiting PKCα (4% control), GF109203X (Bis-1) also inhibits other kinases (*24*), which may also contribute to SP signaling. These results support the hypothesis that SP and the NK_1R signal from endosomes by $G\alpha_q$-mediated mechanisms to activate nuclear ERK and cytosolic PKC and cAMP.

Endocytosis mediates sustained SP-evoked excitation of spinal neurons

The NK_1R mediates nociceptive transmission in second-order spinal neurons, where painful stimuli induce SP release, NK_1R endocytosis,

Downloaded from http://stm.sciencemag.org/ by guest on June 19, 2017

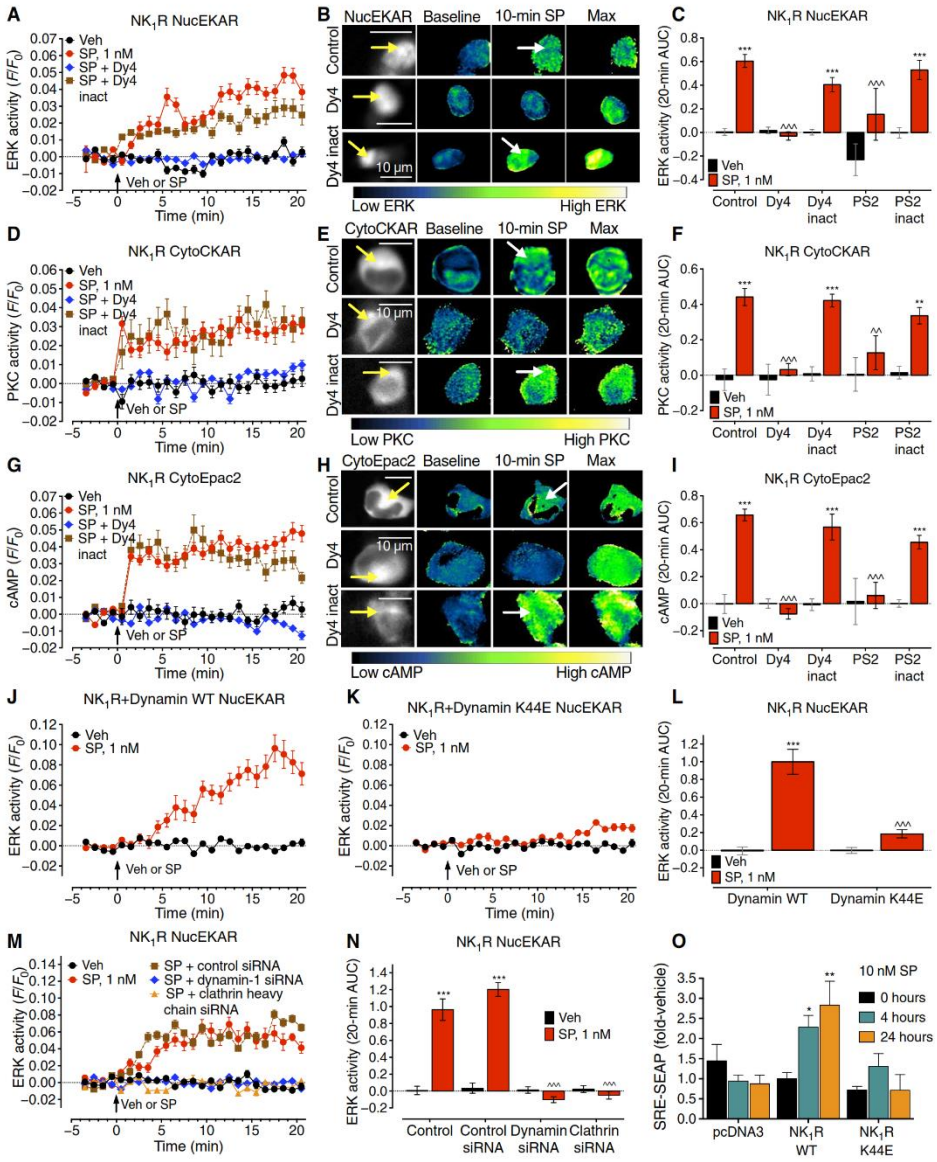

Fig. 1. NK$_1$R endocytosis-dependent compartmentalized signaling. (**A** to **I**) Effect of inhibitors of dynamin (Dy4) and clathrin (PS2), and of inactive (inact) analogs, on SP-induced spatiotemporal signaling profiles for nuclear ERK (NucEKAR) (A to C), cytosolic PKC (CytoCKAR) (D to F), and cytosolic cAMP (CytoEpac2) (G to I) measured in HEK293 cells using FRET biosensors. (A, D, and G) Time course of responses. (B, E, and H). Representative ratiometric images and sensor localization. Max, response to positive controls. Yellow arrows denote localization of FRET sensor and white arrows show the SP-stimulated signals in control cells and cells treated with Dy4 inact. (C, F, and I) Area under the curve (AUC) of (A), (D), and (G). (**J** and **K**) Effect of dynamin WT (J) or dominant negative K44E (K) overexpression on the spatiotemporal profile of SP-induced nuclear ERK. (**L**) AUC of (J) and (K). (**M**) Effect of clathrin heavy chain and dynamin-1 siRNA on the spatiotemporal profile of SP-induced nuclear ERK. (**N**) AUC of (M). (**O**) Effect of dynamin WT or K44E overexpression on the SP-induced SRE-SEAP. *P < 0.05, **P < 0.01, ***P < 0.001, vehicle (Veh); ^^P < 0.01, ^^^P < 0.001, control to inhibitors. (A to N) Thirty to 354 cells, three to five experiments. (O) n = 3 experiments. ANOVA, Tukey's test (C, F, I, and N); Sidak's test (L); Dunnett's test (O).

Downloaded from http://stm.sciencemag.org/ by guest on June 19, 2017

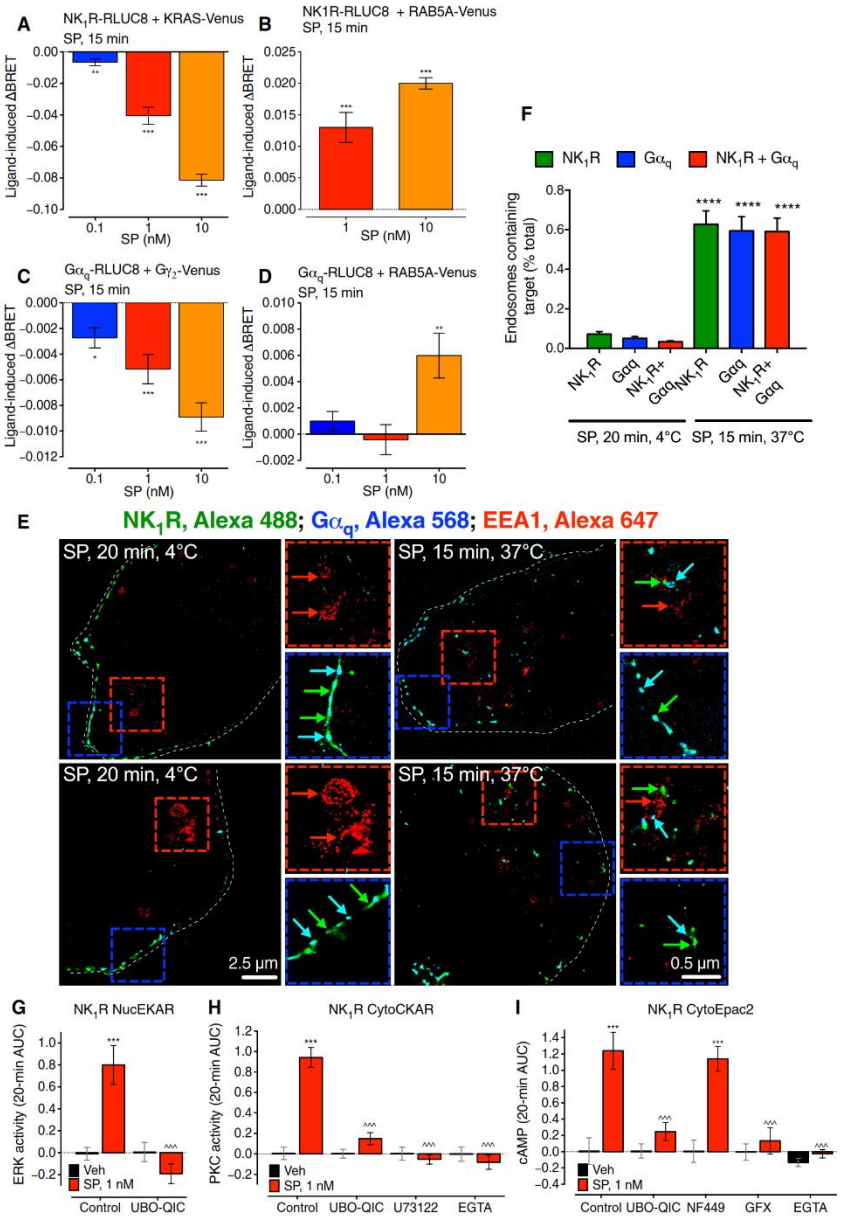

Fig. 2. G protein–dependent NK_1R signaling in endosomes. (**A** to **D**) SP-induced BRET between NK_1R-RLUC8 and KRAS-Venus (A) or RAB5A-Venus (B) and between $G\alpha_q$-RLUC8 and $G\gamma_2$-Venus (C) or RAB5A-Venus (D) in HEK293 cells. $^*P < 0.05$, $^{**}P < 0.01$, $^{***}P < 0.001$ to baseline. Triplicate observations, $n \geq 3$ experiments. (**E**) Localization of NK_1R-IR (green), $G\alpha_q$-IR (cyan), and EEA1-IR (red) in HEK293 cells by super-resolution microscopy. Blue boxes, plasma membrane; red boxes, endosomes. (**F**) Quantification of the proportion of endosomes containing NK_1R-IR and $G\alpha_q$-IR. Sixty to 66 cells per condition (20 to 22 cells from $n = 3$ experiments). $^{****}P < 0.0001$. (**G** to **I**) Effect of inhibitors of $G\alpha_q$ (UBO-QIC) or PLC (U73122) and Ca^{2+} chelation (EGTA) or inhibitors of $G\alpha_s$ (NF449) or PKC (GF109203X, GFX) on SP-induced nuclear ERK (G), cytosolic PKC (H), and cytosolic cAMP (I) measured using FRET biosensors. $^{***}P < 0.001$, SP to vehicle; $^{\wedge\wedge\wedge}P < 0.001$, control to inhibitor. Thirty-five to 67 cells, three experiments. ANOVA, Dunnett's test (A to D); Sidak's test (F and G); Tukey's test (H and I).

Downloaded from http://stm.sciencemag.org/ by guest on June 19, 2017

and ERK activation (*5*, *14*, *25*). SP causes persistent NK_1R-dependent excitation of spinal neurons by unknown mechanisms (*26*). To evaluate whether NK_1R endosomal signaling mediates this sustained excitation, we made cell-attached patch clamp recordings from NK_1R-positive neurons in lamina I of the dorsal horn in slices of rat spinal cord. SP (1 μM, 5 min) stimulated NK_1R-IR endocytosis in spinal neurons (Fig. 3, A and B, and movies S1 to S4). Brief exposure to SP (1 μM, 2 min) triggered rapid-onset action potential firing that was sustained after washout (Fig. 3, C to E). Dy4 but not Dy4 inact inhibited NK_1R endocytosis. Dy4 did not affect the initial onset of SP-induced firing but prevented the sustained response, reducing both the firing rate and firing time, whereas Dy4 inact had no effect. The SP-induced firing rate (events per 2 min, normalized to rate at 2 min) was 342.1 ± 120.7 with Dy4 and 569.0 ± 187.6 with Dy4 inact [$P < 0.05$, analysis of variance (ANOVA), Sidak's test].

To define the signaling pathway that mediates SP-evoked excitation of spinal neurons, slices were preincubated with inhibitors of mitogen-activated protein kinase kinase (MEK) (U0126), PKC (GF109203X), or vehicle (control). U0126 inhibited the SP-induced firing time of lamina I neurons by 67.5 ± 8.3% (control: 10.01 ± 1.8 min, $n = 10$ cells from eight rats; U0126: 3.2 ± 0.8 min, $n = 6$ cells from six rats; $P < 0.05$, ANOVA, Dunn's test) (Fig. 3, F to H). GF109203X reduced SP-induced firing time of lamina I neurons by 56.8 ± 8.2% (control: 10.01 ± 1.8 min, $n = 10$ cells from eight rats; GF109203X: 4.33 ± 0.82 min, $n = 7$ cells from four rats; $P < 0.05$, ANOVA, Dunn's test). U0126 and GF109203X reduced the number of SP-stimulated action potentials by 84 ± 5% and 61 ± 15%, respectively, compared to controls.

Dy4 did not affect the generation of excitatory postsynaptic currents (EPSCs) in lamina I/II_o neurons in response to primary afferent stimulation (Fig. 3, I and J). PS2 and Dy4 did not affect capsaicin-stimulated release of SP or calcitonin gene–related peptide (CGRP) from segments of mouse dorsal spinal cord (Fig. 3, K and L). Thus, NK_1R endocytosis and resultant ERK and PKC signaling mediate sustained SP-induced firing of spinal neurons. The effects of dynamin and clathrin inhibitors in the spinal cord are unrelated to changes in glutaminergic-mediated fast synaptic transmission or the exocytosis of neuropeptides.

Clathrin, dynamin, and βARRs mediate NK_1R endocytosis and nociception in vivo

To determine the involvement of dynamin and clathrin in NK_1R endocytosis in vivo, we injected Dy4, PS2, inactive analogs, or vehicle intrathecally (L3/L4) to rats. After 30 min, vehicle or capsaicin was administered by intraplantar injection. The spinal cord was removed 10 min later, and the NK_1R was localized by immunofluorescence and confocal microscopy. In vehicle-treated control rats, the NK_1R-IR was mostly at the plasma membrane of lamina I neurons (% NK_1R-IR within 0.5 μm of plasma membrane, 80.7 ± 1.6; $n = 3$ rats, 6 neurons analyzed per rat) (Fig. 4, A and C, and movie S5). Intraplantar injection of capsaicin stimulated NK_1R endocytosis (42.1 ± 5.6; $P = 0.0027$ to control, Student's t test) (movie S6). Intrathecal injection of Dy4 or PS2, but not inactive analogs, inhibited capsaicin-stimulated NK_1R endocytosis [Dy4 (59.6 ± 0.2) versus Dy4 inact (49.9 ± 0.8), $P = 0.0004$ (Student's t test); PS2 (69.0 ± 1.1) versus PS2 inact (51.9 ± 1.3), $P = 0.0135$ (Student's t test)] (movies S7 to S10 and Fig. 4, A and C). Painful peripheral stimuli activate ERK in NK_1R-expressing spinal neurons, which contributes to hyperalgesia (*25*). Intraplantar capsaicin stimulated ERK phosphorylation in lamina I/II dorsal horn neurons (Fig. 4, B and D). Dy4 or PS2 prevented capsaicin-stimulated ERK activation in spinal neurons. Thus, painful stimuli induce clathrin- and dynamin-dependent NK_1R endocytosis in spinal neurons, which is required for ERK signaling.

Does NK_1R endocytosis in spinal neurons mediate pain transmission? To evaluate the importance of the NK_1R, clathrin, and dynamin for nociception, we injected vehicle, NK_1R antagonist SR140,333 (*27*), Dy4, PS2, or inactive analogs intrathecally (L3/L4) to mice. After 30 min, vehicle or capsaicin was administered by intraplantar injection into one hindpaw. Withdrawal responses were measured to stimulation of the plantar surface of the ipsilateral (injected) and contralateral (noninjected) hindpaws with von Frey filaments, and edema was assessed by measuring thickness of the ipsilateral paw. In vehicle (intrathecal)–treated mice, capsaicin caused mechanical allodynia and edema for 4 hours. SR140,333 caused a partial and transient inhibition of capsaicin-induced allodynia, whereas Dy4 and PS2, but not inactive analogs, caused a large and sustained inhibition of allodynia (Fig. 4E and fig. S4A). Paw edema was unaffected, confirming that after intrathecal injection, the drugs act locally in the spinal cord (fig. S4B).

Dy4 and PS2 did not affect withdrawal responses of the contralateral paw or rotarod latency, suggesting normal motor behavior (Fig. 4, F and G). Intrathecal Dy4 also inhibited capsaicin-evoked mechanical allodynia in rat, which supports a role for dynamin in nociception in different species (fig. S4C).

Intrathecal injection of dynamin-1 siRNA knocked down dynamin-1–IR (fig. S4D) and inhibited capsaicin-evoked allodynia after 24 and 48 hours in mice (Fig. 4H and fig. S4E). Intrathecal βARR1/2 siRNA knocked down βARR1/2 mRNA (fig. S4F) and inhibited capsaicin-evoked allodynia at 36 hours (Fig. 4I). siRNAs did not affect withdrawal responses of the contralateral paw (fig. S4, G and H), consistent with normal motor function.

Endocytosis and subsequent recycling mediate resensitization and sustained signaling of several GPCRs, including the NK_1R (*28*). Thus, the antinociceptive actions of endocytic inhibitors could be due to disrupted resensitization of plasma membrane signaling rather than to impaired endosomal signaling. Endothelin-converting enzyme-1, which is coexpressed with the NK_1R in spinal neurons (*22*), degrades SP in endosomes and thereby promotes recycling and resensitization of the NK_1R (*29*). However, intrathecal injection of SM-19712, an inhibitor of endothelin-converting enzyme-1 that prevents NK_1R recycling and resensitization (*29*), had no effect on capsaicin-induced allodynia (Fig. 4J). These results suggest that the analgesic actions of endocytic inhibitors are unrelated to disrupted resensitization. Consistent with a role for NK_1R endocytosis and βARRs in SP-evoked nuclear ERK signaling (*9*), intrathecal MEK inhibitor U0126 inhibited capsaicin-evoked allodynia (Fig. 4K) (*25*).

The effects of inhibitors of dynamin and clathrin on noninflammatory and inflammatory pain were examined. Intrathecal injection of Dy4 and PS2 blunted both the early (noninflammatory) and late (inflammatory) phases of the nocifensive response to intraplantar formalin (Fig. 4L). When injected intrathecally 36 hours after intraplantar injection of complete Freund's adjuvant (CFA), which causes sustained inflammatory pain, inhibitors of dynamin and clathrin reversed preexisting mechanical hyperalgesia (Fig. 4M). The NK_1R was robustly internalized in spinal neurons of mice after intraplantar injection of capsaicin, formalin, and CFA (fig. S5, A to D). Intrathecal injection of Dy4 prevented capsaicin- and formalin-induced NK_1R endocytosis and reversed CFA-induced NK_1R endocytosis. These results suggest that clathrin and dynamin mediate pain-evoked endocytosis of NK_1R in spinal neurons, which is required for nociception.

Downloaded from http://stm.sciencemag.org/ by guest on June 19, 2017

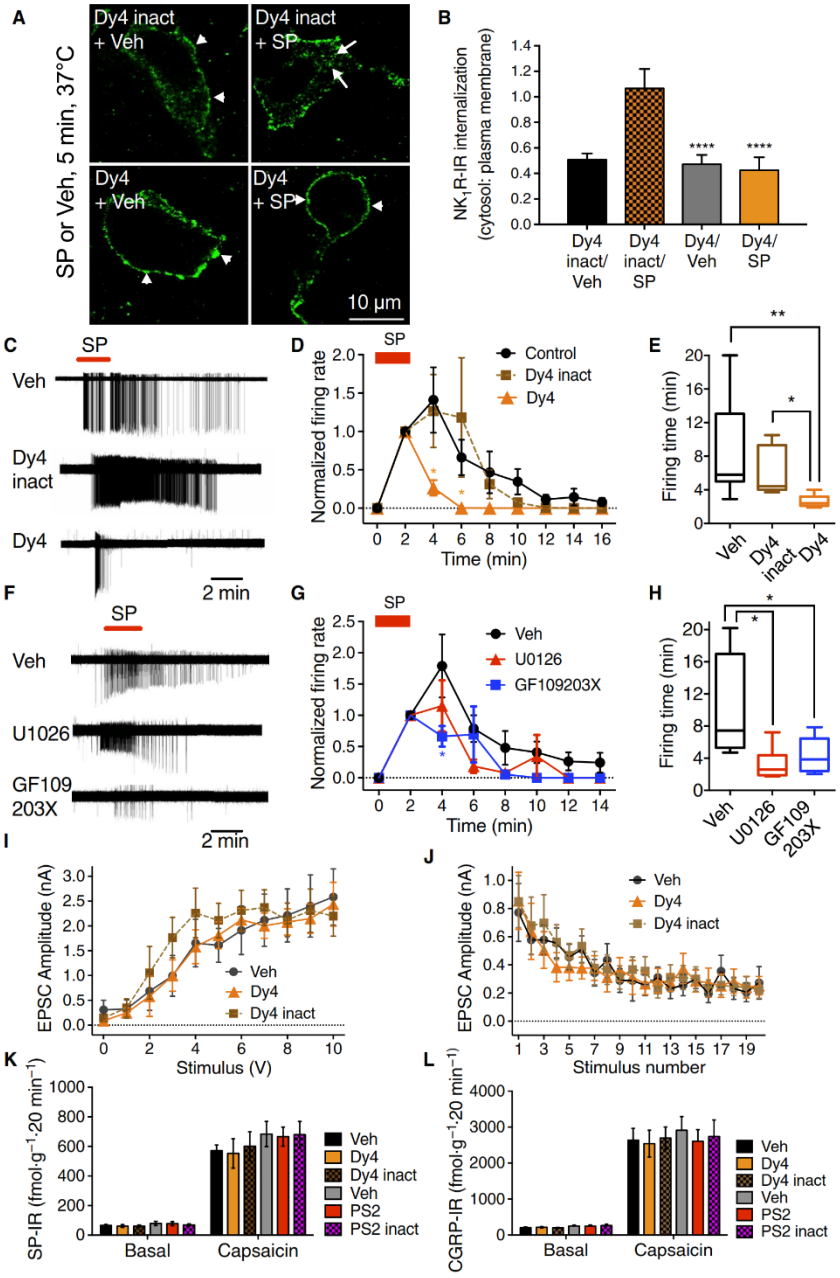

Fig. 3. NK_1R endocytosis and neuronal excitation in spinal cord slices. (**A**) Effect of Dy4 and Dy4 inact on SP-induced endocytosis of NK_1R-IR in rat spinal neurons. Arrows, internalized; arrowheads, cell surface NK_1R. (**B**) Quantification of endocytosis. $^{****}P < 0.0001$. Eighteen neurons per group (six neurons in slices from $n = 3$ rats). (**C** to **H**) Effects of Dy4, Dy4 inact, U0126 (MEK inhibitor), and GF109203X (PKC inhibitor) on SP-induced firing of rat spinal neurons. (C and F) Representative traces. (D and G) Firing rate normalized to 2 min. (E and H) Firing duration to last action potential. Six to 7 neurons per group from $n = 8$ to 17 rats. $^{*}P < 0.05$, $^{**}P < 0.01$. (**I** and **J**) Effect of Dy4 and Dy4 inact on EPSC in lamina I/II$_o$ induced by primary afferent stimulation, $n = 11$ neurons. (**K** and **L**) Effects of Dy4, PS2, and inactive analogs on capsaicin-stimulated SP-IR (K) and CGRP-IR (L) release from segments of mouse spinal cord. $n = 6$ experiments. ANOVA, Tukey's test (B); Sidak's test (D and G); Dunn's test (E and H).

Disruption of NK_1R/βARR interactions inhibits NK_1R endocytosis and nociception in vivo

To substantiate involvement of NK_1R endocytosis in nociception, we devised a pharmacological approach to inhibit NK_1R/βARR interactions and NK_1R endocytosis. G protein receptor kinases (GRKs) phosphorylate S/T-rich regions in the C terminus of GPCRs, which interact with βARRs (*30*). A deletion mutant NK_1Rδ311 lacks the C terminus and corresponds to a naturally occurring NK_1R variant (Fig. 5A) (*5*). NK_1Rδ311 was normally expressed at the plasma membrane of HEK293 cells but did not associate with βARRs or internalize (Fig. 5, B and C, and fig. S6, A to C). In HEK-NK_1Rδ311 cells, SP stimulated cytosolic but not nuclear ERK and did not affect transcription activity, consistent with endocytosis-dependent nuclear ERK signaling and transcription (Fig. 5, D and E). Peptides corresponding to predicted phosphorylation sites in the C terminus of mouse NK_1R were conjugated to membrane-penetrating Tat peptide (Fig. 5A). A combination of three peptides inhibited SP-induced NK_1R-RLUC8/βARR2-YFP BRET and prevented SP-induced NK_1R

Downloaded from http://stm.sciencemag.org/ by guest on June 19, 2017

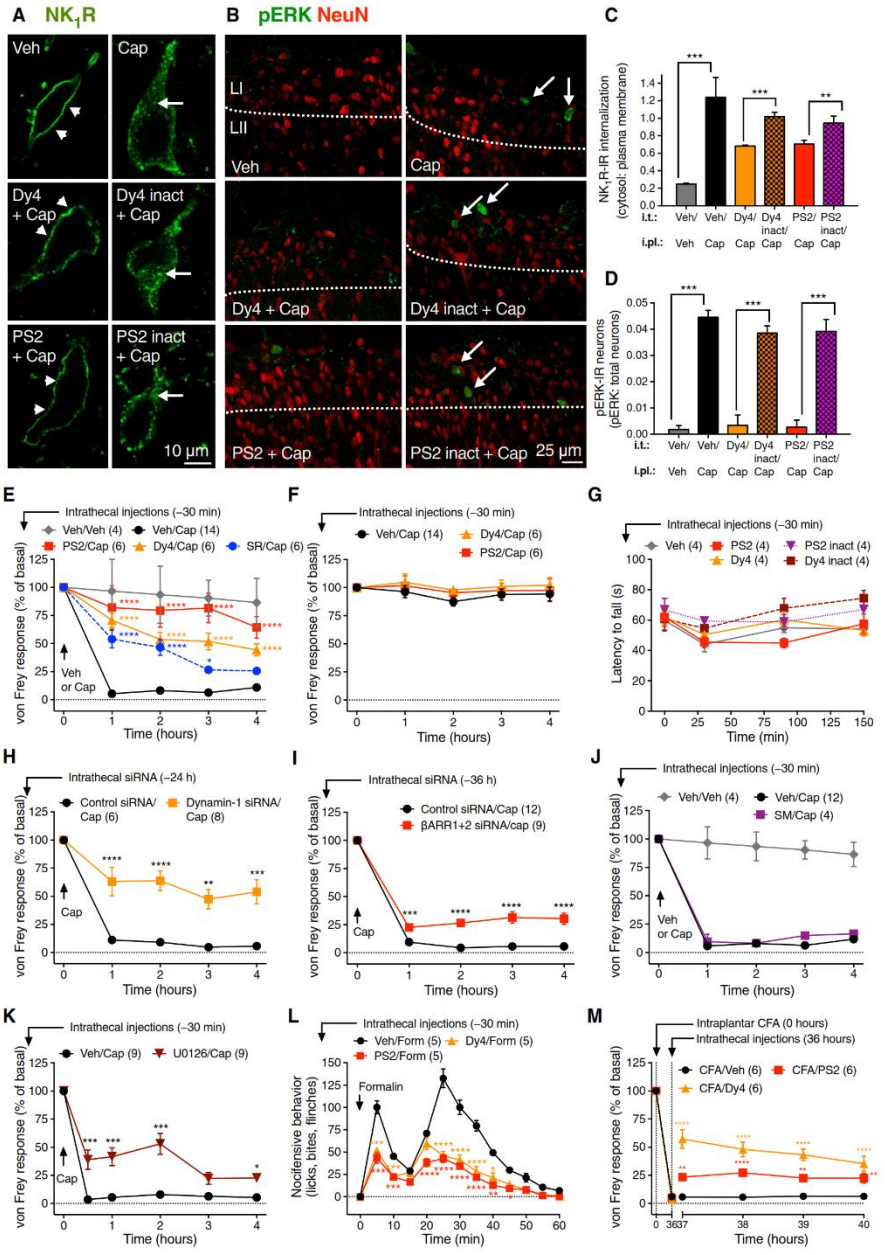

Fig. 4. NK_1R endocytosis, ERK signaling, and nociception in vivo. Effects of intrathecal (i.t.) injections of inhibitors or siRNA. (**A** and **B**) Localization of NK_1R-IR (A) and pERK-IR (B) in rat spinal neurons 10 min after intraplantar (i.pl.) vehicle or capsaicin (Cap). L, lamina. (A) Arrowheads show cell surface and arrows show endosomal NK_1R. (B) Arrows show pERK-IR (green) and red shows NeuN (neuronal marker). (**C** and **D**) Quantification of NK_1R endocytosis (C) and pERK-expressing neurons (D). $^{**}P < 0.01$, $^{***}P < 0.001$. Neuronal numbers: Veh, 54; capsaicin, 52; Dy4, 28; Dy4 inact, 18; PS2, 22; PS2 inact, 19 (≥6 neurons in sections from $n = 3$ rats). (**E**, **F**, **H**, to **K**) Nociception in mice after intrathecal injection of endocytic inhibitors (Dy4, PS2), NK_1R antagonist (SR140,333; SR), dynamin-1 siRNA, βARR1/2 siRNA, endothelin-converting enzyme-1 inhibitor (SM-19712; SM), or MEK inhibitor (U0126). von Frey withdrawal responses of capsaicin-injected (E and H to K) or contralateral (F) paw. (**G**) Rotarod latency. (**L**) Formalin (form) nocifensive behavior. (**M**) von Frey withdrawal responses of the CFA-injected paw. $^{*}P < 0.05$, $^{**}P < 0.01$, $^{***}P < 0.001$, $^{****}P < 0.0001$, to control. Student's *t* test (C and D); ANOVA, Dunnett's test (E to M).

endocytosis, compared to a control peptide, suggesting effective disruption of NK_1R/βARR interactions (Fig. 5, F and G). When injected intrathecally, inhibitors of NK_1R/βARR interactions suppressed capsaicin-evoked allodynia and formalin-induced nociceptive behavior and reversed CFA-induced hyperalgesia (Fig. 5, H to J). Together, these results support a role for βARR-mediated NK_1R endocytosis and endosomal signaling in nociception.

Lipid conjugation delivers NK_1R antagonists to endosomes and selectively blocks sustained endosomal signals

We observed that clathrin, dynamin, and βARR inhibitors and siRNA, including selective inhibitors of NK_1R/βARR interactions, suppress

Downloaded from http://stm.sciencemag.org/ by guest on June 19, 2017

SP-induced NK_1R endocytosis, compartmentalized signaling, transcription, and neuronal excitability, and have antinociceptive actions. These findings support the hypothesis that endosomal NK_1R signaling underlies sustained neuronal excitation and nociception. Thus, selective antagonism of endosomal receptors could be an effective treatment for pain. To investigate this possibility and to provide direct evidence for the importance of endosomal signaling for nociception, we devised an approach to deliver and concentrate GPCR antagonists in early endosomes.

Lipid conjugation anchors drugs at membrane surfaces and promotes endosomal delivery (*31*). We synthesized tripartite probes composed of cholestanol (Chol; promotes membrane insertion and anchoring) or ethyl ester (control; no membrane anchoring), a flexible polyethylene glycol (PEG) linker, and a cargo of either cyanine 5 (Cy5) for localization or spantide I (Span), a peptidic membrane–impermeant NK_1R antagonist (Fig. 6A) (*32*). In addition, we synthesized a probe incorporating Span and Cy5 (Span-Cy5-Chol). When incubated with HEK293 cells, Cy5-Chol inserted into the plasma membrane within 5 min, whereas Cy5–ethyl ester remained entirely extracellular (Fig. 6B and movies S11 and S12). After 4 hours of continuous incubation, Cy5-Chol was concentrated in RAB5A-positive early endosomes, although Cy5-Chol was also detected at the plasma membrane (Fig. 6C). When incubated with HEK-NK_1R–green fluorescent protein (GFP) cells for 4 hours, Cy5-Chol also colocalized with NK_1R-GFP in endosomes (cells were stimulated with SP to induce NK_1R endocytosis) (Fig. 6C). When HEK-NK_1R–GFP cells were pulse-incubated with Cy5-Chol for 30 or 60 min, washed, and allowed to recover for 4 hours, Cy5-Chol was gradually removed from the plasma membrane and accumulated in NK_1R-GFP–positive endosomes, although some probe remained at the plasma membrane (fig. S7, A and C). Cy5–ethyl ester was not taken up by cells after pulse incubation (fig. S7B). Quantification of Cy5-Chol uptake after a 30-min pulse incubation indicated that 69% of cell-bound probe was internalized at 4 hours and 79% was internalized at 8 hours after washing (fig. S7D). After pulse incubation, Cy5-Span-Chol trafficked to NK_1R-GFP–positive endosomes (Fig. 6C). Dy4 inhibited uptake of Chol-conjugated tripartite probes, consistent with constitutive dynamin-mediated endocytosis (fig. S7E).

We used FRET to quantify association of tripartite probes with the NK_1R in endosomes. NK_1R with extracellular N-terminal SNAP-Tag was expressed in HEK293 cells, and cell surface NK_1R was labeled with membrane-impermeant SNAP–Surface-549 (SNAP-549). SP (10 nM, 30 min) evoked translocation of SNAP-549–NK_1R to endosomes (Fig. 6D). Cells were treated with Cy5-Chol, and FRET between SNAP-549–NK_1R and Cy5-Chol was measured in regions of interest within the cytosol. Cy5-Chol/SNAP-549–NK_1R FRET was detected after 5 min and increased for 60 min (Fig. 6, D and E, and movie S13). FRET was not detected in control cells lacking NK_1R (Fig. 6E).

Span-Chol antagonized SP [3 nM; 80% effective concentration (EC_{80})]–stimulated Ca^{2+} signaling in HEK-NK_1R cells [minus log of half maximal inhibitory concentration (pIC_{50}), 8.23 ± 0.21 (Span) and 8.44 ± 0.29 (Span-Chol)] and thus retained activity. Because the tripartite probe was concentrated in endosomes after 4 hours, we examined NK_1R endosomal signaling 4 hours after preincubation with antagonists. When HEK-NK_1R cells were preincubated with Span-Chol, Span, or SR140,333 for 30 min and then immediately challenged with SP, all antagonists blocked nuclear ERK (Fig. 6, F and H) and cytosolic ERK (fig. S8, A and C) activity, indicating effective antagonism of cell surface NK_1R. When cells were pulse-incubated with antagonists for 30 min, washed, and stimulated with SP 4 hours later (to allow lipidated antagonists to concentrate in endosomes), Span-Chol alone inhibited nuclear ERK (derives from endosomal NK_1R) (Fig. 6, G and H), and no antagonist inhibited cytosolic ERK (derives from plasma membrane NK_1R) (fig. S8, B and C). Span-Chol also prevented SP-induced transcription. HEK-NK_1R cells were incubated with Span or Span-Chol for 30 min, washed, recovered for 4 hours, and then stimulated with SP for 20 hours. Span-Chol abolished SP-stimulated SRE-SEAP secretion (derives from endosomal NK_1R), whereas unconjugated Span was ineffective (Fig. 6I). However, when continuously incubated with antagonists, both Span-Chol and Span inhibited transcription. Span-Chol did not affect isoprenaline-induced activation of nuclear ERK, which is mediated by the endogenous β_2-adrenergic receptor (fig. S8D). Thus, the effects of tripartite antagonists are not mediated by a nonspecific disruption of endosomal signaling.

The results show that lipid conjugation promotes the effective delivery and retention of antagonists to endosomes containing the NK_1R. After pulse incubation, Span-Chol caused sustained and selective antagonism of endosomal but not plasma membrane NK_1R. Unconjugated Span and SR140,333, a potent small-molecule antagonist, were unable to effectively inhibit persistent NK_1R signaling in endosomes.

Endosomally targeted NK_1R antagonists block nociception

To assess whether antagonism of the endosomal NK_1R blocks sustained SP-induced excitation of spinal neurons, we incubated slices of rat spinal cord with Span-Chol or Span for 60 min, washed them, and challenged them with SP 60 min later. In vehicle- or Span-treated slices, SP caused brisk firing that was sustained after washout (Fig. 7, A to C). As observed with endocytic inhibitors, Span-Chol did not suppress the initial excitation but prevented sustained excitation. The SP-induced firing rate (normalized to 2 min, events per 2 min) was 196.6 ± 81.6 for Span-Chol and 242.6 ± 95.9 for Span ($P < 0.05$, ANOVA, Sidak's test).

To evaluate whether endosomal targeting improves the efficacy and duration of action of NK_1R antagonists for the treatment of pain, we administered cholestanol-conjugated or conventional antagonists by intrathecal injection 3 hours before intraplantar injection of capsaicin. This time was selected to allow endosomal accumulation of lipidated antagonists. When Cy5-Chol was injected intrathecally, probe was detected in laminae I to III neurons after 6 hours, confirming delivery and retention in pain-transmitting neurons (Fig. 7D). Cy5-Chol did not affect nociception, which excludes nonspecific actions of cholestanol (Fig. 7E). Span-Chol, but not Span or SR140,333, inhibited capsaicin-evoked mechanical allodynia (Fig. 7E). When administered 30 min after capsaicin, intrathecal Span was transiently antinociceptive, whereas Span-Chol caused a delayed (3 hours), persistent (6 hours), and substantial (>50%) antinociception (Fig. 7F).

The small-molecule NK_1R antagonist L-733,060 (*33*) conjugated to Chol antagonized SP (3 nM; EC_{80})–stimulated Ca^{2+} signaling in HEK-NK_1R cells [% inhibition against 1 nM SP: 40.8 ± 8.9 (10 nM L-733,060) and 71.1 ± 9.2 (10 nM L-733,060-Chol)] and thus retained activity. When injected intrathecally 3 hours before intraplantar capsaicin, L-733,060–Chol was antinociceptive from 1 to 4 hours, whereas L-733,060 was antinociceptive only at 1 hour (Fig. 7G).

When injected intrathecally 3 hours before intraplantar formalin, Span-Chol inhibited both phases of nocifensive behavior more completely than Span or SR140,333 (Fig. 7H). When injected intrathecally 36 hours after intraplantar CFA, Span-Chol inhibited mechanical hyperalgesia from 1 to 6 hours, whereas the antinociceptive actions of Span and SR140,333 were minor and transient for Span (Fig. 7, I and J).

Downloaded from http://stm.sciencemag.org/ by guest on June 19, 2017

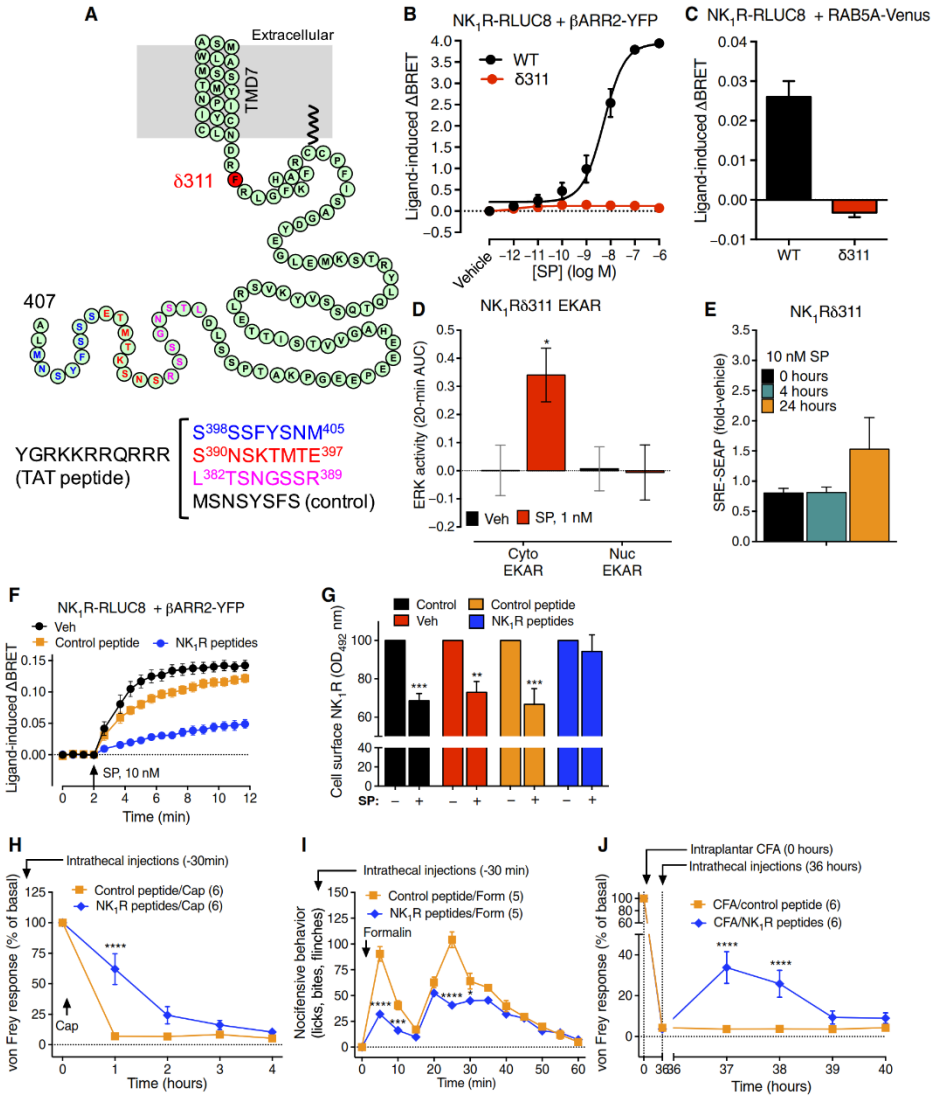

Fig. 5. Disruption of NK_1R/βARR interactions. (**A**) Mouse NK_1R C terminus, indicating $NK_1Rδ311$ truncation and sequences of Tat-conjugated NK_1R and control peptides. (**B** and **C**) SP-induced BRET between WT NK_1R-RLUC8 or $NK_1Rδ311$-RLUC8 and βARR2-YFP (B) or RAB5A-Venus (C). Triplicate observations, $n \geq 3$ experiments. (**D**) SP-induced cytosolic ERK (CytoEKAR) and nuclear ERK (NucEKAR) measured using FRET biosensors. *$P < 0.05$. Forty-nine to 99 cells, three experiments. (**E**) Effect of SP on SRE-SEAP release from HEK-$NK_1Rδ311$ cells. (**F** and **G**) Effect of control and three NK_1R peptides on SP-induced NK_1R-RLUC8/βARR2-YFP BRET (F) and NK_1R endocytosis (G). (**H** to **J**) Effects of intrathecally administered control and NK_1R peptides on capsaicin-induced mechanical allodynia (H), formalin-evoked nocifensive behavior (I), and CFA-induced mechanical hyperalgesia (J) in mice. *$P < 0.05$, **$P < 0.01$, ***$P < 0.001$, ****$P < 0.0001$ to control. ANOVA, Sidak's test (D and G); Dunnett's test (H to J).

The enhanced potency and duration of action of lipidated antagonists could be due to improved metabolic stability rather than to appropriate targeting of endosomal NK_1R. Membrane peptidases rapidly degrade neuropeptides, including SP, and could also degrade peptidic antagonists (*5*). Membranes prepared from mouse spinal cord rapidly degraded SP, but not Span or Span-Chol (Fig. 7K). Span and Span-Chol were also stable in human cerebrospinal fluid (Fig. 7L). These results suggest that enhanced stability does not account for the sustained antinociceptive actions of cholestanol-conjugated antagonists.

Downloaded from http://stm.sciencemag.org/ by guest on June 19, 2017

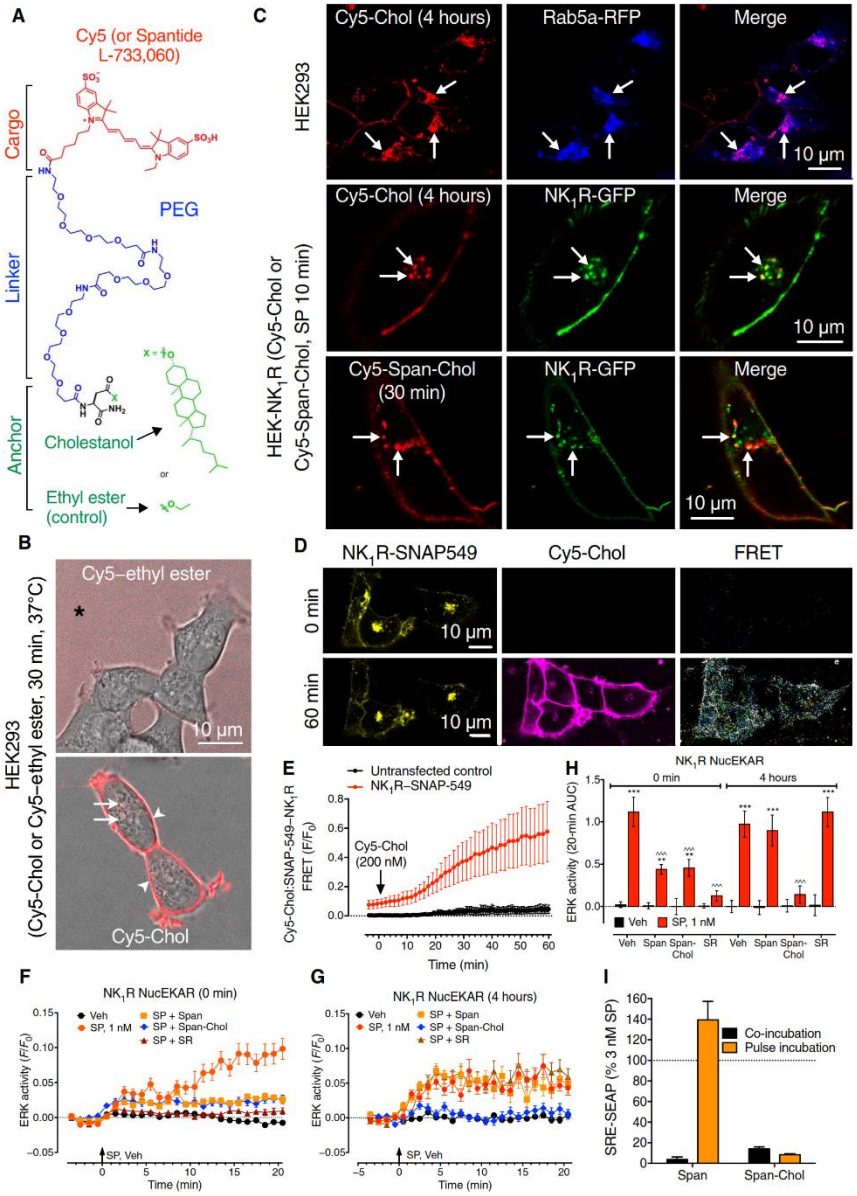

Fig. 6. Antagonism of endosomal NK_1R. (**A**) Structure of tripartite probes. (**B**) Cy5–ethyl ester or Cy5-Chol uptake in HEK293 cells. (**C**) Cy5-Chol or Cy5-Span-Chol (red) trafficking to RAB5A–red fluorescent protein (RFP)–positive (blue) and NK_1R-GFP–positive (green) endosomes. Asterisk, extracellular; arrowheads, plasma membrane; arrows, endosomes. (**D** and **E**) Cy5-Chol:SNAP549-NK_1R FRET, indicating localization of SNAP549-NK_1R, Cy5-Chol, and FRET signals (D) and time course of FRET in the cytosol (E). Six to nine cells, $n = 3$ experiments. (**F** to **H**) FRET assays of nuclear ERK activity (NucEKAR) immediately after (0 min) (F) or 4 hours after (4 hours) (G) 30 min of preincubation with Span, Span-Chol, or SR140,333 (SR). (H) AUC of (G). $^{**}P < 0.01$, $^{***}P < 0.001$, to vehicle; $^{\wedge\wedge\wedge}P < 0.001$, to antagonists. Thirty-one to 417 cells, $n = 3$ to 5 experiments. (**I**) Effects of Span or Span-Chol on SP-induced SRE-SEAP. HEK-NK_1R cells were pulse-incubated with Span or Span-Chol for 30 min, washed, recovered for 4 hours, and then stimulated with SP for 20 hours (pulse incubation) or were coincubated with antagonists throughout the experiment (coincubation). $n = 3$ experiments. ANOVA, Sidak's test (H).

Downloaded from http://stm.sciencemag.org/ by guest on June 19, 2017

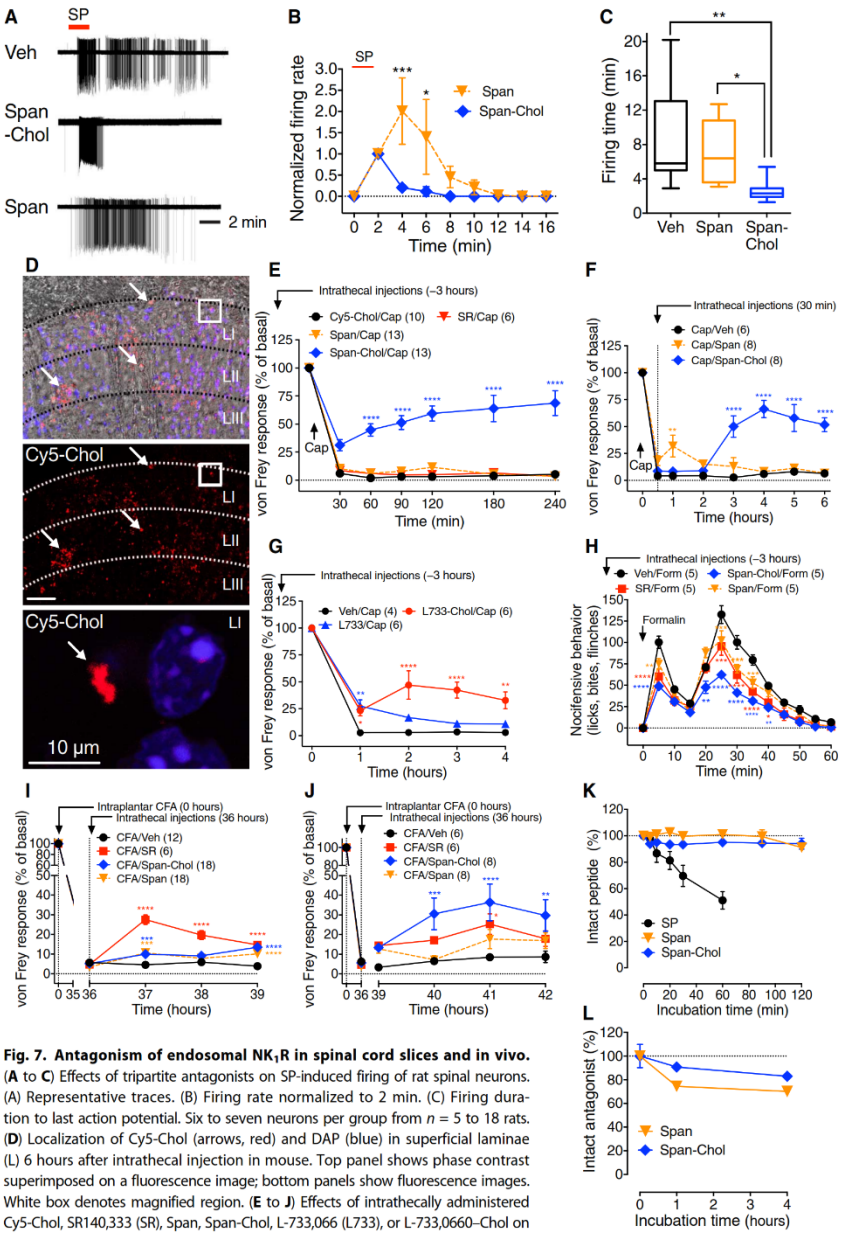

Fig. 7. Antagonism of endosomal NK_1R in spinal cord slices and in vivo. (**A** to **C**) Effects of tripartite antagonists on SP-induced firing of rat spinal neurons. (A) Representative traces. (B) Firing rate normalized to 2 min. (C) Firing duration to last action potential. Six to seven neurons per group from $n = 5$ to 18 rats. (**D**) Localization of Cy5-Chol (arrows, red) and DAP (blue) in superficial laminae (L) 6 hours after intrathecal injection in mouse. Top panel shows phase contrast superimposed on a fluorescence image; bottom panels show fluorescence images. White box denotes magnified region. (**E** to **J**) Effects of intrathecally administered Cy5-Chol, SR140,333 (SR), Span, Span-Chol, L-733,066 (L733), or L-733,0660–Chol on nociception in mice. (E to G) von Frey withdrawal responses of capsaicin-injected paw. (H) Nocifensive behavior after intraplantar formalin. (I and J) von Frey withdrawal responses of CFA-injected paw. $^*P < 0.05$, $^{**}P < 0.01$, $^{***}P < 0.001$, $^{****}P < 0.0001$, to control. (**K**) Kinetics of degradation of SP, Span, and Span-Chol by membranes prepared from mouse spinal cord ($n = 3$). (**L**) Kinetics of degradation of Span and Span-Chol in human cerebrospinal fluid. $n = 2$, mean ± SD. ANOVA, Sidak's test (B); Dunn's test (C); Dunnett's test (E to J).

DISCUSSION

Our results support a reinterpretation of the notion that the primary physiological actions of GPCRs in vivo are mediated by cell surface receptors. By studying the NK_1R as a prototypical GPCR that traffics to endosomes, we show that endosomal receptors convey sustained signals that underlie excitation and nociceptive transmission in spinal neurons and that targeting these receptors in endosomes is required for optimal pharmacological intervention.

We report that endosomal GPCRs generate a spectrum of signals in subcellular compartments. Clathrin and dynamin disruption prevented NK_1R endocytosis and inhibited activation of nuclear ERK, cytosolic PKC, and cytosolic cAMP. Dynamin inhibitors also blocked SP-induced transcription, which is likely mediated by nuclear ERK. A C-terminally truncated mutant, $NK_1R\delta311$, was also unable to internalize, activate nuclear ERK, or stimulate transcription. $G\alpha_q$ inhibition blocked NK_1R endosomal signals, and endosomes contained both activated NK_1R and $G\alpha_q$. Our results are consistent with the hypothesis that the NK_1R in endosomes signals by $G\alpha_q$-dependent processes that activate nuclear ERK, cytosolic PKC, and cytosolic cAMP to cause nociception (Fig. 8A and movie S14). By delivering activated NK_1R to endosomes and serving as a scaffold for signaling complexes, βARRs facilitate these signals (*9*, *22*, *23*). Our findings add to the growing number of GPCRs, including β_2-adrenergic and thyroid-stimulating hormone receptors (*11*, *12*), known to signal from endosomes by G protein–dependent processes, and provide in vivo evidence that this endosomal mechanism is physiologically relevant.

Together, our findings suggest that endosomal NK_1R

Downloaded from http://stm.sciencemag.org/ by guest on June 19, 2017

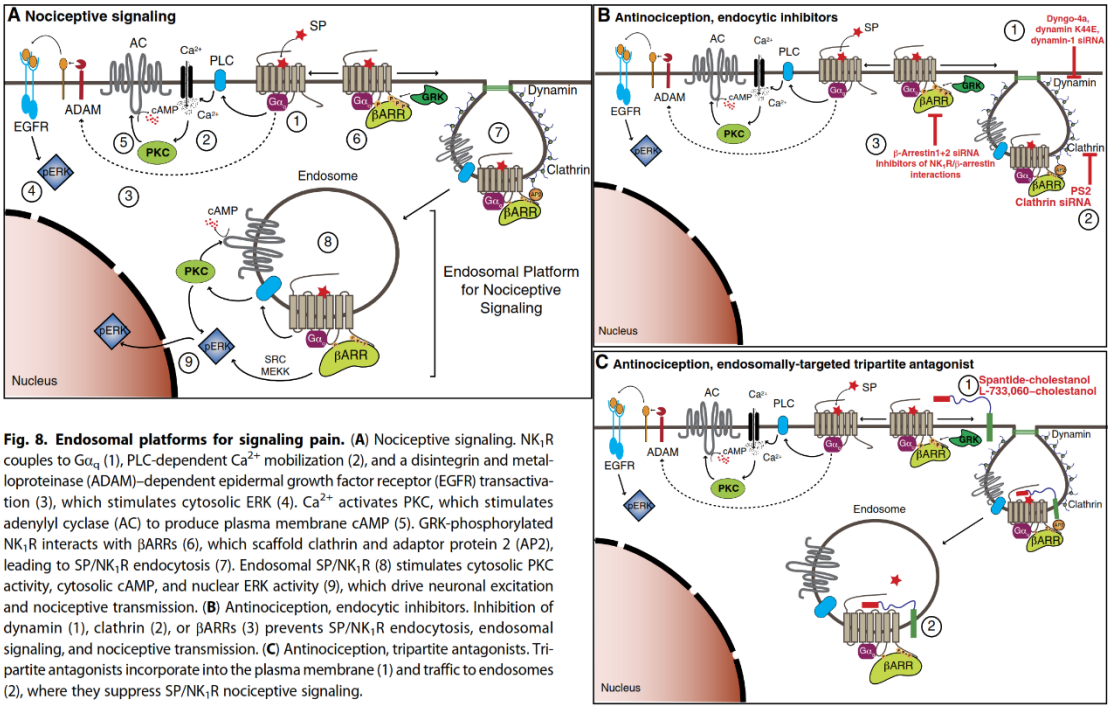

Fig. 8. Endosomal platforms for signaling pain. (**A**) Nociceptive signaling. NK_1R couples to $G\alpha_q$ (1), PLC-dependent Ca^{2+} mobilization (2), and a disintegrin and metalloproteinase (ADAM)–dependent epidermal growth factor receptor (EGFR) transactivation (3), which stimulates cytosolic ERK (4). Ca^{2+} activates PKC, which stimulates adenylyl cyclase (AC) to produce plasma membrane cAMP (5). GRK-phosphorylated NK_1R interacts with βARRs (6), which scaffold clathrin and adaptor protein 2 (AP2), leading to SP/NK_1R endocytosis (7). Endosomal SP/NK_1R (8) stimulates cytosolic PKC activity, cytosolic cAMP, and nuclear ERK activity (9), which drive neuronal excitation and nociceptive transmission. (**B**) Antinociception, endocytic inhibitors. Inhibition of dynamin (1), clathrin (2), or βARRs (3) prevents SP/NK_1R endocytosis, endosomal signaling, and nociceptive transmission. (**C**) Antinociception, tripartite antagonists. Tripartite antagonists incorporate into the plasma membrane (1) and traffic to endosomes (2), where they suppress SP/NK_1R nociceptive signaling.

signaling is necessary for sustained excitation of spinal neurons and nociceptive transmission in the spinal cord, reveal a vital link between endosomal signaling and nociception, and provide information about the contribution of clathrin and dynamin to SP-induced excitation of spinal neurons and nociceptive transmission (Fig. 8B). The observations that dynamin and clathrin inhibitors attenuate NK_1R endocytosis in spinal neurons and suppress neuronal excitation and nociception are consistent with a role for NK_1R endocytosis in pain. The finding that selective disruption of NK_1R-βARR interactions using membrane-permeant peptides and specific antagonism of endosomal NK_1R with lipidated antagonists effectively suppress neuronal excitation and nociception in several models provides direct support for a major contribution of the endosomal NK_1R to pain.

The discovery that endosomes are platforms for compartmentalized GPCR signaling that underlies pathophysiologically important processes in vivo has therapeutic implications. Delivery of antagonists to endosomes might facilitate the disruption of sustained signals from endosomal GPCRs that underlie disease and could provide enhanced efficacy and selectivity for treating pain (Fig. 8C). The accumulation of tripartite probes in NK_1R-positive endosomes demonstrates the feasibility of endosomal delivery. The capacity of Span-Chol and L-733,060–Chol, but not unconjugated antagonists, to specifically antagonize endosomal NK_1R signaling and sustained excitation of spinal neurons and to cause prolonged and more effective antinociception demonstrates the importance of endosomal signaling for pain and illustrates the therapeutic utility of endosomally directed drugs.

Limitations of the use of pharmacological inhibitors of endocytosis include the widespread roles of dynamin and clathrin in vesicular transport and synaptic transmission (*34*, *35*) and possible off-target actions of dynamin inhibitors (*36*). Thus, the actions of clathrin and dynamin inhibitors on excitation of spinal neurons and on nociceptive behavior might be unrelated to impaired NK_1R signaling in endosomes and instead due to disrupted endocytosis or exocytosis of other GPCRs, ion channels, and transmitters that control pain transmission, or an artifact of abnormal motor function. However, clathrin and dynamin inhibitors did not affect fast synaptic transmission in the spinal cord or capsaicin-evoked neuropeptide release from spinal terminals of nociceptors and had no effect on motor coordination in vivo. These results suggest that synaptic transmission and vesicular transport were unaffected. The finding that dynamin 1 knockdown in the spinal cord also inhibited nociception suggests that off-target actions of dynamin inhibitors do not account for their antinociceptive properties. The observation that inhibitors of NK_1R-βARR interactions and lipidated NK_1R antagonists replicate the antinociceptive effects of endocytosis inhibitors supports a role for NK_1R signaling in endosomes for nociception. Additional studies will be required to assess the selectivity of peptide inhibitors of NK_1R-βARR interactions. The antinociceptive actions of lipidated NK_1R antagonists are unlikely to be related to enhanced stability, given the similar rate of metabolism of unconjugated and cholestanol-conjugated spantide, although detailed pharmacokinetic studies will be required to define the tissue distribution and degradation of lipidated NK_1R antagonists in vivo. Evaluation of the therapeutic value of cholestanol-conjugated NK_1R antagonists will require investigation of their potency and efficacy in disease-relevant models of pain.

Downloaded from http://stm.sciencemag.org/ by guest on June 19, 2017

NK_1R redistributes from the plasma membrane to endosomes in chronic inflammatory and neurological diseases that are associated with persistent SP release (*5*). We propose that the inability of conventional antagonists to effectively target the NK_1R in endosomes, where the receptor assembles a multiprotein signalosome in an acidic environment, contributes to their lack of clinical success (*5*). Our study suggests that therapeutic targeting of endosomal GPCRs is a paradigm of drug delivery that offers more effective and selective treatments for pathophysiological conditions, including chronic pain.

MATERIALS AND METHODS

See the Supplementary Materials for full details of Materials and Methods.

Study design

The study was designed to examine the contribution of SP-induced endocytosis of the NK_1R to signal transduction in subcellular compartments, excitation of spinal neurons, and nociception. Endocytosis of the NK_1R was examined in HEK293 cells by using BRET to assess the proximity between the NK_1R and proteins resident in the plasma membrane and early endosomes and by localizing fluorescent SP by confocal microscopy. BRET was also used to examine the assembly of signaling complexes, which were localized in endosomes by immunofluorescence and super-resolution microscopy. Signaling in subcellular compartments of HEK293 cells was studied by expressing genetically encoded FRET biosensors, which allowed analysis of signaling with high spatial and temporal fidelity. NK_1R endocytosis was studied in spinal neurons in slice preparations and in vivo by immunofluorescence and confocal microscopy. To examine the excitation of pain-transmitting neurons, cell-attached patch clamp recordings were made from second-order neurons in slices of rat spinal cord. Nociceptive behavior was evaluated in conscious mice after intraplantar administration of capsaicin, formalin, or CFA. To examine the contribution of NK_1R endocytosis to signaling, neuronal excitation, and nociception, HEK293 cells, rat spinal cord slices, or mice were treated with pharmacological or genetic inhibitors of clathrin, dynamin, or βARRs, or with peptide inhibitors of NK_1R/βARR interactions. Peptidic and small-molecule antagonists of the NK_1R were conjugated to the lipid cholestanol, which facilitated endosomal targeting and retention of antagonists. Cholestanol-conjugated antagonists were used to directly evaluate the contribution of NK_1R signaling in endosomes to SP-induced compartmentalized signaling in HEK293 cells, excitation of spinal neurons, and nociception. Institutional Animal Care and Use Committees approved all studies.

Statistical analyses

Data are presented as means ± SEM, unless noted otherwise. Differences were assessed using Student's *t* test for two comparisons. For multiple comparisons, differences were assessed using one- or two-way ANOVA followed by Dunnett's multiple comparison test, Tukey's multiple comparison test, Sidak's multiple comparisons test, or Dunn's multiple comparisons test. Table S1 provides full details of statistical tests and replicates for each experiment.

SUPPLEMENTARY MATERIALS

www.sciencetranslationalmedicine.org/cgi/content/full/9/392/eaal3447/DC1
Materials and Methods
Fig. S1. Clathrin- and dynamin-dependent NK_1R endocytosis.
Fig. S2. NK_1R compartmentalized signaling.
Fig. S3. G protein–dependent NK_1R signaling in endosomes.
Fig. S4. Nociception and inflammation in vivo.
Fig. S5. NK_1R endocytosis in spinal neurons in vivo.
Fig. S6. NK_1Rß311 expression and trafficking.
Fig. S7. Uptake of tripartite probes.
Fig. S8. Effects of NK_1R tripartite antagonists on ERK signaling.
Fig. S9. Synthesis and analysis of Span-Chol and Span–ethyl ester.
Fig. S10. Synthesis and analysis of L-733,060-Chol.
Table S1. Statistical analyses and cell replicates.
Movie S1. Three-dimensional projections of NK_1R-IR in neurons in spinal cord slices incubated with Dy4 inact and vehicle.
Movie S2. Three-dimensional projections of NK_1R-IR in neurons in spinal cord slices incubated with Dy4 inact and SP.
Movie S3. Three-dimensional projections of NK_1R-IR in neurons in spinal cord slices incubated with Dy4 and vehicle.
Movie S4. Three-dimensional projections of NK_1R-IR in neurons in spinal cord slices incubated with Dy4 and SP.
Movie S5. Three-dimensional projections of NK_1R-IR in neurons in spinal cord 10 min after intraplantar injection of vehicle.
Movie S6. Three-dimensional projections of NK_1R-IR in neurons in spinal cord 10 min after intraplantar injection of capsaicin.
Movie S7. Three-dimensional projections of NK_1R-IR in neurons in spinal cord 10 min after intraplantar injection of capsaicin, with Dy4 injected before capsaicin.
Movie S8. Three-dimensional projections of NK_1R-IR in neurons in spinal cord 10 min after intraplantar injection of capsaicin, with Dy4 inact injected before capsaicin.
Movie S9. Three-dimensional projections of NK_1R-IR in neurons in spinal cord 10 min after intraplantar injection of capsaicin, with PS2 injected before capsaicin.
Movie S10. Three-dimensional projections of NK_1R-IR in neurons in spinal cord 10 min after intraplantar injection of capsaicin, with PS2 inact injected before capsaicin.
Movie S11. Plasma membrane incorporation and endocytosis of Cy5-cholestanol by HEK293 cells.
Movie S12. Lack of uptake of Cy5–ethyl ester by HEK293 cells.
Movie S13. Time lapse images showing FRET between SNAP-549-NK_1R and Cy5-Chol.
Movie S14. Animation showing SP-induced assembly of endosomal signaling platform for pain transmission.
References (*37*–*54*)

REFERENCES AND NOTES

1. A. I. Basbaum, D. M. Bautista, G. Scherrer, D. Julius, Cellular and molecular mechanisms of pain. *Cell* **139**, 267–284 (2009).
2. B. Han, W. M. Compton, C. M. Jones, R. Cai, Nonmedical prescription opioid use and use disorders among adults aged 18 through 64 years in the United States, 2003-2013. *JAMA* **314**, 1468–1478 (2015).
3. M. Audet, M. Bouvier, Insights into signaling from the β_2-adrenergic receptor structure. *Nat. Chem. Biol.* **4**, 397–403 (2008).
4. P. Geppetti, N. A. Veldhuis, T. Lieu, N. W. Bunnett, G protein-coupled receptors: Dynamic machines for signaling pain and itch. *Neuron* **88**, 635–649 (2015).
5. M. S. Steinhoff, B. von Mentzer, P. Geppetti, C. Pothoulakis, N. W. Bunnett, Tachykinins and their receptors: Contributions to physiological control and the mechanisms of disease. *Phys. Rev.* **94**, 265–301 (2014).
6. S. M. DeWire, S. Ahn, R. J. Lefkowitz, S. K. Shenoy, β-Arrestins and cell signaling. *Annu. Rev. Physiol.* **69**, 483–510 (2007).
7. R. Irannejad, M. von Zastrow, GPCR signaling along the endocytic pathway. *Curr. Opin. Cell Biol.* **27**, 109–116 (2014).
8. J. E. Murphy, B. E. Padilla, B. Hasdemir, G. S. Cottrell, N. W. Bunnett, Endosomes: A legitimate platform for the signaling train. *Proc. Natl. Acad. Sci. U.S.A.* **106**, 17615–17622 (2009).
9. K. A. DeFea, Z. D. Vaughn, E. M. O'Bryan, D. Nishijima, O. Déry, N. W. Bunnett, The proliferative and antiapoptotic effects of substance P are facilitated by formation of a β-arrestin-dependent scaffolding complex. *Proc. Natl. Acad. Sci. U.S.A.* **97**, 11086–11091 (2000).
10. K. A. DeFea, J. Zalevsky, M. S. Thoma, O. Déry, R. D. Mullins, N. W. Bunnett, β-Arrestin–dependent endocytosis of proteinase-activated receptor 2 is required for intracellular targeting of activated ERK1/2. *J. Cell Biol.* **148**, 1267–1281 (2000).
11. D. Calebiro, V. O. Nikolaev, M. C. Gagliani, T. de Filippis, C. Dees, C. Tacchetti, L. Persani, M. J. Lohse, Persistent cAMP-signals triggered by internalized G-protein–coupled receptors. *PLOS Biol.* **7**, e1000172 (2009).
12. R. Irannejad, J. C. Tomshine, J. R. Tomshine, M. Chevalier, J. P. Mahoney, J. Steyaert, S. G. F. Rasmussen, R. K. Sunahara, H. El-Samad, B. Huang, M. von Zastrow, Conformational biosensors reveal GPCR signalling from endosomes. *Nature* **495**, 534–538 (2013).

Downloaded from http://stm.sciencemag.org/ by guest on June 19, 2017

13. A. R. B. Thomsen, B. Plouffe, T. J. Cahill III, A. K. Shukla, J. T. Tarrasch, A. M. Dosey, A. W. Kahsai, R. T. Strachan, B. Pani, J. P. Mahoney, L. Huang, B. Breton, F. M. Heydenreich, R. K. Sunahara, G. Skiniotis, M. Bouvier, R. J. Lefkowitz, GPCR-G protein-β-arrestin super-complex mediates sustained G protein signaling. *Cell* **166**, 907–919 (2016).
14. P. W. Mantyh, E. DeMaster, A. Malhotra, J. R. Ghilardi, S. D. Rogers, C. R. Mantyh, H. Liu, A. I. Basbaum, S. R. Vigna, J. E. Maggio, D. A. Simone, Receptor endocytosis and dendrite reshaping in spinal neurons after somatosensory stimulation. *Science* **268**, 1629–1632 (1995).
15. J. M. Jarcho, N. A. Feier, A. Bert, J. A. Labus, M. Lee, J. Stains, B. Ebrat, S. M. Groman, K. Tillisch, A. L. Brody, E. D. London, M. A. Mandelkern, E. A. Mayer, Diminished neurokinin-1 receptor availability in patients with two forms of chronic visceral pain. *Pain* **154**, 987–996 (2013).
16. K. McConalogue, O. Déry, M. Lovett, H. Wong, J. H. Walsh, E. F. Grady, N. W. Bunnett, Substance P-induced trafficking of β-arrestins. The role of β-arrestins in endocytosis of the neurokinin-1 receptor. *J. Biol. Chem.* **274**, 16257–16268 (1999).
17. M. J. Robertson, F. M. Deane, P. J. Robinson, A. McCluskey, Synthesis of Dynole 34-2, Dynole 2-24 and Dyngo 4a for investigating dynamin GTPase. *Nat. Protoc.* **9**, 851–870 (2014).
18. M. J. Robertson, F. M. Deane, W. Stahlschmidt, L. von Kleist, V. Haucke, P. J. Robinson, A. McCluskey, Synthesis of the Pitstop family of clathrin inhibitors. *Nat. Protoc.* **9**, 1592–1606 (2014).
19. F. Schmidlin, O. Déry, K. O. DeFea, L. Slice, S. Patierno, C. Sternini, E. F. Grady, N. W. Bunnett, Dynamin and Rab5a-dependent trafficking and signaling of the neurokinin 1 receptor. *J. Biol. Chem.* **276**, 25427–25437 (2001).
20. M. L. Halls, D. P. Poole, A. M. Ellisdon, C. J. Nowell, M. Canals, Detection and quantification of intracellular signaling using FRET-based biosensors and high content imaging. *Methods Mol. Biol.* **1335**, 131–161 (2015).
21. N. G. Tsvetanova, R. Irannejad, M. von Zastrow, G protein-coupled receptor (GPCR) signaling via heterotrimeric G proteins from endosomes. *J. Biol. Chem.* **290**, 6689–6696 (2015).
22. G. S. Cottrell, B. E. Padilla, S. Amadesi, D. P. Poole, J. E. Murphy, M. Hardt, D. Roosterman, M. Steinhoff, N. W. Bunnett, Endosomal endothelin-converting enzyme-1: A regulator of β-arrestin-dependent ERK signaling. *J. Biol. Chem.* **284**, 22411–22425 (2009).
23. D. D. Jensen, M. L. Halls, J. E. Murphy, M. Canals, F. Cattaruzza, D. P. Poole, T. Lieu, H.-W. Koon, C. Pothoulakis, N. W. Bunnett, Endothelin-converting enzyme 1 and β-arrestins exert spatiotemporal control of substance P-induced inflammatory signals. *J. Biol. Chem.* **289**, 20283–20294 (2014).
24. S. P. Davies, H. Reddy, M. Caivano, P. Cohen, Specificity and mechanism of action of some commonly used protein kinase inhibitors. *Biochem. J.* **351**, 95–105 (2000).
25. R.-R. Ji, K. Befort, G. J. Brenner, C. J. Woolf, ERK MAP kinase activation in superficial spinal cord neurons induces prodynorphin and NK-1 upregulation and contributes to persistent inflammatory pain hypersensitivity. *J. Neurosci.* **22**, 478–485 (2002).
26. K. Murase, M. Randić, Actions of substance P on rat spinal dorsal horn neurones. *J. Physiol.* **346**, 203–217 (1984).
27. X. Emonds-Alt, J. D. Doutremepuich, M. Heaulme, G. Neliat, V. Santucci, R. Steinberg, P. Vilain, D. Bichon, J.-P. Ducoux, V. Proietto, D. Van Broeck, P. Soubrié, G. Le Fu, J.-C. Breliére, In vitro and in vivo biological activities of SR140333, a novel potent non-peptide tachykinin NK_1 receptor antagonist. *Eur. J. Pharmacol.* **250**, 403–413 (1993).
28. D. Roosterman, G. S. Cottrell, F. Schmidlin, M. Steinhoff, N. W. Bunnett, Recycling and resensitization of the neurokinin 1 receptor. Influence of agonist concentration and Rab GTPases. *J. Biol. Chem.* **279**, 30670–30679 (2004).
29. D. Roosterman, G. S. Cottrell, B. E. Padilla, L. Muller, C. B. Eckman, N. W. Bunnett, M. Steinhoff, Endothelin-converting enzyme 1 degrades neuropeptides in endosomes to control receptor recycling. *Proc. Natl. Acad. Sci. U.S.A.* **104**, 11838–11843 (2007).
30. P. Y. Sato, J. K. Chuprun, M. Schwartz, W. J. Koch, The evolving impact of G protein-coupled receptor kinases in cardiac health and disease. *Phys. Rev.* **95**, 377–404 (2015).
31. L. Rajendran, V. Udayar, Z. V. Goodger, Lipid-anchored drugs for delivery into subcellular compartments. *Trends Pharmacol. Sci.* **33**, 215–222 (2012).
32. K. Folkers, R. Håkanson, J. Hörig, J.-C. Xu, S. Leander, Biological evaluation of substance P antagonists. *Br. J. Pharmacol.* **83**, 449–456 (1984).
33. N. M. Rupniak, E. Carlson, S. Boyce, J. K. Webb, R. G. Hill, Enantioselective inhibition of the formalin paw late phase by the NK1 receptor antagonist L-733,060 in gerbils. *Pain* **67**, 189–195 (1996).
34. J. A. Heymann, J. E. Hinshaw, Dynamins at a glance. *J. Cell Sci.* **122**, 3427–3431 (2009).
35. H. T. McMahon, E. Boucrot, Molecular mechanism and physiological functions of clathrin-mediated endocytosis. *Nat. Rev. Mol. Cell Biol.* **12**, 517–533 (2011).
36. R. J. Park, H. Shen, L. Liu, X. Liu, S. M. Ferguson, P. De Camilli, Dynamin triple knockout cells reveal off target effects of commonly used dynamin inhibitors. *J. Cell Sci.* **126**, 5305–5312 (2013).
37. M. Kocan, M. B. Dalrymple, R. M. Seeber, B. J. Feldman, K. D. G. Pfleger, Enhanced BRET technology for the monitoring of agonist-induced and agonist-independent interactions between GPCRs and β-arrestins. *Front. Endocrinol.* **1**, 12 (2010).
38. T.-H. Lan, Q. Liu, C. Li, G. Wu, N. A. Lambert, Sensitive and high resolution localization and tracking of membrane proteins in live cells with BRET. *Traffic* **13**, 1450–1456 (2012).
39. C. D. Harvey, A. G. Ehrhardt, C. Cellurale, H. Zhong, R. Yasuda, R. J. Davis, K. Svoboda, A genetically encoded fluorescent sensor of ERK activity. *Proc. Natl. Acad. Sci. U.S.A.* **105**, 19264–19269 (2008).
40. J. D. Violin, J. Zhang, R. Y. Tsien, A. C. Newton, A genetically encoded fluorescent reporter reveals oscillatory phosphorylation by protein kinase C. *J. Cell Biol.* **161**, 899–909 (2003).
41. V. O. Nikolaev, M. Bünemann, L. Hein, A. Hannawacker, M. J. Lohse, Novel single chain cAMP sensors for receptor-induced signal propagation. *J. Biol. Chem.* **279**, 37215–37218 (2004).
42. S. Wachten, N. Masada, L. J. Ayling, A. Ciruela, V. O. Nikolaev, M. J. Lohse, D. M. Cooper, Distinct pools of cAMP centre on different isoforms of adenylyl cyclase in pituitary-derived GH3B6 cells. *J. Cell Sci.* **123**, 95–106 (2010).
43. O. Déry, K. A. Defea, N. W. Bunnett, Protein kinase C-mediated desensitization of the neurokinin 1 receptor. *Am. J. Physiol. Cell Physiol.* **280**, C1097–C1106 (2001).
44. M. L. Halls, R. A. D. Bathgate, R. J. Summers, Comparison of signaling pathways activated by the relaxin family peptide receptors, RXFP1 and RXFP2, using reporter genes. *J. Pharmacol. Exp. Ther.* **320**, 281–290 (2007).
45. X. H. Yu, A. Ribeiro-da-Silva, Y. De Koninck, Morphology and neurokinin 1 receptor expression of spinothalamic lamina I neurons in the rat spinal cord. *J. Comp. Neurol.* **491**, 56–68 (2005).
46. W. L. Imlach, R. F. Bhola, L. T. May, A. Christopoulos, M. J. Christie, A positive allosteric modulator of the adenosine A_1 receptor selectively inhibits primary afferent synaptic transmission in a neuropathic pain model. *Mol. Pharm.* **88**, 460–468 (2015).
47. S. Amadesi, J. Nie, N. Vergnolle, G. S. Cottrell, E. F. Grady, M. Trevisani, C. Manni, P. Geppetti, J. A. McRoberts, H. Ennes, J. B. Davis, E. A. Mayer, N. W. Bunnett, Protease-activated receptor 2 sensitizes the capsaicin receptor transient receptor potential vanilloid receptor 1 to induce hyperalgesia. *J. Neurosci.* **24**, 4300–4312 (2004).
48. E. F. Grady, P. Baluk, S. Böhm, P. D. Gamp, H. Wong, D. G. Payan, J. Ansel, A. L. Portbury, J. B. Furness, D. M. McDonald, N. W. Bunnett, Characterization of antisera specific to NK1, NK2, and NK3 neurokinin receptors and their utilization to localize receptors in the rat gastrointestinal tract. *J. Neurosci.* **16**, 6975–6986 (1996).
49. F. Alemi, E. Kwon, D. P. Poole, T. Lieu, V. Lyo, F. Cattaruzza, F. Cevikbas, M. Steinhoff, R. Nassini, S. Materazzi, R. Guerrero-Alba, E. Valdez-Morales, G. S. Cottrell, K. Schoonjans, P. Geppetti, S. J. Vanner, N. W. Bunnett, C. U. Corvera, The TGR5 receptor mediates bile acid-induced itch and analgesia. *J. Clin. Invest.* **123**, 1513–1530 (2013).
50. D. P. Poole, S. Amadesi, N. A. Veldhuis, F. C. Abogadie, T. Lieu, W. Darby, W. Liedtke, M. J. Lew, P. McIntyre, N. W. Bunnett, Protease-activated receptor 2 (PAR_2) protein and transient receptor potential vanilloid 4 (TRPV4) protein coupling is required for sustained inflammatory signaling. *J. Biol. Chem.* **288**, 5790–5802 (2013).
51. A. Schlegel, C. Largeau, P. Bigey, M. Bessodes, K. Lebozec, D. Scherman, V. Escriou, Anionic polymers for decreased toxicity and enhanced in vivo delivery of siRNA complexed with cationic liposomes. *J. Control Release* **152**, 393–401 (2011).
52. M. Fa, A. Staniszewski, F. Saeed, Y. I. Francis, O. Arancio, Dynamin 1 is required for memory formation. *PLOS ONE* **9**, e91954 (2014).
53. T. C. Tan, V. A. Valova, C. S. Malladi, M. E. Graham, L. A. Berven, O. J. Jupp, G. Hansra, S. J. McClure, B. Sarcevic, R. A. Boadle, M. R. Larsen, M. A. Cousin, P. J. Robinson, Cdk5 is essential for synaptic vesicle endocytosis. *Nat. Cell Biol.* **5**, 701–710 (2003).
54. N. W. Bunnett, R. Kobayashi, M. S. Orloff, J. R. Reeve, A. J. Turner, J. H. Walsh, Catabolism of gastrin releasing peptide and substance P by gastric membrane-bound peptidases. *Peptides* **6**, 277–283 (1985).

Acknowledgments: We thank C. Nowell for image analysis and F. Chiu for analysis of probe degradation. **Funding:** This work was supported by National Health and Medical Research Council (NHMRC) grants 63303, 1049682, and 1031886; the Australia Research Council Centre of Excellence in Convergent Bio-Nano Science and Technology; and Monash University (to N.W.B.); by NHMRC grants 1047070, 1032771, 1022218, 1017063, and 1011457; the Australian Cancer Research Foundation; and the Ramaciotti Foundation (to P.J.R. and A.M.); and by Takeda Pharmaceuticals Inc. M.L.H. is an NHMRC R.D. Wright Career Development Fellow (1061687) and M.C. is a Monash Fellow. **Author contributions:** D.D.J. analyzed NK_1R trafficking; T.L. studied nociception, inflammation, and motor functions; M.L.H. designed and completed FRET analyses of compartmentalized signaling; N.A.V. studied subcellular trafficking of tripartite probes and FRET analysis of probe/receptor interactions; W.L.I. analyzed excitation of spinal neurons by electrophysiology; Q.N.M. studied subcellular trafficking of tripartite probes; D.P.P. examined NK_1R trafficking by confocal microscopy; T.Q. synthesized and purified tripartite probes; L.A. synthesized and purified tripartite probes; J.C. synthesized and purified tripartite probes; C.K.H. analyzed transcription; N.B. synthesized and purified fluorescent SP; J.S.S. designed tripartite probes; M.J.S. conceived and designed the studies to use tripartite probes to therapeutically target endosomal receptors; B.G. designed tripartite

Downloaded from http://stm.sciencemag.org/ by guest on June 19, 2017

probes; A.M. designed and synthesized inhibitors of endocytosis and inactive control analogs; P.J.R. designed and characterized inhibitors of endocytosis; V.E. designed and prepared cationic liposome and anionic polymer adjuvant for in vivo delivery of siRNA; R.N. measured neuropeptide release from spinal cord; S.M. measured neuropeptide release from spinal cord; P.G. conceived, designed, and analyzed studies to examine neuropeptide release from nociceptors; G.A.H. conceived the studies; M.J.C. conceived, designed, and analyzed studies of excitation of spinal neurons; C.J.H.P. conceived and designed the studies to use tripartite probes to therapeutically target endosomal receptors; M.C. conceived, designed, and completed all BRET analyses of subcellular NK_1R trafficking and G protein activation; and N.W.B. conceived the studies, designed experiments, interpreted the results, and wrote the manuscript. **Competing interests:** Work at N.W.B.'s laboratory was funded, in part, by Takeda Pharmaceuticals Inc. N.W.B. has filed a patent for use of lipidation to target GPCRs in endosomes. All other authors declare that they have no competing interests. **Materials and data availability:** Plasmids encoding the FRET biosensors Epac-camps are available from M. J. Lohse under a material transfer agreement with the University of Wurzburg. Plasmids encoding the FRET biosensors cytoplasmic EKAR and nuclear EKAR are available under a material transfer agreement with Addgene. Dy4 is available from A.M. under a material transfer agreement with the University of Newcastle.

Submitted 4 November 2016
Accepted 17 March 2017
Published 31 May 2017
10.1126/scitranslmed.aal3447

Citation: D. D. Jensen, T. Lieu, M. L. Halls, N. A. Veldhuis, W. L. Imlach, Q. N. Mai, D. P. Poole, T. Quach, L. Aurelio, J. Conner, C. K. Herenbrink, N. Barlow, J. S. Simpson, M. J. Scanlon, B. Graham, A. McCluskey, P. J. Robinson, V. Escriou, R. Nassini, S. Materazzi, P. Geppetti, G. A. Hicks, M. J. Christie, C. J. H. Porter, M. Canals, N. W. Bunnett, Neurokinin 1 receptor signaling in endosomes mediates sustained nociception and is a viable therapeutic target for prolonged pain relief. *Sci. Transl. Med.* **9**, eaal3447 (2017).

Downloaded from http://stm.sciencemag.org/ by guest on June 19, 2017

Science Translational Medicine
AAAS

www.sciencetranslationalmedicine.org/cgi/content/full/9/392/eaal3447/DC1

Supplementary Materials for

Neurokinin 1 receptor signaling in endosomes mediates sustained nociception and is a viable therapeutic target for prolonged pain relief

Dane D. Jensen, TinaMarie Lieu, Michelle L. Halls, Nicholas A. Veldhuis, Wendy L. Imlach, Quynh N. Mai, Daniel P. Poole, Tim Quach, Luigi Aurelio, Joshua Conner, Carmen Klein Herenbrink, Nicholas Barlow, Jamie S. Simpson, Martin J. Scanlon, Bimbil Graham, Adam McCluskey, Phillip J. Robinson, Virginie Escriou, Romina Nassini, Serena Materazzi, Pierangelo Geppetti, Gareth A. Hicks, Macdonald J. Christie, Christopher J. H. Porter,* Meritxell Canals,* Nigel W. Bunnett*

*Corresponding author. Email: nb2733@cumc.columbia.edu (N.W.B.); chris.porter@monash.edu (C.J.H.P.); meri.canals@monash.edu (M.C.)

Published 31 May 2017, *Sci. Transl. Med.* **9**, eaal3447 (2017)
DOI: 10.1126/scitranslmed.aal3447

The PDF file includes:

Other Supplementary Material for this manuscript includes the following:
(available at
www.sciencetranslationalmedicine.org/cgi/content/full/9/392/eaal3447/DC1)

Movie S1 (.mp4 format). Three-dimensional projections of NK_1R-IR in neurons in spinal cord slices incubated with Dy4 inact and vehicle.
Movie S2 (.mp4 format). Three-dimensional projections of NK_1R-IR in neurons in spinal cord slices incubated with Dy4 inact and SP.
Movie S3 (.mp4 format). Three-dimensional projections of NK_1R-IR in neurons in spinal cord slices incubated with Dy4 and vehicle.
Movie S4 (.mp4 format). Three-dimensional projections of NK_1R-IR in neurons in spinal cord slices incubated with Dy4 and SP.
Movie S5 (.mp4 format). Three-dimensional projections of NK_1R-IR in neurons in spinal cord 10 min after intraplantar injection of vehicle.
Movie S6 (.mp4 format). Three-dimensional projections of NK_1R-IR in neurons in spinal cord 10 min after intraplantar injection of capsaicin.
Movie S7 (.mp4 format). Three-dimensional projections of NK_1R-IR in neurons in spinal cord 10 min after intraplantar injection of capsaicin, with Dy4 injected before capsaicin.
Movie S8 (.mp4 format). Three-dimensional projections of NK_1R-IR in neurons in spinal cord 10 min after intraplantar injection of capsaicin, with Dy4 inact injected before capsaicin.
Movie S9 (.mp4 format). Three-dimensional projections of NK_1R-IR in neurons in spinal cord 10 min after intraplantar injection of capsaicin, with PS2 injected before capsaicin.
Movie S10 (.mp4 format). Three-dimensional projections of NK_1R-IR in neurons in spinal cord 10 min after intraplantar injection of capsaicin, with PS2 inact injected before capsaicin.
Movie S11 (.mp4 format). Plasma membrane incorporation and endocytosis of Cy5-cholestanol by HEK293 cells.
Movie S12 (.mp4 format). Lack of uptake of Cy5–ethyl ester by HEK293 cells.
Movie S13 (.mp4 format). Time lapse images showing FRET between SNAP-549-NK_1R and Cy5-Chol.
Movie S14 (.mp4 format). Animation showing SP-induced assembly of endosomal signaling platform for pain transmission.

Materials and Methods

Animals. Institutional Animal Care and Use Committees approved all studies. Rats (Sprague-Dawley, males, 3-8 weeks) and mice (C57BL/6, males, 6-10 weeks) were from the Monash Animal Research Platform, the Animal Resources Centre, Western Australia, and Harlan Laboratories. Animals were maintained in a temperature-controlled environment with a 12 h light/dark cycle and free access to food and water. Animals were sacrificed by inhalation of isoflurane or carbon dioxide, or with sodium pentobartitone (200 mg/kg, i.p.), followed by bilateral thoracotomy or decapitation. Animals were randomized for treatments, and no animals were excluded from studies.

Tripartite probes. Cyanine 5, spantide I, and L-733,060 were conjugated to cholestanol or aspartate ethyl ester via a flexible PEG linker by standard Fmoc solid-phase peptide synthesis (SPPS) on Fmoc-PAL-PEG-PS resin (Life Technologies, 0.17 mmol/g resin loading) (fig. S9A, fig. S10A). Fmoc deprotection reactions were carried out using 20% *v*/*v* piperidine in *N*,*N*-dimethylformamide (DMF). Coupling reactions were carried out using Fmoc-protected amino acids with *O*-(6-chlorobenzotriazol-1-yl)-*N*,*N*,*N*′,*N*′-tetramethyluronium hexafluorophosphate (HCTU) as coupling agent and *N*,*N*-diisopropylethylamine (DIPEA) as activating agent. Cy5-Chol [Cy5-PEG4-PEG3-PEG4-Asp(OChol)-NH_2] was prepared by manual SPPS using Fmoc-Asp(OChol)-OH, Fmoc-PEG4-OH, Fmoc-PEG3-OH, and Fmoc-PEG4-OH as the amino acids. After the final deprotection step, the *N*-terminus was capped using a mixture of Cy5 acid, HCTU, and DIPEA in DMF, and the peptide construct was then cleaved from resin using 95:2.5:2.5 trifluoroacetic acid (TFA)/triisopropylsilane (TIPS)/water. Cy5-Ethyl ester [Cy5-PEG4-PEG3-PEG4-Asp(OEt)-NH_2] was prepared as for Cy5-Chol, except for replacement of Fmoc-Asp(OChol)-OH with Fmoc-Asp(OEt)-OH in the first coupling step. Spantide I [^{D}Arg-Pro-Lys-

Pro-Gln-Gln-^{D}Trp-Phe-^{D}Trp-Leu-Leu-NH_2] was prepared by automated SPPS using the appropriate side-chain protected Fmoc-amino acids. After the final deprotection step, a portion of the material was cleaved from resin using 92.5:2.5:2.5:2.5 TFA/TIPS/1,2-ethanedithiol (EDT)/water and suspended in a 1:1 mixture of acetonitrile (ACN)/water containing 0.1% TFA to ensure complete side-chain deprotection. Spantide-cholestanol [Ac-Asp(OChol)-PEG4-PEG3-PEG4-Spantide-NH_2] was prepared from resin-bound spantide I by manual SPPS using Fmoc-PEG4-OH, Fmoc-PEG3-OH, Fmoc-PEG4-OH, and Fmoc-Asp(OChol)-OH as the amino acids (fig. S9A). After the final deprotection step, the *N*-terminus was capped using a mixture of acetic anhydride and DIPEA in DMF, and the peptide construct was then cleaved from resin using 92.5:2.5:2.5:2.5 TFA/TIPS/EDT/water. Spantide-ethyl ester [Ac-Asp(OEt)-PEG4-PEG3-PEG4-Spantide-NH_2] was prepared as for spantide-cholestanol, except for replacement of Fmoc-Asp(OChol)-OH with Fmoc-Asp(OEt)-OH in the final coupling step (fig. S9A). L-733,060-cholestanol [L-733,060-C8-PEG4-PEG3-PEG4-Asp(OChol)-NH_2] was prepared by manual SPPS using Fmoc-Asp(OChol)-OH, Fmoc-PEG4-OH, Fmoc-PEG3-OH, and Fmoc-PEG4-OH as the amino acids, respectively (fig. S10A). After the final deprotection step, the *N*-terminus was extended by coupling with 8-bromooctanoic acid, HCTU and DIPEA in DMF for 45 minutes. Finally, the bromo-terminated peptide was coupled with L-733,060·HCl, TBAI, and DIPEA for three days, and the construct was then cleaved from resin using 95:2.5:2.5 TFA/TIPS/water. *Purification and LC-MS analysis:* Constructs were purified by reverse-phase high-performance liquid chromatography (HPLC) using a Luna 5 μm C8, 250 × 21.2 mm column (Phenomenex), eluting with gradient mixtures of 0.1% TFA/water and 0.1% TFA/ACN, at a flow rate of 20 ml/min and detection at 214 and 254 nm. Combined fractions were freeze-dried for two days to give the target peptides as TFA salts with 5-10% overall yield (based on initial resin loading).

The identity of the final products were confirmed by liquid chromatography-mass spectrometry (LC-MS) using a Luna 3 µm C8(2), 100 × 2.0 mm column (Phenomenex), eluting with gradient mixtures of 0.05% TFA/water and 0.05% TFA/ACN, at a flow rate of 0.2 ml/min and detection at 214 nm. Mass spectra were acquired in positive ion mode with a scan range of 200-2000 *m/z*. *Spantide I:* gradient = 0-80% ACN over 25 min; t_R = 15.1 min; calcd for $C_{75}H_{110}N_{20}O_{13}$ [M + $2H^+$] *m/z* 749.90; obs. *m/z* 749.95. *Spantide-cholestanol:* gradient = 20-100% ACN over 20 min; t_R = 14.9 min; calcd for $C_{139}H_{223}N_{24}O_{31}$ [M + $3H^+$] *m/z* 908.80; obs. *m/z* 908.95 (fig. S9B). *Spantide-ethyl ester:* gradient = 0-60% ACN over 20 min; t_R = 14.8 min; calcd for $C_{114}H_{181}N_{24}O_{31}$ [M + $3H^+$] *m/z* 794.60; obs. *m/z* 794.90 (fig. S9C). *L-733,060-cholestanol:* gradient = 60-100% ACN over 20 min; t_R = 16.1 min; calcd. for $C_{90}H_{144}F_6N_6O_{19}$ $[M + 2H]^{2+}$ *m/z* 865.05, obs. *m/z* 865.35 (fig. S10B).

Alexa568-SP. AlexaFluor568 NHS ester (Invitrogen; 6.3 µmol) was incubated with SP (1.48 µmol) and triethylamine (2.9 µmol) in DMF (500 µl) (15 h, room temperature, RT). Alexa568-SP was purified by reverse-phase HPLC. The product was confirmed by mass spectrometry: *m/z* 1012.8, calcd for $C_{96}H_{127}N_{19}O_{24}S_3$ [M + $2H^+$] *m/z* 1012.9.

Cell-penetrating NK_1R peptides. Putative GRK2 phosphorylation sites within the intracellular C-terminus of the mouse NK_1R were predicted using Group Based Prediction System (http://gps.biocuckoo.org/wsresult.php?p=1). Peptides corresponding to these domains (S^{398}SSFYSNM^{405}, S^{390}NSKTMTE^{397}, L^{382}TSNGSSR^{389}) or control peptide (MSNSYSFS) with the N-terminal Tat membrane permeant sequence (YGRKKRRQRRR) were from American Peptide Company.

cDNAs. BRET probes NK_1R-RLUC8, KRas-Venus, RAB5A-Venus, βARR1-YFP, βARR2-YFP, $G\alpha_q$-RLUC8, and $G\gamma_2$-Venus have been described (*37, 38*). CytoEKAR and NucEKAR

(*39*) and CytoCKAR and pmCKAR (*40*) were from Addgene (plasmids 18680, 18681, 14870, 14862, respectively). CytoEpac2-camps (*41*) was from M. Lohse (University of Wurzburg) and pmEpac2-camps (*42*) was from D. Cooper (University of Cambridge). GFP-dynamin and GFP-dynamin K44E have been described (*19*). Human NK_1R with extracellular N-terminal Snap-Tag was from Cisbio. Full length and truncated δ311 rat HA-NK_1R have been described (*43*). RLUC8 fusions of these constructs were generated by removal of the stop codon by PCR and subcloning into a pcDNA3.1-RLUC8 vector.

Cell lines, transfection. HEK293 cells stably expressing rat or human NK_1R with N-terminal HA11 epitope have been described (*29*). HEK293 cells were grown in 6-well plates and transiently transfected using polyethylenimine (Polysciences) or FuGene (Promega) (*23*). Cells were grown in Dulbecco's modified Eagle's medium (DMEM) supplemented with 5% FBS (37°C, 5% CO_2). Cells were routinely checked for mycoplasma infection.

BRET. HEK293 cells were transfected with the following cDNAs (per well): 1 µg NK_1R-RLUC8 + 4 µg KRas-Venus, 4 µg RAB5A-Venus, 4 µg βARR1-YFP, or 4 µg βARR2-YFP; or 1 µg NK_1R + 0.5 µg $G\alpha_q$-RLUC8 + 1 µg $G\beta_1$ + 4 µg $G\gamma_2$-Venus; or 1 µg NK_1R + 0.5 µg $G\alpha_q$-RLUC8 + 1 µg $G\beta_1$ + 1 µg $G\gamma_2$ + 4 µg RAB5A-Venus. After 48 h, cells were equilibrated in Hank's balanced salt solution (HBSS) at 37°C, and incubated with the RLuc substrate coelenterazine h (5 µM, 15 min). BRET ratios were determined using a microplate reader LUMIstar Omega (BMG LabTech) before and after challenge with SP (0.1-10 nM) or vehicle (dH_2O) (*23*).

FRET biosensors of compartmentalized signaling. HEK293 cells were transfected with 55 ng/well rat NK_1R with N-terminal HA.11 epitope tag (HA-NK_1R) and 40 ng/well FRET biosensors. FRET was assessed 48 h after transfection, after serum restriction (0.5% FBS

overnight). For experiments using clathrin or dynamin siRNA, cells were transfected with 55 ng/well rat HA-NK_1R, 40 ng/well FRET biosensor, and 25 nM scrambled (control), clathrin heavy chain (Product #67300), or dynamin-1 (Product #13429) ON-TARGETplus SMARTpool siRNA (GE Dharmacon). FRET was assessed 72 h after transfection, after serum restriction (0.5% FBS overnight). Cells were equilibrated in HBSS at 37°C, and FRET was analyzed using a GE Healthcare INCell 2000 Analyzer (*20, 23*). For GFP/RFP emission ratio analysis, cells were sequentially excited using a FITC filter (490/20) with emission measured using dsRed (605/52) and FITC (525/36) filters, and a polychroic filter set optimized for the FITC/dsRed (Quad4). For CFP/YFP emission ratio analysis, cells were sequentially excited using a CFP filter (430/24) with emission measured using YFP (535/30) and CFP (470/24) filters, and a polychroic filter set optimized for the CFP/YFP (Quad3). Cells were imaged every 1 min, allowing image capture of 14 wells per minute. Baseline emission ratio images were captured for 4 min. Cells were challenged with an EC_{50} concentration of SP (1 nM) or vehicle, and images were captured for 20 min. Cells were then stimulated with the positive control (200 nM phorbol 12,13-dibutyrate for ERK; 200 nM phorbol 12,13-dibutyrate with phosphatase inhibitor cocktail for PKC; 10 μM forskolin, 100 μM 3-isobutyl-1-methylxanthine, 100 nM PGE_1 for cAMP) for 10 min to generate a maximal increase, and positive emission ratio images were captured for 4 min. Data were analyzed as described and expressed as emission ratios relative to baseline for each cell (F/F_0) (*20, 23*). Cells with >10% change in F/F_0 after stimulation with positive controls were selected for analysis.

FRET assays of endosomal NK_1R targeting. HEK293 cells were transfected with 50 ng/well of human NK_1R with extracellular N-terminal SNAP-Tag. After 48 h, the cell-surface NK_1R was labeled with SNAP-Surface 549 photostable fluorescent substrate (New England Biolabs) (1 μM, 30

min, 37°C in DMEM, 0.5% BSA). Cells were washed, recovered in DMEM for 30 min, and stimulated with SP (10 nM, 30 min, 37°C) to induce NK_1R endocytosis. Cells were incubated with Cy5-Chol (200 nM, 37°C). SNAP-549/Cy5 sensitized emission FRET was analyzed by confocal microscopy using sequential excitation with Argon (514 nm)/HeNe (633 nm) lasers and emission at 570-620 nm (SNAP-549 donor) and 670-750 nm (Cy5 FRET and Cy5 acceptor) before (F_0) and after (F) addition of Cy5-Chol. Untransfected HEK293 cells (acceptor only) were used as controls. To measure FRET within the cytosol (in endosomes), a region of interest was drawn in the cytosol to exclude the plasma membrane. FRET was measured in the region of interest, and expressed as emission ratios relative to controls (F/F_0). Results are from N=3 separate experiments, with 7-9 cells analyzed per experiment.

Transcription assays. HEK293 cells were transfected with 70 ng/well human or rat NK_1R or $NK_1R\delta311$ and 250 ng/well secreted alkaline phosphatase (SEAP) reporter gene under the control of the specific transcription factor consensus sequence for Serum-Response Element (SRE) (*44*). Some cells were also transfected with 70 ng/well dynamin WT, dynamin K44E, or pcDNA3. After 24 h, cells were placed in phenol-red free DMEM containing 0.5% FBS, 1 mM sodium pyruvate, and 50 units/ml penicillin/streptomycin. The following day, a sample of medium was collected from each well. Cells were then stimulated with vehicle or SP (0.1-100 nM) for 4 or 20 h before collection of a second sample. Samples (5 µl) were mixed with SEAP buffer (45 µl, 2 M diethanolamine, 1 mM $MgCl_2$, pH 10.3) and heat-treated (65°C, 30 min) to denature any endogenous alkaline phosphatases. Samples were cooled to room temperature, mixed with SEAP substrate (5 µl 2 mM 4-methylumbelliferyl phosphate in SEAP buffer). After 1 h of incubation in the dark, the fluorescence intensity (Ex/Em = 360 nm/440 nm) was

measured. The data were analyzed by subtracting the basal from the SP-stimulated SEAP secretion.

Ca^{2+} assays. $[Ca^{2+}]_i$ was measured as described (*23*). HEK293 cells transiently expressing HA-NK_1R or HA-CLR/Myc-RAMP1 were loaded with Fura2-AM (2 μM). To compare the antagonistic capacity of Span and Span-Chol, cells were preincubated for 30 min with antagonists, and then challenged with SP (3 nM, EC_{80}). L-733,060 and L-733,060-Chol (10 nM) were similarly tested for their ability to inhibit SP (1 nM)-stimulated Ca^{2+} signals.

Cell-surface ELISA. HEK293 cells transiently transfected with HA-NK_1R or HA-NK_1Rδ311 were fixed in 4% paraformaldehyde, 100 mM PBS pH 7.4 (PFA, 30 min, 4°C). For analysis of total expression, cells were permeabilized using 0.5% NP-40 in TBS (30 min) after fixation. Cells were incubated in blocking buffer (1% skim milk powder, 0.1 M $NaHCO_3$, 4 h, RT), and then anti-HA (1:5,000, Sigma; overnight, 4°C). Cells were washed and incubated with anti-mouse horseradish peroxidase-conjugated antibody (1:2,000, 2 h, RT). Cells were washed and stained using the SIGMAFAST substrate (SigmaAldrich). Absorbance at 490 nm was measured using an EnVision plate reader (PerkinElmer Life Sciences). Values were normalized to HEK293 cells transfected with pcDNA3 or to untreated cells.

NK_1R trafficking in cell lines. HEK-NK_1R cells were plated on poly-D-Lysine coated glass chamber slides or coverslips and cultured for 48 h. To examine uptake of fluorescent SP, cells were incubated in HBSS with Alexa568-SP (100 nM, 20 min, 4°C), washed, incubated for 30 min at 37°C, and fixed in PFA. Cells were examined by confocal microscopy. To examine NK_1R and $G\alpha_q$ trafficking, cells were incubated in HBSS with SP (100 nM, 15 min) or vehicle and fixed. Cells were blocked in PBS, 0.2% saponin, 3% normal goat serum (1 h, RT). Cells were incubated in primary antibodies: rat anti-HA (1:1,000; Roche), rabbit anti-$G\alpha_q$ (1:2,000, C-19;

Santa Cruz Biotechnology), mouse anti-EEA1 (1:100, 610457; BD Biosciences) (overnight, 4°C). Cells were washed and incubated with donkey anti-rat Alexa488 (1:500), donkey anti-rabbit Alexa568 (1:1,000), and donkey anti-mouse Alexa647 (1:1,000) (Life Technologies or Jackson ImmunoResearch) (1 h, RT). Cells were examined by super-resolution microscopy.

Inhibitors. HEK293 cells were preincubated for 30 min with 30 μM each of Dy4, Dy4 inactive (*17*), PS2, PS2 inactive (*18*), 100 nM UBO-QIC (Institute of Pharmaceutical Biology, University of Bonn, Germany), 1 μM U73122, 10 μM NF449 (Merck Millipore), 1 μM GF109203X, 100 μM EGTA, 30 μM each of cell-penetrating NK_1R peptides (Tat-conjugated $S^{398}SSFYSNM^{405}$, $S^{390}NSKTMTE^{397}$, $L^{382}TSNGSSR^{389}$), 100 μM control peptide (Tat-conjugated MSNSYSFS), or vehicle (dH_2O or 0.1% DMSO). Pitstop and Dyngo are trademarks of Children's Medical Research Institute, Newcastle Innovation, and Freie Universitat Berlin.

Cy5 tripartite probe uptake. HEK293 cells were plated on poly-D-lysine-coated glass coverslips. Cells were infected with CellLight RAB5A-RFP (Life Technologies) or were transfected with rat NK_1R-GFP. After 24 h, cells were equilibrated in HBSS, imaged at 37°C by confocal microscopy, and incubated with Cy5-Chol, Cy5-Ethyl ester, or Cy5-Span-Chol (1.5 μM). Cells expressing NK_1R-GFP were incubated with SP (10 nM).

Spinal cord slices. Parasagittal slices (340-400 μm) were prepared using a vibratome from the lumbar region of the rat spinal cord in ice-cold sucrose-based artificial CSF (sACSF) (mM: 100 sucrose, 63 NaCl, 2.5 KCl, 1.2 NaH_2PO_4, 1.2 $MgCl_2$, 25 glucose, 25 $NaHCO_3$; 95% O_2/5% CO_2). Slices were transferred to N-Methyl-D-Glucamine (NMDG)-based recovery ACSF (rACSF) (mM: 93 NMDG, 93 HCl, 2.5 KCl, 1.2 NaH_2PO_4, 30 $NaHCO_3$, 20 HEPES, 25 glucose, 5 Na ascorbate, 2 thiourea, 3 Na pyruvate, 10 $MgSO_4$, 0.5 $CaCl_2$; 95% O_2/5% CO_2, 15 min, 34°C). Slices were transferred to normal ACSF (mM: 125 NaCl, 2.5 KCl, 1.25 NaH_2PO_4, 1.2 $MgCl_2$,

2.5 $CaCl_2$, 25 glucose, 11 $NaHCO_3$; 95% O_2/5% CO_2) containing 10 μM MK-801 (45 min, 34°C), then maintained at RT.

Electrophysiology. Slices of rat spinal cord were transferred to a recording chamber and superfused with normal ACSF (2 ml/min, 36°C). Dodt-contrast optics were used to identify large (capacitance ≥ 20 pF), putative NK_1R-positive neurons in lamina I based on their position, size, and fusiform shape with dendrites that were restricted to lamina I (*45*). Slices were preincubated with Dy4 or Dy4 inact (30 μM, 0.03% DMSO) for 10 min before recording, or were preincubated with Span-Chol or Span (1 μM, 0.01% DMSO) for 60 min, washed, and incubated in antagonist-free ACSF for a further 60 min before recording. PS2 was not soluble in the low concentrations of DMSO required for electrophysiology. To investigate the signaling mechanisms underlying excitation, slices were incubated with the MEK inhibitor U0126 or the PKC inhibitor GFX109203X (1 μM, 0.01% DMSO) for 30-45 min before recording. Large, NK_1R-positive, presumed nociceptive lamina I neurons were visually identified as described (*46*). Spontaneous currents were recorded in cell-attached configuration (Multiclamp 700B, Molecular Devices), sampled at 10 kHz, high pass filtered at 1 Hz, and capacitatively coupled action potential events were analyzed using Axograph X, V 1.4.4 (Axograph). Patch electrodes (resistance 2.5-3.5 MΩ) contained KMES-based internal solution (mM: 105 KMES, 20 NaCl, 5 HEPES, 10 BAPTA, 1.5 $MgCl_2$, 4 MgATP, 0.4 NaGTP, 0.1% biocytin; 285-295 mosmol/l) to facilitate subsequent recordings of action potential properties in whole-cell configuration. Recordings were made in the presence of CNQX (6-cyano-7-nitroquinoxaline-2,3-dione) (10 μM; AMPA/kainate receptor antagonist), picrotoxin (100 μM; $GABA_A$ receptor antagonist), strychnine (0.5 μM; glycine and acetylcholine receptor antagonist), and AP5 ((2*R*)-amino-5-phosphonovaleric acid; (2*R*)-amino-5-phosphonopentanoate) (100 μM; NMDA receptor

antagonist) to minimize presynaptic influences on action potential properties. Slices were challenged by superfusion with SP (1 μM) for 2 min. Recordings were sampled at 10 kHz and filtered with a high pass filter at 1 Hz, and firing rate was measured in two-minute interval bins. At the end of each cell-attached recording, whole-cell recordings were made in current-clamp mode to confirm retention of normal action potential firing. Data were only included in the analysis if cells had action potential amplitudes that were ≥50 mV above threshold to ensure viable neurons were included. Cells were filled with biocytin, and sections were processed to confirm NK_1R expression by immunofluorescence. The firing rate for each cell was normalized to the response at the 2 min time point, which was not significantly different between groups. The firing time was determined as the duration of the response to last action potential. To assess synaptic transmission, whole-cell configuration recordings were made under control conditions or after exposure to Dy4 or Dy4 inact; a bipolar stimulating electrode was placed at the dorsal root entry zone, and electrically-evoked excitatory postsynaptic currents recorded as described (*46*). To assess NK_1R endocytosis, spinal cord slices (400 μm) were incubated with SP (1 μM, 5 min), fixed in PFA (4 h, RT), cryoprotected, and were processed to localize NK_1R.

Neuropeptide release. Slices (0.4 mm) of mouse dorsal spinal cord (combined cervical, thoracic, lumbar-sacral segments) were superfused (0.4 ml/min) with Krebs' solution (mM: NaCl 119, $NaHCO_3$ 25, KH_2PO_4 1.2, $MgSO_4$ 1.5, $CaCl_2$ 2.5, KCl 4.7, D-glucose 11 mM; 95% CO_2/5% O_2, 37°C) containing 0.1% BSA, 1 μM phosphoramidon, and 1 μM captopril (*47*). Tissues were superfused with Dy4, PS2, inactive analogues (30 μM), or vehicle (0.3% DMSO/saline) for 30 min. Tissues were then superfused with capsaicin (0.3 μM, 10 min) in the presence of inhibitors or controls. Superfusate (10 min collections, 4 ml) was collected before, during, and after capsaicin stimulation, and analyzed for SP-IR and CGRP-IR (Bertin Pharma).

Endocytic inhibitors did not interfere with immunoassays. Detection limits of the assays were 2 pg/ml for SP-IR and 5 pg/ml for CGRP-IR. Results are expressed as fmol/g/20 min.

NK_1R endocytosis in rat spinal neurons. Dy4, Dy4 inact, PS2, PS2 inact (all 50 μM), or vehicle (1% DMSO/saline) was injected intrathecally (10 μl, L3/L4) into conscious rats. After 30 min, rats were sedated (5% isoflurane) and capsaicin (12.5 μg) or vehicle (20% ethanol, 10% Tween 80, 70% saline) was injected subcutaneously into the plantar surface of one hindpaw (25 μl). After 10 min, rats were transcardially perfused with PBS and then 4% PFA. The spinal cord was removed, immersion-fixed in PFA (2 h, 4°C), and cryoprotected (30% sucrose, PBS, 24 h, 4°C). The spinal cord (T12 to L4) was embedded in OCT, and 30 μm serial coronal sections were cut into 48-well plates containing PBS. Free-floating sections were blocked in PBS containing 10% normal horse serum (1 h, RT). Sections were incubated with mouse anti-NeuN (1:20,000; AbCam) and either rabbit anti-NK_1R (*48*) (1:5,000, #94168) or rabbit anti-pERK (1:200; Cell Signaling Technology) in PBS containing 3% normal horse serum (48 h, 4°C). Sections were washed (4 x 20 min in PBS) and incubated with donkey anti-rabbit Alexa488 (1:2,000-1:8,000) and donkey anti-mouse Alexa568 (1:2,000 (Life Technologies) (1 h, RT). Sections were washed, incubated with DAPI (10 μg/ml, 5 min), and mounted in Vectashield (Vector Laboratories).

Nociception in mice and rats, NK_1R endocytosis in spinal neurons in mice. Mice and rats were acclimatized to the experimental apparatus and environment for 1-2 h on 2 successive days before experiments. Mechanical allodynia and hyperalgesia were assessed by paw withdrawal to stimulation of the plantar surface of the hind-paw with graded von Frey filaments (*49*). On the day before the study, von Frey scores were measured in triplicate to establish a baseline for each animal. To assess edema of the paw, hindpaw thickness was measured using digital calipers

before and after treatments (*50*). For intraplantar injections, mice and rats were sedated (5% isoflurane). Capsaicin (5 µg), Complete Freund's Adjuvant (CFA, 2 mg/ml), or vehicle (capsaicin: 20% ethanol, 10% Tween 80, 70% saline; CFA: saline) was injected subcutaneously into the plantar surface of the left hindpaw (10 µl). von Frey scores (left and right paws) and paw thickness (left paw) were measured at 30 or 60 min intervals from 30-240 min after capsaicin, and 36-42 h after injection of CFA. Results are expressed as percent pre-injected values. For assessment of nocifensive behavior, mice were sedated (5% isoflurane), and formalin (4%, 10 µl) was injected subcutaneously into the plantar surface of the left hindpaw. Mice were placed in a Perspex container, and nocifensive behavior (flinching, licking, biting of the injected paw) was recorded for 60 min. The total number of nocifensive events was subdivided into acute (I, 0-10 min) and tonic (II, 10-60 min) phases. At the end of experiments, mice were transcardially perfused with PBS and PFA, and the spinal cord was removed and processed to localize the NK_1R by immunofluorescence, as described for rats. Investigators were blinded to test agents.

Intrathecal injections in mice. Intrathecal injections (5 µl, L3/L4) were made into conscious mice. Dy4, Dy4 inact, PS2, PS2 inact (all 50 µM), SR-140333 (15 µM), SM-19712 (8 mM), U0126 (100 µM), 30 µM each of cell-penetrating NK_1R peptides (Tat-conjugated $S^{398}SSFYSNM^{405}$, $S^{390}NSKTMTE^{397}$, $L^{382}TSNGSSR^{389}$), 100 µM control peptide (Tat-conjugated MSNSYSFS), or vehicle (1% DMSO/saline) was injected intrathecally 30 min before intraplantar injection of capsaicin or formalin, or 36 h after CFA. Span (50 µM), Span-Chol (50 µM), L-733,060 (100 nM), L-733,060-Chol (100 nM), or Cy5-Chol (10 µM) was injected intrathecally 3 h before or 30 min after intraplantar injection of capsaicin, 3 h before formalin, or 36 h after CFA.

Intrathecal siRNA in mice. Cationic liposome and adjuvant anionic polymer (polyglutamate) were used to deliver siRNA (*51*). siRNA targeting mouse dynamin-1 (5' (S-S) UAA GUG UCA AUC UGG UCU C dTdT 3') or control siRNA (5' (S-S) CGU ACG CGG AAU ACU UCG AUU dTdT) (*52*), or siRNA targeting mouse βARR1 (sense 5' AGC CUU CUG CGC GGA GAA U dTdT 3', antisense 5' dTdT U CGG AAG ACG CGC CUC UUA 5') plus mouse βARR2 (sense: 5' CCU ACA GGG UCA AGG UGA A dT dT 3', antisense: 5' UUC ACC UUG ACC CUG UAG G dT dT 3') or control siRNA (sense: 5' AAG GCC AGA CGC GAA UUA U dT dT, 3' antisense: 5' AUA AUU CGC GUC UGG CCU U dT dT 3') (Dharmacon) (50 ng, 0.5 µl of 100 ng.µl^{-1} stock) was mixed with 0.5 µl of adjuvant polyglutamate (0.1 µg/µl stock) and 1.5 µl sterile 0.15 M NaCl. Liposome solution, cationic lipid 2- {3-[bis-(3-amino-propyl)-amino]-propylamino}-N-ditetradecylcarbamoylmethyl-acetamide (DMAPAP) and L-α-dioleoyl phosphatidylethanolamine (DOPE) (DMAPAP/DOPE, 1/1 M:M) (2.5 µl of 200 µM) was added to siRNA/adjuvant, vortexed for 1 min, and incubated (30 min, RT). The siRNA lipoplexes were administered to mice by intrathecal injection (L1-L4, 5 µl). After behavioral testing (24-48 h), the spinal cord (L1-L4) was collected for analysis of dynamin-1 expression by Western blotting and βARR1 and βARR2 expression by q-PCR.

Western blotting. *Cell lines.* HEK293 cells were lysed in 150 µl of RIPA buffer containing HALT protease and phosphatase inhibitors (Thermo Scientific). Samples were sonicated on ice, centrifuged, and supernatant (20 µg protein) was fractionated by 10% SDS-PAGE and transferred to PVDF membranes. Membranes were blocked (1 h, RT) in Odyssey blocking buffer (LI-COR Biosciences), and incubated with sheep anti-dynamin-1 (*53*) (1:1,000) or rabbit anti-clathrin (1 µg/ml, AbCam) antibodies in PBS, 0.2% Tween-20, 50% Odyssey blocking buffer (16 h, 4°C). Membranes were washed and incubated with donkey anti-goat 680 or goat anti-

rabbit 680 (1:10,000; LI-COR Biosciences) (1 h, RT). Membranes were washed and imaged with the LI-COR Odyssey infrared scanner. Membranes were stripped and re-probed with rabbit anti-β-actin (1:1,000; Cell Signaling Technology, 16 h, 4°C), washed, incubated with goat anti-rabbit 800 (1:10,000, 1 h at RT, LI-COR), and re-imaged. Signals were quantified using ImageJ (NIH).

Spinal cord. The dorsal half of the spinal cord was placed in 100 µl of ice-cold RIPA buffer containing HALT protease and phosphatase inhibitors (Thermo Scientific). Tissues were homogenized, centrifuged, and supernatant (20 µg protein) was separated by 10% SDS-PAGE and transferred to PVDF membranes. Membranes were processed to detect dynamin-1 and β-actin as described above.

q-PCR. Mouse lumbar spinal cord (L1-L4) was placed in RNA*later* (Qiagen), and total RNA was isolated using RNeasy RNA Isolation kit (Qiagen). Total RNA (500 ng) was reverse-transcribed using Superscript III cDNA Synthesis Kit (Invitrogen). cDNA was amplified using Eppendorf RealPlex Real Time PCR System. Twenty microliters of amplification reaction included cDNA template, TaqMan Universal Master Mix, and TaqMan Gene Expression Assays for one of the following genes (catalog no.): *Arrb2* (Mm00520666_g1), *Arrb1* (Mm00617540_m1), *Actb* (Mm02619580_g1), *Gapdh* (hs00363153_m1). Samples were amplified in triplicates. For real-time quantitative PCR, the ΔΔCt method (Applied Biosystems) was used to calculate relative changes in mRNA abundance. The threshold cycle (Ct) values for the housekeeping genes *Actb* and *Gapdh* were subtracted from the Ct value for the gene of interest (Δ*C*t). Data were expressed as relative abundance using the equation: $2^{-\Delta Ct} * 1000$, where $\Delta Ct = Ct_{\text{gene of interest}} - Ct_{Actb,Gapdh.}$ The results are presented as mRNA abundance (fold-change or percentage of housekeeping genes).

Rotarod latency. Mice were acclimatized by three trials on two successive days before experiments. Mice were trained to remain on the rotarod for three consecutive periods. On the experimental day, three baseline time trials (cut-off 120 s) were recorded. Dy4, PS2, inactive analogues (50 μM), or vehicle was injected intrathecally (5 μl, L3/L4). After 30 min, mice were placed on the rotarod with accelerating velocity for up to 120 s. Times were recorded in three successive trials, and latency time to fall was determined at 30, 90, and 120 min.

Confocal microscopy, image analysis. Tissues and cells were examined using a Leica SP8 confocal microscope using HCX PL APO 40x (NA 1.30) and HCX PL APO 63x (NA 1.40) oil objectives. Z stacks were collected of NK_1R-positive neurons in lamina I of the dorsal horn. Video projections of Z stacks were made using Imaris Software (Bitplane). NK_1R endocytosis and pERK expression were quantified using ImageJ. To quantify NK_1R internalization in lamina I neurons, the border of the cytoplasm of the neuronal soma was defined by NeuN fluorescence, and NK_1R fluorescence within 5 pixels (0.5 μm) of the border was defined as plasma membrane-associated receptor. The ratio of plasma membrane to cytosolic NK_1R-IR fluorescence was determined in ≥6 lamina I neurons per animal per condition. To quantify ERK activation, the ratio of the number of pERK-IR neurons to total NeuN-N-positive neurons in lamina I was determined in ≥6 fields (x40 objective) per condition.

Super-resolution microscopy. Coverslips were mounted and sealed on a concave slide containing 100 mM cysteamine (MEA). Cells were observed using a Leica DMI6000 Ground State Depletion microscope with a HCX PL APO 100x (NA 1.49) objective, a SuMo Stage, an Andor iXon 3 897 camera using LAS AF software (version 3.2.0.9652, Leica). Fluorophores were imaged sequentially starting with the 647 channel to avoid photo bleaching of lower wavelength channels. Pumping occurred at 100% laser power for each fluorophore until the

frame correlation dropped to <0.2. Channels were acquired at 50% laser power, and 27,000-30,000 frames per channel were captured. The number of EEA-IR endosomes per cell containing NK_1-IR and $G\alpha_q$-IR was determined. A 300 nm diameter region of interest (average size of EEA1 positive structures) was drawn around all EEA1-IR endosomes in an image using ImageJ. The proportion of regions of interest that contained detectable NK_1R-IR and $G\alpha_q$-IR was determined. Results are expressed as the percentage of EEA1-IR endosomes containing NK_1R-IR, $G\alpha_q$-IR, or both NK_1R-IR and $G\alpha_q$-IR. Images were analyzed from 20 (SP, 37°C) or 22 (SP, 4°C) cells.

Metabolic stability of tripartite probes. Membranes were prepared from mouse spinal cord as described (*54*), with final centrifugation at 40,000 *g*. Normal human cerebrospinal fluid was provided by Dr. Paul Myles, Alfred Hospital Melbourne. To assess stability, SP, Span, or Span-Chol (10 $\mu g.ml^{-1}$) was incubated with mouse spinal cord membranes (40 µg/ml protein) or human cerebrospinal fluid (0-4 h, 37°C), and then snap frozen. Proteins were precipitated using ACN. Samples were analyzed by LC/MS using a Waters Xevo TQ triple quadrupole mass spectrometer coupled to a Waters Acquity UPLC. Chromatographic separation of peptides was achieved on a Merck Millipore Chromolith RP-18e monolithic column (50 x 2 mm; mouse spinal membranes) or a Supelco Ascentis Express Peptide ES C18 column (50 x 2.1 mm, 2.7 µm particle size; human cerebrospinal fluid) using 0.05% formic acid in H_2O and ACN as solvents. Peptides were quantified using positive electrospray ionization by comparison to a calibration standard (10-20,000 ng/ml) and by Multiple Reaction Monitoring using an internal standard (6.25 ng/ml diazepam in 50% ACN-water).

Statistical analyses. Data are presented as mean±SEM, unless noted otherwise. Table S1 indicates the statistical tests and the cell replicates for each figure.

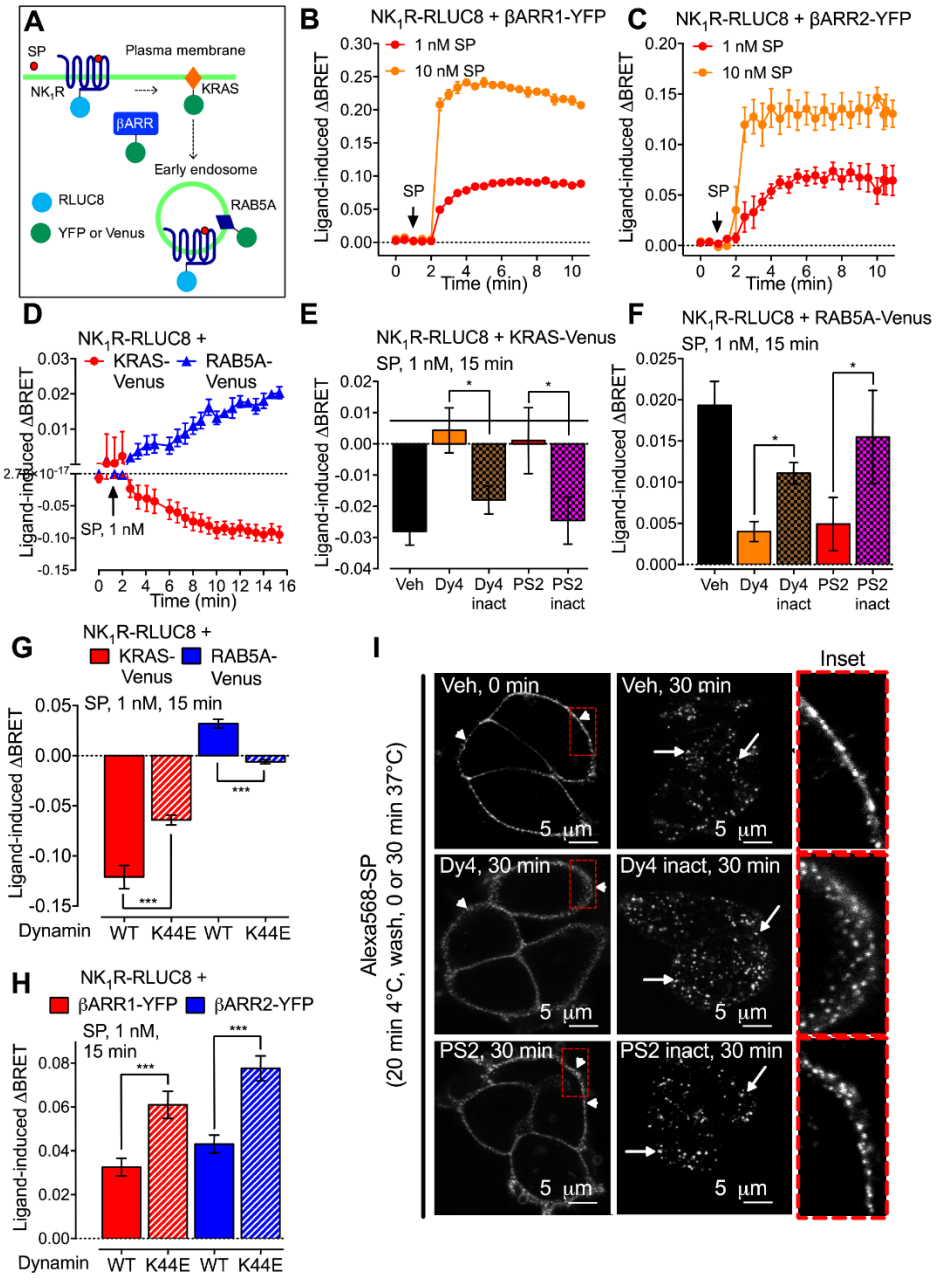
A
SP
Plasma membrane
NK1R
KRAS
βARR
Early endosome
RLUC8
RAB5A
YFP or Venus
B
NK1R-RLUC8 + βARR1-YFP
1 nM SP
10 nM SP
SP
Ligand-induced ΔBRET
Time (min)
C
NK1R-RLUC8 + βARR2-YFP
1 nM SP
10 nM SP
SP
Ligand-induced ΔBRET
Time (min)
D
NK1R-RLUC8 +
KRAS-Venus
RAB5A-Venus
SP, 1 nM
Ligand-induced ΔBRET
Time (min)
E
NK1R-RLUC8 + KRAS-Venus
SP, 1 nM, 15 min
Ligand-induced ΔBRET
Veh
Dy4
Dy4 inact
PS2
PS2 inact
F
NK1R-RLUC8 + RAB5A-Venus
SP, 1 nM, 15 min
Ligand-induced ΔBRET
Veh
Dy4
Dy4 inact
PS2
PS2 inact
G
NK1R-RLUC8 +
KRAS-Venus
RAB5A-Venus
SP, 1 nM, 15 min
Ligand-induced ΔBRET
Dynamin
WT
K44E
WT
K44E
H
NK1R-RLUC8 +
βARR1-YFP
βARR2-YFP
SP, 1 nM, 15 min
Ligand-induced ΔBRET
Dynamin
WT
K44E
WT
K44E
I
Inset
Alexa568-SP
(20 min 4°C, wash, 0 or 30 min 37°C)
Veh, 0 min
Veh, 30 min
Dy4, 30 min
Dy4 inact, 30 min
PS2, 30 min
PS2 inact, 30 min
5 μm

Fig. S1. Clathrin- and dynamin-dependent NK_1R endocytosis. A. Schematic of BRET assays for βARR recruitment and NK_1R trafficking. **B** to **D.** SP (1 or 10 nM) -induced changes in BRET between NK_1R-RLUC8 and βARR1-YFP (**B**), βARR2-YFP (**C**), KRAS-Venus (**D**), or RAB5A-Venus (**D**) in HEK293 cells. **E** to **H.** Effects of inhibitors of dynamin (Dyngo4a; Dy4) or clathrin (Pitstop-2; PS2), inactive (inact) analogues, or dominant negative dynamin K44E (K44E) and wild-type (WT) dynamin on SP-induced changes in BRET between NK_1R-RLUC8 and KRas-Venus (**E** and **G**), or RAB5A-Venus (**F** and **G**), or βARR2-YFP (**H**) at 15 min. **I.** Alexa568-SP endocytosis in HEK-NK_1R cells preincubated with vehicle (Veh), Dy4, PS2, or inactive analogues. Arrowheads, cell surface; arrows, endosomes. **P*<0.05, ***P*<0.01, ****P*<0.001. Triplicate observations, *N*≥3 experiments. ANOVA, Dunnett's test (E-H).

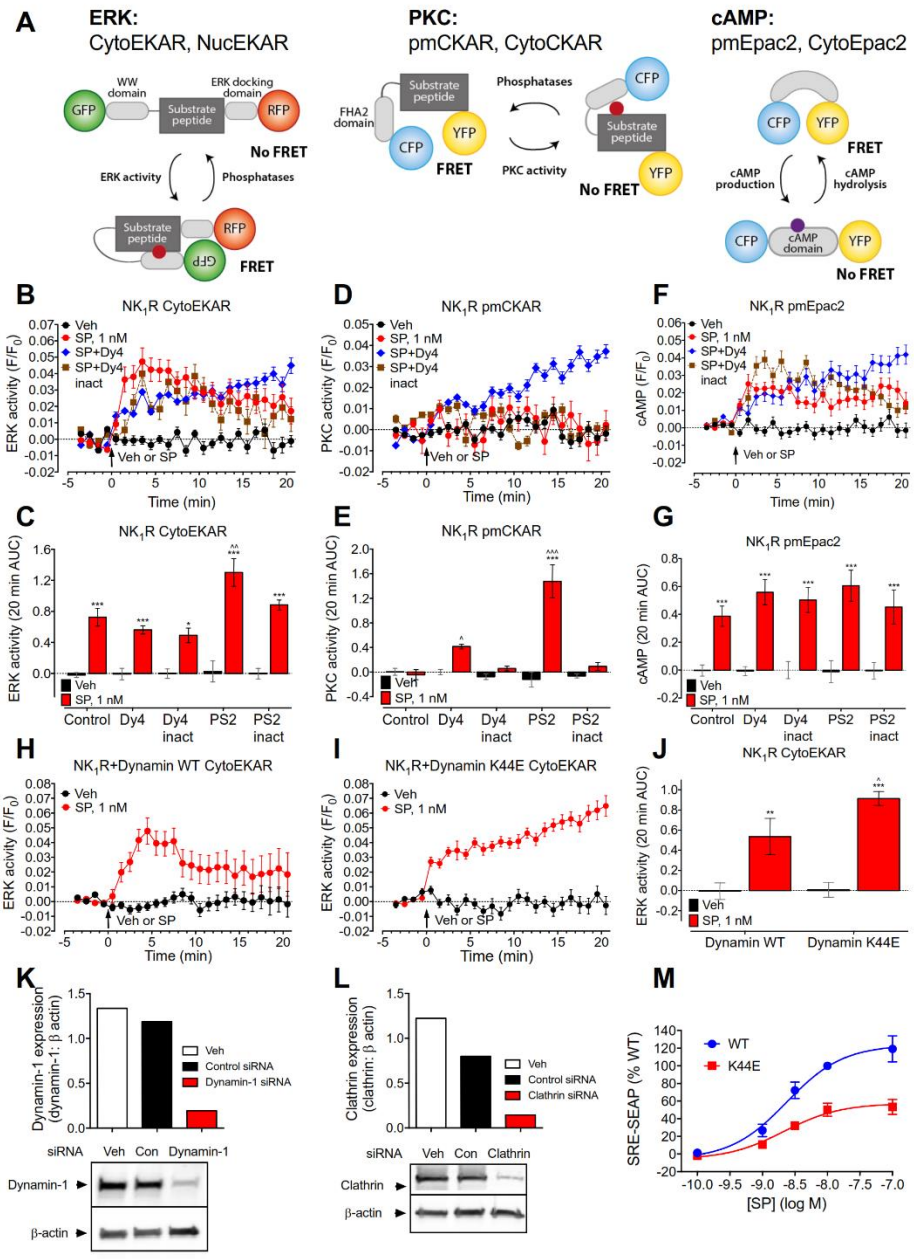
A
ERK:
CytoEKAR, NucEKAR
WW domain
ERK docking domain
GFP
Substrate peptide
RFP
No FRET
ERK activity
Phosphatases
FRET
PKC:
pmCKAR, CytoCKAR
FHA2 domain
Phosphatases
PKC activity
cAMP:
pmEpac2, CytoEpac2
cAMP production
cAMP hydrolysis
cAMP domain
B
NK1R CytoEKAR
ERK activity (F/F0)
Veh
SP, 1 nM
SP+Dy4
SP+Dy4 inact
Veh or SP
Time (min)
D
NK1R pmCKAR
PKC activity (F/F0)
F
NK1R pmEpac2
cAMP (F/F0)
C
ERK activity (20 min AUC)
Control
Dy4
Dy4 inact
PS2
PS2 inact
E
PKC activity (20 min AUC)
G
cAMP (20 min AUC)
H
NK1R+Dynamin WT CytoEKAR
I
NK1R+Dynamin K44E CytoEKAR
J
Dynamin WT
Dynamin K44E
K
Dynamin-1 expression (dynamin-1: β actin)
Control siRNA
Dynamin-1 siRNA
siRNA
Veh
Con
Dynamin-1
β-actin
L
Clathrin expression (clathrin: β actin)
Clathrin siRNA
Clathrin
M
SRE-SEAP (% WT)
WT
K44E
[SP] (log M)

Fig. S2. NK_1R compartmentalized signaling. A. Schematic of FRET biosensors for cytosolic (CytoEKAR) and nuclear (NucEKAR) ERK, plasma membrane (pmCKAR) and cytosolic (CytoCKAR) PKC, and plasma membrane (pmEpac2) and cytosolic (CytoEpac2) cAMP. **B** to **J.** FRET assays of compartmentalized signaling in HEK293 cells. **B** and **C.** Cytosolic ERK. **D** and **E.** Plasma membrane PKC. **F** and **G.** Plasma membrane cAMP. **B** to **F.** Effect of dynamin (Dy4) and clathrin (PS2) inhibitors and inactive (inact) analogues on the spatiotemporal profile of SP-induced signals. **C** to **G.** Area under the curve (AUC) analysis of data from **B** to **I.** Effect of dynamin WT (**H**) or dominant negative dynamin K44E (**I**) on the spatiotemporal profile of SP-induced activation of cytosolic ERK. **J.** AUC of **H** to **L.** siRNA knockdown of dynamin-1 (**K**) and clathrin heavy chain (**L**) (Western blots) in HEK293 cells. **M.** Effect of dynamin WT or dominant negative dynamin K44E on SRE-SEAP release 24 h after stimulation with graded concentrations of SP. **P*<0.05, ***P*<0.01, ****P*<0.001 SP to vehicle; ^*P*<0.05, ^^*P*<0.01, ^^^*P*<0.001 inhibitors to control. B-J, 16 to 354 cells, 3 experiments. ANOVA, Tukey's test (C, E, G); Sidak's test (J).

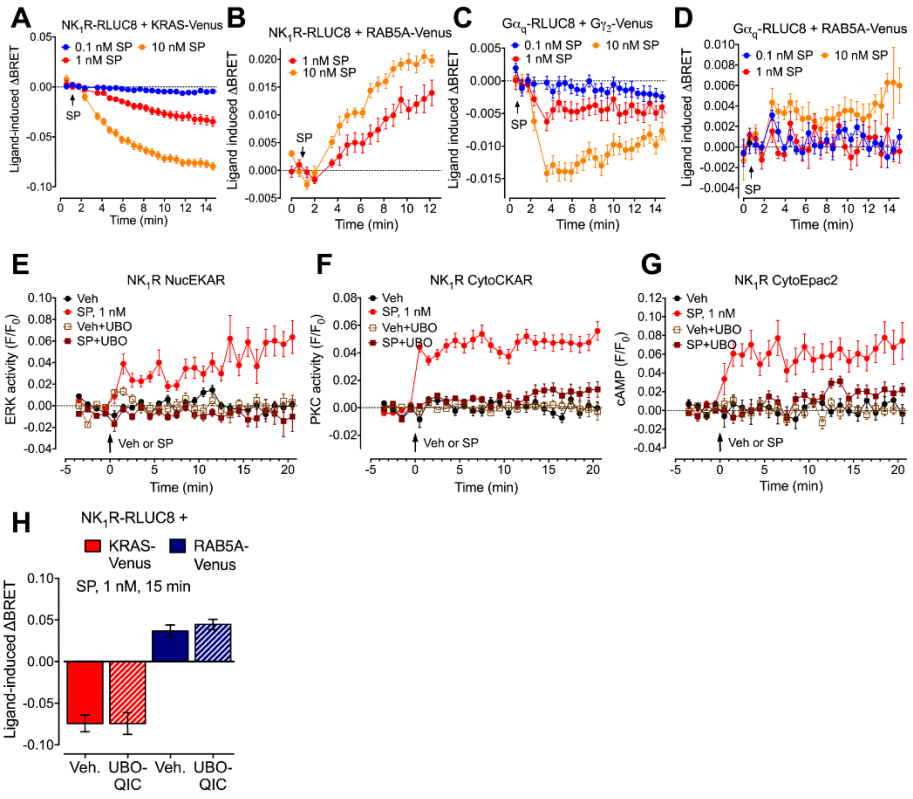

Fig. S3. G protein–dependent NK_1R signaling in endosomes. A to **D.** SP-induced BRET between NK_1R-RLUC8 and KRas-Venus (**A**) or RAB5A-Venus (**B**), and between $G\alpha_q$-RLUC8 and $G\gamma_2$-Venus (**C**) or RAB5A-Venus (**D**) in HEK293 cells. Triplicate observations, $N \geq 3$ experiments. **E** to **G.** Effect of $G\alpha_q$ inhibitor (UBO-QIC, UBO) on SP-induced spatiotemporal profiles of nuclear ERK (NucEKAR, **E**), cytosolic PKC (CytoCKAR, **F**), and cytosolic cAMP (CytoEpac2, **G**) measured in HEK293 cells using FRET biosensors. 35-67 cells, 3 experiments. **H.** SP-induced changes in BRET between NK_1R-RLUC8 and KRas-Venus or RAB5A-Venus in the absence (Veh) or presence of the $G\alpha_q$ inhibitor UBO-QIC.

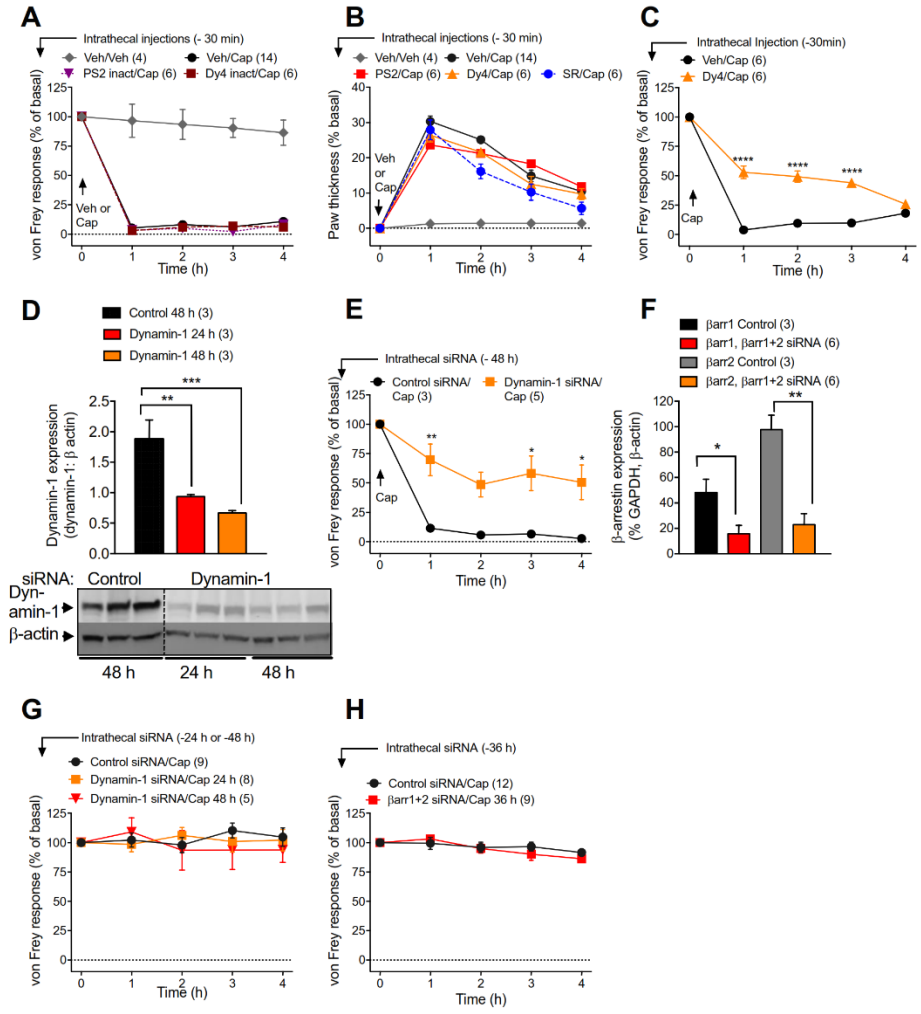

Fig. S4. Nociception and inflammation in vivo. A to **E.** von Frey withdrawal responses of capsaicin-injected paw after intrathecal injection of indicated inhibitors or inactive controls. **B.** Thickness of the capsaicin-injected paw after intrathecal injection of indicated inhibitors or inactive controls. **D** and **F.** Validation of siRNA knockdown of dynamin-1 (**D**, Western blot) and

βARR1+2 (**F,** qPCR) in the spinal cord. **G** and **H.** von Frey withdrawal responses of contralateral paw after siRNA knockdown of dynamin (**G**) or βARR1+2 (**H**). **P*<0.05, ***P*<0.01, ****P*<0.001, *****P*<0.0001 to control. All experiments were in mice except C, which was in rats. (*N*) animal number. ANOVA, Dunnett's test (A-C, E, G-H); Student's t test (D, F).

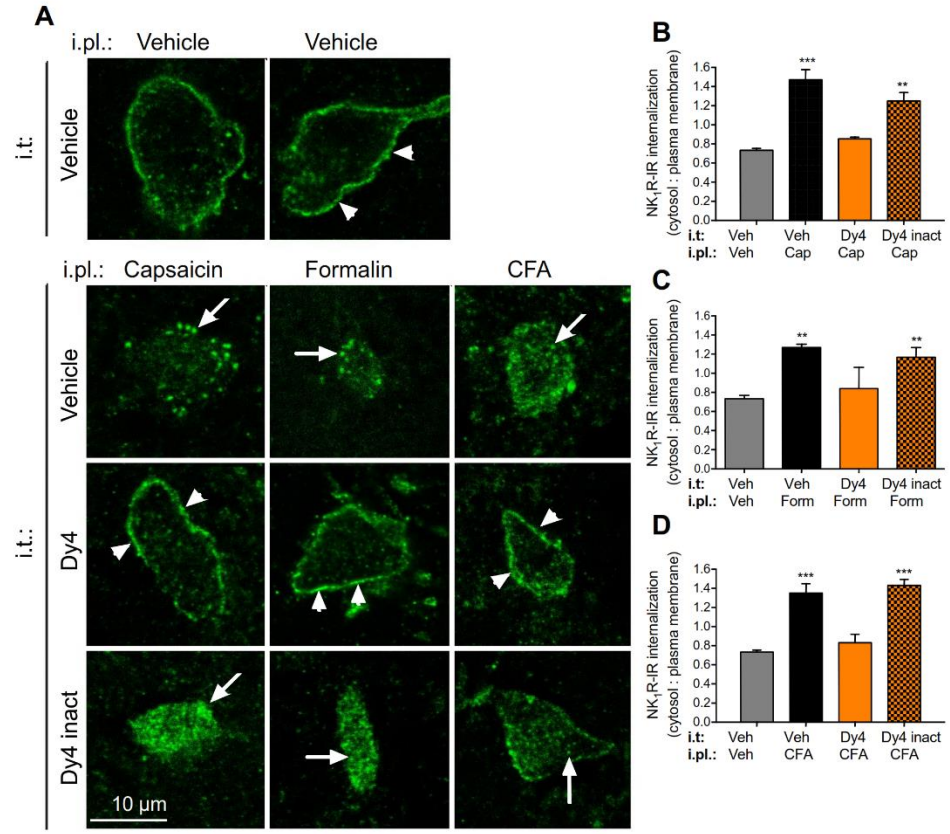

Fig. S5. NK$_1$R endocytosis in spinal neurons in vivo. A. NK$_1$R-IR localization in mouse spinal cord, 30 min after intraplantar (i.pl.) capsaicin, 90 min after intraplantar formalin, and 40 h after intraplantar CFA. Vehicle, Dy4, or Dy4 inact was injected intrathecally (i.t.) 30 min before intraplantar injection of capsaicin or formalin, or 36 h after intraplantar injection of CFA. Arrowheads, cell surface; arrows, endosomes. **B** to **D**. Cytosolic:plasma membrane NK$_1$R-IR in mouse spinal neurons. ***P*<0.01, ****P*<0.001 to vehicle. 18 neurons per condition (6 neurons from *N*=3 mice). Student's t test (B-D).

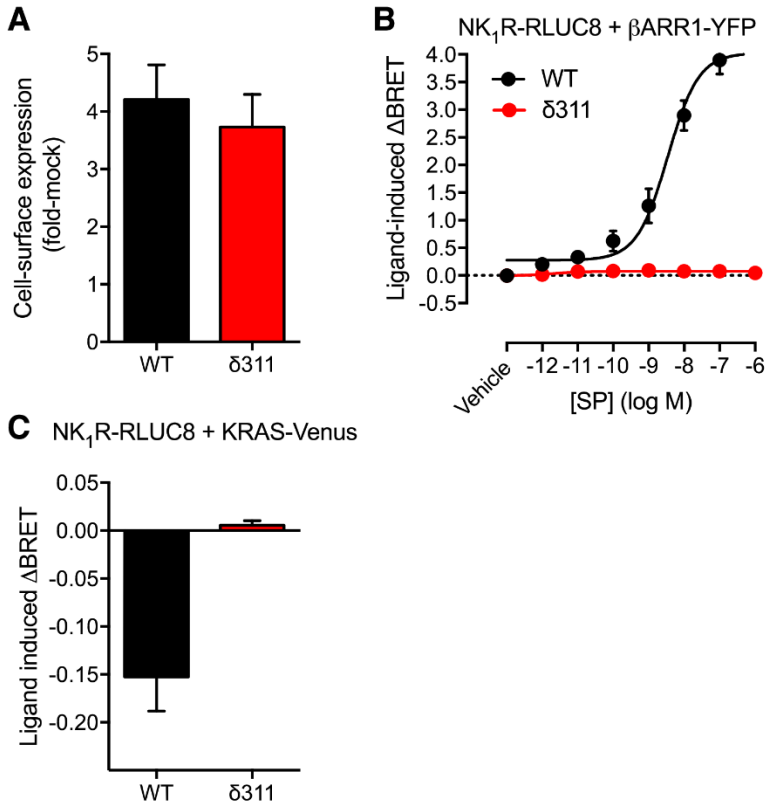

Fig. S6. NK$_1$Rδ311 expression and trafficking. A. Cell-surface ELISA of wild-type (WT) NK$_1$R and NK$_1$Rδ311 in HEK293 cells. **B** and **C.** SP-induced BRET between WT NK$_1$R-RLUC8 or NK$_1$Rδ311-RLUC8 and βARR1-YFP (**B**) or KRas-Venus (**C**). Triplicate observations, $N \geq 3$ experiments.

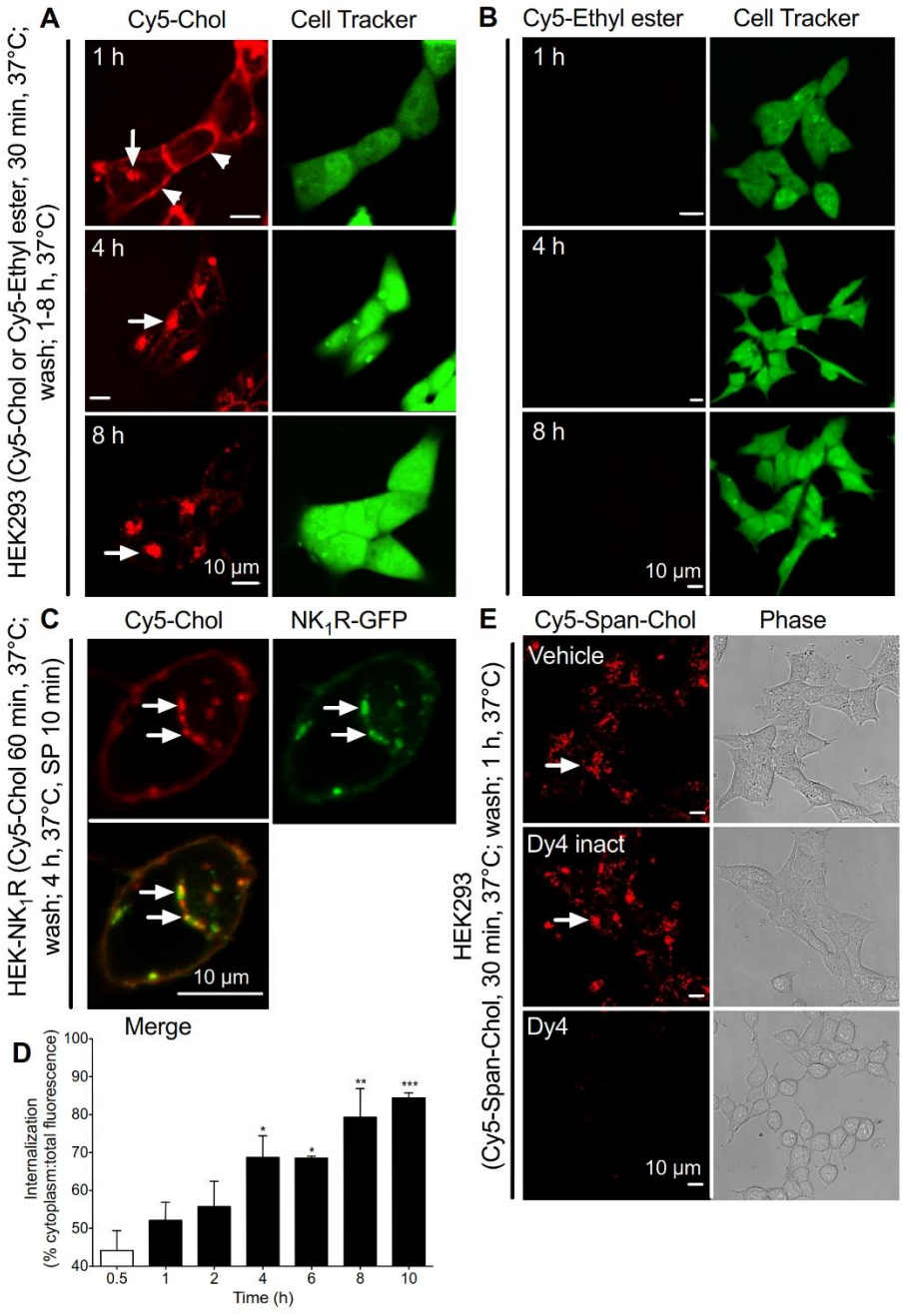
A
Cy5-Chol
Cell Tracker
1 h
4 h
8 h
10 µm
HEK293 (Cy5-Chol or Cy5-Ethyl ester, 30 min, 37°C; wash; 1-8 h, 37°C)
B
Cy5-Ethyl ester
Cell Tracker
1 h
4 h
8 h
10 µm
C
Cy5-Chol
NK1R-GFP
Merge
10 µm
HEK-NK1R (Cy5-Chol 60 min, 37°C; wash; 4 h, 37°C, SP 10 min)
D
Internalization (% cytoplasm:total fluorescence)
100
90
80
70
60
50
40
0.5
1
2
4
6
8
10
Time (h)
*
*
**
***
E
Cy5-Span-Chol
Phase
Vehicle
Dy4 inact
Dy4
10 µm
HEK293 (Cy5-Span-Chol, 30 min, 37°C; wash; 1 h, 37°C)

Fig. S7. Uptake of tripartite probes. A and **B.** Time course of Cy5-Chol (**A**) and Cy5-Ethyl ester (**B**) uptake into HEK293 cells. HEK293 cells were pulse-incubated with tripartite probes for 30 min, washed, and imaged at 1, 4, or 8 h after washing. Arrow heads, plasma membrane Cy5-Chol; arrows, internalized Cy5-Chol. **C.** Colocalization of Cy5-Chol and NK_1R-GFP. HEK-NK_1R cells were pulse-incubated with Cy5-Chol for 60 min, washed, and recovered for 4 h. Cells were then challenged with SP to induce NK_1R endocytosis. Arrows, colocalization of Cy5-Chol and NK_1R-GFP. **D.** Quantification of Cy5-Chol uptake. Cells were pulse-incubated with Cy5-Chol (as in A), washed, and recovered for 1-10 h. Cy5-Chol uptake was quantified. **P*<0.05, ***P*<0.001 to control. 6-9 cells, *N*=3 experiments. **E.** Effect of Dy4 and Dy4 inact on Cy5-Span-Chol uptake. Cells were pulse-incubated with Cy5-Span-Chol (as in A), washed, and recovered for 1 h. Arrows, Cy5-Chol in endosomes. ANOVA, Dunnett's test (D).

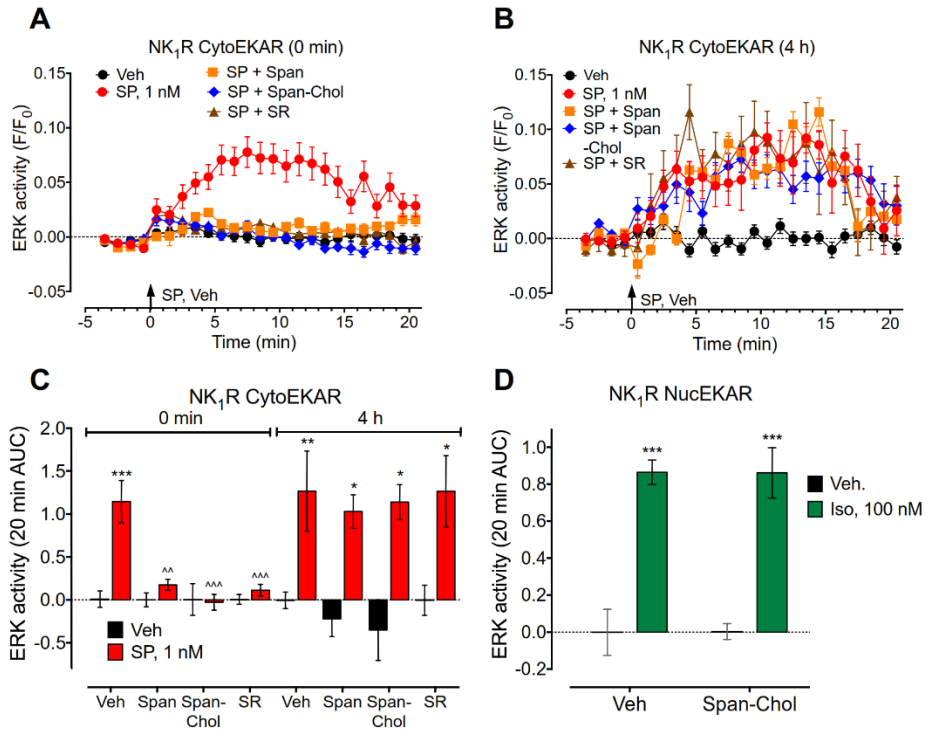

Fig. S8. Effects of NK$_1$R tripartite antagonists on ERK signaling. A to **C.** FRET assays for cytosolic ERK (CytoEKAR) immediately after (**A**, 0 min) or 4 h after (**B**, 4 h) 30 min preincubation with Span, Span-Chol, or SR140333 (SR). **C**. AUC for A and B. **D.** Effect of 4 h incubation with Span-Chol on the nuclear ERK response of endogenously expressed β_2AR. Iso, isoproterenol. **P*<0.05, ***P*<0.01, ****P*<0.001 SP to vehicle; ^^*P*<0.01, ^^^*P*<0.001 antagonist to control. 31-333 cells, 3 experiments. ANOVA, Tukey's test (C, D).

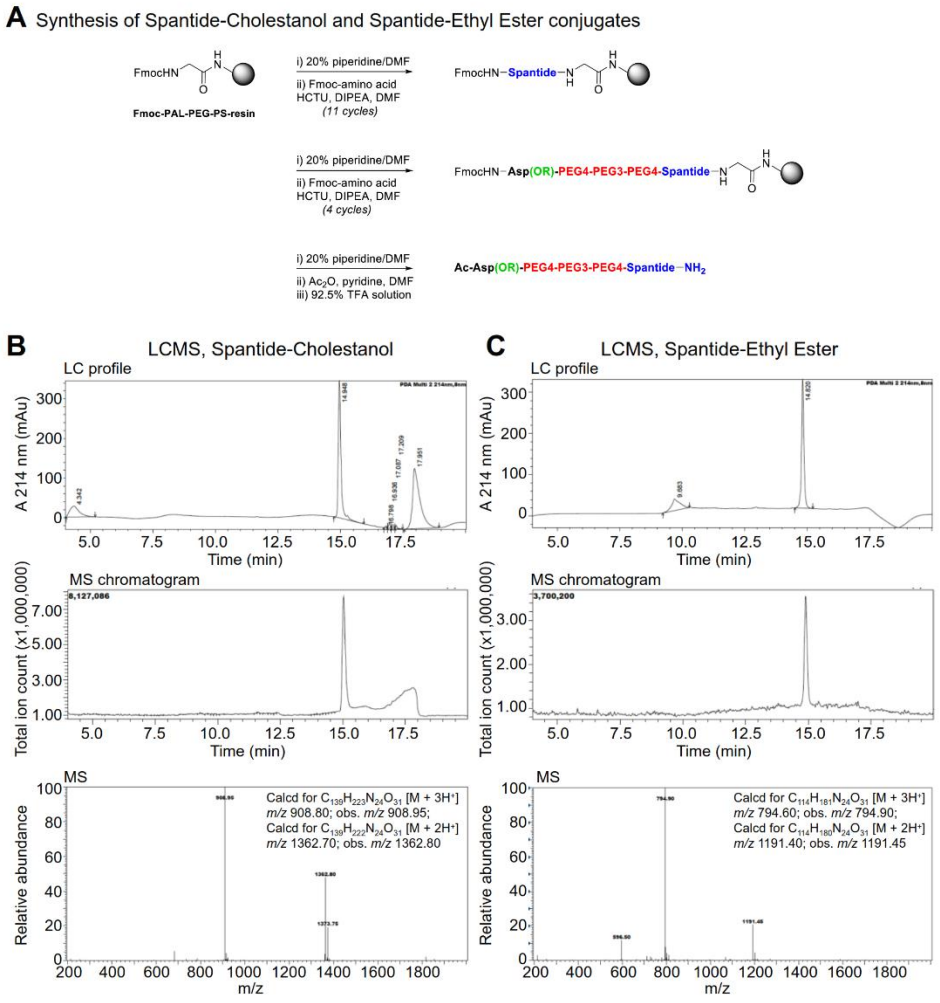

Fig. S9. Synthesis and analysis of Span-Chol and Span–ethyl ester. A. Synthesis of tripartite probes. **B.** LCMS analysis of Span-Chol. Peaks at t_R 4.34 and 17.95 min in the LC profile reflect changes in the baseline of the LC-MS gradient, as confirmed by injection of a blank solvent sample using the same method. **C.** LCMS analysis of Span-Ethyl ester. The peak at t_R 9.68 min

in the LC profile reflects changes in the baseline of the LC-MS gradient, as confirmed by injection of a blank solvent sample using the same method.

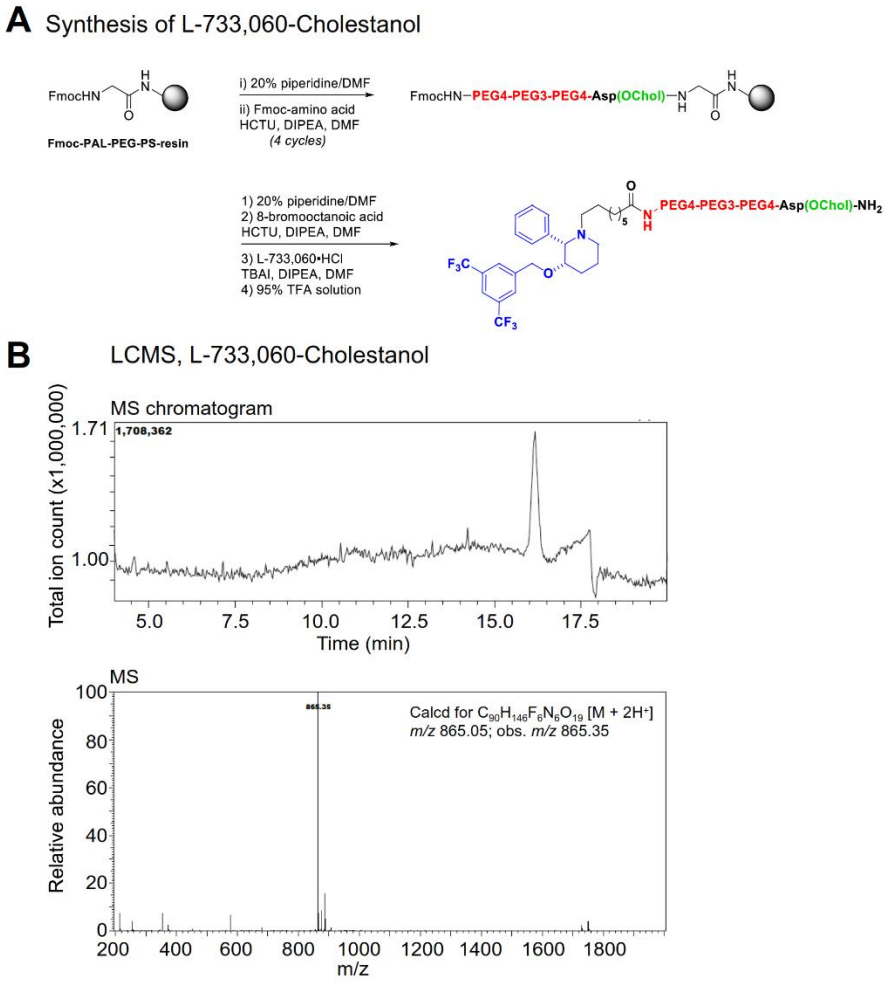

Fig. S10. Synthesis and analysis of L-733,060-Chol. A. Synthesis of tripartite probe. **B.** LCMS analysis. A UV spectrum for L-733,060-Chol could not be obtained because the absorbance of the construct was very low at both 214 and 254 nm, and the dominant peaks obtained were from the diluent buffer. The total ion trace (TIC) by MS is provided.

Table S1. Statistical analyses and cell replicates.

Figure	Test	Cell Number
Fig. 1 C, F, I, N	2-way ANOVA with Tukey's test	30-354 cells
Fig. 1 L	2-way ANOVA with Sidak's test	30-354 cells
Fig. 1 O	1-way ANOVA with Dunnett's test	Population based assay, N=3 experiments
Fig. 2 A-D	1-way ANOVA with Dunnett's test	Population based assay, $N \geq 3$ experiments
Fig. 2 F	1-way ANOVA with Sidak's test	60-66 cells
Fig. 2 G	2-way ANOVA with Sidak's test	35-67 cells
Fig. 2 H, I	2-way ANOVA with Tukey's test	35-67 cells
Fig. 3 B	2-way ANOVA with Tukey's test	6 neurons / animal / group
Fig. 3 D, G	2-way ANOVA with Sidak's test	6-7 neurons / animal / group
Fig. 3 E, H	1-way ANOVA with Dunn's test	6-7 neurons / animal / group
Fig. 4 C, D	Student's t-test unpaired	3 rats, ≥6 neurons or fields / rat
Fig. 4 E-M	1-way ANOVA with Dunnett's test	
Fig. 5 D	2-way ANOVA with Sidak's test	44-99 cells
Fig. 5 G	2-way ANOVA with Sidak's test	Population based assay, N=3 experiments
Fig. 5 H-J	1-way ANOVA with Dunnett's test	
Fig. 6 H	2-way ANOVA with Sidak's test	31-417 cells
Fig. 7 B	2-way ANOVA with Sidak's test	6-7 neurons / group
Fig. 7 C	1-way ANOVA with Dunn's test	6-7 neurons / group
Fig. 7 E-J	1-way ANOVA with Dunnett's test	

Supplementary Figures

Figure	Test	Cell Number
Fig. 1 E-H	1-way ANOVA with Dunnett's test	Population based assay, N=3 experiments
Fig. 2 C, E, G	2-way ANOVA with Tukey's test	16-354 cells
Fig. 2 J	2-way ANOVA with Sidak's test	16-354 cells
Fig. 4 A-C, E, G-H	1-way ANOVA with Dunnett's test	
Fig. 4 D, F	Student's T-test unpaired	
Fig. 5 B-D	Student's t-test unpaired	6 neurons / group
Fig. 7 D	1-way ANOVA with Dunnett's test	6-9 cells
Fig. 8 C, D	2-way ANOVA with Tukey's test	31-333 cells

Movie S1. Three-dimensional projections of NK_1R-IR in neurons in spinal cord slices incubated with Dy4 inact and vehicle. 3D projections of confocal images showing localization of NK_1R-IR in lamina I neurons in dorsal horn of rat spinal cord slices. Slices of spinal cord were preincubated with Dy4 inact (10 min), then incubated with vehicle (5 min), and fixed. Neurons from 3 animals are shown.

Movie S2. Three-dimensional projections of NK_1R-IR in neurons in spinal cord slices incubated with Dy4 inact and SP. 3D projections of confocal images showing localization of NK_1R-IR in lamina I neurons in dorsal horn of rat spinal cord slices. Slices of spinal cord were preincubated with Dy4 inact (10 min), then incubated with SP (1 μM, 5 min), and fixed. Neurons from 3 animals are shown.

Movie S3. Three-dimensional projections of NK_1R-IR in neurons in spinal cord slices incubated with Dy4 and vehicle. 3D projections of confocal images showing localization of NK_1R-IR in lamina I neurons in dorsal horn of rat spinal cord slices. Slices of spinal cord were preincubated with Dy4 (10 min), then incubated with vehicle (5 min), and fixed. Neurons from 3 animals are shown.

Movie S4. Three-dimensional projections of NK_1R-IR in neurons in spinal cord slices incubated with Dy4 and SP. 3D projections of confocal images showing localization of NK_1R-IR in lamina I neurons in dorsal horn of rat spinal cord slices. Slices of spinal cord were preincubated with Dy4 (10 min), then incubated with and SP (1 μM, 5 min), and fixed. Neurons from 3 animals are shown.

Movie S5. Three-dimensional projections of NK_1R-IR in neurons in spinal cord 10 min after intraplantar injection of vehicle. 3D projections of confocal images showing localization

of NK_1R-IR in lamina I neurons in dorsal horn of rat spinal cord. Tissues were collected 10 min after intraplantar injection of vehicle. Neurons from 3 animals are shown.

Movie S6. Three-dimensional projections of NK_1R-IR in neurons in spinal cord 10 min after intraplantar injection of capsaicin. 3D projections of confocal images showing localization of NK_1R-IR in lamina I neurons in dorsal horn of rat spinal cord. Tissues were collected 10 min after intraplantar injection of capsaicin. Neurons from 3 animals are shown.

Movie S7. Three-dimensional projections of NK_1R-IR in neurons in spinal cord 10 min after intraplantar injection of capsaicin, with Dy4 injected before capsaicin. 3D projections of confocal images showing localization of NK_1R-IR in lamina I neurons in dorsal horn of rat spinal cord. Tissues were collected 10 min after intraplantar injection of capsaicin. Dy4 was administered intrathecally 30 min before intraplantar capsaicin. Neurons from 3 animals are shown.

Movie S8. Three-dimensional projections of NK_1R-IR in neurons in spinal cord 10 min after intraplantar injection of capsaicin, with Dy4 inact injected before capsaicin. 3D projections of confocal images showing localization of NK_1R-IR in lamina I neurons in dorsal horn of rat spinal cord. Tissues were collected 10 min after intraplantar injection of capsaicin. Dy4 inact was administered intrathecally 30 min before intraplantar capsaicin. Neurons from 3 animals are shown.

Movie S9. Three-dimensional projections of NK_1R-IR in neurons in spinal cord 10 min after intraplantar injection of capsaicin, with PS2 injected before capsaicin. 3D projections of confocal images showing localization of NK_1R-IR in lamina I neurons in dorsal horn of rat spinal cord. Tissues were collected 10 min after intraplantar injection of capsaicin. PS2 was

administered intrathecally 30 min before intraplantar capsaicin. Neurons from 3 animals are shown.

Movie S10. Three-dimensional projections of NK_1R-IR in neurons in spinal cord 10 min after intraplantar injection of capsaicin, with PS2 inact injected before capsaicin. 3D projections of confocal images showing localization of NK_1R-IR in lamina I neurons in dorsal horn of rat spinal cord. Tissues were collected 10 min after intraplantar injection of capsaicin. PS2 inact was administered intrathecally 30 min before intraplantar capsaicin. Neurons from 3 animals are shown.

Movie S11. Plasma membrane incorporation and endocytosis of Cy5-cholestanol by HEK293 cells. Time lapse images showing plasma membrane incorporation and endocytosis of Cy5-cholestanol by HEK293 cells at 37°C. Cy5-cholestanol was added at 0 min.

Movie S12. Lack of uptake of Cy5–ethyl ester by HEK293 cells. Time lapse images showing lack of uptake of Cy5-ethyl ester by HEK293 cells at 37°C. Cy5-ethyl ester was added at 0 min.

Movie S13. Time lapse images showing FRET between SNAP-549-NK_1R and Cy5-Chol. Time lapse images showing FRET between SNAP-549-NK_1R and Cy5-cholestanol. SNAP-549-NK_1R was internalized by SP (10 nM, 30 min), and Cy5-cholestanol was added at 0 min. Scale, 10 μm.

Movie S14. Animation showing SP-induced assembly of endosomal signaling platform for pain transmission.

Part II: Lipidation improves antagonist potency and the inhibition of NK_1R signalling in endosomes

Quynh N. Mai,[a, c] Tim Quach,[b, d] Priyank Shenoy,[a, c] Jeffri Retamal-Santibanez,[a, c] Holly R. Yeatman[1], Luigi Aurelio,[b, c] Josh W. Conner,[b] Meritxell Canals,[a, f] Bimbil Graham[b], Stephen J. Briddon,[e] Stephen J. Hill, [e] Christopher J. Porter,[a ,c, d] Nigel W. Bunnett,[a, f, g, h], Michelle L. Halls[a, c*], and Nicholas A. Veldhuis[a,c *]

a. Drug Discovery Biology, Monash Institute of Pharmaceutical Sciences, Monash University, Parkville, Victoria 3052, Australia
b. Medicinal Chemistry, Monash Institute of Pharmaceutical Sciences, Monash University, Parkville, Victoria 3052, Australia
c. ARC Centre of Excellence in Convergent Bio-Nano Science and Technology, Monash Institute of Pharmaceutical Sciences, Monash University, Parkville, Victoria 3052, Australia
d. Drug Delivery Disposition and Dynamics, Monash Institute of Pharmaceutical Sciences, Monash University, Parkville, Victoria 3052, Australia
e. Cell Signalling Research Group, School of Life Sciences, The University of Nottingham Medical School, Nottingham, UK
f. Department of Pharmacology and Therapeutics, University of Melbourne, Parkville, VIC 3010, Australia
g. Department of Surgery, Columbia University, New York, NY 10032
h. Department of Pharmacology, Columbia University, New York, NY 10032

2.1 Abstract

Stimulation of some G protein-coupled receptors (GPCRs) can lead to rapid phosphorylation and β-arrestin-mediated recruitment to endosomes. While endocytosis events were historically considered to terminate signalling by directing GPCRs to recycling or degradative pathways, recent investigations demonstrate that GPCRs can remain in G protein or β-arrestin complexes to promote sustained signalling from endosomal compartments. Substance P (SP)-dependent stimulation of the Neurokinin 1 receptor (NK_1R) and β-arrestin-mediated internalisation is essential for the complete SP-NK_1R signalling repertoire. Furthermore, endosomal signalling is required for pathophysiologically relevant processes such as pain transmission. The endosomal NK_1R population is therefore proposed to be a distinct therapeutic target. To target endosomal receptors, we recently conjugated a soluble NK_1R peptide antagonist Spantide I to cholestanol, a sterol-based lipid-anchor, to promote membrane association and internalisation. Spantide-cholestanol (Span-Chol) enhances the inhibition of endosomal signalling and analgesia, but the mechanisms through which lipidated compounds inhibit endosomal signalling has not been investigated in detail. In this study, the potential for lipidated antagonists to regulate receptor trafficking and spatiotemporal NK_1R signalling was assessed using live cell imaging, biophysical approaches and nociceptive behavioural assays. While the soluble antagonist Spantide targets short-term inhibition of cell surface processes, lipid-conjugation provides sustained inhibition of β-arrestin coupling, plasma membrane-delimited signalling, and selective inhibition NK_1R endosomal-derived nuclear ERK activity and cytosolic cAMP production. Nociceptive assays demonstrate that Span-Chol, but not a Cholestanol-PEG conjugate, offers sustained analgesia. These studies demonstrate that membrane-anchoring enhances the

intracellular drug distribution of GPCR antagonists for sustained inhibition of endosomal receptor signalling and pain transmission.

2.2 Introduction

G protein-coupled receptors (GPCRs) mediate cell signalling processes that are influenced by intracellular localisation and hence, dysregulation of receptor localisation or trafficking can contribute to pathophysiological states (Arora *et al.,* 2007, Nikolaev *et al.,* 2010). The canonical view of the GPCR signalling-trafficking relationship suggests GPCRs are internalised as a mechanism to arrest signalling leading to desensitisation by lysosomal-mediated receptor degradation, or receptor resensitisation following recruitment into recycling endosomes (Pierce *et al.,* 2002, Sorkin *et al.,* 2009). The development of sensitive biophysical tools to measure receptor trafficking and spatiotemporal cellular signalling has revealed that stimulated, internalised GPCRs can form distinct G protein or βArr signalling complexes and continue to signal from intracellular locations such as the endosomal network (Luttrell 1999, Slessareva *et al.,* , Sorkin *et al.,* 2009, Jensen *et al.,* 2017). Furthermore, we and others have demonstrated that endosomal-mediated signalling processes are required for unique and physiologically important processes (Nikolaev *et al.,* 2004, Calebiro *et al.,* 2009, Murphy *et al.,* 2009, Irannejad *et al.,* 2013, Yarwood *et al.,* 2017). Endosomes are therefore recognised as spatially and temporally distinct signalling platforms and should be considered as distinct therapeutic targets (12).

Limited drug accessibility to internalised receptors may explain why some antagonists show a high level of selectivity and potency in cell-based assays, but very poor clinical outcomes in pathophysiological states. This may be the case for the Neurokinin 1 Receptor (NK_1R) where attempts to use antagonists to treat pain in humans have failed (Goldstein *et al.,* 1997, Dionne *et*

al., 1998, Diener 2003). The NK_1R is a GPCR of the tachykinin family that is expressed in human central neurons of the dorsal horn, endothelia, vascular smooth muscle and the gastrointestinal tract and performs critical roles in nociception, cognition and inflammation (Greeno *et al.,* 1993, Renzi *et al.,* 2000, Hargreaves 2002, Caberlotto *et al.,* 2003, Pinto *et al.,* 2004, Steinhoff *et al.,* 2014). Noxious stimuli result in the release of Substance P (SP), an endogenous neuropeptide, from peripheral and central projections of primary afferent neurons. In the periphery, SP stimulates NK_1R signalling at the site of injury to promote oedema and plasma extravasation (neurogenic inflammation). At central projections, pre-synaptic SP release from peripheral neurons leads to excitation of second order neurons of the spinal cord and central pain transmission.

Activation of the NK_1R results in distinct spatiotemporal signalling outcomes. At the plasma membrane SP-bound NK_1R activates $G\alpha_q$ to promote phospholipase C (PLC)-dependent formation of inositol triphosphate and diacylglycerol (DAG) and calcium mobilisation (Ca^{2+}). DAG and Ca^{2+} activate protein kinase C (PKC), a key signalling protein in the pain pathway, capable of activating signalling proteins and ion channels that regulate nerve excitation (Quartara *et al.,* 1997, Sorkin *et al.,* 2009, Pelayo *et al.,* 2014, Steinhoff *et al.,* 2014). SP-dependent NK_1R stimulation also leads to cell surface $G\alpha_q$-mediated adenylate cyclase (AC) activity and cAMP production, and transactivation of epidermal growth factor receptor (EGFR) to stimulate extracellular signal-regulated kinase (ERK) activity in the cytoplasm. SP-bound NK_1R is then rapidly phosphorylated and recruited into endosomes *via* βArr-mediated processes (Bowden *et al.,* 1994, Mantyh *et al.,* 1995). Within endosomes, the SP-NK_1R-$G\alpha_q$ complex stimulates sustained signalling of cytosolic cAMP, cytosolic PKC activity and recruitment of Src and MEKK to activate nuclear ERK, independently of EGFR (Cottrell *et al.,* 2009, Murphy *et al.,* 2009, Jensen *et al.,* 2014). Importantly, NK_1R signalling from internalised membranes in spinal neurons is strongly

associated with sustained mechanical and inflammatory pain transmission (Mantyh *et al.,* 1995, Zhang *et al.,* 2013).

We propose that the efficacy and selectivity of NK_1R antagonists for pathophysiologically relevant signalling may be improved by directing antagonists to the endosomes and have recently developed lipid-anchored NK_1R antagonists and fluorescent probes that can be directed to endosomal membranes (7). Inspired by prior lipid-drug conjugate optimisation studies, a series of constructs were synthesised, consisting of the sterol cholestanol as a lipid-conjugate for anchoring a pharmacophore to membranes *via* a flexible polyethylene glycol linker (PEG4-PEG3-PEG4). Cargo included the soluble fluorophore Cyanine 5 (Cy5) to generate a fluorescent lipid reporter (Cy5-Chol), or lipid-anchored NK_1R antagonist, Spantide I (Figure. 2.1). A non-lipidated control construct was also generated, consisting of Cy5 and PEG linker terminated with a soluble ethyl-ester group (Cy5-ethyl ester; Cy5-EE). Initial characterisation demonstrated that lipid-conjugation of NK_1R-selective antagonists *via* a PEG linker improves analgesic outcomes in mice relative to their unmodified, soluble counterparts. Moreover, cholestanol-conjugated Spantide (Spantide-PEG-Cholestanol; Span-Chol) selectively inhibited NK_1R-mediated nuclear ERK signalling, a pathway driven from endosomal NK_1R signalling complexes and critical for pain transmission (Jensen *et al.,* 2017). However, whether lipidated antagonists can inhibit other NK_1R endosomal-derived signalling processes (including cytosolic cAMP and cytosolic PKC activity) or directly influence NK_1R endocytosis remains unknown.

We have combined live cell imaging, biophysical techniques, cell signalling and trafficking, and behavioural pain assays to investigate the potential for cholestanol-anchored drugs to target established NK_1R signalling pathways initiated from endosomes. Cy5-Chol co-distributes with fluorescent-fusion organelle resident proteins of endocytic and secretory pathways, including

the plasma membrane and endosomes, where stimulated NK_1R resides. The lipidated antagonist Span-Chol has the potential to target NK_1R at the cell surface and in endosomes, leading to short-term inhibition of NK_1R-βArr coupling and endocytosis, and sustained inhibition of endosomal-selective NK_1R signalling pathways, including nuclear ERK activity and cytosolic cAMP production. Consistent with this, behavioural pain studies demonstrate that lipidation of Spantide prolongs the analgesic effect of the drug. This study reveals new insights about lipid-anchors for enhancing the membrane affinity of soluble GPCR antagonists and targeting endosome-derived signalling pathways of pathophysiological importance.

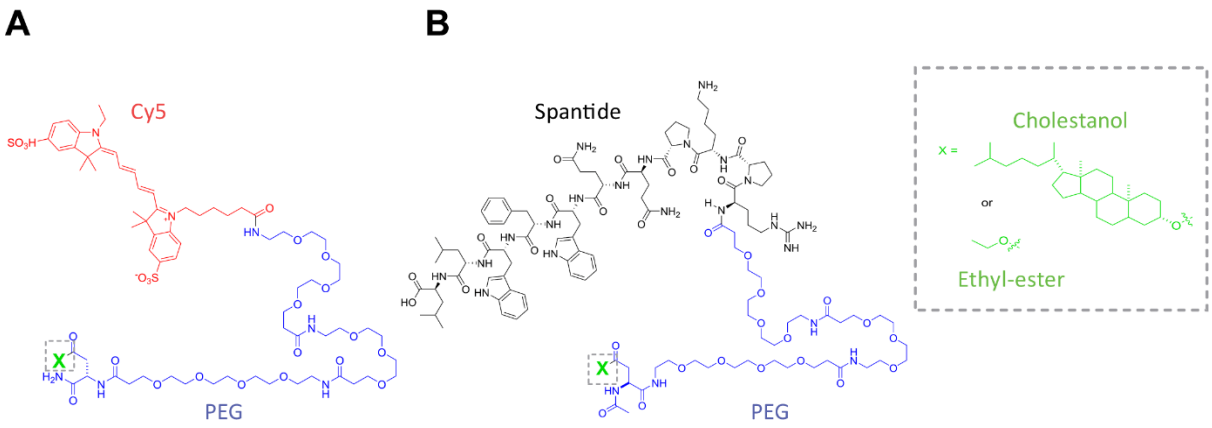

Figure 2.1 Tripartite compound structure. Tripartite compounds are comprised of soluble cargo, conjugated to cholestanol via a polyethylene glycol (PEG) chain. **A,** cy5 fluorescent reporter (red) conjugated via PEG (blue) to either ethyl ester or a lipid moiety, cholestanol (green, dashed box). **B,** Spantide 1 (black), conjugated to cholestanol (green), via a PEG linker (blue).

2.3 Methods

2.3.1 Synthesis

Synthesis of the tripartite ligands Spantide-Cholestanol, Cy5-Cholestanol and Cy5-Ethyl ester are as described previously (Jensen *et al.,* 2017). Tetramethylrhodamine (TAMRA)-labelled Substance P peptide (TAMRA-SP) was synthesised by GL Biochem (Shanghai, China).

2.3.2 cDNA

Rat NK_1R-GFP and HA-NK_1R have been described previously (Cattaruzza *et al.,* 2009, Jensen *et al.,* 2014). The cytoEKAR GFP/RFP (plasmid 18680) and nucEKAR GFP/RFP (plasmid 18682), and cytoCKAR (plasmid 14870) and pmCKAR (plasmid 14862) were obtained from Addgene (Cambridge, MA). CytoEpac2-camps was provided by M. Lohse (University of Wurzburg) and pmEpac2-camps was provided by D. Cooper (University of Cambridge) (Nikolaev *et al.,* 2004, Wachten *et al.,* 2010). NK1R-RLuc8, Venus-Arr, KRAS, Rab5 (Kocan *et al.,* 2011, Lan *et al.,* 2012) and SNAP-NK1R from Cisbio.

2.3.3 ***Cell lines, Transfection***

HEK293 cells were maintained in Dulbecco's modified Eagle's medium (DMEM) supplemented with 5% v/v FBS (37°C, 5% CO_2). HEK-FlpIn (human embryonic kidney cells) stably expressing rat HA-NK_1R (HEK-NK_1R) have been described (Cottrell *et al.,* 2007). HEK-NK_1R cells were maintained in DMEM supplemented with 10% v/v FBS and 100 µg/mL Hygromycin B (37°C, 5% CO_2). For FRET, HEK293 cells were plated into poly-D-lysine coated 96 well black-walled, optically clear plates for imaging by the InCell Analyzer or into 8-well Ibidi chamber slides for imaging by confocal. Cells were grown to 50% confluency in DMEM supplemented with 5% v/v

FBS and 100 U/mL penicillin and 100 µg/mL streptomycin. Cells were transiently transfected with 55 ng/well HA-NK_1R and 40 ng/well cytoEKAR, pmEpac2, cytoEpac2 or cytoCKAR using a 1:6 ratio of DNA to polyethylenimine (1 mg/mL; Polysciences, Warrington, PA). After 24 h, culture medium was replaced with serum restricted medium (DMEM supplemented with 0.5% v/v FBS and 100 U/mL penicillin and 100 µg/mL streptomycin) and FRET was assessed 48 h after transfection. For bioluminescence resonance energy transfer (BRET), HEK293 cells were transfected with 1 µg of NK_1R-RLuc8 and 4 µg β-arrestin 2-YFP, KRas-Venus or Rab5a-Venus. After 24 h, cells were plated in poly-D-lysine-coated 96 well CulturPlates (PerkinElmer).

2.3.4 Fluorescence Correlation Spectroscopy

Prior to each experiment, calibration was performed for the 633 nm laser line. Cy5 (GE healthcare, Buckingham, UK) was used to calibrate the 633 nm laser, diffusion coefficient of $3.16x10^{-10}$ m^2/s. (Schwille *et al.,* 1996, Schwille 2006, Poyner *et al.,* 2009). HEK cells stably expressing NK_1R-SNAP were plated into Nunc Lab-Tek 8-well coverglass (SLS, Nottingham, UK). Cy5-Chol and Cy5-EE were prepared in HBSS. Cells were incubated with 400 µL of each ligand at 37ºC. A reference fluorescent image of each cell was captured. A fluorescence intensity scan in the z direction was used to determine the plasma membrane and the focal point was positioned at intervals above the plasma membrane. FCS was recorded (ex λ: 633 nm HeNe, em λ: LP650 nm filter) for 20 sec, at an AOTF of 10 and a laser power of 60%, using a Zeiss LSM510Meta Confocor 3 microscope fitted with a c-Apochromat 40x NA 1.2 water immersion objective lens (Kilpatrick *et al.,* 2012). Autocorrelation analysis was performed with a 1 component, 3D Brownian model fit using Zeiss 2010 black software (Briddon *et al.,* 2007).

2.3.5 Fluorescent Competition Binding

HEK-ratNK_1R cells were plated into poly-D-lysine coated black-walled 96 well plates and grown to >80% confluence. Cells were treated with increasing concentrations of antagonist and an EC_{50} concentration (0.5 nM) of carboxy tetramethylrhodamine-labeled SP (SP-TAMRA). Cell nuclei were stained with Hoechst (1 µg/mL, 30 min, 37°C). Images were acquired using an ImageXpress Ultra confocal high-content plate reader (Molecular Devices, Sunnyvale, CA, USA) with Fluor 40 × NA0.6 objective. Cells were imaged using the 405 and 561 laser excitations for Hoechst and TAMRA, respectively. For each well, four fields of view were imaged. Images were analysed with MetaXpress 2.0 software (Molecular Devices), using an automated granularity module with the granule range set to 5-10 µm and intensity thresholds for granule classification set for each experiment based on the positive and negative controls. A nuclear count from the Hoechst 33342 image was obtained and the granularity analysis calculated the average intensity per cell (Kilpatrick *et al.,* 2010, Stoddart *et al.,* 2015).

2.3.6 Localisation of Cy5 Tripartite Compounds

For confocal imaging, HEK293 cells expressing endosomal markers and NK_1R-GFP were plated onto 30 mm poly-D-lysine coated coverslips and cultured to 60% confluency. Cells were transiently transfected with 1 µg/coverslip rat NK_1R-GFP using FuGene (Promega, Sydney, Australia) according to the manufacturer's instructions. To identify endosomal compartments, Rab5a-RFP or Rab7a-GFP fusion proteins were transiently expressed by transducing cells for 16 h with CellLight™ Bacmam 2.0 virus (Life Technologies, Mulgrave, Victoria). Lysosomes were labelled with lysosomal pH sensitive dye, LysoTracker green (Life Technologies). Cells were equilibrated in Hanks' Balanced Salt Solution (HBSS) for 30 min prior to imaging. Images were

obtained using a Leica TCS SP8 Laser-scanning confocal microscope with HCX PL APO 40x (NA 1.30) and HCX PL APO 63x (NA 1.40) oil objectives in a humidified and temperature-controlled chamber (37°C). Three baseline images were captured (4-6 optical sections) before addition of Cy5-Cholestanol (Cy5-Chol) or Cy5-ethyl ester (1.5 µM). Cells were imaged at time points indicated or imaged at 2 min intervals for 1 h. Cells expressing NK_1R-GFP were incubated with Cy5-Chol (1.5 µM, washout after 30 min incubation). Excess probe was removed by washing cells with HBSS and incubated with medium for 3 h. Cells were then stimulated with SP (10 nM, 10 min), washed with HBSS and incubated for 20 min before imaging. Imaging experiments were performed more than 3 times on different days with separate drug preparations.

2.3.7 Bioluminescence Resonance Energy Transfer

HEK293 cells were transiently transfected with NK_1R-RLuc and β-arrestin 2-YFP, KRas-Venus or Rab5a-Venus. Cells were incubated with antagonists for 4 h before the medium was replaced with HBSS and cells were equilibrated for 30 min at 37°C, or for 30 min in HBSS. Coelenterazine h (Promega) was added at a final concentration of 5 µM and the cells were incubated for a further 5 min. BRET was measured at 1 min intervals with, 4 baseline measurements, a manual 1 nM SP addition, and a further 25 measurements. BRET was measured sequentially at 475 ± 30 nm and 535 ± 30 nm with filters for the appropriate band pass in the PHERAstar Omega microplate reader (BMG Labtech). Data were presented as a BRET ratio of the YFP signal to the *Renilla* luciferase signal and corrected for the vehicle and baseline.

2.3.8 Förster Resonance Energy Transfer (FRET)

HEK293 cells transiently transfected with NK_1R-HA, and cytoEKAR, nucEKAR (cytosolic or nuclear ERK biosensors) , cytoCKAR (cytosolic PKC biosensor) , pmEpac2 or cytoEpac2 (plasma membrane or cytosolic cAMP biosensors) (Nikolaev *et al.*, 2004, Wachten *et al.*, 2010). Cells were incubated with 1 μM of the antagonists for 4 h before the medium was replaced with HBSS and cells were equilibrated for 30 min at 37°C. FRET was measured at 1 min intervals using the INCell 2000 Analyzer with a Nikon Plan Fluor ELWD 40× (NA, 0.6) objective and FRET module (GE Healthcare) (Jensen *et al.*, 2014, Halls *et al.*, 2016). Using these settings, approximately 100 cells were imaged for each drug treatment in one experiment. For the Epac2 biosensors, cells were sequentially excited using a CFP filter (430/24) with emission measured using YFP (535/30) and CFP (470/24) filters with a polychroic optimised for this FRET pair (Quad 3). For EKAR biosensors, cells were sequentially excited using a FITC filter (490/20) with emission measured using dsRed (605/52) and FITC (525/36) filters with a polychroic optimised for this FRET pair (Quad4). Basal FRET images were captured for 4 min. Cells were stimulated with vehicle control (MilliQ H_2O) or SP (1 nM), and images were captured for 20 min. Cells were stimulated with positive controls for 10 min (10 μM forskolin with 100 μM 3-isobutyl-1-methylxanthine for Camp and 200 nM phorbol 12,13-dibutyrate (PDBu) for ERK) and imaged for 4 min.

For the PKC biosensor, cells were imaged for CFP (ex λ= 458, em λ= 481 ± 18 nm) and YFP (em λ= 540 ± 20 nm) using a Zeiss LSM710 confocal fluorescence microscope with a Zeiss 40X (NA, 1.34), oil immersion objective, with pinhole set to 2 AU. Using these settings, up to 20 cells were imaged in each experiment. Basal FRET images were captured at 3 sec intervals for 30 sec. Cells were manually stimulated with vehicle control (MiliQ H_20) or SP (1 nM) and captured for 2 min. Cells were stimulated with positive control, PDBu (200 nM) and imaged for 5 min.

The data were analysed by identifying individual cells as regions of interest. For the images captured using the InCell, up to 200 cells with the lowest expression of biosensor were selected and up to 20 cells were selected in the confocal experiments. Each biosensor was expressed as a FRET ratio and normalised to the baseline. Only the cells that responded with at least a 5% increase in FRET ratio in response to the positive controls were collated in the graphs. Details of the analysis are further described in Halls *et al*., 2015.

2.3.9 Measurement of $[Ca^{2+}]_i$

Stable HEK-NK_1R were plated into clear 96 well plates. Cells were washed with calcium buffer and were loaded with Fura-2 AM ester (1 μM, 45 min, 37°C) in calcium buffer (10 mM HEPES, 0.5% BSA, 10 mM D-glucose, 2.2 mM $CaCl_2.H_2O$, 1.18 mM $MgCl_2.6H_20$, 2.6 mM KCl, 150 mM NaCl), containing 4 mM probenecid and 0.05% v/v pluronic F127, pH 7.4. Cells were then stimulated with 1 nM SP at 1, or 4 h post-antagonist addition, or with ionomycin (1 μM) to obtain a maximal $[Ca^{2+}]_i$ response. Fluorescence was measured at 4 s intervals for 45 secs per well (excitation: 340 nm/ 380 nm; emission: 520 nm) using a FlexStation 1/3 plate reader (Molecular Devices, Sunnyvale, CA). SoftMax Pro (v5.4.4) software was used to obtain the area under the curve from the kinetic data for >4 experiments performed in duplicate.

2.3.10 In vivo studies

2.3.10.1 Animals

A total of 72 male C57Bl/6 mice (6-12 weeks old) were used in this study. Mice were maintained in a temperature and humidity-controlled room (23ºC ± 2º C) under a 12 h light/dark cycle with food and water *ad libitum*. The study was conducted in accordance with the ethical guidelines of

the International Association for the Study of Pain and was approved by the animal ethics committee of Monash Institute of Pharmaceutical Sciences, Monash University.

2.3.10.2 Drugs administration

50μM of Spantide-cholestanol, Spantide, Cholestanol-PEG-Biotin and vehicle (1% DMSO/Saline) (n=6 each group) were injected intrathecally (5 μL) 3, 6 and 12 h before intra-plantar injection of capsaicin in a single dose in the L3-L4 region under isoflurane anaesthesia (1-3 % delivered in oxygen).

2.3.10.3 Mechanical hyperalgesia

The behavioural assessment of mechanical hyperalgesia by von Frey method was performed by an investigator blinded to the treatments. Experimental mice were acclimatised and habituated to the experimental conditions of von Frey testing for 2 successive days for around 1-2 h. Mechanical hyperalgesia was assessed by measuring the paw withdrawal thresholds elicited by the filaments of ascending magnitudes of force applied to the plantar surface of the hind paws as per the previously established protocol (Alemi *et al.,* 2013, Jensen *et al.,* 2017). On the day of the study, von Frey paw withdrawal thresholds were measured in duplicate to establish baseline readings for each of the animal in different groups. At time 0 mice were anaesthetised (1-3 % isoflurane in oxygen) and capsaicin (5 μg, vehicle: 20% ethanol, 10% Tween 80, 70% saline solution) was injected subcutaneously in the plantar surface of the left hind paw (10 μL). Following capsaicin injection, von Frey thresholds were measured for both the ipsilateral and contralateral hind paws every hour for up to 4 h. The data were subsequently normalised to the baseline paw withdrawal thresholds of the respective animal.

2.3.11 Data Processing and Analysis

Drug uptake and FRET biosensor images were processed and analysed using FIJI (v 1.51d) software. Graphs were generated using GraphPad Prism 6.01 (San Diego, CA). For the analysis of FRET data, two-way analysis of variance (ANOVA) and post hoc Tukey's multiple comparisons test was applied (* $p<0.05$; ** $p<0.01$, ***$p<0.001$). Data are presented as mean ± S.E.M. For BRET data, one-way ANOVA and the Dunnett's post-test relative to the Vehicle control (** $p<0.01$). Ligand binding data are presented as mean ± S.E.M and fitted with a competitive binding, one site, fit logIC_{50} model and compared log IC_{50} using an extra sum-of-squares F test ($P<0.05$).

2.4 Results

2.4.1 Cholestanol lipid-anchor increases Cy5 probe cell membrane association

FCS is a sensitive fluorescence spectroscopy technique that can be used to quantitatively measure and resolve the biophysical properties of fluorescent molecules (Briddon *et al.*, 2017). The technique involves the measurement of fluorescence intensity fluctuations within a diffraction-limited confocal volume and the application of autocorrelative analysis to determine concentration and diffusion characteristics (Briddon *et al.*, 2017). We have used this approach to quantitatively determine soluble and lipidated Cy5 probes in the extracellular fluid immediately above the plasma membrane and at increasing distance intervals above the cell. The position of the plasma membrane was identified by performing a fluorescence intensity scan in the z-direction at one fixed x and y position. The fluorescence was measured at intervals increasing by 2 µm for 5 measurements (2-10 µm), subsequent measurements were performed by intervals of 5 µm, and the distances were normalised to the raw values of the z-position. The concentration of Cy5-Chol

measured within the first 5 µm of extracellular fluid above the plasma membrane was 26.8 ± 8.29 nM and decreased to 2.38 ± 0.22 nM at 200 µm. In contrast, measured concentrations of the control construct, Cy5-EE, were 6.77 ± 0.35 nM at 5 µm above the plasma membrane and increased to 26.2 ± 3.05 nM at 200 µm. Consistent with Cy5 probe imaging (Figure 2.2A), a comparison of probe concentrations at increasing intervals indicates an enrichment of Cy5-Chol in the plasma membrane, while ethyl-ester-terminated Cy5-PEG molecules freely diffuse through the extracellular fluid (Figure 2.2B-D).

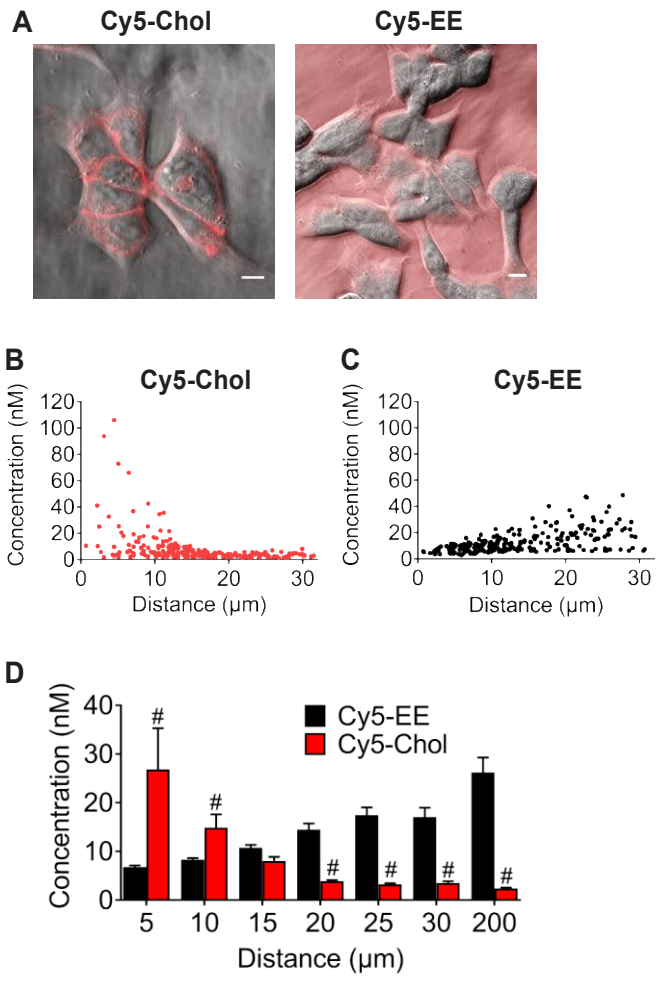

Figure 2.2. Extracellular distribution and concentration of Cy5 probes at the plasma membrane. A, HEK293 cells imaged following incubation with Cy5-Cholestanol (Cy5-Chol) or Cy5-Ethyl ester (Cy5-EE) (both 1 µM, 55 min, 37˚C). Incubation (10 min, 37˚C) of HEK293 cells with 10nM Cy5-Chol, **B**, or Cy5-EE, **C**, followed by measurement of Cy5 probe concentration at increasing distances above the plasma membrane by fluorescence correlation spectroscopy. **D**, Average Cy5 probe concentration at 5 µm increasing intervals above the plasma membrane. #p> 0.001, Unpaired *t*-test, Holm-Sidak multiple comparisons. Combined cell data from n=4 experiments. Scale bar, 10 µm.

2.4.2 Cholestanol Fluorescent Reporter Internalises into NK_1R-positive Endosomes

We have previously demonstrated that the Cy5-Chol probe significantly internalises into endosomal compartments after continuous incubation for 4 h (Jensen *et al.,* 2017). To determine the intracellular distribution of a lipid-conjugated pharmacophore following acute or chronic treatment, Cy5-Chol (1.5 µM) was incubated for times indicated, in cells transiently expressing fluorescent reporter proteins, including endosomal markers or NK_1R-GFP. Organelles were visually defined as early endosomes (Rab5a-RFP), late endosomes (Rab7a-GFP), recycling endosomes (Rab11-GFP), the *trans*-Golgi network (GalT2-GFP) or the endoplasmic reticulum (Calreticulin-GFP). After a 30 min incubation with Cy5-Chol, fluorescence was readily observed at the plasma membrane in live cells, and within Rab5a-GFP and Rab7a-GFP positive endosomes (Figure 2.3A), but not markers of the recycling endosome, *trans*-Golgi network or endoplasmic reticulum. Using a pulsed incubation protocol, consisting of a 30 min incubation, wash and 3.5 h recovery, plasma membrane fluorescence was reduced, while intracellular co-internalisation was observed with Rab5a and Rab7a positive endosomes (Figure 2.3B). In addition, Cy5-Chol internalises into endosomes that also contain stimulated, internalised NK_1R-GFP, after challenging cells with SP (10 nM, 10 min, wash) (Figure. 3B). This indicates sustained association with NK_1R-positive compartments when using a pulsed incubation protocol and was supported by the co-distribution of Cy5-Chol and NK_1R-GFP in these conditions. To determine the long-term intracellular distribution of a lipidated probe, cells were incubated with Cy5-Chol for 24 h (Figure 2.4). In these conditions, Cy5-Chol fluorescence was detected, indicating that cholestanol conjugates are not diminished by metabolic processes. Co-distribution was observed with Rab5, Rab7, Rab11 and a lysosomal dye. Although they are markers of different endosomal fates, co-distribution was observed between the Rab5 and Rab7 markers and between the Rab 11 and

Lysosomal markers. This may be due to the continuous incubation of cholestanol for 24 h which may affect the fluidity of the plasma membrane and endosomal membranes. Together, these observations indicate that at early timepoints of up to 4 h, the cholestanol can promote trafficking specifically into the early and late endosomal compartments.

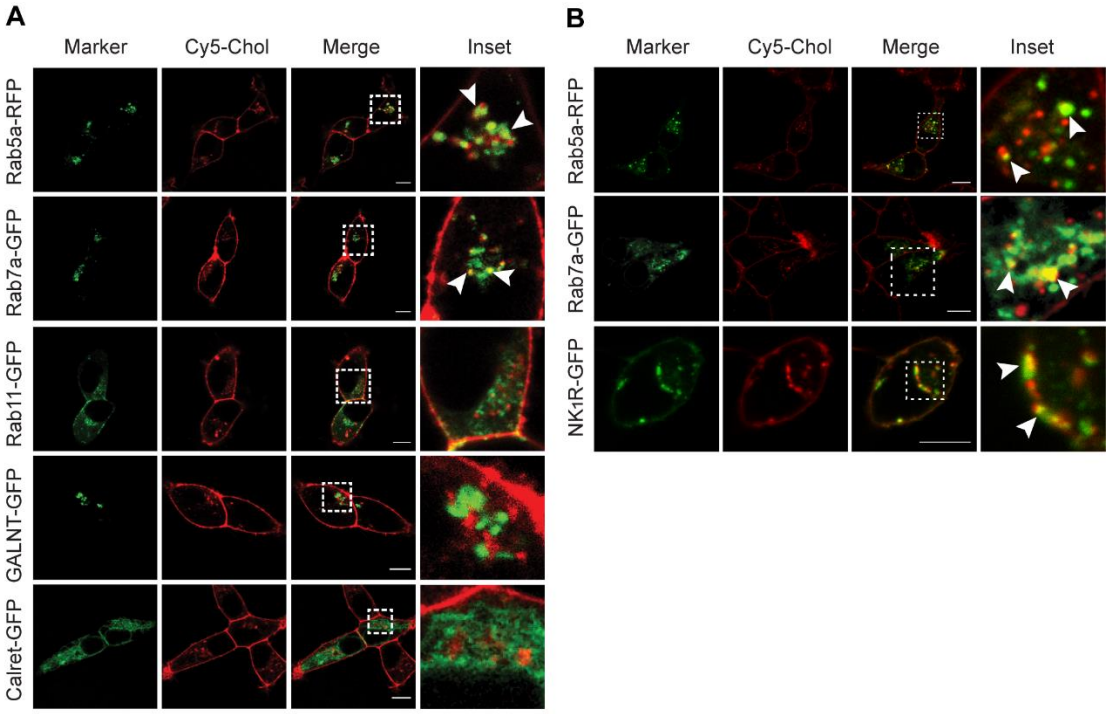

Figure 2.3. Cholestanol conjugation increases the association of fluorescent probes with endosomes. A, Stable HEK NK_1R-HA cells transduced with CellLight markers to transiently express GFP-tagged Rab5a (Early endosome), Rab7a (Late endosome), Rab11 (Recycling endosome), GALNT (Golgi) or Calreticulin signal with KDEL retention peptide (endoplasmic reticulum) markers and incubated with Cy5-Cholestanol (1.5 µM, 30 min, 37°C), washed and imaged by confocal microscopy. **B**, Untransfected HEK293 cells incubated with 1.5 µM Cy5-Chol (30 min, washed and replaced in buffer 3.5 h) with endosomal markers, Rab5a-RFP, Rab7a-GFP and SP stimulated NK_1R (1 nM SP, 10 min). Representative images and overlap coefficients from n=3 individual experiments. White arrows indicate regions of overlap. Scale bar, 10 µm.

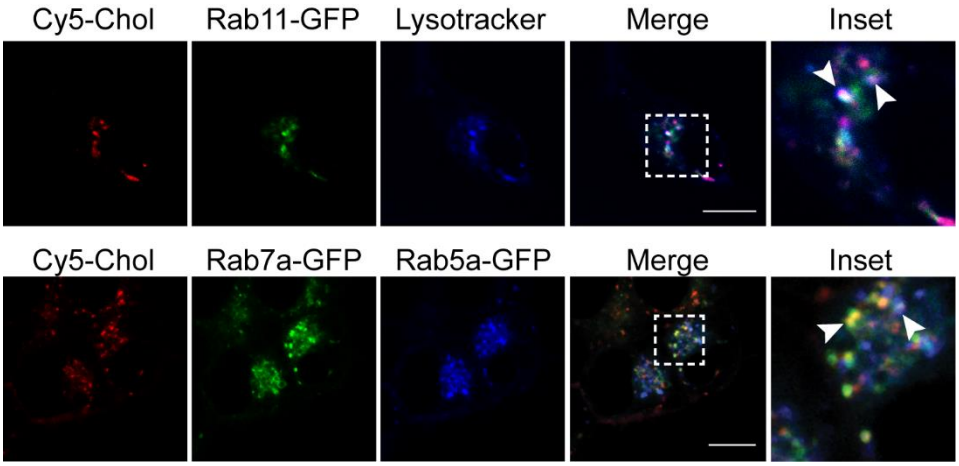

Figure 2.4. Sustained incubation of Cy5-Chol leads to accumulation in lysosomes. HEK-NK_1R cells were transduced with CellLight markers to transiently express Rab5-GFP, Rab7-RFP, or Rab11a-GFP, to visualise early, late or recycling endosomes, respectively. Cells incubated with Lysotracker Red to enabled visualisation lysosomes. Cells were incubated with 1.5 µM Cy5-Chol (red channel) for 24 h, washed and imaged in HBSS. Organelle markers were pseudo-coloured to differentiate fluorescent channels. Representative images from n=2 experiments. White arrows indicate regions of overlapping fluorescence. Scale bar 10µm.

2.4.3 Lipid-conjugated antagonists retain affinity for the NK_1R antagonist

To determine how lipid-conjugation influences the affinity of Spantide for the NK_1R, we used TAMRA-labelled SP agonist (SP-TAMRA) in a whole cell fluorescence-based competitive ligand binding assay. Live HEK-NK_1R cells were co-incubated with SP-TAMRA (0.5 nM) and increasing concentrations of Spantide or Span-Chol for 30min. Cells were subsequently imaged and analysed using an established granularity algorithm (Stoddart *et al.,* 2012, Stoddart *et al.,* 2015). At 30min, Span-Chol showed a modest increase in affinity for NK_1R, when compared to the soluble Spantide control (pIC_{50} 6.26 ± 0.16 and 5.96 ± 0.11, respectively; Figure 2.5B).

Sustained ligand binding was also assessed, by pre-incubating cells with antagonist for 3.5 h, then incubated with SP-TAMRA for a further 30 min (Figure 2.5C). In these conditions, the measured affinity for Spantide was reduced after 4 h (pIC_{50} 5.54 ± 0.34), whereas Span-Chol (6.32 ± 0.17) was consistent with the affinity measured after 30 min binding. This indicates that lipidation does not diminish the affinity of Spantide for the NK_1R, and that Span-Chol maintains its ability to compete TAMRA-SP for sustained periods. The co-incubation of the Spantide or Span-Chol with the TAMRA-SP indicated no changes in Spantide affinity. However, a shift in the affinity of Spantide was observed when the antagonists were pre-incubated for 3.5 h. Together, these data suggest that the longer pre-incubation time allows for more of the lipid-conjugated drug to partition into the plasma membrane, increasing the local concentration for competition with the TAMRA-SP over the 30 min equilibration.

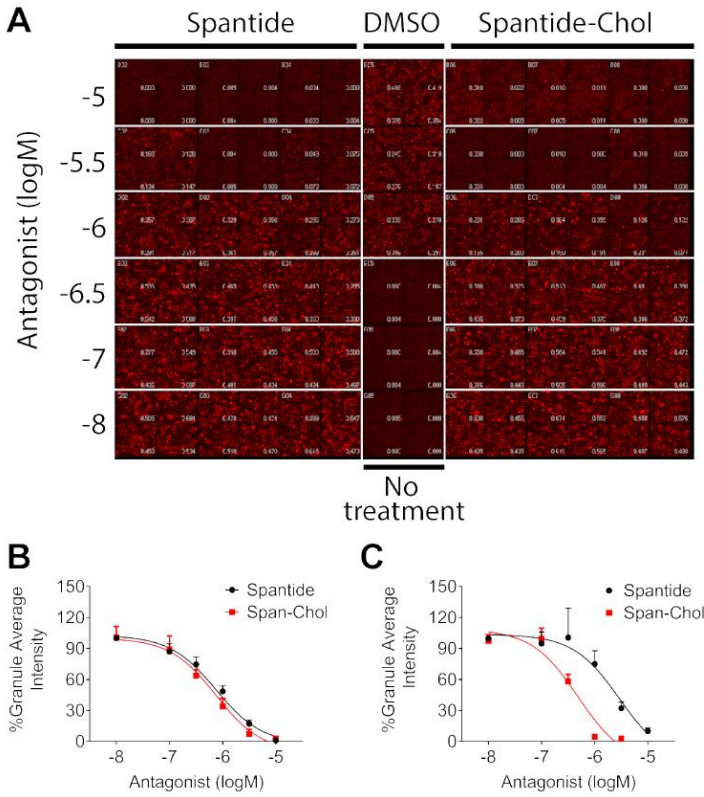

Figure 2.5. Competition binding of SP-NK_1R interactions. A, Representative images of SP-TAMRA (0.5 nM) fluorescence in cells co-incubated with Vehicle (0.1% DMSO+HBSS) or competing antagonists, Spantide and Span-Chol. Concentration-dependent competition of SP-TAMRA binding (intracellular SP-TAMRA fluorescence) following pre-incubation with Spantide and Span-Chol for 30 min, **B**, or 3.5 h, **C**. Data expressed as a percentage of the intensity of fluorescent granules

measured for 10nM Spantide. n=5, mean ± S.E.M.

2.4.4 Cholestanol-conjugated Spantide can prevent SP mediated increase in intracellular calcium via activation of NK1R

To determine if lipid-conjugation influences the potency of Spantide on an acute SP-dependent NK_1R response, the soluble and lipidated molecules were compared by Ca^{2+} signalling in HEK-NK_1R cells. Following a pre-incubation with increasing concentrations of Spantide or Span-Chol for 30 min, cells were challenged with 1nM SP (EC_{80} concentration) and $G\alpha_q$-coupled Ca^{2+} transients were measured for 90 s post-stimulation. Pre-incubation of cells with Spantide or Span-Chol caused a concentration-dependent inhibition of Ca^{2+} flux (Figure 2.6A) and a comparison of pIC_{50} values for Spantide and Span-Chol (4.87 ± 0.33 and 6.25 ± 0.19, respectively) revealed a significant increase in the potency of the lipidated antagonist (p=0.0112). This may be due to the lipid-anchoring of the antagonist to the plasma membrane and increasing the local concentration near the receptor. As lipid probes are continuously internalised from the plasma membrane, and this may affect the relative potency of Spantide compared with Span-Chol over time, we repeated the experiment using progressively longer pre-incubation periods. Continuous exposure to the antagonists was compared to a "pulsed" administration whereby the cells were pre-incubated with antagonist for 30 min, washed to remove any excess antagonist, and then challenged with 1 nM SP, 4 h after antagonist addition (Figure 2.6B). There was no significant change in the IC_{50} of the antagonists over time when the cells were continuously incubated with the antagonists. As expected, following pulsed administration only Span-Chol inhibited Ca^{2+} signalling and this effect was consistent up to 4 h post wash. This is likely due to the wash decreasing the available concentration of free Spantide in the extracellular space. In contrast, relatively little Span-Chol would be lost during the wash, as lipidation allowed the antagonist to be rapidly incorporated into

the cell membrane resulting in prolonged retention at the plasma membrane. These data demonstrate that cholestanol-conjugated antagonists, not only maintain antagonist function, but increase the retention and effective concentration, regardless of a washout.

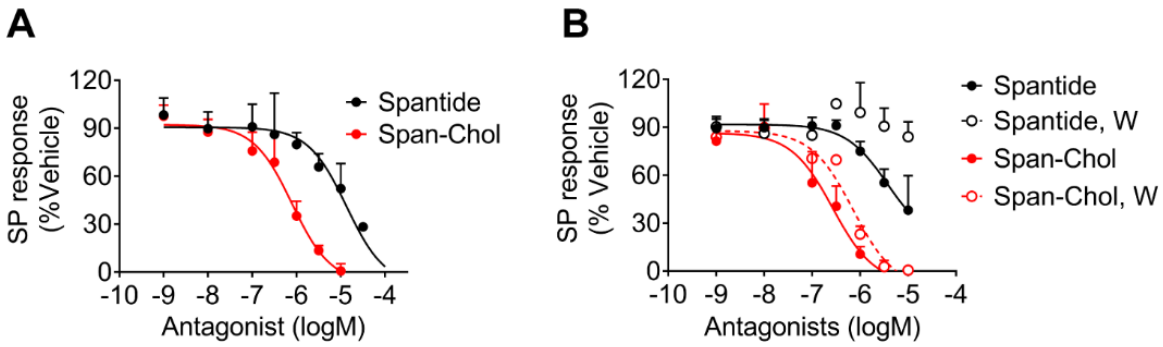

Figure 2.6. Inhibition of NK_1R Ca^{2+} signalling. Ca^{2+} transients measured in HEK293 stably expressing HA-NK_1R and loaded with FURA2-AM. **A**, Effects of pre-incubating with graded concentrations of Spantide or Span-Chol for 30 min, followed by stimulation with SP. **B**, Pre-incubation of cells with graded concentrations of Spantide and Span-Chol continuously for 4 h (solid symbols) or pre-incubated for 30 min, washed (W) and recovered for 3.5 h (open symbols), and then stimulated with SP. Mean and S.E.M. from n=3 experiments.

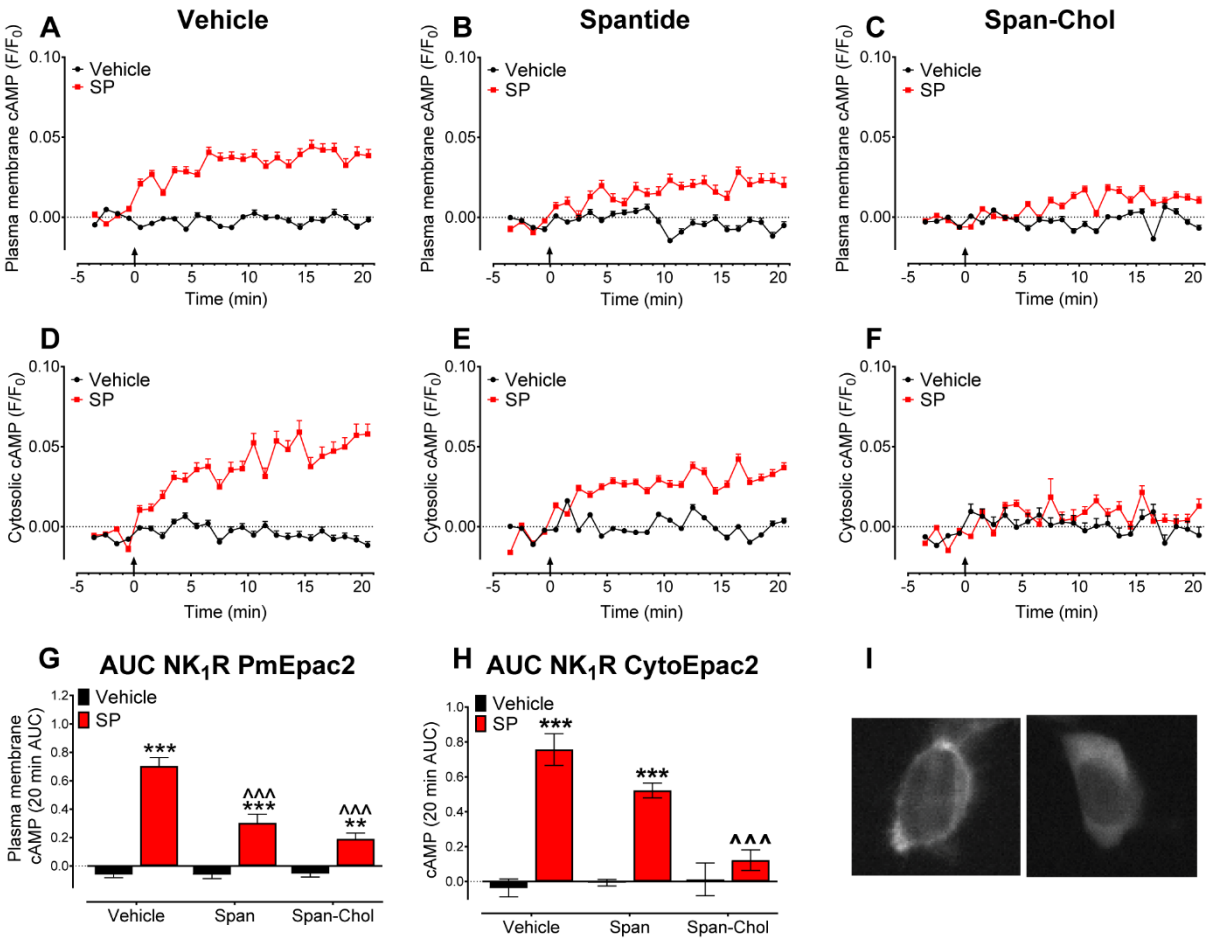

Figure 2.7. Inhibiting NK$_1$R-mediated Spatiotemporal cAMP production. HEK293 cells were transiently transfected with HA-NK$_1$R and mEpac2 or cytoEpac2 FRET biosensors to measure cAMP activity in the plasma membrane and cytosol, respectively. **A-F,** Time course of SP (1 nM, arrow) activation of cAMP production at the plasma membrane (**A-C**) or in the cytosol (**D-F**). Cells were pre-incubated for 4 h with vehicle (0.1% v/v DMSO; **A, D**), 1 µM Spantide (Span; **B, E**), or 1 µM Span-Chol (**C, F**). **G** and **H,** group data showing effects of Span or Span-Chol on cAMP production at the plasma membrane (**G**) or in the cytosol (**H**) over 20 min (Area Under the Curve, AUC). **I**, Representative images of plasma membrane and cytosolic localised cAMP FRET biosensors, respectively. n=123-304 cells from 3 independent experiments; Symbols/bars show mean ± S.E.M. * p<0.05, ** p<0.01 and *** p<0.001 versus vehicle control; ^ p<0.05, ^^ p<0.01 and ^^^ p<0.001 versus DMSO control; two-way ANOVA with Tukey's multiple comparison test.

2.4.5 Spantide-Cholestanol can Inhibit Spatiotemporal Signalling of NK_1R

Subcellular targeted FRET biosensors have been utilised to determine the relationship between NK_1R signalling and trafficking, by measuring SP-stimulated NK_1R signalling in cells pre-treated with the dynamin inhibitor, Dyngo 4a, or the clathrin inhibitor, Pitstop2. These findings indicated that only endosomal pools of NK_1R can stimulate cytosolic cAMP production, cytosolic PKC activity and nuclear ERK activity (Jensen *et al.,* 2017). Previously, pulsed pre-administration of Span-Chol selectively inhibited SP-induced increases in nuclear but not cytosolic ERK, with no effect of free Spantide (Jensen *et al.,* 2017).

To determine the effect of incubation protocols and whether Span-Chol exclusively antagonises the endosomally-localised NK_1R, we compared continuous and pulsed administration of antagonists and measured the spatiotemporal regulation of nuclear ERK (nucEKAR), cytosolic cAMP production (cytoEpac2), and cytosolic PKC activity (cytoCKAR). PKC activity was measured over a shorter time scale to capture fast peaks of PKC activity due to calcium transients and over 20 min for the sustained response. SP stimulation of NK_1R activated sustained cAMP in cytosol (Figure 2.7), sustained ERK activity in the nucleus (Figure 2.9), and a rapid initial peak of PKC activity within 30 sec and sustained activity over 20 min (Figure 2.8). Preincubation with 1 μM Spantide had no effect on nuclear ERK but significantly inhibited the cytosolic cAMP, and inhibited PKC at early and longer timepoints. Span-Chol (1 μM) completely abolished cytosolic cAMP and nuclear ERK and inhibited the rapid PKC peak but not the sustained PKC activity over 20 min. These data suggest that lipidation of Spantide improves the inhibition of SP-dependent signalling of NK_1R that is associated with endosomes. These results may also indicate the contribution of receptor signalling from the plasma membrane detected in the fast PKC peak by the cytosolic PKC biosensor.

We have previously shown that stimulation of plasma membrane localised NK_1R prior to internalisation activates plasma membrane localised cAMP and cytosolic ERK (Jensen *et al.*, 2014, Jensen *et al.*, 2017). The effect of Span-Chol on plasma membrane delimited signalling of NK_1R was determined by measuring plasma membrane cAMP (pmEpac2) and cytosolic ERK (cytoEKAR). Previous studies showed that cAMP production at the plasma membrane is transient, current data instead revealed a sustained production of cAMP at the plasma membrane. These differences may be due to expression levels of either the receptor or the biosensor. High levels of receptor expression relative to the biosensor may result in a more sustained cAMP profile. SP stimulation of NK_1R activated transient ERK activity in the cytosol. Continuous pre-incubation with Spantide inhibited SP-stimulated cAMP production at the plasma membrane (Figure 2.7) and abolished cytosolic ERK activity (Figure 2.9). Span-Chol significantly inhibited plasma membrane derived cAMP but had no effect on cytosolic ERK activity. This suggests that after 4 h, some Span-Chol is retained in the plasma membrane.

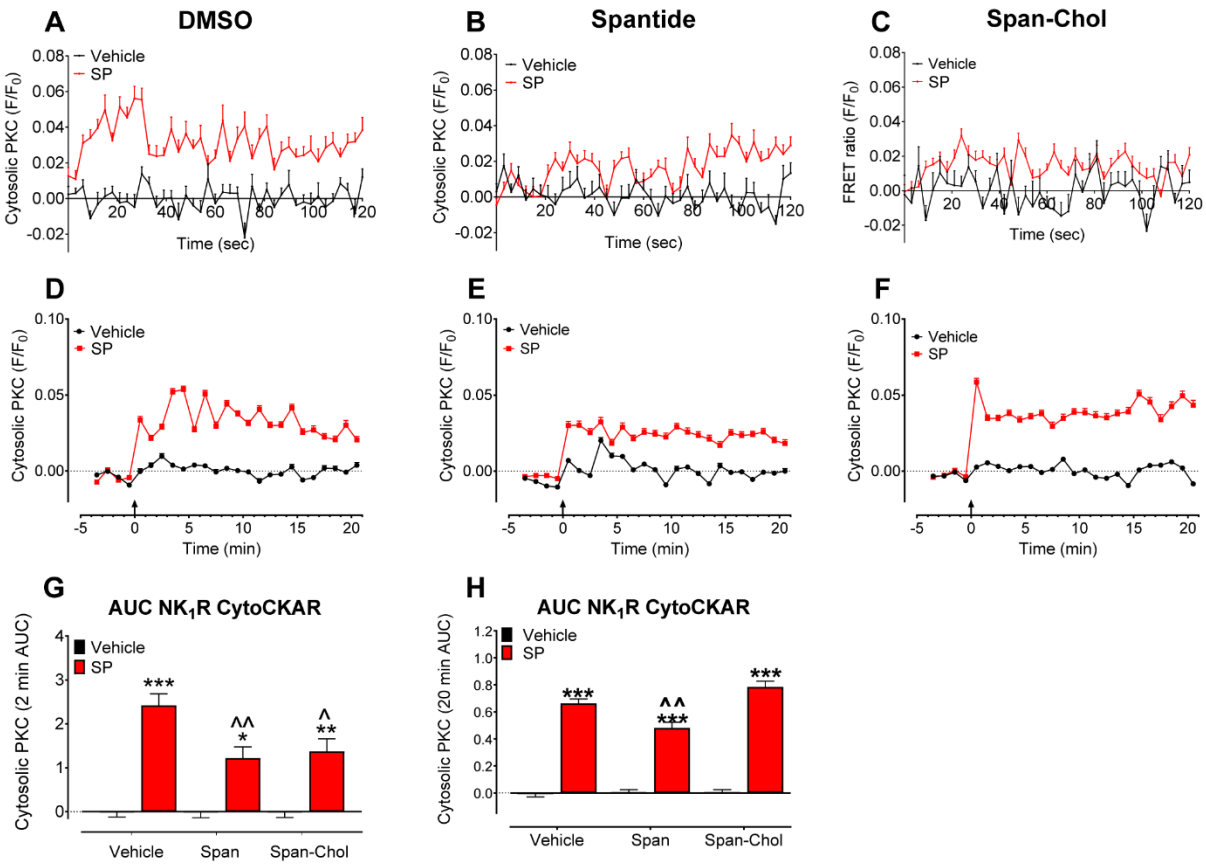

Figure 2.8. Inhibiting NK_1R-mediated PKC activity. HEK293 cells were transiently transfected with HA-NK_1R and cytoCKAR FRET biosensors to measure PKC activity in the cytosol. **A-F**, Time course of SP (1 nM, arrow) activation of cytosolic PKC activity acquired rapidly for 2 min at 3 sec intervals (**A-C**) or over 20 min at 1 min intervals (**D-F**). Cells were pre-incubated for 4 h with vehicle (0.1% v/v DMSO; **A, D**), 1 µM Spantide (Span; **B, E**), or 1 µM Span-Chol (**C, F**). **G** and H, group data showing effects of Span or Span-Chol on cytosolic PKC activity over 2 min (**G**) and 20 min (**H**), measured by area under curve (AUC). n=24-51 cells (2 min cytosolic PKC activity) and n=158-304 cells (20 min cytosolic PKC activity); from 3 independent experiments. Symbols/bars show mean ± S.E.M. * $p<0.05$, ** $p<0.01$ and *** $p<0.001$ versus vehicle control; ^ $p<0.05$, ^^ $p<0.01$ and ^^^ $p<0.001$ versus DMSO control; two-way ANOVA with Tukey's multiple comparison test.

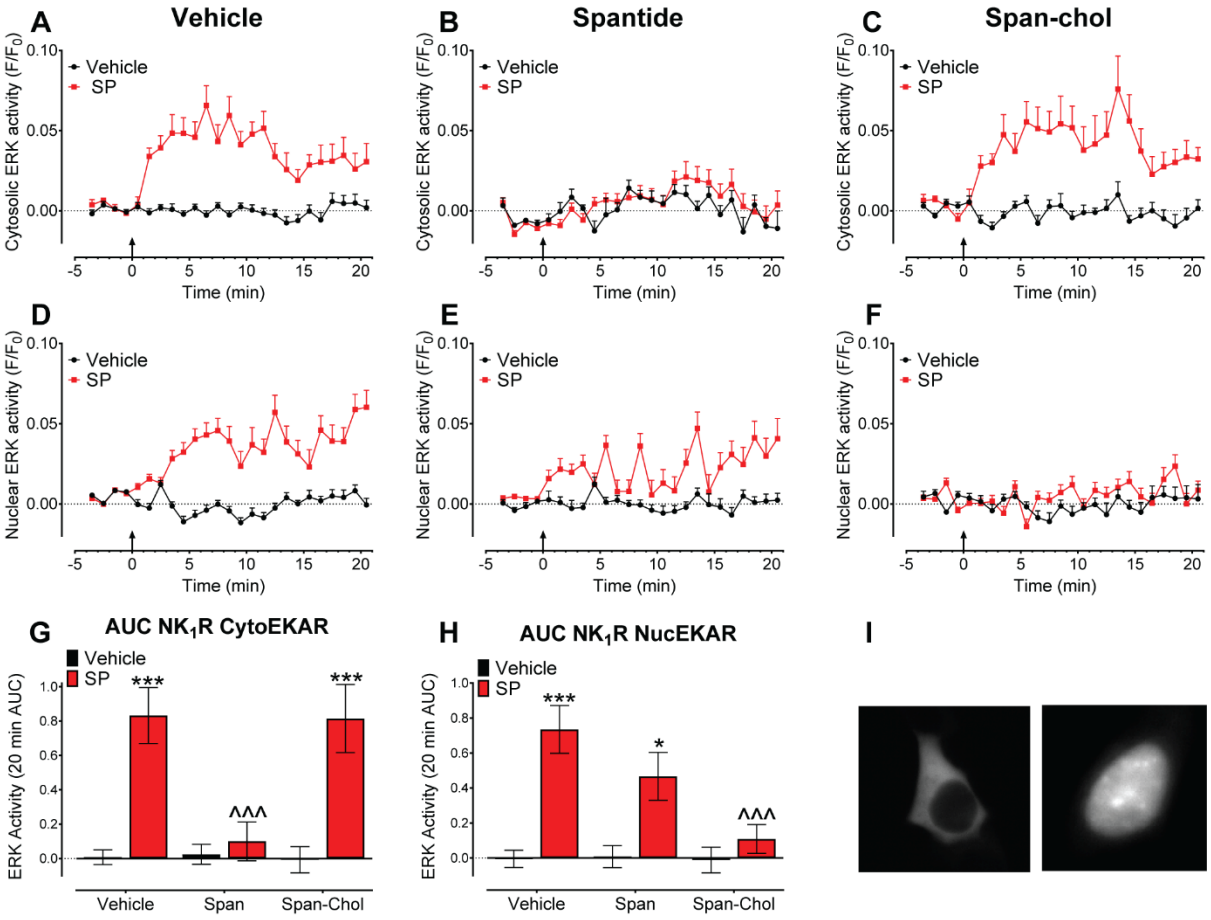

Figure 2.9. Inhibiting NK_1R-mediated ERK activity. HEK293 cells were transiently transfected with HA-NK_1R and either cytoEKAR or nucEKAR FRET biosensors to measure ERK activity in the cytosol and nucleus, respectively. **A-F**, Time course of SP (1 nM, arrow) activation of cytosolic (**A-C**) or nuclear ERK (**D-F**). Cells were pre-incubated for 4 h with vehicle (0.1% v/v DMSO; **A, D**), 1 µM Spantide (Span; **B, E**), or 1 µM Span-Chol (**C, F**). **G** and **H**, group data showing effects of Span or Span-Chol on ERK activity in the cytosol (**G**) or nucleus (**H**) over 20 min (area under curve, AUC). **I**, Representative images showing localisation of cytosolic and nuclear FRET EKAR biosensors, respectively. n=31-82 cells from 3 independent experiments; Symbols/bars show mean ± S.E.M. * $p<0.05$, ** $p<0.01$ and *** $p<0.001$ versus vehicle control; ^ $p<0.05$, ^^ $p<0.01$ and ^^^ $p<0.001$ versus DMSO control; two-way ANOVA with Tukey's multiple comparison test.

2.4.6 Cholestanol-conjugated Spantide reduces SP mediated trafficking of NK_1R

The addition of the cholestanol group promotes internalisation of the ligand into endosomes and ligand retention is still observed at the plasma membrane prior to its translocation into endosomes. When the cholestanol-ligand is present at the plasma membrane, this could also bind to the receptor at the cell surface and prevent the trafficking of the receptor into endosomes. It is important to determine whether this is the case after both acute or chronic exposure to the Chol-antagonist, as decreased receptor trafficking to endosomes, in addition to antagonism of receptors within endosomes, would contribute to the global effects of the chol-antagonist on endosomal signalling and pain transmission. It is also important to probe the effect of cholestanol on membrane trafficking. Therefore, we used BRET to determine the effect of a cholestanol-biotin control, Spantide and Span-Chol on NK_1R-Rluc recruitment of βArr (βArr 2-YFP), trafficking away from the plasma membrane (KRas-Venus) and translocation to early endosomes (rab5a-YFP). Although there is a decrease in the potency of SP at NK_1R-Rluc (pEC50 8.67) compared to the wild type receptor, SP has been shown to robustly recruit βArr in BRET assays (Fong *et al.*, 1992, Jensen *et al.*, 2014, Rupniak *et al.*, 2018). Preincubation of cells with both free and chol-conjugated Spantide for 30 minutes, resulted in a concentration-dependent inhibition of SP-dependent-NK_1R βArr recruitment and translocation away from the plasma membrane, into early endosomes (Figure 2.10A-C). In contrast, a sustained incubation resulted in a concentration-dependent inhibition of SP-dependent trafficking of the NK_1R-Rluc, in Span-Chol, but not Spantide treated cells (Figure 2.10D-H). Previous studies with these lipid-conjugated antagonists have been carried out using 1 μM which does not significantly affect trafficking after 4 h. However, higher concentrations of ligand in plate-based assays will affect receptor trafficking and would have to be carefully monitored. These BRET data suggest that the Span-Chol, regardless of a washout can bind to the

receptor on the cell surface and prevent receptor activation and trafficking. These data are consistent with the images captured after 4 h of Cy5-Chol in which ligand retention on the plasma membrane was still observed.

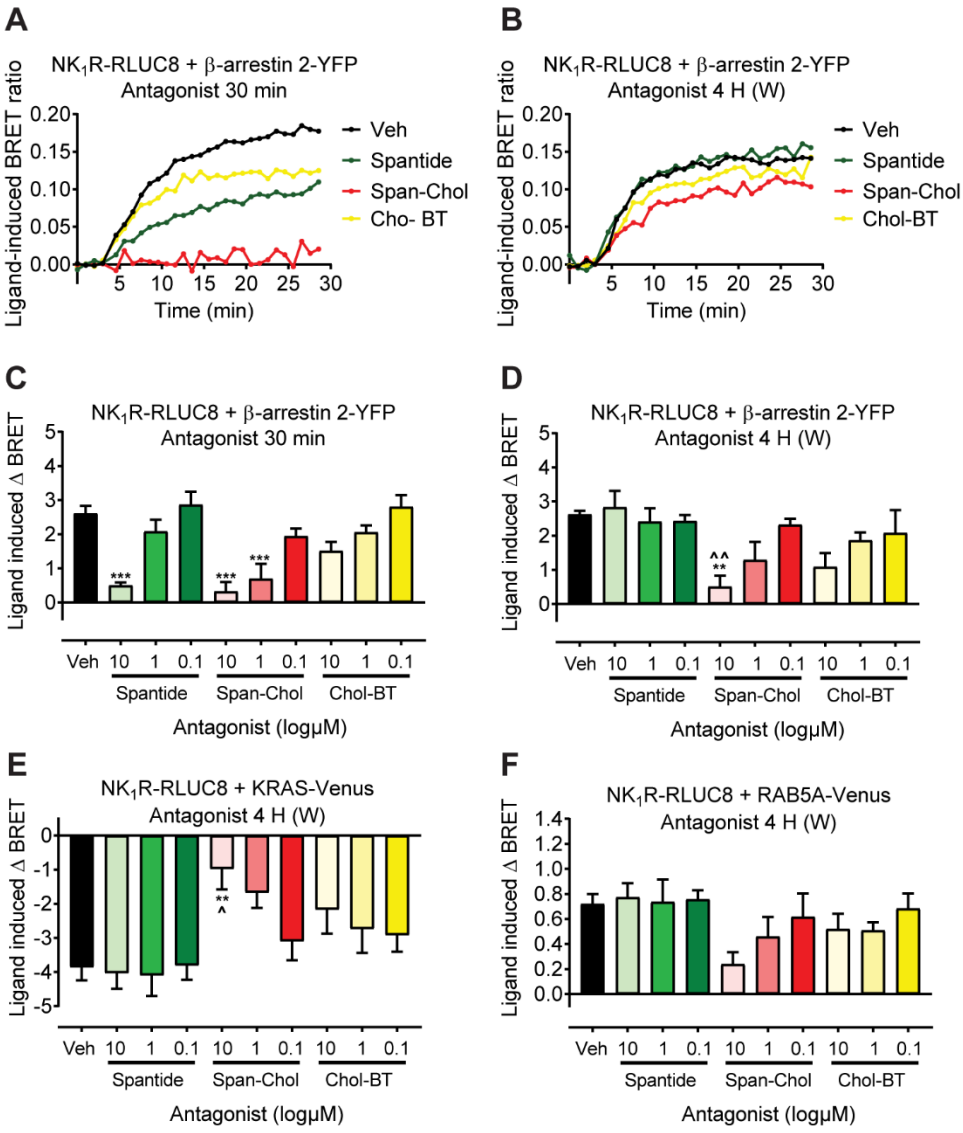

Figure 2.10. Effect of lipid-conjugates on NK$_1$R interactions with the plasma membrane, endosomes and β-Arrs. A and **B**, Representative time course of SP-induced BRET interactions between NK$_1$R-Rluc8 and β-arrestin 2-YFP in HEK cells after incubation with 1 μM of Spantide, Span-Chol or cholestanol-PEG-biotin (Chol-BT, control). Cells were incubated with antagonist or control for 30 min (**A**) or for 3 h followed by a wash (W) and 60 min recovery (total 4 h; **B**). **C** and **D**, SP-induced BRET between NK$_1$R-Rluc8 and β-arrestin 2-YFP in HEK cells (Δ BRET

measured over 25 min) after 30 min (**C**) or 4h antagonist incubation (**D**). SP-induced Δ BRET was also measured after 4 h antagonist treatment, between NK_1R-Rluc8 and a resident protein of the plasma membrane (KRAS-Venus, **E**) or early endosomes (Rab5A-Venus, **F**). n=5, mean ± SEM. ** P< 0.01; *** P<0.001, One-way ANOVA, Dunnett's test, compared to vehicle. ^P<0.1, ^^P<0.01 compared to equivalent concentration of Spantide, Holm-Sidak multiple comparisons test.

2.4.7 Cholestanol-conjugated Spantide sustains inhibition of mechanical hyperalgesia

Mechanical hyperalgesia was assessed with Von Frey filaments. Filaments of ascending magnitudes of force were applied to the plantar surface of the hind paws to measure the paw withdrawal thresholds. Previous studies assessed the effect of intrathecal administration of Span-Chol on intraplantar capsaicin-induced hyperalgesia over 7 h. Span-Chol was shown to sustain anti-hyperalgesia up to 7 h after antagonist administration. Here we evaluate the effect of Span-Chol on mechanical hyperalgesia up to 16 h post Span-Chol administration. Chol-PEG-Biotin, a control in the BRET trafficking studies, was also used to determine the effect of cholestanol on mechanical hyperalgesia. Mice were intrathecally administered with Spantide, Span-Chol, Chol-PEG-Biotin, or vehicle at 3, 6, or 12 h prior to an intraplantar injection of capsaicin. Mechanical hyperalgesia was then measured every hour for 4 h. Span-Chol but not Spantide was anti-hyperalgesic up to 9 h after injection (Figure 2.11). Chol-PEG-Biotin, a control for non-specific actions of cholestanol, had no effect. This suggests that only Span-Chol is retained in membranes and maintains antagonist function to inhibit nociception.

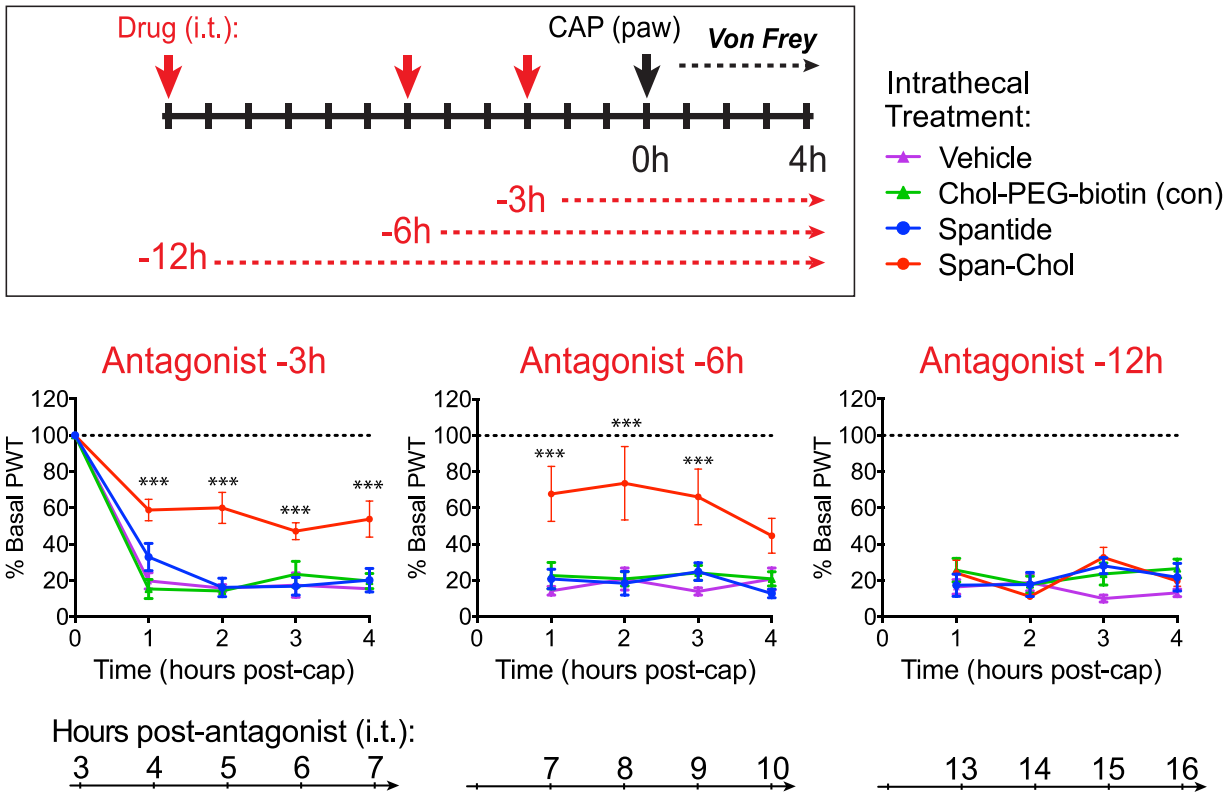

Figure 2.11. Anti-hyperalgesic effect of Spantide-Cholestanol in capsaicin evoked inflammatory hindpaw hypersensitivity in mice. Spantide-chol (n=6, intrathecal; 5 µL, 50 µM), Spantide (n=6, intrathecal; 5 µL, 50 µM), Chol-PEG-Biotin (n=6, intrathecal; 5 µL, 50 µM) or vehicle-1% DMSO/Saline (n=6, intrathecal; 5 µL) were injected at different time points prior to Capsaicin (5 µg / 10 µL / hindpaw) injection. **A,** Drugs injected 3 h prior to capsaicin injection. **B,** Drugs injected 6 h prior to capsaicin injection. **C,** Drugs injected 12 h prior to capsaicin injection. ***p<0.001 compared to mice that received intrathecal vehicle (Two-way ANOVA, *post hoc* Bonferroni test).

2.5 Discussion

There is increasing evidence to show that signalling of receptors in endosomes encodes for distinct signal amplification, regulation and specificity leading to different physiological outcomes (Johannessen *et al.*, 2011, Merriam *et al.,* 2013, Zhang *et al.*, 2013, Jensen *et al.,* 2014, Tsvetanova *et al.,* 2014). It is therefore important to consider the subcellular location of GPCRs in pathophysiological conditions as intracellular receptors may not be accessible to soluble drugs. Reduced bioavailability of the NK_1R has been observed in patients suffering from chronic visceral pain , which may contribute to the limited clinical success for drug discovery programs targeting the NK_1R for chronic pain (Jarcho *et al.,* 2013, Steinhoff *et al.,* 2014). Given that signalling from intracellular receptors often results in a distinct cellular outcome, it is imperative to design drug delivery techniques to specifically target this receptor population by increasing local drug delivery at intracellular locations.

Hydrophobicity of drugs and cell permeability of drugs have been associated with activation of receptors at different locations, resulting in differential effects on pathophysiological profiles (Irannejad *et al.,* 2017). A recent study of distinct pools of β_1-adrenergic receptor has indicated that a cell permeable, but not a cell impermeable antagonist inhibits the Golgi localised pools of receptor. As such, differential effects of cell permeable and impermeable β-blockers have also been observed in the clinic (Irannejad *et al.,* 2017). Increasing the lipophilic properties of soluble drugs, such as GPCR antagonists, would increase their association with membranes and may therefore enhance their local potency within the endosomal network (Vauquelin *et al.,* 2010, Rose *et al.,* 2012). Lipid-conjugation to drugs has previously been explored as a means of delivering drugs to intracellular compartments. For example, the lipophilic group, cholestanol, was successful in targeting inhibitors to the cycling endopeptidase, β-site amyloid precursor protein

cleaving enzyme 1 (BACE-1), which localises to early endosomes (Rajendran *et al.,* 2008, Rajendran *et al.,* 2012). Scanning FCS measurements of the partitioning coefficient of sterol, cholesterol-BODIPY, palmityl, and oleyl anchored probes into supported bilayers revealed that the sterol-anchored probes preferentially partitioned into the liquid ordered phase (Rajendran *et al.,* 2008). These studies suggested that sterol-conjugation increased ligand association to the plasma membrane and possibly sterol-enriched domains to promote internalisation into endosomal compartments (Rajendran *et al.,* 2008, Levental *et al.,* 2010). A lipid-conjugated, but not a free antagonist inhibited the cleavage of amyloid precursor protein at the BACE-1 ectodomain, a rate limiting step in the production of the β-amyloid peptide. Importantly, these data indicate that sterol conjugation increases targeting to specific membranes or microdomains within the cell.

Here we report the lipid-dependent changes in the distribution of a probe in solution. The quantitative measurement of Cy5-Chol and Cy5-EE concentration by FCS revealed two distinct gradient distributions. Cy5-Chol preferentially diffused towards the cell with the greatest concentrations measured directly above the plasma membrane. In contrast, Cy5-EE was measured at low concentrations above the plasma membrane and likely equilibrated in the medium. These results are supported with our observations of Cy5-Chol and Cy5-EE association with the plasma membrane, allowing the internalisation of Cy5-Chol into the endosomal network. Interestingly, after extended periods of incubation, Cy5-Chol is retained at the plasma membrane and is co-distributed with the endosomal and lysosomal pathways. Together, these observations indicate that lipid-conjugation would be an effective method of promoting association of ligands with intracellular membranes and retention in the plasma membrane.

To comprehensively explore the effects of lipid-conjugation to Spantide on plasma membrane localised NK_1R, we assessed the ability of Span-Chol to bind, inhibit signalling and

trafficking of NK_1R at the plasma membrane. Fluorescent ligand binding of Span-Chol confirmed that the antagonist was able to bind to the receptor at the plasma membrane and the affinity Spantide and Span-Chol during short incubations (30 min) were not significantly different. However, after a long incubation (4 h), the affinity of the Spantide decreased while Span-Chol remained unchanged. The ability of the antagonist to inhibit plasma membrane localised NK_1R was assessed by measuring calcium mobilisation, plasma membrane cAMP and cytosolic ERK. The inhibition of SP-NK_1R Ca^{2+} was sustained after a continuous and pulse administration of Span-Chol. In contrast, Spantide only inhibited Ca^{2+} mobilisation after a continuous administration. Compartmentalised biosensors were expressed in cells to measure plasma membrane cAMP and cytosolic ERK revealing that Span-Chol and Spantide inhibited cAMP but only Spantide inhibited the ERK signalling. These data do not conclusively show that Span-Chol can bind the plasma membrane localised receptor. The mechanism by which the Span-Chol inhibits plasma membrane derived cAMP and PKC, but not ERK remains unknown. However, it may be an effect of the localisation of the ligand in the membrane as well as the effect of the cholestanol on the localisation of lipid-bound proteins such as adenylate cyclase. BRET receptor trafficking studies revealed that up to 4 h after the pulse administration of Span-Chol, high concentrations of Span-Chol inhibited receptor trafficking by blocking internalisation. The cholestanol control used in this study, Chol-PEG-Biotin, also influenced receptor trafficking which have investigated further in *in vivo* studies. These observations suggest that Span-Chol is retained in the plasma membrane up to 4 h to bind the receptor and inhibit signalling. This is also supported by our observations of Chol-Cy5 at the plasma membrane after 4 hr. The inhibition of Ca^{2+} mobilisation and receptor trafficking also suggest that Span-Chol is retained after the removal of the antagonist (pulse protocol). Although these data suggest that lipidation may prevent the

internalisation of the receptor, our imaging studies demonstrated that using 1.5 μM of Cy5-Chol, the probe was internalised and co-distributed with NK_1R. Together, these observations suggest that lipidation of a peptide antagonist can maintain antagonist activity at the plasma membrane and while also promoting internalisation to prolong the antagonism of the NK_1R in intracellular compartments.

Our previous study demonstrated that the pulse administration of Span-Chol, but not free Spantide, inhibited nuclear ERK signalling from the endosomally-localised NK_1R. (Jensen *et al.*, 2017). We also showed that selectively targeting intracellular NK_1R translated to the significant increase of Span-Chol efficacy to inhibit sustained pain transmission. Here we explore the effect of Span-Chol on other endosomal signalling events, including cAMP and PKC, the effect of administration procedures and receptor trafficking. Span-Chol was more effective at inhibiting endosomally derived, cytosolic cAMP, nuclear ERK and cytosolic PKC at early time points. This effect on PKC was not sustained over the 20 min measurement which is inconsistent with the profiles shown with ERK and cAMP. This demonstrates that Span-Chol can internalise and remains functional at low pH to inhibit NK_1R in the endosome. The nuclear ERK data is also consistent with our previous assessment of Span-Chol using the pulse administration. The receptor trafficking measurement by BRET gave an insight into the effect of Span-Chol on receptor distribution revealing that association with endosomes was reduced. This is likely due to the inhibition of βArr binding and translocation away from the plasma membrane. Although Span-Chol may affect receptor trafficking, in a pathophysiological state in which the NK_1R has been activated and internalised, the location of the antagonist may play a larger role in the therapeutic potential of a drug.

The effect of the cholestanol control and of prolonged Span-Chol administration on mechanical hyperalgesia was measured using Von Frey filaments. This allowed for a more comprehensive understanding of the analgesic profile of Span-Chol than our previous study, revealing that the anti-hyperalgesia was sustained up to 8 h (Jensen *et al.,* 2017). Importantly, the cholestanol control, Chol-PEG-Biotin had no effect on paw withdrawal threshold and therefore the effect of the cholestanol observed in the plate-based assay may not translate into an *in vivo* model.

This study demonstrates that lipidation is a viable approach, not only for enhancing membrane affinity of soluble GPCR antagonists, but also for selectively targeting compartmentalised NK_1R signalling pathways of pathophysiological importance. We have assessed the potential for selective targeting of receptor-mediated signalling events from endosomes. Furthermore, this novel approach improves the pharmacological properties of an otherwise low potency NK_1R antagonist for the selective inhibition of signalling events associated with central pain transmission. Although we have observed ligand retention at the plasma membrane up to 4 h, there is potential to improve the uptake or to target drugs to different subcellular compartments by characterising and exploring other lipid-anchors.

Conflict of Interest. Research in the authors' laboratory is funded in part by Takeda Pharmaceuticals Inc.

Footnotes. Supported by NHMRC 63303, 1049682, 1031886, ARC Centre of Excellence in Convergent Bio-Nano Science and Technology and Monash University (N.W.B.)

Chapter 3

Characterising the biophysical and molecular dynamic profile of lipidated ligands using fluorescence correlation spectroscopy

3.1 Introduction

The dynamic activation of GPCRs from different cellular compartments can lead to distinct location-dependent signalling outcomes (Irannejad *et al.,* 2013). GPCR internalisation *via* arrestin/clathrin/dynamin-mediated endocytosis and subsequent endosomal signalling has been extensively studied (DeWire *et al.,* 2007, Hanyaloglu *et al.,* 2008, Shukla *et al.,* 2011). However, GPCRs have also been demonstrated to signal from other intracellular membranes and organelles such as the endoplasmic reticulum (Revankar *et al.,* 2005), nucleus (Joyal *et al.,* 2014, Sergin *et al.,* 2017), and Golgi membranes (Godbole *et al.,* 2017, Irannejad *et al.,* 2017). Together, signalling from different intracellular compartments within the cell may lead to distinct phenotypic outcomes and may be important therapeutic targets.

As demonstrated in **Chapter 2**, NK_1R can signal from endosomes in a sustained manner, distinct from the transient signalling profile of the plasma membrane-delimited receptor population (Mantyh *et al.,* 1995, Cottrell *et al.,* 2009, Murphy *et al.,* 2009, Zhang *et al.,* 2013, Jensen *et al.,* 2014, Jensen *et al.,* 2017). The spatial profile and reduced access of drugs to NK_1R may account for the limited clinical success of NK_1R directed therapeutic efforts (Jarcho *et al.,* 2013, Zhang *et al.,* 2013). Therefore, the spatial and temporal profile of receptors and drugs should be considered when developing therapeutic compounds.

One method to achieve directed intracellular targeting is by enhancing the cell permeability of drugs. The β-1 adrenoreceptor (β1AR) is a GPCR localised at the plasma membrane and in the Golgi network and independently be activated and signal from both locations (Irannejad *et al.,* 2017). Cell impermeable antagonists of the β1AR inhibits the plasma membrane, but not the Golgi receptor population (Irannejad *et al.,* 2017). Similar results have also been observed with a cell impermeant antagonist used in conjunction with a cell permeable agonist with intracellular populations of metabotropic glutamate 5 receptor (Sergin *et al.,* 2017). An alternative approach to developing new cell permeable drugs is to employ

drug delivery strategies such as lipid-conjugation. Lipid-conjugation promotes partitioning of ligands into the lipid bilayer to internalise into endosomes (Rajendran *et al.,* 2008, Rajendran *et al.,* 2012).

In **chapter 2**, cholestanol-conjugated, fluorescent probes and NK_1R antagonists were developed to study the use of lipid-conjugation to direct drugs to the NK_1R. We demonstrated that cholestanol-conjugated *via* PEG to a Cy5 fluorophore (Cy5-Chol) promoted plasma membrane anchoring and internalisation when compared to a non-lipidated control (Cy5-EE) (Jensen *et al.,* 2017). Cholestanol conjugation *via* PEG to an NK_1R antagonists, Spantide (Spantide-Chol), inhibited the intracellular signalling of the receptor when compared to unmodified Spantide in cell lines. Investigation revealed that administration of lipid-conjugated Spantide improved analgesic outcomes in mice compared to the unmodified drug (Jensen *et al.,* 2017). This may have been a result of anchoring to cell membranes and increasing local concentrations of the drug at the plasma membrane and in endosomes. Although modifications to change the hydrophobic properties of the ligands improved targeting and selectivity, these changes may have had consequences on the molecular dynamic profile of the compounds. As a result, the effective concentrations, diffusion profiles, and biophysical properties of cholestanol-conjugated ligands remain unknown.

The molecular dynamic profile of a drug or delivery system can include its diffusion, distribution, concentration, and molecular interactions. These parameters have previously been measured as indicators or predictors of pharmacokinetics, target engagement, and drug transport (Tatarkova *et al.,* 2005, Navratil *et al.,* 2006, Reitan *et al.,* 2008, Röcker *et al.,* 2009). Therefore, molecular dynamic profiles have been assessed for potential therapeutics in extracellular matrices, tissues, and cells, typically in cancer and tumour models (Lombardi Borgia *et al.,* 2005, Reitan *et al.,* 2008, Lynch *et al.,* 2009). This can be assessed using fluorescence correlation spectroscopy (FCS), a sensitive, biophysical technique, which

measures fluctuations in intensity caused by the diffusion of fluorescent species that passes through a confocal volume (Schwille 2006, Poyner *et al.*, 2009). Statistical autocorrelation analysis of these intensity fluctuations can be applied to quantitatively determine the diffusion coefficient and the concentration and a photon counting histogram can be used to determine the molecular brightness of fluorescent species (Schwille 2006, Poyner *et al.*, 2009).

To the best of our knowledge, the biophysical and molecular dynamic profiles of lipidated ligands have not been studied. Therefore, the aim of this study is to use FCS to characterise the molecular dynamic profile of fluorescently labelled lipidated ligands. Concentrations and diffusion coefficients of Cy5-Chol, Cy5-EE and Spantide-Cy5-Chol were determined in solution and were measured at significantly lower concentrations compared to the nominal concentrations. This reduced measured concentration was not time-dependent. Concentration measurements at height intervals above the chamber slide coverslip indicated non-specific binding of the ligands to the chamber slide. The addition of a stabilising agent reduced the non-specific binding and increased the measured concentrations. However, analysis of the diffusion coefficients revealed that the stabilising agent reduced the rate of diffusion for the cholestanol-conjugated ligands. The particle number and diffusion coefficients of ligands were also measured at the plasma membrane using FCS. The Cy5-Chol and Spantide-Cy5-Chol were both measured to have higher particle numbers and slower diffusion coefficients than the Cy5-EE control, suggesting that the cholestanol conjugation promotes interaction of the drug with the plasma membrane.

3.2 Methods

3.2.1 Synthesis

Synthesis of the tripartite ligands Spantide-Cy5-cholestanol, Cy5-cholestanol and Cy5-ethyl ester are as described in (Jensen *et al.*, 2017).

3.2.2 Cell lines

HEK293 cells were maintained in Dulbecco's modified Eagle's medium (DMEM) supplemented with 5% v/v FBS (37°C, 5% CO_2). HEK cells stably expressing N-terminally tagged NK_1R-SNAP were plated into Nunc Lab-Tek 8-well cover glass (SLS, Nottingham, UK) coated with 20 ng/well poly-D-lysine 48 h prior to the experiment.

3.2.3 SNAP-labelling

Cells were labelled with 0.1 µM SNAP Surface Alexa Fluor 488 (AF488) (30 min, 37°C, 5% CO_2). Cells were washed with Hanks' Balanced Salt Solution (HBSS) and incubated with fluorescent ligands at room temperature for 10 min.

3.2.4 Fluorescence Correlation Spectroscopy

Fluorescence correlation spectroscopy (FCS) is a confocal technique which can be used to measure low concentrations of fluorescent particles in small fixed detection volume approximately 0.2 fL and dimensions of 0.2 x 1 µm at 488 nm. The detection volume is defined by the diffraction limit of the light, i.e. the numerical aperture of the lens and the wavelength of the light. Accurate FCS measurements require a small diffraction limited focal point which can be achieved using an objective with a high numerical aperture. Fluorescent species that diffuse through the detection volume are excited and their emission is detected by a single-photon detector. The random diffusion of fluorescent species through the detection volume result in fluctuations in fluorescence intensity that can be statistically analysed using autocorrelation statistical analysis (Poyner *et al.*, 2009). This technique was used to determine diffusion time and concentration of the lipid-conjugated probes in solution.

3.2.5 FCS Calibration

FCS measurements were recorded using a Zeiss LSM510Meta Confocor 3 microscope fitted with a c-Apochromat 40x NA 1.2 water immersion objective lens. The pinhole diameter was set to 1 airy unit. The alignment of the pinhole is required to ensure that the measurement is taking place in the centre of the diffraction limited spot where the point spread function is defied and the signal to noise is at the highest. Therefore calibration of the optical system must be performed for each laser line required prior to an experiment (Schwille 2006, Poyner *et al.,* 2009). Cy5 NHS Ester (GE healthcare, Buckingham, UK) was used to calibrate the 633 nm laser as it has a known literature value for the diffusion coefficient of 3.16×10^{-10} m^2/s (Poyner *et al.,* 2009). Rhodamine 6G was used to calibrate the 488 nm laser line (diffusion coefficient 2.80×10^{-10} m^2/s) (Poyner *et al.,* 2009). The method of calibration and FCS measurement has been described previously (Schwille *et al.,* 1996, Poyner *et al.,* 2009). The microscope laser power was adjusted to obtain ~90kHz cpm/s for Rh6G or ~40kHz cpm/s for Cy5. After the alignment has been performed, FCS measurements of 10 sec measurements were repeated 10 times and a 60 sec read was taken for autocorrelation analysis and photon counting histogram (PCH) analysis. The autocorrelation analysis of the 10sec x10 recording is used to calculate the radius ω_0, the height ω_1 and volume of the Gaussian shaped detection volume(Ayling *et al.,* 2012) . The PCH analysis of the 60 sec recording can be used to calculate the molecular brightness of the fluorophore. PCH analysis is also used to obtain the first order correction factor which can correct for deviation from an ideal Gaussian observation volume (Huang *et al.,* 2004).

3.2.6 FCS measurements

FCS measurements of AF488 (ex λ: 488 nm argon, em: BP530-610 nm filter) and Cy5 (ex λ: 633 nm HeNe, em: LP650 nm filter) were performed using a Zeiss Confocor 3 fitted with a C-

Apo 40X NA/1.2 water immersion objective lens. Solutions were prepared in HBSS in the presence or absence of 0.1% w/v Bovine Serum Albumin (BSA). 200 µL of each solution was plated into Nunc Lab-Tek 8-well cover glass (SLS, Nottingham, UK). The focal point was positioned 200 µm into the solution and FCS measurements were taken at 633nm for 20s using equivalent laser powers unless specified otherwise. For FCS measurements in cells, the focus was set on the plasma membrane by placing the detection volume at the peak of an intensity scan of the SNAP label over a 4 µm z-range, with a 0.5 µm step interval (Dampening 1%, AOTF 5%). The measurements were then carried out for 60 sec (Dampening 1%, AOTF 60%), described previously (Kilpatrick *et al.*, 2012).

3.2.7 FCS analysis

Zeiss 2010 software (Carl Zeiss, Jena, Germany) was used for autocorrelation and photon counting histogram (PCH) analysis. The autocorrelation curve is derived from the time dependent fluctuations (Figure 3.1). The analysis calculates fluctuation ($\delta I(t)$) from the mean intensity, $\langle I \rangle$, at a given time, t, and the fluctuation a short time later ($\delta I(t+\tau)$). The product of these fluctuations is normalised to the square of the average intensity, $\langle I \rangle^2$, and this calculation is repeated over a range of lag times (τ) to produce an autocorrelation curve (equation 1). Curve fitting of the solution data was performed using a 1 component fit for diffusion in the x, y and z direction (3D Brownian diffusion) with a pre-exponential to account for a triplet state, a 2 component 2D model was used for the labelled receptor and ligands at the plasma membrane. From the autocorrelation curve, the particle number can be calculated as it is inversely proportional to the theoretical amplitude of the curve at G(0). The average dwell time of the fluorescent ligand can be calculated from the midpoint of the decay of the $G(\tau)$. In addition, the calculation of the detection volume and volume diameter can be used to calculate the concentration of each fluorescent species as well as the diffusion coefficient (Schwille 2005).

PCH analysis has previously been described (Huang *et al.*, 2004). For this study, data were analysed using a 1 component PCH model with a binning time of 20 µs.

$$G(\tau) = 1 + \frac{< \delta I(t).\delta I(t+\tau) >}{< I >^2}$$

Equation 1. Normalised autocorrelation equation.

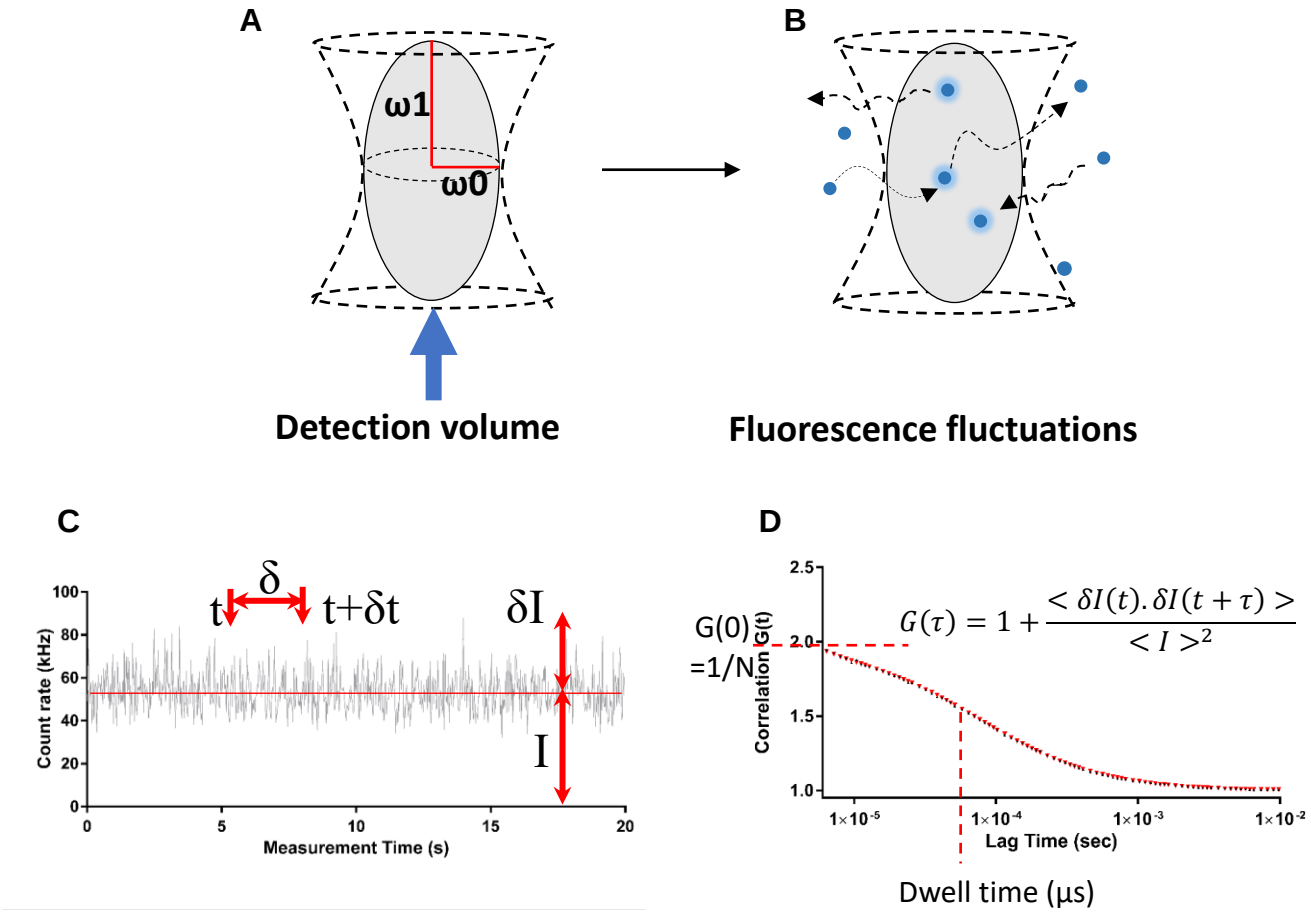

Figure 3.1. Detection and analysis. A, Illuminated confocal volume and the FCS detection volume (grey) are shown with the half axis for the lateral (ω0) and axial (ω1) parameters **B,** Fluorescent species that randomly diffuse through the illuminated volume are excited and fluorescent species that emit photons from within the detection volume are counted using avalanche photodiodes. **C**, Representative image of an FCS acquisition, recording fluctuations over time. The parameters used in the derivation of the autocorrelation curve are also shown.

D, The autocorrelation function shown graphically with a 1 component 3D Brownian model fit.

3.2.8 Data Processing and Analysis

Graphs were generated using GraphPad Prism 6.01 (San Diego, CA). Data comparing nominal and FCS measured concentrations were analysed using two-way analysis of variance (ANOVA) and post hoc Tukey's multiple comparisons test. Kinetic data were analysed with two-way ANOVA with a post hoc Dunnett's multiple comparisons test. For the analysis of FCS plasma membrane measurements one-way ANOVA and post hoc Tukey's test was applied (* $p<0.05$; ** $p<0.01$, ***$p<0.001$). Data are presented as mean ± S.E.M.

3.3 Results

3.3.1 Initial characterisation and optimisation

The main objective of this study was to examine the lipid and PEG conjugation-dependent changes in ligand interactions with solutions and cell membranes. This study used cyanine 5 conjugated *via* PEG to either cholestanol (Cy5-Cholestanol; Cy5-Chol) or an ethyl ester soluble end group (Cy5-ethyl ester; Cy5-EE) (Jensen *et al.,* 2017). An NK_1R antagonist Spantide, conjugated *via* PEG to cholestanol and cyanine 5 (Spantide-Cy5-Cholestanol; Span-Cy5-Chol) was also examined (Jensen *et al.,* 2017). To determine optimal FCS measurement conditions, Cy5-cholestanol (Cy5-Chol), Cy5-ethyl ester (Cy5-EE) and Spantide-Cy5-Cholestanol (Span-Cy5-Chol) fluorescence were measured at a range of laser powers. Each compound was prepared at 50 nM in HBSS, which is the highest concentration of ligand used in the FCS experiments in this study. The 633 nm laser power was varied at intervals between 5% and 100%. Each solution was continuously excited for 20 secs and the count rate of the photons over time were detected. Autocorrelation analysis with a 1 component 3D Brownian motion

model was applied to calculate the concentration. For each ligand, the calculated concentration did not vary with laser power over the range tested. An inflection was observed at the 100% laser power in the Cy5 (Figure 3.2A). Photon-counting histogram with a 1 component fit, with a 20 sec binning time was applied to calculate the molecular brightness. As the laser power increased, the molecular brightness of each ligand increased (Figure 3.2B). The consistency of the concentration measurements as well as the linearity of the molecular brightness calculations suggests that laser powers below the 100% may be used to perform future FCS experiments.

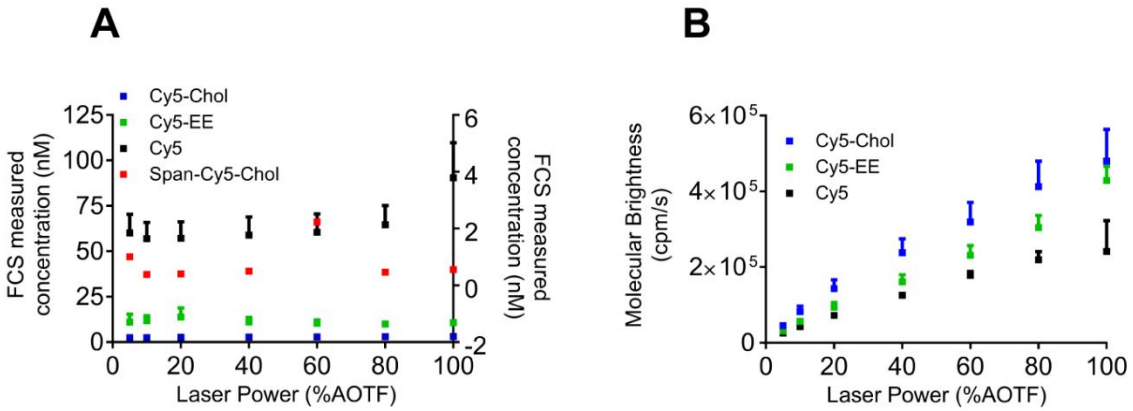

Figure 3.2. Optimisation of fluorescence correlation spectroscopy. A, Effect of varying laser on concentration of ligands measured. **B,** The effect of varying laser power on molecular brightness η. n=3; mean ±S.E.M.

3.3.2 Measured concentrations of Cy5, Cy5-ethyl ester and Cy5-cholestanol in HBSS

To determine the concentrations of each ligand Cy5-EE, Cy5-Chol, and Span-Cy5-Chol were prepared to 5 nM, 10 nM, 25 nM and 50 nM in HBSS at room temperature. The solutions were measured by FCS for 20 sec. Analysis by autocorrelation with a 1 component, 3D Brownian model with a pre-exponential for triplet states was applied to calculate the concentration of each ligand. A linear increase in concentration was measured relative to the nominal

concentration of ligand (Figure 3.3A-C) with R^2 values of 0.8121, 0.9366, and 0.1803 for Cy5-EE, Cy5-Chol, and Span-Cy5-Chol respectively. The measured concentrations of the 50 nM solutions of Cy5-Chol (3.1 ± 0.3 nM), Cy5-EE (11.8 ± 1.8 nM), and Span-Cy5-Chol (0.4 ± 0.1 nM) were all significantly lower than the nominal concentration prepared (Figure 3.3D). At the other nominal concentrations, the measured concentration of all three ligands were consistently lower.

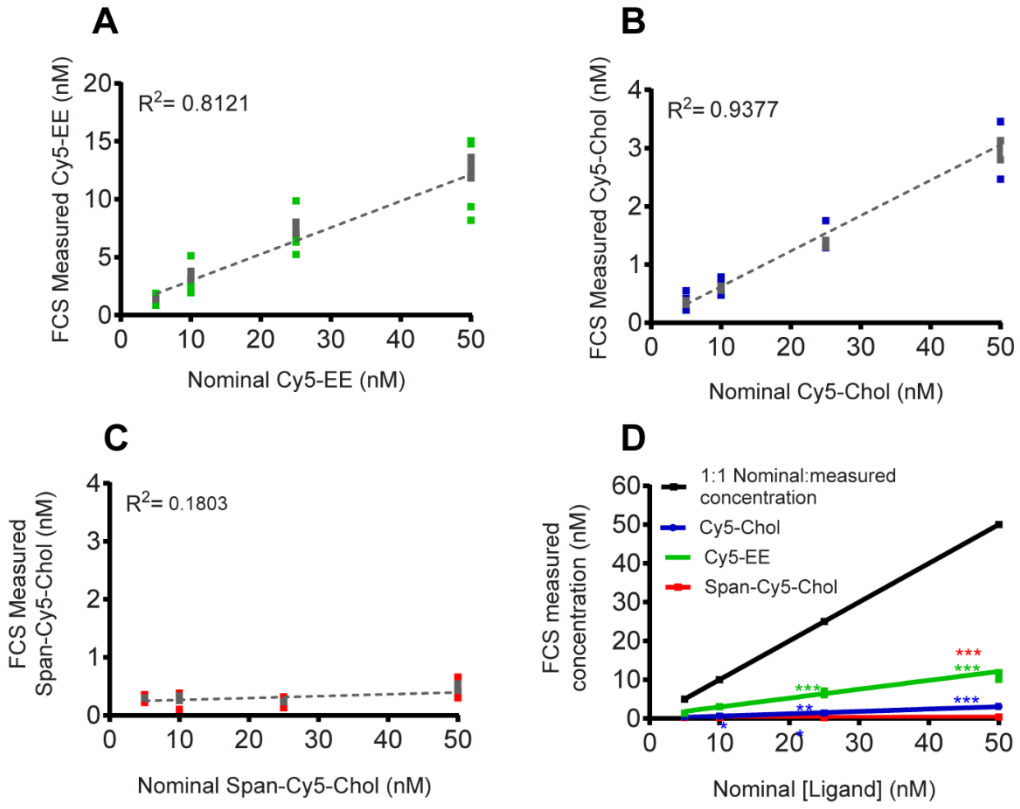

Figure 3.3. FCS measurement of Cy5, Cy5-ethyl ester and Cy5-cholestanol concentrations in HBSS. Measurements of each individual experiment and the averaged concentrations are shown in **A.** Cy5-ethyl ester (Cy5-EE), **B,** Cy5-cholestanol (Cy5-Chol), and **C,** Spantide-Cy5-cholestanol (Span-Cy5-Chol). **D,** Compiled graph of each ligand relative to the theoretical concentration. The solid black line demonstrates a theoretical 1:1 linear relationship between the measured and nominal ligand concentration. Two-way analysis of

variance (ANOVA) and post hoc Tukey's multiple comparisons test (* $p<0.05$, ** $p<0.01$, ***$p<0.001$). Data are n=3-4, presented as a mean ± S.E.M.

3.3.3 Kinetic concentration measurements of ligands

To investigate if the loss of ligand is time dependent, a range of concentrations of each ligand was measured by FCS over time. Cy5-EE, Cy5-Chol and Span-Cy5-Chol were prepared fresh in HBSS at room temperature and were measured immediately. Each solution was measured by FCS for 20 secs at 5 min intervals over 30 min. At all concentrations of each ligand, the concentration remained consistent over the 30 min (Figure 3.4A-C). This was confirmed by a two-way analysis of variance (ANOVA) and post hoc Dunnett's multiple comparisons test, comparing each value to the concentration at the corresponding 0 min time point.

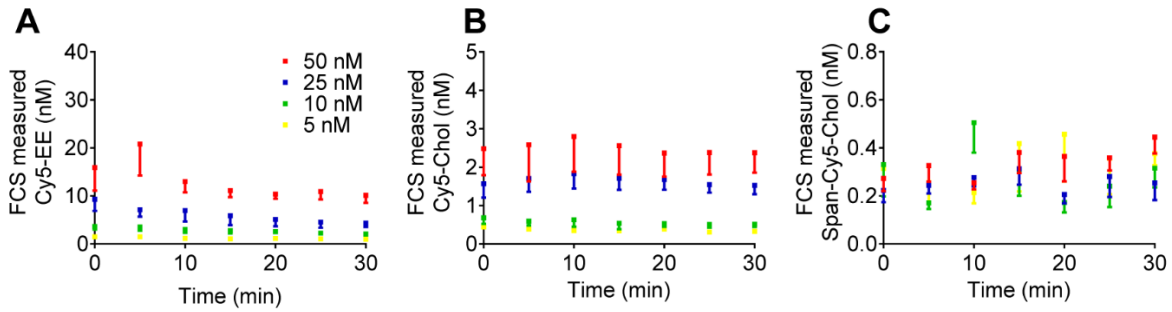

Figure 3.4. Kinetic profile of Cy5, Cy5-ethyl ester and Cy5-Cholestanol in HBSS. A, Cy5-ethyl ester (Cy5-EE), **B,** Cy5-Cholestanol (Cy5-Chol), and **C,** Spantide-Cy5-Cholestanol (Span-Cy5-Chol) concentrations were measured over 30 min. Data are n=3-4, presented as a mean ± S.E.M.

3.3.4 Measured concentrations of ligands in HBSS and bovine serum albumin

To determine if the deviation of measured concentrations were due to adhesion to surfaces during the drug preparation, HBSS was supplemented with bovine serum albumin (BSA) to prevent non-specific binding. Each ligand was prepared at a concentration range between 5 - 50 nM in HBSS with 0.1% w/v BSA. Compared to the concentrations of the ligands prepared in HBSS (Figure 3.3), the ligands prepared with BSA was measured at greater concentrations (Figure 3.5A-C). The relationship between the measured and nominal concentration remained linear with R^2 values of 0.9949, 0.9318 and 0.8572 for Cy5-EE, Cy5-Chol, and Span-Cy5-Chol, respectively. When compared to theoretical concentration of the solutions, the Cy5-EE ligand concentration was completely recovered at all concentration measured, with no significant deviation from the theoretical values. Conversely, the Cy5-Chol and Span-Cy5-Chol concentrations were partially recovered by blocking non-specific binding. Despite the partial recovery, the Cy5-Chol was still significantly different at the 50 nM nominal concentration measured to be 23.8 ±1.9 nM (Figure 3.5D). The Span-Cy5-Chol solutions prepared to 50 nM and 25 nM were measured by FCS to be at 2.1 ± 0.4 nM and 1.1 ± 0.1 nM, significantly lower (25-fold) than the nominal concentration. The Span-Cy5-Chol is significantly larger than the Cy5-Chol and Cy5-EE, affecting the solubility and hydrophobicity of the compound, this may have resulted in loss in the preparation of stocks, of the sample solutions, or may have resulted in complexes being formed.

3.3.5 Kinetic concentration measurements of ligands in preparations containing BSA

To investigate if the loss of the ligand in the preparations with BSA were time dependent, each ligand was measured by FCS at a range of concentrations over time. Cy5-EE, Cy5-Chol, Span-Cy5-Chol were prepared fresh in HBSS with 0.1% w/v BSA at room temperature and were measured immediately. Each solution was measured by FCS for 20 secs at 5 min intervals over

30 min. For each ligand, at all concentrations, the concentration remained consistent over the 30 min (Figure 3.6A-C). This was confirmed by a two-way analysis of variance (ANOVA) and post hoc Dunnett's multiple comparisons test, comparing each value to the concentration at the corresponding 0 min time point.

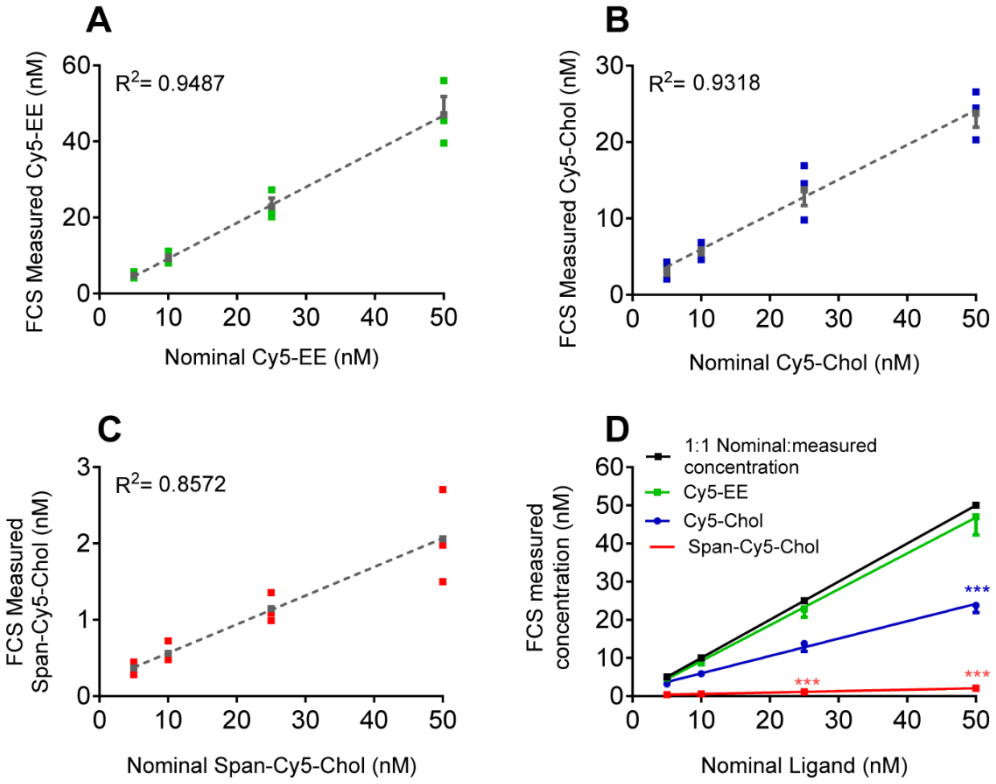

Figure 3.5. FCS measurement of Cy5, Cy5-ethyl ester and Cy5-Cholestanol concentrations in HBSS and BSA. Measurements of each individual experiment and the averaged data are shown in **A.**, Cy5-ethyl ester (Cy5-EE), **B**, Cy5-Chol (Cy5-Chol), and **C**, Span-Cy5-Chol (Span-Cy5-Chol). **D,** Compiled graph of each ligand relative to the theoretical concentration. Two-way analysis of variance (ANOVA) and post hoc Tukey's multiple comparisons test (***p <0.001). Data are n=3, presented as a mean ± S.E.M.

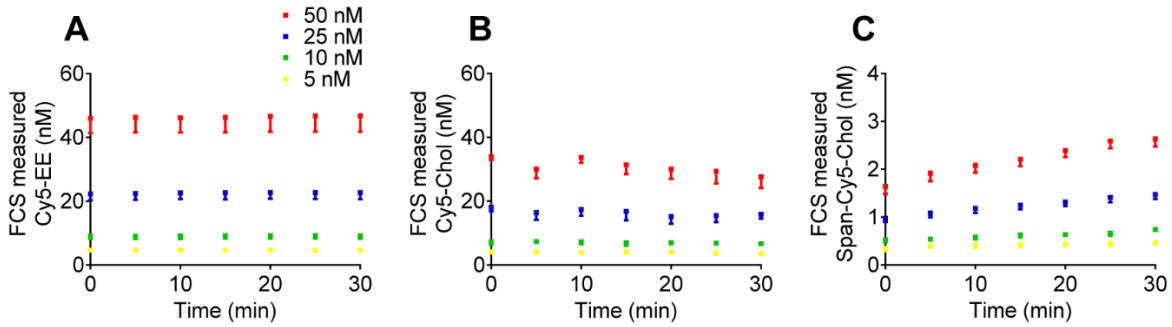

Figure 3.6. Kinetic profile of Cy5, Cy5-ethyl ester and Cy5-Cholestanol in HBSS with BSA. A, Cy5-ethyl ester (Cy5-EE), **B**, Cy5-Cholestanol (Cy5-Chol), and **C,** Spantide-Cy5-Cholestanol (Span-Cy5-Chol) concentrations were measured over 30 min. Data are n=3, presented as a mean ± S.E.M.

3.3.6 Diffusion coefficient measurements of ligands

To investigate the effect of conjugation of a PEG chain or a PEG chain conjugated to cholestanol on the diffusion of each ligand, the dwell time of was determined from the abscissa of the autocorrelative function and diffusion coefficients were calculated from FCS measurements (Figure 3.7A). Each ligand was prepared at a concentration range of 5-50 nM in HBSS. The diffusion coefficient was obtained from the experiments performed in Figure 3.3. The diffusion coefficients remained constant for all concentrations with similar diffusion coefficients measured for the Cy5-EE and Cy5-Chol. Conversely, Span-Cy5-Chol diffused through the confocal volume at half the speed of the Cy5-EE and Cy5-Chol probes. The diffusion coefficients of Cy5-EE, Cy5-Chol, and Span-Cy5-Chol averaged from 4 individual experiments were 203.5 ± 5.7 $\mu m^2/s$, 207.5 ± 6.7 $\mu m^2/s$, and 109.1 ± 18.8 $\mu m^2/s$ respectively in 25 nM preparations. To determine the effect of solubilising the ligands with BSA, on the

diffusion coefficient, the same experiment was repeated in preparations containing 0.1% w/v BSA (Figure 3.7B). The diffusion remained constant for all concentrations of Cy5-EE, Cy5-Cholestanol, and Span-Cy5-Chol with the average of 211.8 ± 10.3 $\mu m^2/s$, 51.6 ± 1.1 $\mu m^2/s$ and 44.3 ± 1.3 $\mu m^2/s$, respectively in 25 nM preparations. The diffusion coefficient of the Cy5-EE was not impacted by the addition of BSA into the preparation. In contrast, the Cy5-Chol and Span-Cy5-Chol diffusion coefficients decreased to similar diffusion coefficients.

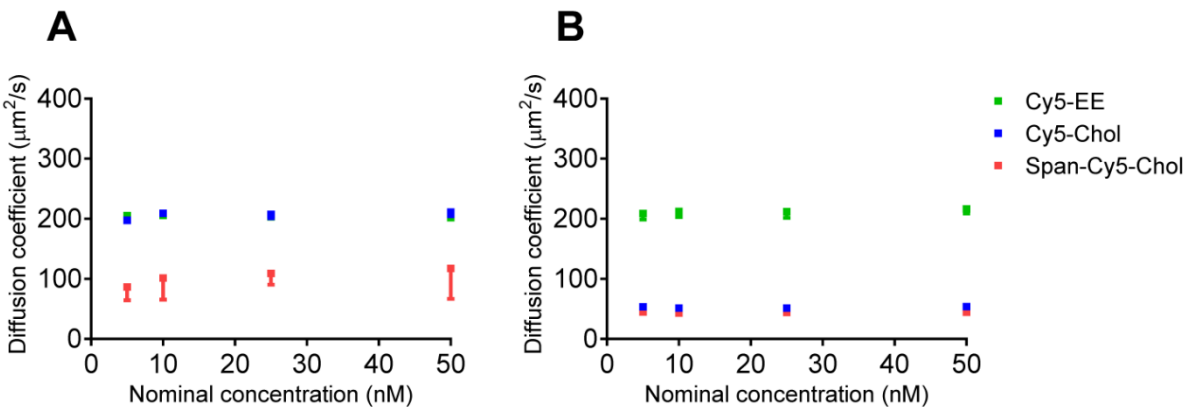

Figure 3.7. Diffusion coefficients of Cy5, Cy5-ethyl ester and Cy5-Cholestanol. A, Diffusion coefficients of Cy5-ethyl ester (Cy5-EE), Cy5-Cholestanol (Cy5-Chol), Spantide-Cy5-Cholestanol (Span-Cy5-Chol) prepared in HBSS at 5, 10, 25 and 50 nM. **B,** Diffusion coefficients of Cy5, Cy5-ethyl ester, and Cy5-Chol prepared in HBSS with BSA at 5, 10, 25 and 50 nM. Data are n=3-4, presented as a mean ± S.E.M.

3.3.7 Measured concentrations of ligands at intervals above the coverslip

The investigation into the reduced FCS measured concentrations compared to the nominal concentrations indicated that the loss was not time-dependent and further investigation has demonstrated at least a partial recover with a solubilising agent which has led to the hypothesis that the ligands are non-specifically adhering to surfaces. To confirm this, concentrations of ligands at intervals above the coverslip were measured to determine if there is loss of ligands

in solution due to adhesion. Cy5-EE, Cy5-Chol, and Span-Cy5-Chol were prepared to 10 nM in HBSS and were measured immediately. Each solution was measured for 15 secs at intervals ranging from 2 µm to 50 µm above the coverslip (Figure 3.8A). The highest concentration of each ligand was measured within 2-4 µm of the coverslip. As the distance from the coverslip increased, the measured concentration decreased until the concentration reached a plateau. These experiments were repeated in the presence of BSA to determine the effect of the solubilising agent on ligand adhesion. In the preparations containing 0.1% w/v BSA (Figure 3.8B), the measured concentration of each ligand remained consistent over the distance measured. The concentration of the Cy5-EE was completely recovered to the nominal concentration. Similar to the results in Figure 3.5, the Cy5-Chol and Span-Cy5-Chol concentrations were only partially recovered.

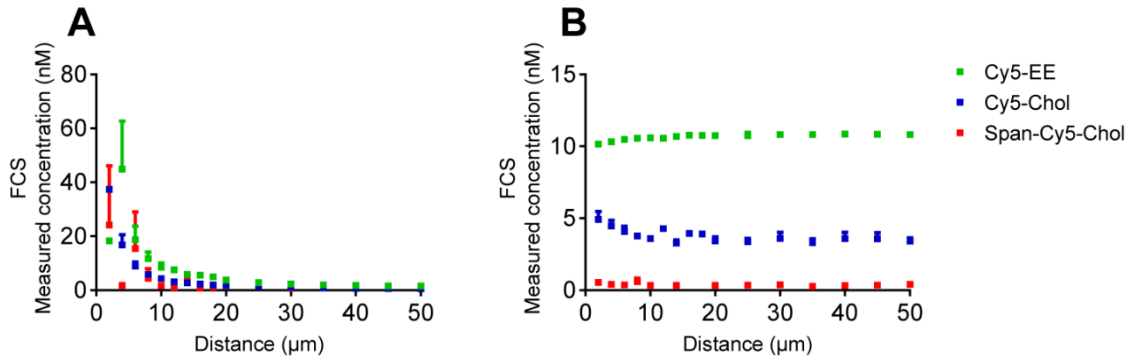

Figure 3.8. FCS measurement of Cy5, Cy5-ethyl ester and Cy5-Cholestanol at intervals from the coverslip. FCS measurements at intervals starting from a distance of 2 µm from the coverslip to 50 µm. Cy5, Cy5-ethyl ester (Cy5-EE), and Cy5-Cholestanol (Cy5-Chol) were prepared in **A,** HBSS or **B,** HBSS containing 0.1% w/v BSA. Data are n=3-4, presented as a mean ± S.E.M.

3.3.8 Measured concentrations of ligands at the plasma membrane

Cy5-EE, Cy5-Chol and Span-Cy5-Chol particle number and diffusion coefficients were measured at the plasma membrane to investigate possible interactions of the ligands with the plasma membrane or the NK_1R. In this part of the study, 10 nM of Cy5-Chol, Cy5-EE or Span-Cy5-Chol were incubated in mixed population HEK293, stably expressing SNAP-NK_1R. The binding affinity of SP to fluorescein labelled SNAP-NK_1R has been measured in fluorescent competition binding assays with a Kd value of 9.8 nM, which is approximately five-times lower than the Kd for the wild-type receptor (Zwier *et al.*, 2010). For FCS measurements at the plasma membrane, the particle number is presented instead of the concentration to account for the 2D lateral distribution of ligands rather than 3D Brownian motion (Kilpatrick *et al.*, 2010). The particle number of the Cy5-EE was significantly greater than the Cy5-Chol with 12.3 ± 7.0 N/μm^2 and 2.8 ±1.2 N/μm^2 measured respectively (Figure 3.9). The diffusion coefficient of Cy5-EE was also greater than Cy5-Chol with respective measurements of 47.8 ± 17.4 $\mu m^2 s^{-1}$ and 2.8 ± 0.6 $\mu m^2 s^{-1}$. The high diffusion coefficient of the Cy5-EE may indicate that the ligand is diffusing above or interacting with the plasma membrane rather than anchoring into the lipid bilayer. Span-Cy5-Chol has previously been investigated as an imaging probe in time-dependent internalisation assays using 1µM of the ligand in which the Cy5 was observed in punctate regions in the cell membrane (Jensen *et al.*, 2017). Span-Cy5-Chol was also measured at the plasma membrane of high expressing and low expressing NK_1R-SNAP cells labelled with SNAP surface-Alexa Fluor 488 (AF488). The particle number of the Span-Cy5-Chol in the low and high expressing NK_1R cells were 0.304 ± 0.35 N/μm^2 and 1.793 ± 3.29 N/μm^2 respectively. Given that the Span-Cy5-Chol was used primarily as an imaging probe, there is currently no binding or potency data for the ligand to NK_1R. However, based on the data presented here, we observe a receptor density-dependent increase in the particle number. This is likely due to an interaction with the receptor based on the slower diffusion coefficient

compared to the Cy5-Chol, which is also anchored into the plasma membrane. To interpret this data further, it is imperative that the binding affinity and potency of the Span-Cy5-Chol be measured in future experiments.

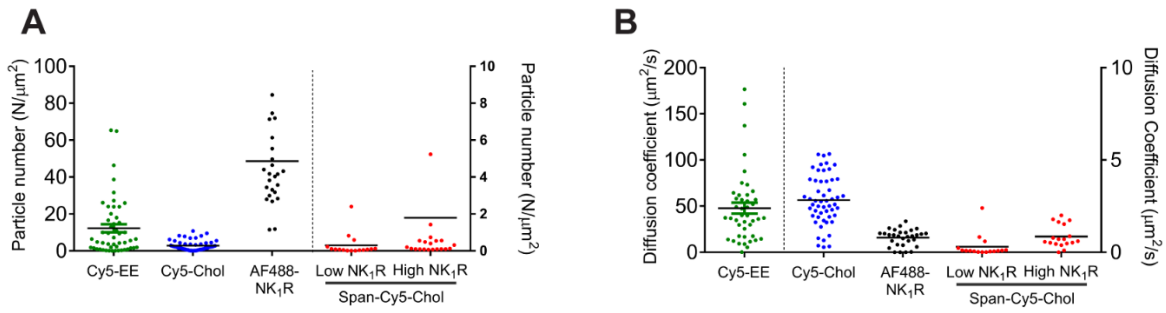

Figure 3.9. Cell membrane FCS measurements in mixed population AF488 SNAP-labelled NK_1R cells A, Particle number (Span-Cy5-Chol right y-axis) and **B,** diffusion coefficients of Cy5-EE (left y-axis), after 4 h incubations with 10 nM of Cy5-Chol and Spantide-Cy5-Chol in cells with high or low expression of NK_1R. n= 16-54 cells in 3-5 individual experiments.

The expression of cells was manually categorised using the camera. The diffusion coefficient of the Span-Cy5-Chol in low and high expressing NK_1R cells were measured at 0.7 ± 0.37 $\mu m^2 s^{-1}$ and 0.857 ± 0.35 $\mu m^2 s^{-1}$. Lastly, the NK_1R-SNAP labelled with AF488 and cells with medium expression was measured at the plasma membrane with a particle number of 48.62 ± 26.45 $N/\mu m^2$ and diffusion coefficient of 0.793 ± 0.26 $\mu m^2 s^{-1}$. Given that the particle number varied within individual experiments, the variability of the NK_1R particle number detected at the plasma membrane is likely due to the mixed cell line, rather than a variability in receptor labelling. Compared to the cholestanol-conjugated ligands, the Cy5-EE has the fastest diffusion rate and is approximately 18-fold greater than the diffusion coefficient of Cy5-Chol. The diffusion coefficient of Cy5-Chol was greater than Span-Cy5-Chol in the high and low

expression cells, although this was not statistically significant. Interestingly, the Span-Cy5-Chol diffused with a similar diffusion coefficient to the receptor, suggesting possible receptor interactions of the ligand.

Table 3.1. The average particle number (N/μm^2) and Diffusion coefficient (μm^{2}s^{-1}) at the plasma membrane. NK_1R expressing cells were incubated with 10 nM of ligand prepared in HBSS and incubated at 37°C for 30 min. n= 16-54 cells in 3-5 individual experiments and presented as mean ± S.E.M.

Ligand	Particle number	Diffusion coeff.
Cy5-EE	12.3 ± 7.0	47.8 ± 17.4
Cy5-Chol	2.8 ±1.2	2.8 ± 0.6
Span-Cy5-Chol (low exp.)	0.3 ± 0.4	0.7 ± 0.4
Span-Cy5-Chol (high exp.)	1.8 ± 3.3	0.9 ± 0.4
NK_1R-SNAP AF488	48.6 ± 26.5	0.8 ± 0.3

3.4 Discussion

Lipid-conjugation to drugs have previously been explored and proposed as a means of delivering drugs intracellularly, including the recycling endopeptidase, β-site amyloid precursor protein cleaving enzyme 1 (BACE-1) which is expressed in central neurons of the brain (Rajendran *et al.,* 2012). In **chapter 2,** we used lipidated NK_1R antagonists to probe intracellular NK_1R signalling through which the antagonist, Span-Chol, was demonstrated to inhibit endosomal but not plasma membrane derived ERK signalling. However, in previous imaging experiments, Cy5-Chol is still present at the cells surface 4 h after the initial addition of the probe (Jensen *et al.,* 2017). Despite the extensive characterisation of the effect of cholestanol conjugation of Spantide on signalling events and analgesia, there is little understanding of the molecular dynamic and biophysical profile that lipid-conjugation has on ligands.

To further understand the mechanism by which cholestanol conjugation changes the properties of a compound and how that promotes directed targeting, we characterised the properties of the cholestanol linked probes. When we examined the Cy5-EE, Cy5-Chol, and Span-Cy5-Chol, prepared in HBSS we have observed significantly lower concentrations of the ligands when compared to the nominal concentrations. These results suggested that the loss was due to the conjugation to both the PEG chain and the cholestanol. Although the ligands were measured immediately after they were prepared, the kinetic measurements of the concentrations showed that there was no time dependent decrease. FCS measurements were recorded near the coverslip and at intervals away from the coverslip. The concentrations of all ligands were higher near the coverslip and decreased as the focal volume and hence, detection volume was moved further from the coverslip. These data indicated that there was significant loss of ligands due to adhesion to the coverslip and to the chamber walls. This also suggested that the adhesion of the ligands occured rapidly and was not detected in the kinetic reads in

which FCS was measured over 30 minutes at 5-minute intervals. Therefore, the low measured concentrations relative to the nominal may have been due to adhesion of the ligands to tubes and pipette tips in the preparation of the solutions.

An approach to reduce the adhesion of ligands to surfaces may include the coating of tubes, pipette tips, and plates However, formulation approaches such as solubilising agents or carrier particles may be more advantageous, by preventing the adhesion of ligands throughout the preparation process regardless of the tools and vessels used. Serum albumins have been commonly used to solubilise hydrophobic ligands and have also been investigated in nanocarriers and drug formulations (Jiang *et al.,* 2001, Kratz 2008, Zhao *et al.,* 2010, Chaturvedi *et al.,* 2015). Furthermore, BSA has previously been included in preparations of lipophilic compounds for FCS measurements (Fujii *et al.,* 1992, Kilpatrick *et al.,* 2012). Therefore, to solubilise the PEG and lipid-conjugated ligand solutions, 0.1% w/v BSA was included in the HBSS. In contrast to ligands in HBSS, the concentrations of solutions prepared in HBSS and 0.1% w/v BSA had higher concentrations. Cy5-EE measured concentrations completely recovered to the nominal concentration, whereas the Cy5-Chol and Span-Cy5-Chol were only partially recovered. The complete recovery of Cy5-EE but not the cholestanol-conjugated ligands suggested that the cholestanol promotes non-specific adherence during the preparation of the stock or to the BSA. The measured concentration of ligands over time yielded a similar result to the ligands in HBSS. These results suggested that the addition of BSA in the HBSS increased the measured concentration by increasing solubilisation of the ligands. The consistent concentration of ligands measured at distances ranging from 2-50 μm from the coverslip further supported that losses in concentration were attributed to the ligands partitioning to the solution-glass interface.

The diffusion profiles of Cy5-EE, Cy5-Chol, and Span-Cy5-Chol were also measured by FCS. The diffusion coefficients of all ligands were consistent regardless of concentration.

Interestingly, when prepared in HBSS, the Cy5-EE and Cy5-Chol had similar diffusion coefficients, while the Span-Cy5-Chol diffused through HBSS with approximately half the diffusion rate. Changes in diffusion coefficient can be induced by chemical reactions or changes in the hydrodynamic radius. In this study, the ligands have not been subject to chemical reactions and thus the differences in diffusion coefficient are likely due to factors affecting the hydrodynamic radius such as temperature, viscosity, folding structure, or mass (Schwille *et al.*, 2001, Poyner *et al.*, 2009). Given that the ligands were all measured under the same conditions, temperature and viscosity are unlikely to have contributed to the change in diffusion. Changes in diffusion coefficients should correlate to the molecular weight of each of the ligands of 3526.44 g/mol, 1498.79 g/mol and 1842.40 g/mol for the Span-Cy5-Chol, Cy5-EE and Cy5-Chol respectively. In order to achieve a 1.6 fold difference in diffusion time, a 6 fold difference in the mass is required as the diffusion time is proportional to the cube root of the difference in molecular weight (Meseth *et al.*, 1999, Schwille *et al.*, 2001, Poyner *et al.*, 2009). The difference in molecular weight of the Cy5-Chol and Cy5-EE is not significant enough to affect the diffusion coefficient. Although the mass of Span-Cy5-Chol is approximately two-fold greater than Cy5-EE and Cy5-Chol, this difference in mass should not be enough to halve the diffusion coefficient. In the absence of BSA, the low diffusion coefficient of the Span-Cy5-Chol may be due to complexes or oligomers of Span-Cy5-Chol. The diffusion coefficients of the ligands were also measured in HBSS supplemented with BSA. The presence of BSA decreased the diffusion coefficients of the Cy5-Chol and Span-Cy5-Chol. Compared to the Cy5-EE control, the Cy5-Chol and Span-Cy5-Chol diffusion coefficients were 0.25-fold of the control. Although the diffusion coefficient of Span-Cy5-Chol in HBSS indicated possible oligomerisation, further reduction of the diffusion coefficient from 109.1 ± 18.8 $\mu m^2/s$ to 44.3 ± 1.3 $\mu m^2/s$ in the presence of BSA suggests that the ligand may interact with BSA. Together, considering the mass of BSA (66.4 kDa), the change in the diffusion coefficient of the Cy5-

Chol and Span-Cy5-Chol ligands are likely due to interactions with the protein. The similar diffusion coefficients of the Cy5-Chol and Span-Cy5-Chol were also indicative of the predominate effect that the BSA had on the ligands due to the great mass comparative to the ligands with an approximate 35-fold and 19-fold difference in mass respectively. However, further experiments and analysis are required for the determination if the change in diffusion is due to complexation of these ligands.

In the development of new drugs or drug delivery devices, it is important to elucidate the molecular dynamic profiles of ligands in solution and in cells to develop a comprehensive understanding of the ligand interactions. Previously, we have reported the use of FCS to measure the concentration of Cy5-EE and Cy5-Chol in media directly above cells and at increasing distances from the plasma membrane. Cy5-EE concentrations were observed to decrease as the concentration was measured closer to the plasma membrane. In contrast, Cy5-Chol concentrations increased as the focal volume measured approached the plasma membrane. These results provided critical understanding of the behaviour of lipid-conjugated ligands as they distribute in media or cell membranes. To further our understanding of ligand interactions with cell membranes, FCS was measured at the plasma membrane. The Cy5-EE when compared to Cy5-Chol and Span-Cy5-Chol was detected with a greater particle number/μm^2. However, the diffusion coefficient of the Cy5-EE was also significantly greater than the Cy5-Chol and Span-Cy5-Chol. Compared to the diffusion coefficient of the ligands in solution, the diffusion coefficients measured in cells was significantly lower. This suggested that the Cy5-EE measured interacted with the plasma membrane but did not anchor into the lipid bilayer. The Span-Cy5-Chol was present at the lowest concentration in cells. When comparing high and low expression of NK_1R the particle number was greater in the high expression cells. The diffusion coefficient of the Span-Cy5-Chol present was comparable to the diffusion coefficient of the NK_1R in the cell line. To further this study, it would be

informative to compare the properties of Span-Cy5-Chol in the plasma membrane in presence and absence of the receptor, to determine if the antagonist is interacting with NK_1R.

These studies have provided valuable insight into the molecular dynamic profile of lipid-conjugated ligands. We have also elucidated the spatial profile of lipid-conjugates in solution in the presence and absence of cells. Together with the previous imaging and signalling studies, the measured concentrations of the ligands in previous studies were likely to be significantly lower than the nominal concentrations. In addition, the number of lipid-conjugate particles that partition towards and interact with the cell may also be lower than expected. Despite the concentration of Span-Chol likely to have been lower than that of Spantide in previous studies, it was still effective in inhibiting intracellular signalling. Therefore, the inhibitory effect of the Span-Chol may be a function of the interactions at the plasma membrane and in endosomes. In future experiments, Spantide-Cy5 characterisation would further the current understanding of the effect of cholestanol conjugation on antagonists.

Given that the lipid-modification of the Spantide resulted in an increase in non-specific adhesion, formulation approaches such as nanocarriers and solubilising agents may be employed to reduce this effect. Nanocarriers are highly dynamic and are capable of encapsulating hydrophobic ligands through covalent and non-covalent means. Non-covalent encapsulation of drugs is particularly advantageous as it does not require a mechanism of cleavage to release the drug and no modifications are made to the structure of the ligand (Ulbrich *et al.,* 2016). Furthermore, nanocarriers can also be designed to release the drug in response to different stimuli including temperature, pH, specific wavelengths of light, and redox conditions (Ganta *et al.,* 2008, Zhang *et al.,* 2008, Gao *et al.,* 2010, Peng *et al.,* 2013). Similarly, solubilising agents can reduce non-specific adhesion of the ligands by increasing the hydrophobicity of the solution itself. This reduces the energy required for the compounds to

interact with the buffer, decreasing the adhesion to non-specific, hydrophobic materials (Van Oss 2006).

Together, this study has emphasised the importance of understanding the hydrophobic and diffusion characteristics of potential therapeutic ligands. Therefore, newly developed drugs should also be examined in solutions, at the plasma membrane with potential for measurements in endosomal compartments to gain a comprehensive understanding of the molecular dynamic and spatial profile. Future work to elucidate the molecular dynamic profile and mechanism of action of lipid-conjugated ligands may also include FCS in microdomains of the cell such as endosomes to determine the local concentration of drugs to access endosomal signalling of GPCRs.

Chapter 4

Incorporation of Di(Ethylene Glycol) Methyl Ether Methacrylate (DEGMA) to Reduce Polycation-Dependent Cytotoxicity of pH-Sensitive Nanoparticles

Quynh N. Mai,[a, b] Ngoc M. Vu, [b, c] Nghia Truong,[b, c] Paulina Ramirez-Garcia,[b, c] An Huu Tran-Doan,[b, c] John F. Quinn, [b, c] Michael R. Whittaker, [b, c] Nigel W. Bunnett,[b, d, e, f] Nicholas A. Veldhuis[a, b] and Thomas P. Davis[b, c, g]

a. Drug Discovery Biology, Monash Institute of Pharmaceutical Sciences, Monash University, Parkville, Victoria 3052, Australia
b. ARC Centre of Excellence in Convergent Bio-Nano Science and Technology, Monash Institute of Pharmaceutical Sciences, Monash University, 381 Royal Parade, Victoria 3052, Australia
c. Drug Delivery Disposition and Dynamics, Monash Institute of Pharmaceutical Sciences, Monash University, Parkville, Victoria 3052, Australia
d. Department of Pharmacology and Therapeutics, University of Melbourne, Parkville, VIC 3010, Australia
e. Department of Surgery, Columbia University, New York, NY 10032
f. Department of Pharmacology, Columbia University, New York, NY 10032
g. Department of Chemistry, University of Warwick, Gibbet Hill, Coventry CV4 7AL, United Kingdom

4.1 Abstract

Stimulus-responsive nanoparticles have shown great potential, for selective drug targeting and delivery, to treat globally important diseases such as cancer and inflammation. These nanoparticles can be beneficial due to selective targeting of therapeutics while avoiding off-target effects, the primary goal of stimulus-responsive nanoparticle drug delivery is to exploit the unique microenvironments observed within disease states, including distinct pH, redox conditions or protein expression. The use of pH as a stimulus has been particularly attractive for nanoparticles because monomers with different pK_a characteristics can be readily incorporated to achieve fine-tuned drug release in specific pH conditions observed in tumours, inflamed tissue undergoing acidosis and in distinct acidic intracellular micro-environments of endocytic compartments. However, polycationic polymers such as polyethylenimine, which has been widely used in gene delivery, have also been shown to be cytotoxic through the induction of apoptosis. Here we investigate the toxicity of two widely exploited monomers, 2-(Diethylamino) ethyl methacrylate (DEAEMA) (pK_a ~7.1) and 2-(Diisopropyl amino) ethyl methacrylate (DIPMA) (pK_a ~6.1) for pH-responsive self-assembling nanoparticle systems. Nanoparticle disassembly and cell health was assessed *via* multiple approaches and although DEAEMA rapidly disassembles to release intracellular cargo within endosomes, it was more cytotoxic than DIPMA. To overcome this, di(ethylene glycol) methyl ether methacrylate (DEGMA) was incorporated into the hydrophobic portion of the block copolymer; to protect or shield against polycation-dependent cytotoxicity without affecting pH-sensitivity or cellular uptake of particles. Together, this demonstrates the importance of using a combination of cell health indicators to understand the cytotoxicity profiles of macromolecules in cells and offers a new and valuable approach for reducing the cytotoxicity of pH-responsive materials *in vivo*.

4.2 Introduction

In recent years, nanoparticles have offered significant therapeutic promise due to their versatility and potential for clinical applications, including drug delivery, utility as biosensors and diagnostic systems. In particular, nanoparticles can be engineered to elicit a physio-chemical response to external biological stimuli such as enzymatic cleavage (Ghadiali *et al.,* 2008), temperature (You *et al.,* 2008), light (You *et al.,* 2010), or pH (Zhang *et al.,* 2011, Zhou *et al.,* 2011). The unique pH microenvironments found in affected tissues of diseases, such as cancer, or chronic inflammation, are considered particularly attractive stimuli, which has encouraged the development of multiple pH-responsive nanoparticle systems for targeted and stimulated delivery of a range of therapeutics agents (Wike-Hooley *et al.,* 1984, Webb *et al.,* 2011), including intracellular delivery of siRNA or cytotoxic compounds (Meyer *et al.,* 2008, You *et al.,* 2010, Du *et al.,* 2011, He *et al.,* 2013).

The internalisation of non-targeted nanoparticles into cells occurs through multiple constitutive endocytic processes. Nanoparticles with radii greater than 500 nm generally are internalised *via* phagocytosis (Zhao *et al.,* 2018). Smaller nanoparticles internalise by micropinocytosis, caveolin-dependent, clathrin-dependent endocytosis, or clathrin-independent endocytosis (Doherty *et al.,* 2009, Hillaireau *et al.,* 2009, Zhang *et al.,* 2015). The endocytic route for nanoparticle internalisation is dependent on a multitude of factors including size, surface charge, stiffness and shape (Osaki *et al.,* 2004, He *et al.,* 2010, Zhang *et al.,* 2015, Zhao *et al.,* 2018). Particles internalised *via* receptor-mediated, clathrin-dependent endocytosis have been shown to vary in size up to 200 nm (Rejman *et al.,* 2004, dos Santos *et al.,* 2011). Modifying nanoparticle surface chemistry or decoration with ligand or antibodies can improve protein interactions and enhance uptake *via* receptor-mediated endocytosis (Figure 4.1) (Sperling *et al.,* 2010, Mahon *et al.,* 2012, Sapsford *et al.,* 2013).

Following the internalisation of nanoparticles into vesicles that pinch off the cell surface membrane and fuse with early endosomes, particles are sorted throughout the tubulo-vesicular endosomal network and have multiple cellular fates (Doherty *et al.,* 2009, Hillaireau *et al.,* 2009). As early endosomes mature, they fuse and frequently share cargo with late endosomes, and it is from here that nanoparticles or macromolecules can be shuttled back out of the cell *via* sorting into recycling endosomes, or can be targeted towards lysosomes or proteasomes in the degradative pathway (Doherty *et al.,* 2009, Hillaireau *et al.,* 2009, Huotari *et al.,* 2011, Zhao *et al.,* 2018). Once nanoparticles enter endocytic pathways, they are exposed to reducing pH gradients mediated by V-ATPases, or proton pumps (Beyenbach *et al.,* 2006, Marshansky *et al.,* 2008). The acidification increases as the endosomal compartments mature from early endosomes (pH 6.1-6.8) to late endosomes (pH 4.8-6.0) and deeper endocytic compartments such as lysosomes (pH >5.5) (Mellman *et al.,* 1986, Huotari *et al.,* 2011).

Endosomal pH gradients have been exploited in the design of nanosensors and nanomedicines by conjugating pH-labile crosslinkers, pH-dependent protein transduction domains for cell penetration, or amine-containing monomers (Ganta *et al.,* 2008, Lee *et al.,* 2008, Gao *et al.,* 2010, Mura *et al.,* 2013). Nanoparticles assembled from materials containing tertiary amines, such as 2-(Diethylamino)ethyl methacrylate (DEAEMA) (pK_a ~7.1) or Poly(l-histidine) (pK_b <6.0) are used for fine tuning of polymer pKa. In endosomal pH environments, nanoparticle disassembly is proposed to be initiated through polymer protonation, leading to a hydrophobic to hydrophilic switch and with contributions from like charge-mediated repulsion (Lee *et al.,* 2003, Hu *et al.,* 2007, Kim *et al.,* 2008, Wu *et al.,* 2010). Importantly, while there are many therapeutic applications of pH responsive materials, it has been widely demonstrated that some polycationic materials may reduce cell health (Fischer *et al.,* 2003, Hunter *et al.,* 2010, Parhamifar *et al.,* 2010).

Polycationic polymers such as polyethylenimine (PEI) are widely studied materials with applications as a metal chelator, flocculating agent, and as an efficient gene delivery system (Fischer *et al.,* 1999, Kunath *et al.,* 2003, Lungwitz *et al.,* 2005). However, these polycationic polymers have also been reported to modulate metabolic function (Parhamifar *et al.,* 2010) and significantly reduce cell viability due to membrane perforation and rupture (Bieber *et al.,* 2002, Clamme *et al.,* 2003), or interaction with essential cellular proteins such as protein kinases (Leroy *et al.,* 1995, Vepa *et al.,* 1997, Bachrach *et al.,* 2001). The polycationic properties of pH-responsive materials have also been reported to influence cell viability through endosomal escape, due to a proposed "proton-sponge effect", where unsaturated amines in polymers form a proton sink when in acidic endosomal environments, which increases retention of chloride ions and water molecules, leading to endosomal swelling and eventual membrane rupture (Haensler *et al.,* 1993, Behr 1997, Fischer *et al.,* 1999, Nel *et al.,* 2009).

The increased charge state of pH-responsive polymeric materials in acidic environments are at risk of affecting cell health, typically due to the presence of charged tertiary amines (Meyer *et al.,* 2008, Won *et al.,* 2009, Parhamifar *et al.,* 2010, Zhou *et al.,* 2011), and hence, measuring cell viability is a critical factor for determining the success of nanoparticles in *in vitro* or pre-clinical settings. Particle-dependent cell toxicity can be reduced by exploring different pH-responsive monomers and the incorporation of PEG (Petersen *et al.,* 2002, Park *et al.,* 2005, Luo *et al.,* 2012), pluronic acid (Gebhart *et al.,* 2002) or dextran (Tseng *et al.,* 2003), to shield the positive charge. In this study, we have characterised the toxicity profiles of nanoparticles which have been self-assembled from amphiphilic block copolymers that undergo a solubility switch in response to pH, consisting of hydrophilic P(PEGMA-c-DMAEMA) component along with a hydrophobic block consisting of DEAEMA or 2-(diisopropyl amino) ethyl methacrylate (DIPMA). The DEAEMA and DIPMA have differing

pKa values with $pKa_{DEAEMA} > pKa_{DIPMA}$ (Hu *et al.*, 2008, Ma *et al.,* 2014). We also assess the ability of di(ethylene glycol) methyl ether methacrylate (DEGMA) to reduce the cell toxicity by shielding endosomal membranes from cationic DEAEMA and DIPMA. It is now appreciated that using a single cell viability assay is inadequate to comprehensively gain an understanding of the extent and the mechanism of cell toxicity. Therefore, we applied three different indicators of cell health. Propidium iodide sequestration measures the permeability of the cell membrane as an indicator or plasma membrane damage, whereas mitochondrial health and metabolic activity were assessed using AlamarBlue and CellTiter Glo® to measure ATP biosynthesis, or using 3-(4,5-dimethylthiazol-2-yl)-2,5-diphenyltetrazolium bromide (MTT) to measure NAD(P)H-dependent cellular oxidoreductase enzyme activity (Lv *et al.,* 2006, Parhamifar *et al.,* 2010, Riss *et al.,* 2016). These studies have revealed that DEAEMA nanoparticles (pKa ~7.1) were consistently more damaging to cells than the DIPMA particles (pKa ~6.1) (Riss *et al.,* 2016). We also observe the recovery of the cell health with increasing incorporation of Di(Ethylene Glycol) Methyl Ether Methacrylate (DEGMA) into the block copolymers used to assemble nanoparticles. The three cell health indicators indicated that the DEAEMA monomers affected all cellular processes measured, whereas DIPMA had a greater effect on the ATP production relative to the plasma membrane integrity. DEGMA incorporation may therefore be a useful approach for abrogating cell toxicity in a range of copolymer systems.

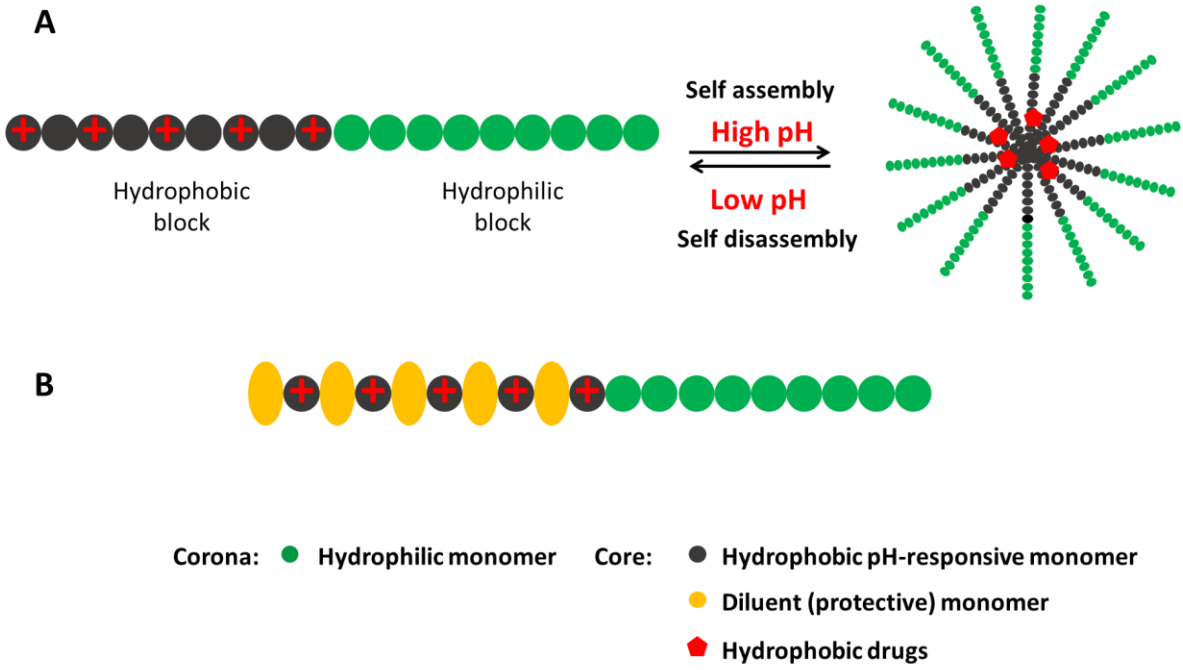

Figure 4.1. Schematic representation of a pH responsive star particle. A, Diblock copolymer consistent of a pH-responsive hydrophobic polymer and a hydrophilic copolymer self assembles into micelles at high pH. **B,** Shielding the cation with ethylene glycol (DEGMA) monomer to minimise cytotoxicity.

4.3 Methods

4.3.1 Materials

Poly(ethylene glycol) methacrylate (PEGMA) (M_n = 300 g mol^{-1}), 2- dimethylaminoethyl methacrylate (DMAEMA) (M_n = 157 g mol^{-1}), Di(ethylene glycol) methyl ether methacrylate (DEGMA) (M_n = 188.22 g mol^{-1}), 2-diethylaminoethyl methacrylate (DEAEMA) (M_n = 185.26 g mol^{-1}), initiator, azobis(isobutyronitrile) (AIBN), and the raft reagent, 4- cyano-4-(phenyl carbonothio) pentanoic acid, were purchased from Sigma-Aldrich. Solvents were purchased from Merck Millipore. CellTiter Glo was purchased from Promega.

4.3.2 Gel permeation chromatography (GPC)

A Shimadzu (Kyoto, Japan) liquid chromatography system was used for the GPC analysis of polymers to determine the molecular weight. The system comprised of a SIL-10AD autoinjector, a 5.0 µm bead-size guard column (50 x 7.8 mm) followed by four Polymer Laboratories (Styragel) columns (105, 104, 103, and 500 Å) and an RID10A differential refractive-index detector. The eluent N,N-dimethylacetamide (DMAc; 0.03% w/v LiBr, 0.05% 2, 7-di-Butyl-4-methylphenol) was used at 50 °C with a flow rate of 1 mL/min. A molecular weight calibration curve was produced using commercial polystyrene standards with narrow molecular weight distribution ranging from 500 to 106 g/mol.

4.3.3 ^{1}H NMR analysis

The ^{1}H-NMR spectra were recorded using Bruker Avance III 400 Ultrashield Plus spectrometer at 400 mHz running Topspin, version 1.3. Spectra were recorded in either chloroform-d ($CDCl_3$) or dimethyl formamide (DMF).

4.3.4 Self-assembly of Micelles

P(PEGMA-*co*-DMAEMA)-*b*-P(DEAEMA-*co*-DEGMA) and P(PEGMA-*co*-DMAEMA)-*b*-P(DIPMA-*co*-DEGMA) were self-assembled into micelles. The diblock copolymers were prepared by dissolving 5 mg into 0.5 mL of acetone. A syringe pump set at a flow rate of 1.2 mL/h was used to titrate the mixture into 4.5 mL of phosphate-buffered solution (PBS) and continuously mixed at room temperature (Harvard apparatus, 11 Elite). The micelles were then dialysed (MWCO 3500 Da) at room temperature for 24 h in PBS to remove organic solvent.

4.3.5 Dynamic Light Scattering

The size distribution of the assembled nanoparticles was measured by DLS using a Malvern Instruments Zetasizer Nano ZS ZEN3600 (Malvern, UK). DEAEMA with 10, 20 and 40% DEGMA were prepared at a concentration of 1 mg/mL in PBS and was filtered using a 0.45 μm nylon filter. Measurements were performed in polystyrene cuvettes, at 25°C to determine the hydrodynamic diameter/particle size and polydispersity index at pH 7 and at pH 6.

4.3.6 Synthesis of P(PEGMA-co-DMAEMA) macromer

P(PEGMA-co-DMAEMA) copolymer was prepared by reversible addition-fragmentation chain transfer (RAFT) polymerisation method as per Scheme 1 below: Dimethylaminoethyl methacrylate (DMAEMA, 0.628 g, 0.004 mol), poly(ethylene glycol) monomethyl ether methacrylate (PEGMA, 12 g, 0.04 mol), 2,2-azobisisobutyronitrile (AIBN, 0.0108 g, 0.067 mmol) and 2-cyanoprop-2-yl dithiobenzoate (CPDB, 0.1472 g, 0.67 mmol) were dissolved in toluene (60 mL) and placed in a vial with a magnetic stirrer bar. The vial was sealed and the mixture deoxygenated by purging with nitrogen for 30 minutes. The deoxygenated mixture was then placed on a magnetic stirrer plate set at 70 °C, 400 RPM for 21 h. After 21 h the polymer product was exposed to the air and cooled in an ice bath and the P(PEGMA-co-DMAEMA) macromerwas recovered after exhaustive dialysis against methanol for 48 h and acetone for 48 (MWCO 3500 Da). The P(PEGMA-co-DMAEMA) macromer was characterised via gel permeation chromatography (GPC) and proton-nuclear magnetic resonance (^{1}H-NMR).

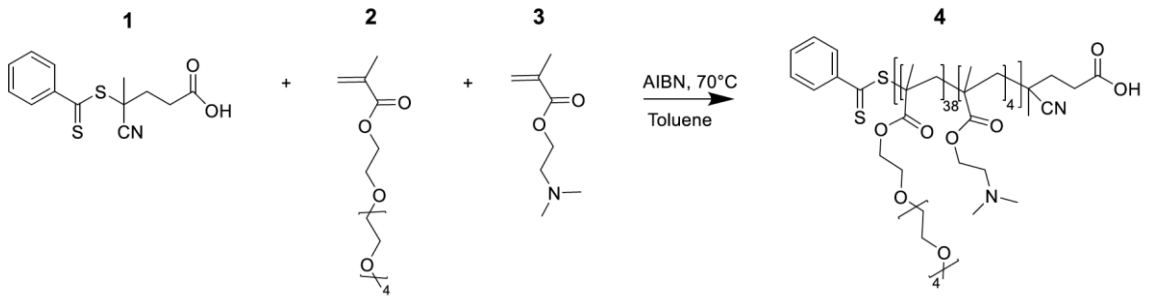

Scheme 1 Synthesis of hydrophilic portion of the P(PEGMA-co-DMAEMA) block copolymer. 1) Raft reagent (4- cyano-4-(phenyl carbonothio) pentanoic acid)**, 2)** poly(ethylene glycol) methacrylate (PEGMA) and **3)** 2- dimethylaminoethyl methacrylate (DMAEMA), initiation with azobisisobutyronitrile (AIBN), 70ºC, in toluene. **4)** Hydrophilic polymer product, P(PEGMA-*co*-DMAEMA).

4.3.7 Synthesis of P(PEGMA-co-DMAEMA)-block-(DEAEMA-co-DEGMA)

The synthesis of was carried out using reversible addition-fragmentation chain transfer (RAFT) polymerisation method as per Scheme 2 below. This chain extension reaction was performed at different [DEAEMA]: [DEGMA] ratios to give a polymer library with 0%, 5%, 10%, 20%, 40% or 50% DEGMA content in the hydrophobic block via the addition of appropriate amount of DEGMA: all others remained constant.

A typical chain extension reaction is given for the 10% DEGMA: Diethylaminoethyl methacrylate (DEAEMA, (0.3 g, 2.03×10^{-3} mol) , diethylene glycol monomethyl ether methacrylate (DEGMA, 0.0421g , 2.237×10^{-4} mol), 2,20-azobisisobutyronitrile (AIBN, 0.5 mg, 3.04×10^{-6} mol) and P(PEGMA-co-DMAEMA) macromer (0.2628 g, 2.03×10^{-5} mol) were dissolved in toluene (2 mL) and placed in a vial with a magnetic stirrer bar. The vial was sealed and the mixture deoxygenated by purging with nitrogen for 30 min. The deoxygenated mixture was then placed on a magnetic stirrer plate set at 70 °C, 400 RPM for 17.5 h after which the reaction mixture was exposed to the air. P(PEGMA-co-DMAEMA)-block-(DEAEMA-co-DEGMA) product was recovered after exhaustive dialysis against methanol for 48 h and acetone for 48 (MWCO 3500 Da). The P(PEGMA-co-DMAEMA)-block-(DEAEMA-co-DEGMA) was characterised via gel permeation chromatography (GPC) and proton-nuclear magnetic resonance (^{1}H-NMR).

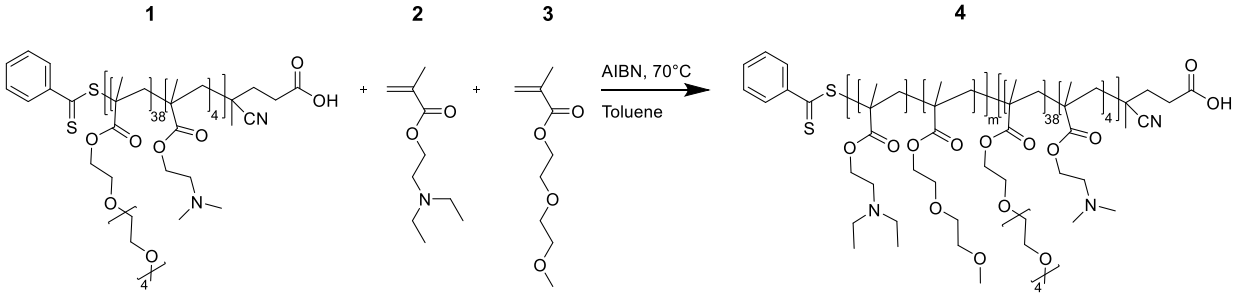

Scheme 2 Synthesis of hydrophobic portion of the P(PEGMA-co-DMAEMA)-b-P(DEAEMA-co-DEGMA) diblock copolymer. Reagents and conditions. **1)** Hydrophilic polymer synthesised in scheme 1, **2)** 2-diethylaminoethyl methacrylate (DEAEMA), **3)** Di(ethylene glycol) methyl ether methacrylate (DEGMA), **4)** Block copolymer, P(PEGMA-*co*-DMAEMA)-*b*-P(DEAEMA-*co*-DEGMA). Initiation with AIBN, 70ºC, in toluene.

Synthesis of P(PEGMA-co-DMAEMA)-block-(DIPMA-co-DEGMA)

The synthesis of P(PEGMA-co-DMAEMA)-block-(DIPMA-co-DEGMA) was carried out using reversible addition-fragmentation chain Transfer (RAFT) polymerisation method as per Scheme 3 below. This chain extension reaction was performed at different [DIPMA]: [DEGMA] ratios to give a polymer library with 0%, 5%, 10%, 20% and, 40% or 50% DEGMA content in the hydrophobic block via the addition of appropriate amount of DEGMA: all others remained constant.

A typical chain extension reaction is given for the 10% DEGMA: Di-isopropyl aminoethyl methacrylate (DIPMA, (0.432 g, 2.03×10^{-3} mol) , diethylene glycol monomethyl ether methacrylate (DEGMA, 0.0421g , 2.237×10^{-4} mol), 2,20-azobisisobutyronitrile (AIBN, (0.5 mg, 3.04×10^{-6} mol) and P(PEGMA-co-DMAEMA) macromer (0.2628 g, 2.03×10^{-5} mol) were dissolved in toluene (2 mL) and placed in a vial with a magnetic stirrer bar. The vial was sealed, and the mixture deoxygenated by purging with nitrogen for 30 min. The deoxygenated mixture was then placed on a magnetic stirrer plate set at 70 °C, 400 RPM for 17.5 h after which the reaction mixture was exposed to the air. P(PEGMA-co-DMAEMA)-block-(DIPMA-co-DEGMA) product was recovered after exhaustive dialysis against methanol for 48 h and acetone for 48 (MWCO 3500 Da). The P(PEGMA-co-DMAEMA)-block-(DIPMA-co-DEGMA) was characterised via gel permeation chromatography (GPC) and proton-nuclear magnetic resonance (^{1}H-NMR).

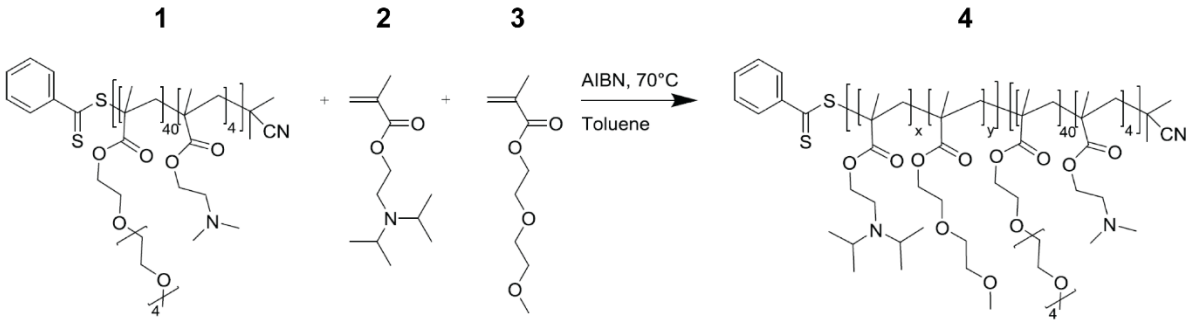

Scheme 3 Synthesis of hydrophobic portion of the P(PEGMA-co-DMAEMA)-b-P(DIPMA-co-DEGMA) diblock copolymer. Reagents and conditions. **1)** Hydrophilic polymer synthesised in scheme 1, **2)** 2-(Diisopropyl amino) ethyl methacrylate (DIPMA), **3)** Di(ethylene glycol) methyl ether methacrylate (DEGMA), **4)** Block copolymer, P(PEGMA-*co*-DMAEMA)-*b*-P(DIPMA-*co*-DEGMA).

4.3.8 Cell lines and Transfection

HEK293 (human embryonic kidney cells) were maintained in Dulbecco's modified Eagle's medium (DMEM) supplemented with 10% v/v FBS (37°C, 5% CO_2). For imaging, cells were plated in poly-D-lysine-coated, 8-well Ibidi chamber slides. For cell viability assays, 25,000 cells/well were plated into poly-D-lysine-coated 96 well CulturPlates (PerkinElmer) and incubated for 24 h for the AlamarBlue assay or 48 h for the CellTiter Glo and propidium iodide assays. For Coumarin 153 loaded nanoparticle internalisation assays, poly-D-lysine coated 96 well black-walled, optically clear plates were used. Cells were at 80% confluency on day of assessing cell viability.

4.3.9 Localisation of nanoparticles

For confocal imaging, HEK293 cells expressing the Rab5a-GFP endosomal marker were cultured to 60% confluency. Cells were transiently transduced with CellLight™ Early Endosome Bacmam 2.0 virus (Life Technologies, Mulgrave, Victoria), 2 µL/10,000 cells for a minimum of 16 h. Mitochondria were labelled with MitoTracker green (Life Technologies) (50 nM, 30 min). Cells were equilibrated in Hanks' Balanced Salt Solution (HBSS) (Sigma Aldrich) for 30 min prior to imaging. Images were obtained using a Leica TCS SP8 Laser-scanning confocal microscope with HCX PL APO 63x (NA 1.40) oil objectives in a humidified and temperature-controlled chamber (37°C). Imaging are representative of three or more experiments.

4.3.10 Cell Viability assays

For all assays, nanoparticle dilutions were prepared in PBS under sterile conditions. Cells were treated with 0.2% TritonX-100 as a control for cell death and PBS as the vehicle control. Cells were then incubated at 37°C supplemented with 5% CO_2. Treatments were carried out in triplicate with increasing concentrations of nanoparticles with a total volume of 100 µL of volume across all wells.

4.3.11 Cellular uptake of Coumarin 153 dye loaded nanoparticles

HEK 293 cells were cultured to 60% confluency in clear bottom, black, 96 well plates. Coumarin 153 dye (5 mg) was loaded into 5 mL of self-assembled DEAEMA, DIPA and non-disassembling (n-butyl methacrylate) particles. Fluorescence was imaged on an Operetta plate-based high content imaging system (ex: λ = 405 nm and em: λ = 555 nm) and average fluorescent units were determined by pixel densitometry and normalised to vehicle (DMSO) control. With estimates of critical micelle concentration (CMC) of each NP at 1-5ug/ml, cells were exposed to 40ug/ml nanoparticles for 30min, to ensure NP concentrations ~10-fold above CMC.

4.3.12 CellTiter Glo cell viability assay

Reagent was prepared according to the manufacturer instructions (Promega, USA). Cells grown to 80% confluence were treated with nanoparticles (concentrations as indicated in results) and incubated at room temperature for 30 min. 50 µL of cell media was first removed from each well and discarded. The remaining contents of each well was treated with 50 µL of the CellTiter Glo reagent. Cells were incubated at room temperature for a minimum of 10 min and the bioluminescence was measured at $\lambda = 555 \pm 40$ nm, using the CLARIOstar (BMG labtech). Cell viability was then calculated by subtracting the TritonX-100 control and

expressing the values as a percentage of the vehicle control. Data are presented as mean ± S.E.M of 5 individual experiments.

4.3.13 The propidium iodide cell toxicity

Cells were incubated with propidium iodide dye (final well concentration of 500 nM) for 30 min at room temperature. The fluorescence was detected using the CLARIOstar (ex: $\lambda = 535 \pm 10$ nm and em: $\lambda = 617 \pm 10$ nm). Cell toxicity values were calculated by a vehicle baseline subtraction and expressed as a percentage of the TritonX-100 control for cell death. Data are presented as mean ± S.E.M of 5 individual experiments.

4.3.14 AlamarBlue cell viability assay

Cell media was removed and replaced with 100 µL of fresh media. Cells were treated with a range of particle concentrations (0.4- 250 µg/mL) for 12, 24, 48 and 72 h at 37 °C, 5% CO_2. Cells were washed twice with chilled HEPES buffered saline solution (HBSS) (Sigma Aldrich) and then 10% (v/v) AlamarBlue reagent (Life Technologies) in media was added. Cells were incubated for 4 h further and the fluorescence was measured using the CLARIOstar (ex: $\lambda = 570 \pm 10$ nm, em: $\lambda = 605 \pm 15$ nm). Cell viability was then calculated by subtracting the Triton X-100 control and expressing the values as a percentage of the vehicle control. Data are then presented as the mean ± S.E.M of 3 individual experiments.

4.3.15 Data Processing and Analysis

Images were processed and analysed using FIJI (v 1.51d) software (Pelayo *et al.,* 2011). Graphs were generated using GraphPad Prism 6.01 (San Diego, CA). For the analysis of cell viability

data, two-way analysis of variance (ANOVA) and post hoc Tukey's multiple comparisons test was applied (* $p<0.05$; ** $p<0.01$, ***$p<0.001$). Data are presented as mean ± S.E.M.

4.4 Results and Discussion

4.4.1 Synthesis and characterisation of diblock copolymers.

Polycations have been implicated as the cytotoxic component of block copolymers (Fischer *et al.*, 2003). One proposed method of reducing polycation-related toxicity is to shield the charge with biocompatible monomers such as ethylene glycol (Putnam *et al.*, 2001). Precedence for charge shielding has been demonstrated by Putnam *et al*. and Thomas *et al.* (Putnam *et al.*, 2001, Thomas *et al.*, 2002). Therefore, we investigated the shielding of polycations by incorporating DEGMA into the pH switchable component. We characterised the diblock copolymer P(PEGMA-*co*-DMAEMA)-*b*-P(DEAEMA-*co*-DEGMA) (scheme 2) which consists of a hydrophilic copolymer P(PEGMA-*co*-DMAEMA). The hydrophobic copolymer consists of a pH responsive monomer, DEAEMA (pKa 7.1) and the shielding monomer DEGMA. The products were prepared in chloroform-d ($CDCl_3$) and characterised by ^1H NMR to confirm successful polymer synthesis by identifying monomeric groups incorporated into the polymer chains as shown in the representative spectra (Figure 4.2). The macromer was confirmed to comprise of poly(ethylene glycol) methacrylate and 2- dimethylaminoethyl methacrylate groups as shown in the assigned peaks in Figure 4.2A. Given that the DEAEMA and DIPMA polymers were synthesised with the macromer, only the Di(ethylene glycol) methyl ether methacrylate and 2-diethylaminoethyl methacrylate (Figure 4.2B) or Di(ethylene glycol) methyl ether methacrylate groups (Figure 4.2C) have been assigned in the representative spectra. GPC analysis was also performed to characterise the DEAEMA and DIPMA nanoparticle series are shown (Table 1). The polydispersity index (PDI), is the ratio of the weight average molecular weight to the number average molecular weight and is indicative of the distribution of the molecular mass of the polymer chains synthesised. In all cases the polymerisations yielded diblock copolymers with narrow molecular weight

distributions <1.34. Narrow molecular weight distributions are indicative of a controlled polymerisation of the block copolymers and allow for consistent sizes and shapes of the self-assembled particles (Lynd *et al.*, 2008).

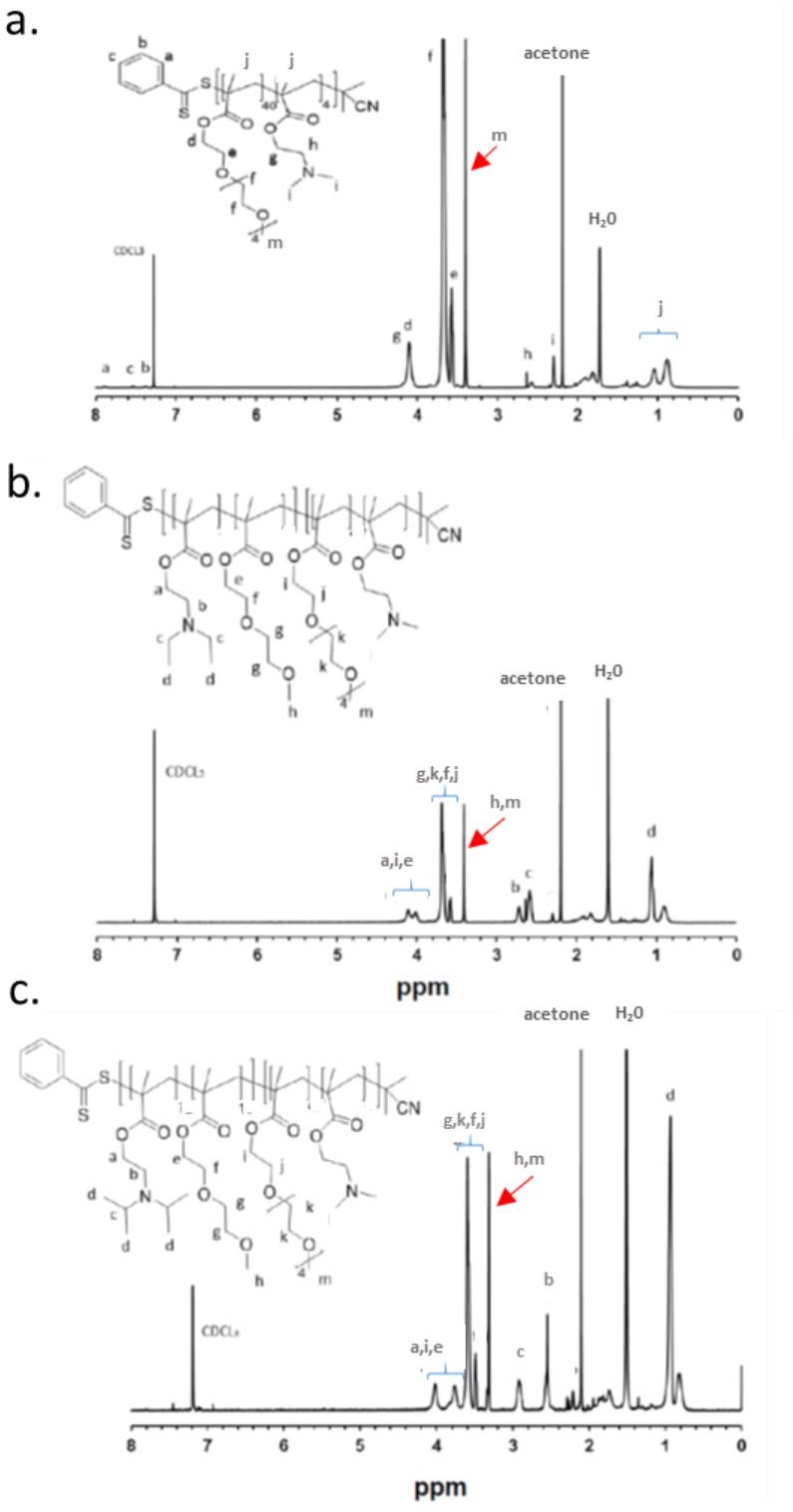

Figure 4.2: ^{1}H NMR spectra of **a,** macromer, **b,** DEAEMA-10 and **c,** DIPMA-10 in $CDCl_3$ with representative peaks assigned as shown.

Table 4.1. GPC of the P(PEGMA-*co*-DMAEMA)-*b*-P(DEAEMA-*co*-DEGMA) and P(PEGMA-*co*-DMAEMA)-*b*-P(DIPMA-*co*-DEGMA) diblock copolymers. Size exclusion chromatography (SEC) analysis of DEAEMA and DIPMA particles with 00-50% DEGMA. The number average molecular weight, weight average molecular weight, and polydispersity indices (PDI) are shown. The PDI is a measure of molecular weight distribution of a polymer.

	Polymer code	**% DEGMA**	***SEC***		
			Mn (g/mol)	**Mw (g/mol)**	**PDI [(c)]**
	Macromer	**n/a**	12500	14000	1.15
DEAEMA Series	**DEAEMA-0**	**0**	20500	24500	1.20
	DEAEMA-5	**5**	19000	23500	1.27
	DEAEMA-10	**10**	20500	27000	1.32
	DEAEMA-20	**20**	20500	27500	1.34
	DEAEMA-40	**40**	23500	30000	1.28
	DEAEMA-50	**50**	20000	24000	1.24
DIPMA Series	**DIPMA-0**	**0**	20000	25000	1.25
	DIPMA-5	**5**	19500	25500	1.30
	DIPMA-10	**10**	22000	27000	1.25
	DIPMA-20	**20**	20000	26000	1.29
	DIPMA-40	**40**	n/a	n/a	n/a
	DIPMA-50	**50**	24000	31000	1.30

4.4.2 Nanoparticle assembly and characterisation of pH sensitivity

A subset of the library DEAEMA and DIPMA were self-assembled into nanoparticles as described in the experimental but where loaded with Nile red dye through the process. Nile red, hydrophobic fluorophore, self-quenches when exposed to aqueous solvents and therefore, can be used as an indicator for *in vitro* assessment of particle disassembly. The pH sensitivity of these nanoparticles was assessed by titrating 1 N HCl into the nanoparticle solution and Nile red intensity was measured as a function of pH by spectrofluorophotometry (excitation λ= 475 nm, emission λ = 565 nm). The Nile red fluorescence intensity decreased with decreasing pH for all the DIPMA and DEAEMA nanoparticles as a consequence of the slight dilution on the addition of acid. However, at pH 6, most of the Nile red from the DEAEMA nanoparticles was quenched. In contrast, the dye released from the DIPMA particles was quenched when the pH reached 5. This is indicative of nanoparticle disassembly and cargo release into the aqueous environment (Figure 4.3). The complete disassembly of the DEAEMA nanoparticles was observed to occur at a higher pH than that of the DIPMA which is consistent with the pKa for each block copolymer (Ma *et al.*, 2014).

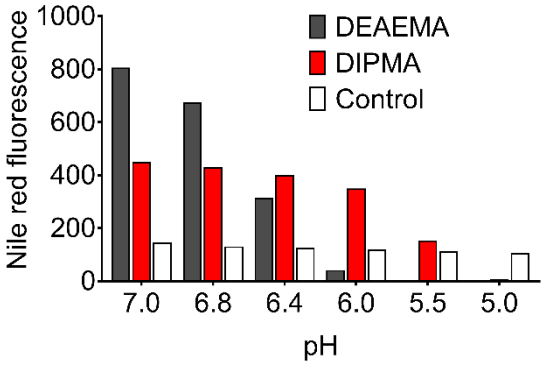

Figure 4.3. Disassembly of pH-responsive nanoparticles. Fluorescence emission intensity of nanoparticle assembled with Nile Red in PBS with copolymers with distinct pKa including DEAEMA (pKa 7.1), DIPMA (pKa 6.1) or non-disassembling control.

DEAMEA nanoparticles were also analysed by dynamic light scattering to determine size and the polydispersity index (Figure 4.4). The mean size of the DEAEMA nanoparticles were between 21-24 d.nm and showed a PDI below 0.68 at pH 7. This indicated that the block copolymers assembled into nanoparticles and with low variation in particle size. In contrast, when the pH of the buffer was decreased to pH 6, the mean particle size decreased to approximately 7.5 d.nm and PDI of approximately 0.5. The increase in variation and decrease in measured particle size suggested that the block copolymers in solution were present as unimers and not in ordered larger micelle structures. Critically the data indicated that nanoparticles synthesised with DEGMA units in the core retain pH sensitivity.

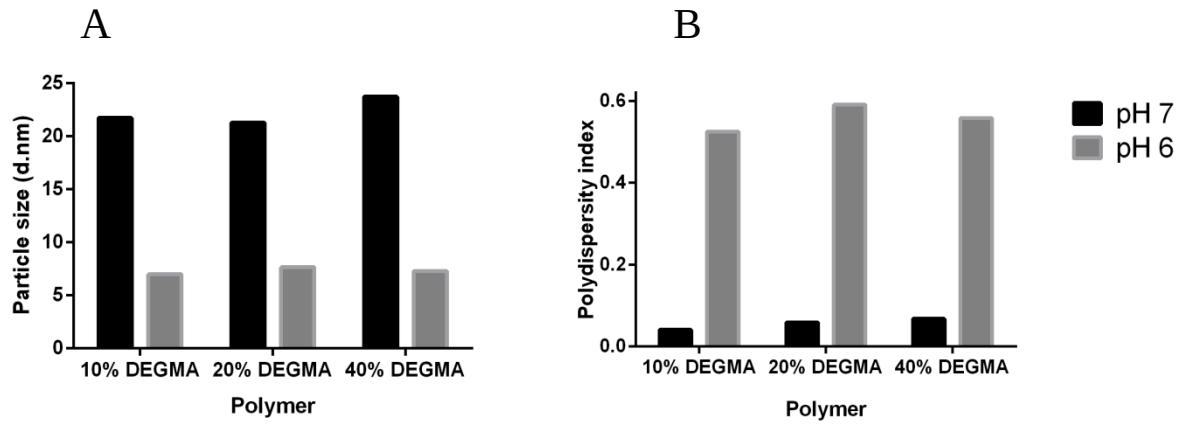

Figure 4.4 pH sensitivity of DEGMA-incorporated DEAEMA particles. A, Particle sizes of each nanoparticle of varying DEGMA content at pH 7 (black) and pH 6 (grey). **B,** Polydispersity index of each nanoparticle at pH 7 (black) and pH 6 (grey).

4.4.3 The effect of incorporating DEGMA into nanoparticles on internalisation and translocation

To study the internalisation and intracellular trafficking of the DEAEMA nanoparticles, DEAEMA-0 and DEAEMA-5 (0% and 5% DEGMA, respectively) were labelled with tetramethyl rhodamine (TMR) using published end group modification strategies. These particles were imaged after treatment in cells expressing Rab5-GFP early endosomal resident

protein, or MitoTracker Green, a mitochondrial-selective dye (Abel *et al.,* 2016). The internalised nanoparticles showed partial co-distribution with Rab5-positive early endosomes. TMR, an analogue of rhodamine B, which is a cationic fluorescent marker known to diffuse through membranes and can become sequestered in the mitochondria. It was important to determine if the TMR-conjugated nanoparticle translocates to this location as a function of the TMR. The DEAEMA-0 nanoparticle does not co-distribute with the mitochondria. The results have demonstrated that the incorporation of the protective short DEGMA side-chains and the fluorophore did not affect the internalisation or translocation of the nanoparticle into the endosomal network. The DEAEMA-0 and DEAEMA-5 polymers were the only TMR labelled particles available and additional imaging was beyond the scope of the study at the time of imaging. However, future efforts to make end group modifications to fluorescently label the 10, 20, and 50% DEGMA particles would also be informative as well as further live cell, volumetric imaging using other organelle markers and deconvolution techniques to gain further understanding of the localisation of the nanoparticles in cells.

4.4.4 Assessing drug release of pH-tunable nanoparticles in cells

The DEAEMA and DIPMA particles were loaded with Coumarin 153, a hydrophobic dye that remains quenched in hydrophobic environments, including in the hydrophobic core of an assembled copolymer. Hence, it can be used as a fluorescent model for understanding the cellular release of a hydrophobic drug (Figure 4.6). Cells were treated with nanoparticles and the intracellular fluorescence was measured using a high-content imaging system. The fluorescence intensity in the cells treated with DEAEMA nanoparticles increased and plateaued after nanoparticle addition. This was indicative of nanoparticle uptake and disassembly and immediately releasing the hydrophobic dye. The DIPMA particle showed a similar trace to the control nanoparticle, which increased with time. DIPMA and DEAEMA particles have the same hydrophilic monomer and only differ in the pH-responsive component. Figure 4.5 shows

colocalisation between the particles and early endosomes which have a luminal pH of 6.1-6.8. Given that the DIPMA has a low pKa, the early endosomes may not be acidic enough to induce nanoparticle disassembly. Therefore, DIPMA was likely to have disassembled at later time points after translocation into late endosomes (pH 4.8-6.0) or lysosomes (pH 5.5)

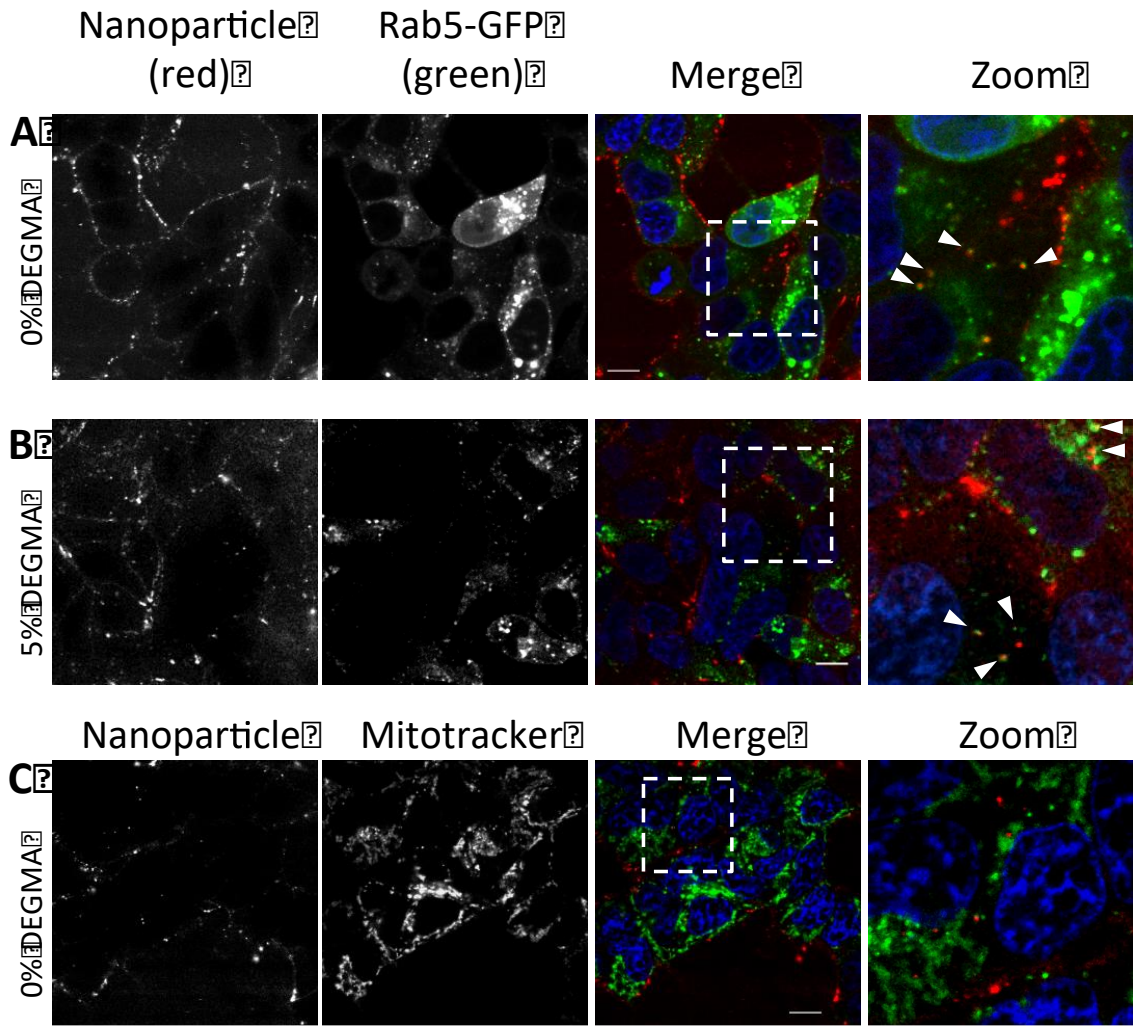

Figure 4.5. **Uptake of DEAEMA and DEAEMA-DEGMA nanoparticles into HEK 293 cells.** HEK 293 cells transiently expressing Rab5a-GFP were incubated for 20 min with either **A,** 0% DEGMA-DEAEMA TMR-labelled nanoparticles or **B,** 5% DEGMA-DEAEMA TMR-nanoparticles. **C,** Parental HEK 293 cells stained with MitoTracker dye were incubated for 20

min with 0% DEGMA-DEAEMA TMR-labelled nanoparticles. The merge panels are composite images of the nanoparticle (red), organelle marker (green), and nuclear marker. Co-distribution of nanoparticles with Rab5a-positive endosomal membranes are indicated by white arrows in the magnified images. Shown here are representative images of 3 individual experiments. Scale bar 10 μm.

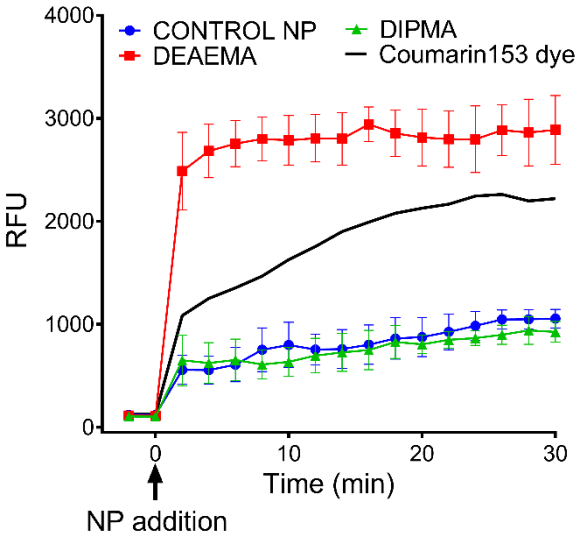

Figure 4.6. Disassembly of DEAEMA and DIPMA particles and release of Coumarin153 cargo in HEK293 cells. Fluorescence intensity of Coumarin dye assembled into DEAEMA, DIPMA nanoparticles and a non-disassembling control. Fluorescence was measured in HEK293 cells.

4.4.5 Assessment of particle effect on ATP production

Historically, the toxicity of nanoparticles have been assessed using a myriad of different assays for cell health. We used CellTiter Glo, propidium iodide and AlamarBlue to assess the effect of the nanoparticles on mitochondrial health, plasma membrane integrity and the cytosolic

redox potential, respectively. These commonly used assays measure different indicators of cell health, which need to be considered prior to selecting a suitable assay.

As a measure of mitochondrial activity, we used the CellTiter Glo assay to assess the effect of nanoparticles on ATP production. The assay uses an ATP-dependent Ultra-Glo recombinant luciferase enzymatic conversion of Beetle Luciferin to produce oxyluciferin and light. The bioluminescence produced from this enzymatic interaction can be measured and correlated with the intracellular presence of ATP to determine cell viability. It is sensitive (detection limit of 50 HEK293 cells), rapid (single reagent addition followed by 10 min incubation at RT for a steady luminescent signal) and unaffected by serum or phenol red (common pH indicator in growth media). However, the CellTiter Glo reagent contains a detergent and ATPase inhibitors to lyse the cells and release the ATP for end-point detection and therefore cannot be used monitor cell viability over time. Cells were incubated with graded concentrations of DEAEMA and DIPMA nanoparticles incorporating 0-50% DEGMA and viability was assessed with CellTiter Glo 8 h or 24 h later. Following 8 h incubation with DEAEMA and DIPMA nanoparticle, toxicity was only observed at concentrations of 50 µg/mL. At 24 h, the 10 µg/mL and 50 µg/mL nanoparticle concentrations reduced the cell viability of both nanoparticles. The introduction of 50% DEGMA significantly increased the cell viability of the cells treated with 50 µg/mL of DEAEMA nanoparticles at 2, 4, 6, and 8 h. In the DIPMA treated cells, the 0-20% DEGMA particles reduced the cell viability when compared to the 0% particle. Interestingly, there was some variability observed in the cell viability after 24 h of incubation with the DIPMA particles. However, these differences were not statistically significantly when comparing the 0% DEGMA-DIPMA particle at different concentrations or when comparing the 0% DEGMA-DIPMA particles to the 5-50% DEGMA nanoparticles at each concentration.

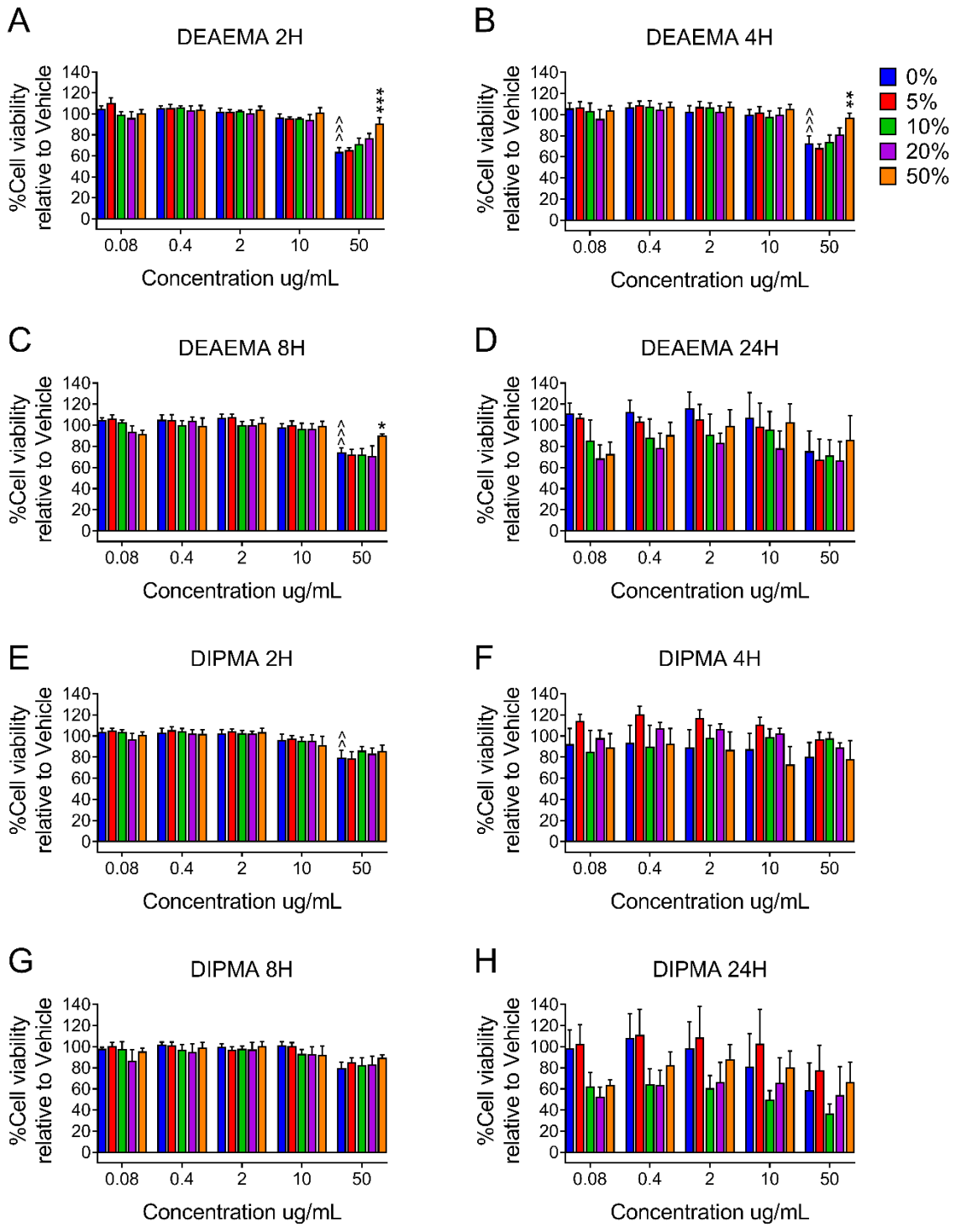

Figure 4.7. Mitochondrial function as an indicator of cell viability in cells treated with DEAEMA and DIPMA particles. Cell viability was determined by measuring mitochondrial activity using CellTiter Glo. Cells were treated up to 24 h with DEAEMA (**A-D**) or DIPMA (**E-H**) particles containing 0%, 5%, 10%, 20% and 50% of DEGMA at increasing. The cell

viability was expressed as a percentage of vehicle controls. Mean ± S.E.M; n=4-5 individual experiments. Symbols show * $p<0.05$, ** $p<0.01$ and *** $p<0.001$ versus 0% DEGMA at each concentration; ^^ $p<0.01$ and ^^^ $p<0.001$ versus 0% DEGMA at 0.08 ug/mL; two-way ANOVA with Tukey's multiple comparison test.

4.4.6 Assessment of particle effect on membrane integrity and permeability

To determine if the nanoparticles disrupted membrane integrity, propidium iodide (PI) assays were performed. In healthy cells, PI is a cell-impermeant dye. However, disruption of the plasma membrane allows PI to diffuse into the cell and counterstain the nucleus and chromosomes by intercalating nucleic bases which can be used as an indicator of cell death. Consistent with the ATP detection assay, 50µg/ mL of the DEAEMA particles incubated for 2-24 h induced up to 40% cell death in the PI detection assay. The toxicity of the DEAEMA particle was significantly reduced with the introduction of 50% DEGMA when incubated with cells for 2, 8 and 24 h. Interestingly, the DEAEMA particles induce more toxicity at 4 h compared to the 8 and 24 h incubations. This may be due to contact or interaction of the polymers with the plasma membrane which is recovered after the 4 h timepoint, resulting in a sustained increase in cell viability up to 24 h at the 0.08, 0.4, 2, and 10 µg/mL concentrations. The DIPMA particles were less toxic and showed ~15% death of the cell population at the highest concentration of particles after 24 h of incubation. This is low comparative to the ATP detection which showed ~40% loss in cell viability with the DIPMA particle at the equivalent concentration and time. The differences in the cell toxicity measured between the ATP detection assay and the plasma membrane permeability assay may due to the disassembly of the DIPMA nanoparticle further along the endosomal pathway where polymers still induce toxicity intracellularly but cause little disruption at the plasma membrane. The differences in DEAEMA and DIPMA toxicity may be due to the pKa which can affect the fate of the

translocation of the particles through the endosomal network. The DEAEMA has a higher pKa than DIPMA with the reported pKa of 7.1 and 6.1, respectively. Therefore, DEAEMA likely to disassembled earlier in the endosomal maturation process at a higher pH, whereas the DIPMA particle is likely to remained intact further in the endosomal network. The delayed dissociation may result in slower onset of polycationic-dependent cell death and may also determine the mechanism of cell death.

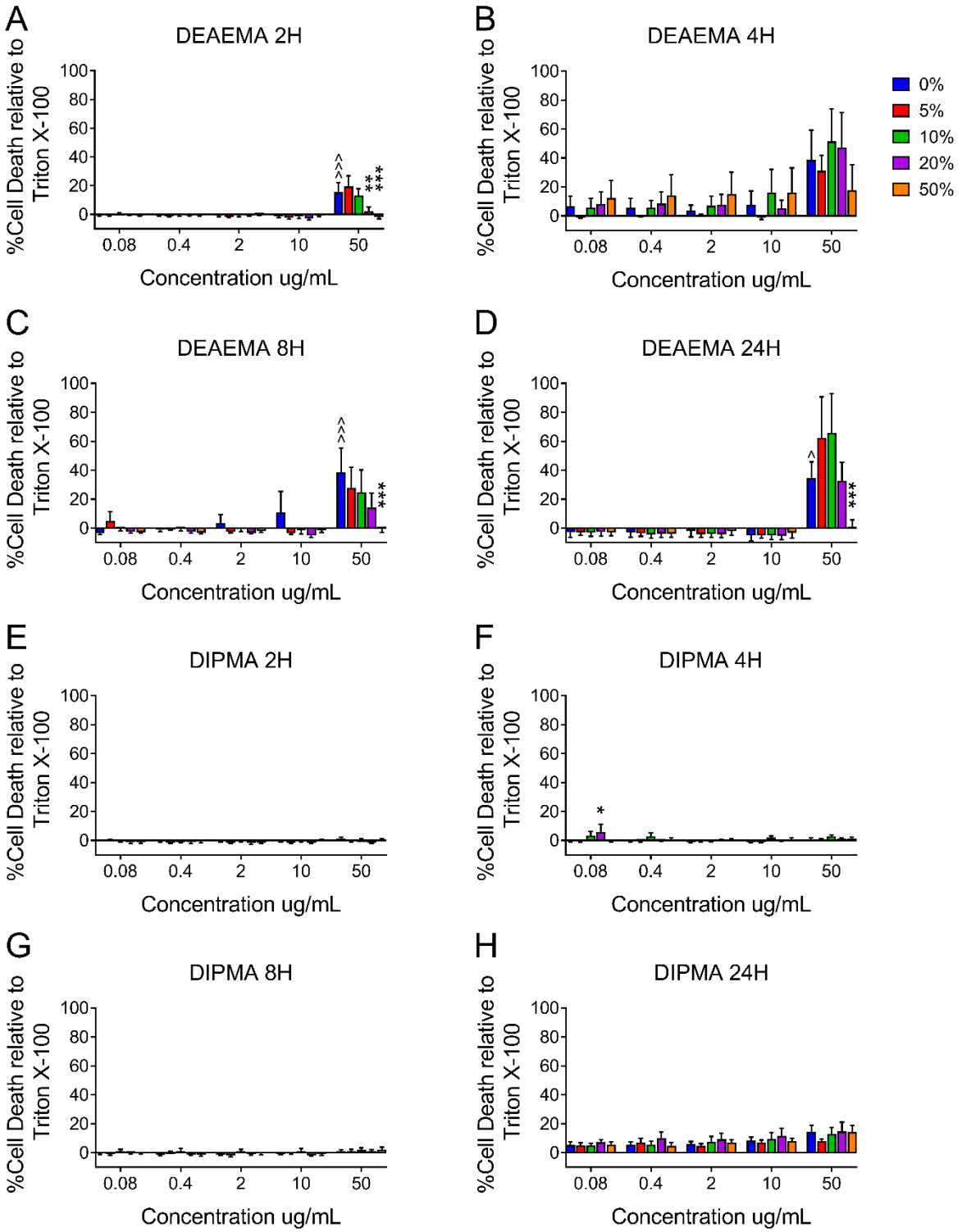

Figure 4.8. **Plasma membrane permeability as an indicator of cell death in cells treated with DEAEMA and DIPMA particles.** Cell death was determined by measuring plasma membrane permeability using propidium iodide. Cells were treated up to 24 h with DEAEMA (**A-D**) or DIPMA (**E-H**) particles containing 0%, 5%, 10%, 20% and 50% of DEGMA at

increasing. The cell death was expressed as a percentage of 0.2% Triton X-100 (maximal cell death). Mean ± S.E.M; n=4-5 individual experiments. Symbols show * $p<0.05$, ** $p<0.01$ and *** $p<0.001$ versus 0% DEGMA at each concentration; ^^^ $p<0.001$ versus 0% DEGMA at 0.08 ug/mL; two-way ANOVA with Tukey's multiple comparison test.

4.4.7 Assessment of particle effect on intracellular redox potential

The differences in the cell viability when measuring the plasma membrane integrity and the ATP production is indicative of the different mechanisms of cell death that can be induced by nanoparticles. Understanding the location of the interactions that result in cell death can be informative for the design of new nanoparticles. Another marker of cell death is the intracellular redox potential which is indicative of cellular respiration and ATP production. The effect of these particles on ATP production has already been measured using the CellTiter Glo assay and both the membrane integrity and ATP production assays indicated that the DEAEMA and DIPMA particles did not lead to complete cytotoxicity. Therefore, to observe the full cytotoxic profile of the particles, we investigated the effect of higher concentrations (0.4-250 µg/mL) and prolonged exposure (12-72 h) of the particles on the intracellular redox potential using AlamarBlue reagent. AlamarBlue (resazurin) is a cell permeable redox indicator that is reduced to the fluorescent product, resorufin, in the cytoplasm of cells with active metabolisms. The fluorescence measured correlates to the number of viable cells in a population. Consistent with the membrane integrity and ATP production assays, DEAEMA particles induced cell death at 50 µg/mL over 72 h. We also observe 100% cytotoxicity at 250 µg/mL of the DEAEMA particle. The incorporation of 50% DEGMA completely recovered cell viability of 50 µg/mL up to and including 72 h and recovered 14.4 ± 5.5% cell viability at 250 µg/mL (12 h). The DIPMA particle induced cell death after 48 h of treatment with 50 µg/mL and 250 µg/mL and after 72 h of incubation with 10-250 µg/mL. The incorporation of 50% DEGMA

improved the biocompatibility of the DIPMA particle in the 48 h treated cells. However, the shielding effect of the 50% DEGMA only partially improved cell viability when cells were incubated with concentrations of 50 μg/mL (22.5 ± 7.5%) and 250 μg/mL (19.6 ± 2.0%). At 72 h, when incubated with 10 μg/mL of the nanoparticles, 5% and 10% DEGMA prevented cytotoxicity, and 20% and 50% partially increased cell viability. After a 72 h incubation with higher concentrations of particles, DEGMA incorporation had a minimal effect on cell viability.

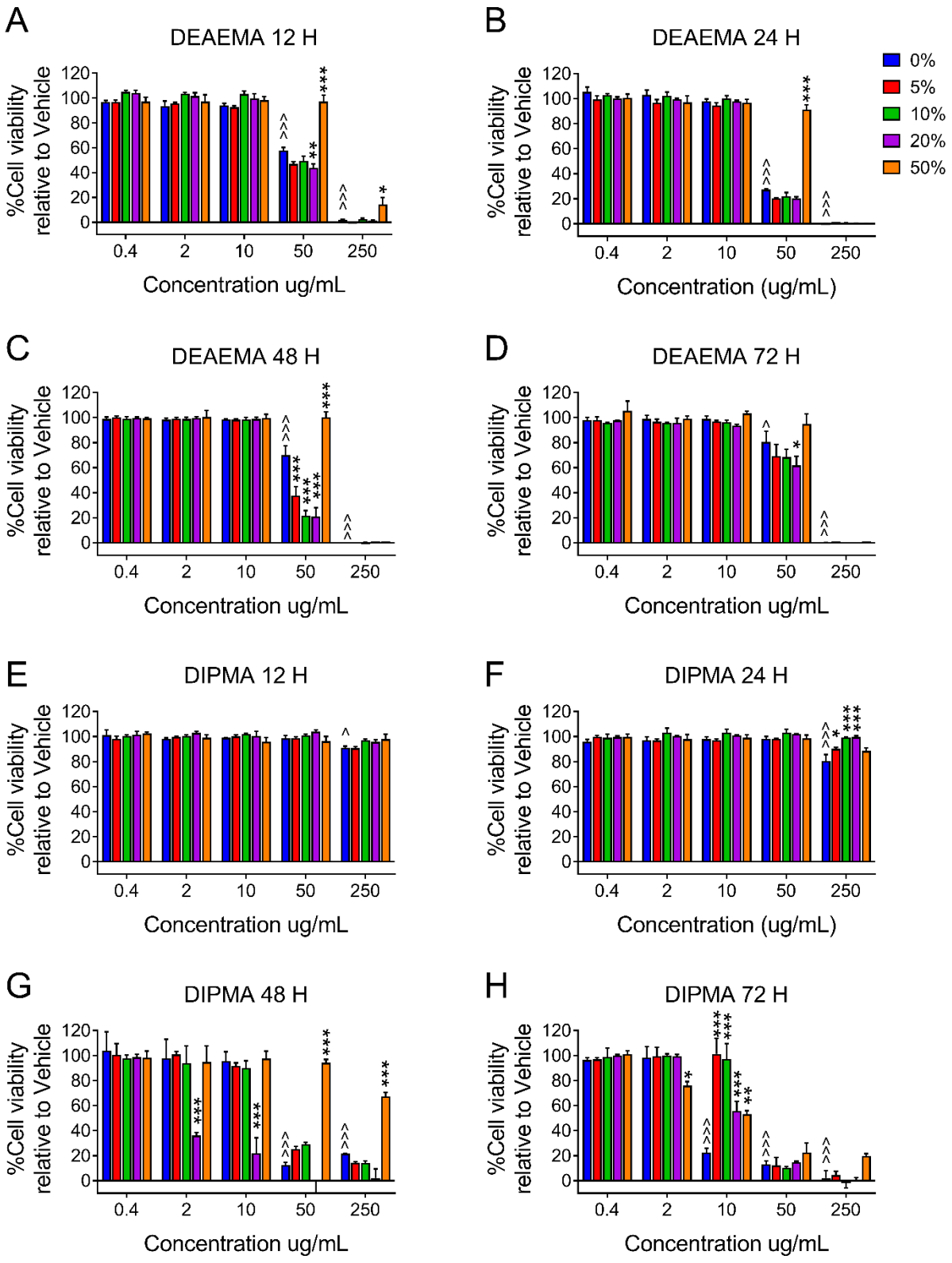

Figure 4.9. **Cytoplasmic reducing activity as an indicator of cell viability in cells treated with DEAEMA and DPA particles.** Cell death was determined by measuring cytoplasmic reducing activity with AlamarBlue. Cells were treated up to 72 h with DEAEMA (**A**-**D**) or

DPA (**E-H**) particles containing 0%, 5%, 10%, 20% and 50% of DEGMA at increasing. The cell death was expressed as a percentage of the vehicle. Mean ± S.E.M; n=3 individual experiments. Symbols show * $p<0.05$, ** $p<0.01$ and *** $p<0.001$ versus 0% DEGMA at each concentration; ^$p<0.05$, ^^^ $p<0.001$ versus 0% DEGMA at 0.4 ug/mL; two-way ANOVA with Tukey's multiple comparison test.

4.5 Conclusion

Nanoparticle polycation-dependent cytotoxicity is multifaceted, complex and requires adequate characterisation to ensure their safety as drug carriers. Here we have synthesised P(PEGMA-*co*-DMAEMA)-*b*-P(DEAEMA-*co*-DEGMA) and P(PEGMA-*co*-DMAEMA)-*b*-P(DIPMA-*co*-DEGMA). These diblock copolymers were self-assembled and characterised to confirm that low pH can induce disassembly and release of loaded dyes. We have shown that DEAEMA particles were consistently more cytotoxic than the DIPMA across the three indicators of cell health. When we incorporated DEGMA into 50% of the hydrophobic region of the block copolymer, we were able to shield the endosomes and prevent cell death. Interestingly, we observed different degrees of cytotoxicity of the DIPMA when comparing the effects on membrane integrity and ATP production, whereas the effect of the DEAEMA was similar across assays. This indicated that DEAEMA and DIPMA particles drive different mechanisms of cell death. This will require further investigation to understand how these particles induce apoptosis to gain a better understanding of polycation-dependent cell death. PEI, a commonly studied polycationic drug carrier has been shown to induce two phases of cell death, a necrotic and apoptotic phase. The necrotic phase affects the plasma membrane integrity, phosphatidylserine translocation and lactate dehydrogenase release (Zhang *et al.*, 2017) and the apoptotic phase is a result of permeabilisation of the mitochondria releasing cytochrome c which subsequently activates caspases (Moghimi *et al.*, 2005, Symonds *et al.*,

2005, Hunter *et al.*, 2010, Parhamifar *et al.*, 2010). The characterisation of multiple cell-death markers would be required to gain a comprehensive understanding of particle-dependent cytotoxicity. However, this is time consuming and may not be an accurate predictor of other variants of the particle such as different sizes. This has been observed when comparing low and high molecular weight poly(l-lysine) which can activate mitochondrial-mediated apoptosis differently (Symonds *et al.*, 2005). Therefore, high-throughput assays measuring the ATP production, membrane permeability and the redox potential such as the CellTiter Glo, propidium iodide, and AlamarBlue assays are valuable tools for screening polymers and particles for their biocompatibility. Although these assays are commonly used as stand-alone screens for biocompatibility, ATP and redox processes may continue to during the first phase of apoptosis and the plasma membrane may be affected from interactions with nanocarriers during internalisation that may not necessarily lead to cell death. Therefore, a combination of these assays would provide a more comprehensive and accurate understanding of the cytotoxicity of drug carriers.

Chapter 5
General Discussion

The endosomal signalling platform has led to a shift in the classical receptor signalling and trafficking paradigm (Wang *et al.,* 2018). With the development of new tools to probe compartmentalised signalling, there has been a growing number of receptors that have demonstrated active conformations and signalling from intracellular platforms (Horwitz *et al.,* 2003, Murphy *et al.,* 2009, Irannejad *et al.,* 2017, Wang *et al.,* 2018). This compartmentalised signalling of receptors such as the PTHR and β_1AR have been associated with distinct physiological outcomes (Horwitz *et al.,* 2003, Irannejad *et al.,* 2017). Therefore, there has also been a growing interest in cell permeable and impermeable drugs for the selective treatment of intracellular-derived signalling associated with disease (Horwitz *et al.,* 2003, Irannejad *et al.,* 2017, Sergin *et al.,* 2017). However, to our knowledge, this is the first study to employ drug delivery devices to achieve selectivity for intracellular GPCR populations. Therefore, the main aim of this thesis is to investigate and characterise two drug delivery tools, lipid-conjugation, and pH responsive nanoparticles to specifically deliver drugs to endosomes.

Lipid-conjugation has previously been explored and proposed as a means of delivering drugs intracellularly to inhibit a recycling endopeptidase, β-site amyloid precursor protein cleaving enzyme 1 (BACE-1), which is expressed in the central neurons of the brain (Rajendran *et al.,* 2012). However, in this study, we apply lipid-conjugation for the purpose of specifically targeting intracellular signalling of GPCRs. A fluorescently labelled tripartite ligand, Cy5-Chol was localised at the plasma membrane and internalised into cells, whereas the lipid-free control, Cy5-EE, remained in solution. When the location of the intracellular pools of Cy5-Chol was investigated, it was shown to co-distribute with endosomal compartments, lysosomes with limited co-distribution to the endoplasmic reticulum, and the trans-Golgi network. This illustrates the potential of the lipid to anchor to the plasma membrane and promote endocytosis. One of the key findings of this study was that the lipidated NK_1R antagonists attenuated

intracellular signalling, while the control (lipid-free) drugs were significantly less effective in cell lines. The treatment of NK_1R expressing cell lines with the NK_1R antagonist Spantide and the lipid-conjugate, Span-Chol demonstrated that only the free Spantide inhibited SP-dependent cytosolic ERK signalling of NK_1R, a plasma membrane delimited event. Conversely, Span-Chol but not Spantide selectively inhibited the nuclear ERK signalling of NK_1R, which is an endosomal delimited event. This distinct pattern of inhibition was further supported with the measurement of cAMP production localised at the plasma membrane and in the cytosol. SP stimulation of the NK_1R led to an increase in cytosolic PKC, but no plasma membrane PKC was detected. Upon further investigation with a dynamin inhibitor, Dyngo 4a, stimulation with SP increased the PKC activation at the plasma membrane and no cytosolic PKC was detected. Together, these measurements of PKC suggest that the activation of cytosolic PKC is an endosomal signalling event. Interestingly, the Spantide and Span-Chol were equally effective in inhibiting cytosolic PKC. The binding affinity of Span-Chol and Spantide indicated that there were no significant difference in the binding affinity of the two compounds to NK_1R. These findings may suggest that the differences in the ability of each compound to inhibit plasma membrane and endosomal delimited signalling is a result of location bias. An alternative approach for this may be to use internalisation inhibitors such as Dyngo 4a to ensure that both the antagonists and the receptor remain on the cell surface for the binding experiments (Robertson *et al.,* 2014).

Previous studies examining the NK_1R have demonstrated that noxious stimuli such as capsaicin induces the release of SP from primary sensory neurons into the dorsal horn of the spinal cord (Mantyh *et al.,* 1995). This SP-mediated nociception also induces robust internalisation of the receptor in the second order neurons (Mantyh *et al.,* 1995). Similar observations of SP-dependent internalisation of NK_1R have also been observed in the striatum of rats (Mantyh *et al.,* 1995). In human patients with inflammatory bowel disease and irritable

bowel syndrome, NK_1R was diminished from the cortical and subcortical regions of the brain (Hargreaves 2002, Bergström *et al.*, 2004, Jarcho *et al.*, 2013). The diminished NK_1R detected may be due to an increased SP-dependent receptor activation, but it has also been hypothesised that the intracellular signalling of the receptor may contribute to the disease. In this study, we examined the role of NK_1R internalisation on neuronal excitability in rat spinal cord slices, and pain responses in mice. The treatment of Dyngo 4a to inhibit dynamin-dependent internalisation had a delayed inhibitory effect on neuronal firing rates. Similar results were also observed using MEK and PKC inhibitors. These findings indicate that the internalisation of NK_1R is required for the sustained excitability and hence sustained nociceptive transmission. A caveat to this approach is that dynamin-dependent internalisation is an important cellular process and the inhibition of dynamin is not specific to NK_1R. Therefore, the use of lipidated NK_1R antagonists is a more selective approach in probing the role of NK_1R internalisation in neuronal excitability. The treatment of Span-Chol had no effect on the initial firing but inhibited sustained firing of the neurons supported the previous hypothesis that sustained pain transmission is dependent on intracellular NK_1R signalling. Our data also demonstrated that the inhibition of endocytosis or the treatment of Span-Chol have antinociceptive actions when measuring Von Frey paw withdrawal responses. Collectively, these findings highlight the role of internalisation and intracellular signalling of NK_1R in pain transmission, as well as the therapeutic potential of targeting drugs to modulate intracellular signalling.

To further understand the mechanism by which cholestanol-conjugation improves selectivity, the molecular dynamic properties of the cholestanol linked probes were characterised by FCS. The diffusion coefficients of Cy5-EE, Cy5-Chol and Span-Cy5-Chol were consistent regardless of concentration. However, Span-Cy5-Chol diffusion coefficient was significantly slower than the Cy5-Chol and Cy5-EE. The diffusion coefficient of a compound can be affected by the viscosity and temperature of the solution. However, given

the consistent conditions maintained for all FCS experiments, the differences in diffusion coefficients are likely due to a greater molecular weight. In order to achieve a 1.6 fold difference in diffusion time, a 6 fold difference in mass is required as the diffusion time is proportional to the cube root of the difference in molecular weight (Meseth *et al.,* 1999). However, these do not account for the changes in diffusion coefficient between the Cy5-Chol, Cy5-EE, and Span-Cy5-Chol ligands. Together, these findings indicated that the Span-Cy5-Chol may be forming clusters in solution leading to an increase in the molecular weight of the fluorescent species. To investigate this further, photon counting histogram analysis can be applied to determine the molecular brightness of the fluorophores measured. Theoretically, aggregation or clusters of a fluorescent ligand will have yield a greater brightness than individual fluorescent ligands but will diffuse together in one cluster to be measured as one fluctuation. This may result in lower measurements of Span-Cy5-Chol concentrations as the autocorrelation analysis assumes that fluctuations are a result of singular fluorescent species. If there is clustering of the Span-Cy5-Chol, there is also potential for using PCH analysis to determine the number of ligands per cluster based on the molecular brightness of Cy5 in a soluble form (Reiner *et al.,* 2009, Johnson *et al.,* 2010). This will allow for a more accurate determination of the number of ligands prepared in solution. Concentration measurements of Cy5-EE, Cy5-Chol and Span-Cy5-Chol were significantly lower than the nominal concentrations prepared in HBSS. This may suggest that there is loss occurring due to non-specific binding of the ligands as a result of conjugation to the PEG chain and the cholestanol. Although the ligands were measured immediately after preparation, the kinetic measurements of concentrations demonstrated that there was no time dependent decrease. BSA was added to preparations to prevent the non-specific binding of the lipophilic compounds for FCS measurements (Fujii *et al.,* 1992, Kilpatrick *et al.,* 2012). In the presence of BSA, the concentration of Cy5-EE was completely recovered, whereas there was only partial recovery

of the Cy5-Chol and Span-Cy5-Chol concentrations, confirming the hypothesis that the ligands can bind non-specifically. Thus, the addition of BSA resulted in an even distribution of all ligands within the solution. Given that in the previous experiments, both soluble and cholestanol-conjugated drugs were diluted in HBSS or PBS, the actual concentration would have been significantly lower. This would result in a lower concentration of Span-Chol, in comparison to soluble Spantide. Despite the concentration of Spantide-cholestanol being lower, it is still effective than Spantide in inhibiting intracellular signalling, neuronal firing and nociception. Interestingly, when treating NK_1R expressing cells with these ligands, the concentrations at the plasma membrane of Cy5-EE was greater than Cy5-Chol and Span-Cy5-Chol. However, when examining the diffusion coefficient of each ligand, Cy5-EE was measured to have the highest diffusion coefficient, followed by Cy5-Chol and Span-Cy5-Chol. The Span-Cy5-Chol diffusion coefficients were similar to that of the receptor. This may suggest that the improved potency of anchored drugs may not only be dependent on a high local concentration at the receptor, but also a low diffusion coefficient at the receptor for receptor-ligand interactions to occur. Therefore, a focus on measuring the ligand concentrations in solution, in the presence of cells, concentration and diffusion coefficients at the plasma membrane will provide valuable insight into the spatial profile of cholestanol-conjugated antagonists. Furthermore, FCS has also previously been used to quantify and measure ligands intracellularly (Yoshida *et al.,* 2000, Schwille 2001). An extension of the current study may include the characterisation of cell permeable and impermeable ligands using FCS in conjunction with PCH analysis to determine their potential for the translocation to intracellular therapeutic targets.

Nanoparticles can be extremely versatile delivery devices as they can be designed to release drugs in response to pH, redox reactions, enzymatic cleavage, or temperature (Ganta *et al.,* 2008, Mura *et al.,* 2013). The size, surface charge and surface ligands of the nanoparticles

can also be engineered to promote targeting to specific cells and endosomal pathways (Gao *et al.,* 2010, He *et al.,* 2010, Zhou *et al.,* 2011, Mahon *et al.,* 2012). Therefore, the development of stimuli responsive nanoparticles can be valuable for drug delivery to intracellular locations, such as endosomes. Given the rapid and robust acidification of endosomes during the maturation process, a pH-sensitive nanoparticle would provide a consistent and well characterised mechanism of drug release (Beyenbach *et al.,* 2006, Marshansky *et al.,* 2008). A common method of imparting pH sensitivity into nanoparticles involves incorporating monomers in the hydrophobic core that ionise at acidic pH, resulting in the repulsion of the core and subsequent disassembly of the particle (Ganta *et al.,* 2008, Gao *et al.,* 2010). At acidic pH the disassembled copolymers are polycationic which has previously been identified as a contributing factor to nanoparticle-dependent cytotoxicity (Bieber *et al.,* 2002, Petersen *et al.,* 2002, Ganta *et al.,* 2008, Gao *et al.,* 2010, Benjaminsen *et al.,* 2013). It has previously been hypothesised that the polycation-dependent toxicity is due to interactions between the charged polymers and endosomal membranes. In this study we have identified the use of diethylene glycol incorporation into the nanoparticle core as a method of shielding the cell membrane to reduce cytotoxicity (Luo *et al.,* 2012). In addition, we have also explored the used of two different pH sensitive monomers, DEAEMA (pKa 7.1) and DIPMA (pKa 6.1) to determine if the pKa of the polymer influences cytotoxicity. The cytotoxicity of the nanoparticles were measured using ATP biosynthesis, membrane integrity, and cytosolic redox potential as various indicators of cell viability. Using these three methods, we demonstrated that DIPMA, the monomer with a lower pKa, results in a nanoparticle that disassembles at a lower pH and is consistently less cytotoxic than DEAEMA. The reduced cytotoxicity of DIPMA may be due to the disassembly of the nanoparticle further along the endocytic pathway. Future investigations focusing on the role of polymer pKa in the endocytic pathway may provide a

more comprehensive understanding of nanoparticles and lead to the development of non-toxic nanoparticles.

5.1 Summary and future directions

In summary, this thesis has provided insights into the importance of endosomal NK_1R signalling and the design of location bias ligands. This was investigated by studying the effect of endocytic inhibitors and lipid-conjugated NK_1R antagonists on intracellular NK_1R signalling. Moreover, this study also focused on the development of non-toxic, pH responsive nanoparticles. Looking forward, the development of safe, stimuli responsive nanoparticles may be the ideal direction for drug delivery to endosomes and other intracellular compartments. Although, anchoring drugs to the plasma membrane using lipids has demonstrated increased therapeutic potential compared to the soluble drug, they are translocated throughout the entire cell rather than to one specific compartment. Therefore, nanoparticles provide a means to tailor drugs that can target specific pathophysiological outcomes, without significantly affecting all receptor-mediated physiological outcomes. Thus, nanoparticles have the potential to significantly improve the way we treat disease.

References

Abel, B. A. and C. L. McCormick (2016). ""One-Pot" Aminolysis/Thiol–Maleimide End-Group Functionalization of RAFT Polymers: Identifying and Preventing Michael Addition Side Reactions." Macromolecules **49**(17): 6193-6202.

Alemi, F., E. Kwon, D. P. Poole, T. Lieu, V. Lyo, F. Cattaruzza, F. Cevikbas, M. Steinhoff, R. Nassini and S. Materazzi (2013). "The TGR5 receptor mediates bile acid–induced itch and analgesia." The Journal of clinical investigation **123**(4): 1513-1530.

Allen, J. A., R. A. Halverson-Tamboli and M. M. Rasenick (2007). "Lipid raft microdomains and neurotransmitter signalling." Nature reviews neuroscience **8**(2): 128.

Allen, T. M. and P. R. Cullis (2004). "Drug delivery systems: entering the mainstream." Science **303**(5665): 1818-1822.

Almeida, T., J. Rojo, P. Nieto, F. Pinto, M. Hernandez, J. Martin and M. Candenas (2004). "Tachykinins and tachykinin receptors: structure and activity relationships." Current medicinal chemistry **11**(15): 2045-2081.

Amigo, L., H. Mendoza, S. Zanlungo, J. F. Miquel, A. Rigotti, S. González and F. Nervi (1999). "Enrichment of canalicular membrane with cholesterol and sphingomyelin prevents bile salt-induced hepatic damage." Journal of lipid research **40**(3): 533-542.

Arora, P., T. K. Ricks and J. Trejo (2007). "Protease-Activated Receptor Signalling, Endocytic Sorting and Dysregulation in Cancer." Journal of Cell Science **120**(6): 921-928.

Ayling, L. J., S. J. Briddon, M. L. Halls, G. R. V. Hammond, L. Vaca, J. Pacheco, S. J. Hill and D. M. F. Cooper (2012). "Adenylyl cyclase AC8 directly controls its micro-environment by recruiting the actin cytoskeleton in a cholesterol-rich milieu." Journal of Cell Science **125**(4): 869-886.

Bachrach, U., Y.-C. Wang and A. Tabib (2001). "Polyamines: New Cues in Cellular Signal Transduction." Physiology **16**(3): 106-109.

Bae, Y. H., T. Okano, R. Hsu and S. W. Kim (1987). "Thermo-sensitive polymers as on-off switches for drug release." Die Makromolekulare Chemie, Rapid Communications **8**(10): 481-485.

Bai, T. R., D. Zhou, T. Weir, B. Walker, R. Hegele, S. Hayashi, K. McKay, G. P. Bondy and T. Fong (1995). "Substance P (NK1)-and neurokinin A (NK2)-receptor gene expression in inflammatory airway diseases." American Journal of Physiology-Lung Cellular and Molecular Physiology **269**(3): L309-L317.

Barak, L. S., K. Warabi, X. Feng, M. G. Caron and M. M. Kwatra (1999). "Real-time visualization of the cellular redistribution of G protein-coupled receptor kinase 2 and β-arrestin 2 during homologous desensitization of the substance P receptor." Journal of Biological Chemistry **274**(11): 7565-7569.

Baron, S. A., B. M. Jaffe and A. R. Gintzler (1983). "Release of substance P from the enteric nervous system: direct quantitation and characterization." Journal of Pharmacology and Experimental Therapeutics **227**(2): 365-368.

Behr, J.-P. (1997). "The proton sponge: a trick to enter cells the viruses did not exploit." CHIMIA International Journal for Chemistry **51**(1-2): 34-36.

Benjaminsen, R. V., M. A. Mattebjerg, J. R. Henriksen, S. M. Moghimi and T. L. Andresen (2013). "The Possible "Proton Sponge " Effect of Polyethylenimine (PEI) Does Not Include Change in Lysosomal pH." Molecular Therapy **21**(1): 149-157.

Benns, J. M., J.-S. Choi, R. I. Mahato, J.-S. Park and S. W. Kim (2000). "pH-sensitive cationic polymer gene delivery vehicle: N-Ac-poly (L-histidine)-graft-poly (L-lysine) comb shaped polymer." Bioconjugate chemistry **11**(5): 637-645.

Bergström, M., R. J. Hargreaves, H. D. Burns, M. R. Goldberg, D. Sciberras, S. A. Reines, K. J. Petty, M. Ögren, G. Antoni and B. Långström (2004). "Human positron emission tomography studies of brain neurokinin 1 receptor occupancy by aprepitant." Biological psychiatry **55**(10): 1007-1012.

Beyenbach, K. W. and H. Wieczorek (2006). "The V-type H+ ATPase: molecular structure and function, physiological roles and regulation." Journal of Experimental Biology **209**(4): 577-589.

Bieber, T., W. Meissner, S. Kostin, A. Niemann and H.-P. Elsasser (2002). "Intracellular route and transcriptional competence of polyethylenimine–DNA complexes." Journal of Controlled Release **82**(2): 441-454.
Bourne, H. R., D. A. Sanders and F. McCormick (1991). "The GTPase superfamily: conserved structure and molecular mechanism." Nature **349**(6305): 117.
Boutaghou-Cherid, H., C. Porcher, M. Liberge, Y. Jule, N. W. Bunnett and M.-O. Christen (2006). "Expression of the neurokinin type 1 receptor in the human colon." Autonomic Neuroscience **124**(1): 9-17.
Bowden, J. J., A. M. Garland, P. Baluk, P. Lefevre, E. F. Grady, S. R. Vigna, N. W. Bunnett and D. M. McDonald (1994). "Direct Observation of Substance P-induced Internalization of Neurokinin 1 (NK1) Receptors at Sites of Inflammation." Proceedings of the National Academy of Sciences **91**(September): 8964-8968.
Briddon, S. J. and S. J. Hill (2007). "Pharmacology Under The Microscope: The Use of Fluorescence Correlation Spectroscopy to Determine the Properties of Ligand–Receptor Complexes." Trends in Pharmacological Sciences **28**(12): 637-645.
Briddon, S. J., L. E. Kilpatrick and S. J. Hill (2017). "Studying GPCR Pharmacology in Membrane Microdomains: Fluorescence Correlation Spectroscopy Comes of Age." Trends in Pharmacological Sciences.
Caberlotto, L., Y. L. Hurd, P. Murdock, J. P. Wahlin, S. Melotto, M. Corsi and R. Carletti (2003). "Neurokinin 1 receptor and relative abundance of the short and long isoforms in the human brain." European Journal of Neuroscience **17**(9): 1736-1746.
Calebiro, D., V. O. Nikolaev, M. C. Gagliani, T. de Filippis, C. Dees, C. Tacchetti, L. Persani and M. J. Lohse (2009). "Persistent cAMP-Signals Triggered by Internalized G-Protein–Coupled Receptors." PLoS Biology **7**(8): e1000172.
Candenas, L., A. Lecci, F. M. Pinto, E. Patak, C. A. Maggi and J. N. Pennefather (2005). "Tachykinins and tachykinin receptors: effects in the genitourinary tract." Life sciences **76**(8): 835-862.
Castagliuolo, I., A. C. Keates, B. Qiu, C. P. Kelly, S. Nikulasson, S. E. Leeman and C. Pothoulakis (1997). "Increased substance P responses in dorsal root ganglia and intestinal macrophages during Clostridium difficile toxin A enteritis in rats." Proceedings of the National Academy of Sciences **94**(9): 4788-4793.
Castagliuolo, I., M. Riegler, A. Pasha, S. Nikulasson, B. Lu, C. Gerard, N. P. Gerard and C. Pothoulakis (1998). "Neurokinin-1 (NK-1) receptor is required in Clostridium difficile-induced enteritis." The Journal of clinical investigation **101**(8): 1547-1550.
Caswell, P. T., S. Vadrevu and J. C. Norman (2009). "Integrins: masters and slaves of endocytic transport." Nature Reviews Molecular Cell Biology **10**: 843.
Cattaruzza, F., G. Cottrell, N. Vaksman and N. Bunnett (2009). "Endothelin-converting enzyme 1 promotes re-sensitization of neurokinin 1 receptor-dependent neurogenic inflammation." British journal of pharmacology **156**(5): 730-739.
Cattaruzza, F., G. S. Cottrell, N. Vaksman and N. W. Bunnett (2009). "Endothelin-Converting Enzyme 1 Promotes Re-Sensitization of Neurokinin 1 Receptor-Dependent Neurogenic Inflammation." British Journal of Pharmacology **156**(5): 730-739.
Cattaruzza, F., D. P. Poole and N. W. Bunnett (2013). Arresting inflammation: contributions of plasma membrane and endosomal signalling to neuropeptide-driven inflammatory disease, Portland Press Limited.
Chaturvedi, S. K., E. Ahmad, J. M. Khan, P. Alam, M. Ishtikhar and R. H. Khan (2015). "Elucidating the interaction of limonene with bovine serum albumin: a multi-technique approach." Molecular BioSystems **11**(1): 307-316.
Chawla, M. K., G. M. Gutierrez, W. S. Young III, N. T. McMullen and N. E. Rance (1997). "Localization of neurons expressing substance P and neurokinin B gene transcripts in the human hypothalamus and basal forebrain." Journal of Comparative Neurology **384**(3): 429-442.

Chen, H., D. Redelman, S. Ro, S. M. Ward, T. Ordog and K. M. Sanders (2007). "Selective labeling and isolation of functional classes of interstitial cells of Cajal of human and murine small intestine." American Journal of Physiology-Cell Physiology **292**(1): C497-C507.
Chen, P., S. D. Douglas, J. Meshki and F. Tuluc (2012). "Neurokinin 1 receptor mediates membrane blebbing and sheer stress-induced microparticle formation in HEK293 cells." PloS one **7**(9): e45322.
Claing, A., S. A. Laporte, M. G. Caron and R. J. Lefkowitz (2002). "Endocytosis of G protein-coupled receptors: roles of G protein-coupled receptor kinases and ß-arrestin proteins." Progress in neurobiology **66**(2): 61-79.
Clamme, J.-P., G. Krishnamoorthy and Y. Mély (2003). "Intracellular dynamics of the gene delivery vehicle polyethylenimine during transfection: investigation by two-photon fluorescence correlation spectroscopy." Biochimica et Biophysica Acta (BBA)-Biomembranes **1617**(1-2): 52-61.
Cooper, P. E., M. H. Fernstrom, O. P. Rorstad, S. E. Leeman and J. B. Martin (1981). "The regional distribution of somatostatin, substance P and neurotensin in human brain." Brain research **218**(1-2): 219-232.
Cottrell, G. S., B. Padilla, S. Pikios, D. Roosterman, M. Steinhoff, E. F. Grady and N. W. Bunnett (2007). "Post-endocytic Sorting of Calcitonin Receptor-like Receptor and Receptor Activity-modifying Protein 1." Journal of Biological Chemistry **282**(16): 12260-12271.
Cottrell, G. S., B. E. Padilla, S. Amadesi, D. P. Poole, J. E. Murphy, M. Hardt, D. Roosterman, M. Steinhoff and N. W. Bunnett (2009). "Endosomal endothelin-converting enzyme-1: a regulator of beta-arrestin-dependent ERK signaling." The Journal of biological chemistry **284**: 22411-22425.
Cottrell, G. S., B. E. Padilla, S. Amadesi, D. P. Poole, J. E. Murphy, M. Hardt, D. Roosterman, M. Steinhoff and N. W. Bunnett (2009). "Endosomal Endothelin-converting Enzyme-1: A Regulator of beta-arrestin-dependent ERK Signaling." Journal of Biological Chemistry **284**: 22411-22425.
Daaka, Y., L. M. Luttrell, S. Ahn, G. J. Della Rocca, S. S. G. Ferguson, M. G. Caron and R. J. Lefkowitz (1998). "Essential Role for G Protein-coupled Receptor Endocytosis in the Activation of Mitogen-activated Protein Kinase." Journal of Biological Chemistry **273**(2): 685-688.
DeFea, K., Z. Vaughn, E. O'bryan, D. Nishijima, O. Dery and N. Bunnett (2000). "The proliferative and antiapoptotic effects of substance P are facilitated by formation of a β-arrestin-dependent scaffolding complex." Proceedings of the National Academy of Sciences **97**(20): 11086-11091.
DeFea, K., J. Zalevsky, M. Thoma, O. Dery, R. Mullins and N. Bunnett (2000). "β-Arrestin–dependent endocytosis of proteinase-activated receptor 2 is required for intracellular targeting of activated ERK1/2." The Journal of cell biology **148**(6): 1267-1282.
DeFea, K. A. (2011). "Beta-arrestins as regulators of signal termination and transduction: How do they determine what to scaffold?" Cellular Signalling **23**(4): 621-629.
DeWire, S. M., S. Ahn, R. J. Lefkowitz and S. K. Shenoy (2007). "β-arrestins and cell signaling." Annu. Rev. Physiol. **69**: 483-510.
Di Fiore, P. P. and M. von Zastrow (2014). "Endocytosis, signaling, and beyond." Cold Spring Harbor perspectives in biology **6**(8): a016865.
Di Guglielmo, G. M., C. Le Roy, A. F. Goodfellow and J. L. Wrana (2003). "Distinct endocytic pathways regulate TGF-β receptor signalling and turnover." Nature cell biology **5**(5): 410.
Diener, H. (2003). "RPR100893, a substance-P antagonist, is not effective in the treatment of migraine attacks." Cephalalgia **23**(3): 183-185.
Dionne, R. A., M. B. Max, S. M. Gordon, S. Parada, C. Sang, R. H. Gracely, N. F. Sethna and D. B. MacLean (1998). "The substance P receptor antagonist CP-99,994 reduces acute postoperative pain." Clinical Pharmacology & Therapeutics **64**(5): 562-568.
Doherty, G. J. and H. T. McMahon (2009). "Mechanisms of Endocytosis." Annual Review of Biochemistry **78**(1): 857-902.
dos Santos, T., J. Varela, I. Lynch, A. Salvati and K. A. Dawson (2011). "Effects of Transport Inhibitors on the Cellular Uptake of Carboxylated Polystyrene Nanoparticles in Different Cell Lines." PLOS ONE **6**(9): e24438.

Du, J.-Z., X.-J. Du, C.-Q. Mao and J. Wang (2011). "Tailor-made dual pH-sensitive polymer–doxorubicin nanoparticles for efficient anticancer drug delivery." Journal of the American Chemical Society **133**(44): 17560-17563.
Duncan, R. (2003). "The dawning era of polymer therapeutics." Nature reviews Drug discovery **2**(5): 347.
Elkin, S. R., A. M. Lakoduk and S. L. Schmid (2016). "Endocytic pathways and endosomal trafficking: a primer." Wiener Medizinische Wochenschrift **166**(7-8): 196-204.
Ferrandon, S., T. N. Feinstein, M. Castro, B. Wang, R. Bouley, J. T. Potts, T. J. Gardella and J.-P. Vilardaga (2009). "Sustained cyclic AMP production by parathyroid hormone receptor endocytosis." Nature chemical biology **5**(10): 734.
Fischer, D., T. Bieber, Y. Li, H.-P. Elsässer and T. Kissel (1999). "A novel non-viral vector for DNA delivery based on low molecular weight, branched polyethylenimine: effect of molecular weight on transfection efficiency and cytotoxicity." Pharmaceutical research **16**(8): 1273-1279.
Fischer, D., Y. Li, B. Ahlemeyer, J. Krieglstein and T. Kissel (2003). "In vitro cytotoxicity testing of polycations: influence of polymer structure on cell viability and hemolysis." Biomaterials **24**: 1121-1131.
Folk, D. S., J. C. Torosian, S. Hwang, D. G. McCafferty and K. J. Franz (2012). "Monitoring β-Secretase Activity in Living Cells with a Membrane-Anchored FRET Probe." Angewandte Chemie International Edition **51**(43): 10795-10799.
Fong, T. M., S. A. Anderson, H. Yu, R. Huang and C. D. Strader (1992). "Differential activation of intracellular effector by two isoforms of human neurokinin-1 receptor." Molecular pharmacology **41**(1): 24-30.
Fong, T. M., H. Yu, R. R. C. Huang and C. D. Strader (1992). "The extracellular domain of the neurokinin-1 receptor is required for high-affinity binding of peptides." Biochemistry **31**(47): 11806-11811.
Fredriksson, R., M. C. Lagerström, L.-G. Lundin and H. B. Schiöth (2003). "The G-Protein-Coupled Receptors in the Human Genome Form Five Main Families. Phylogenetic Analysis, Paralogon Groups, and Fingerprints." Molecular Pharmacology **63**(6): 1256-1272.
Fredriksson, R. and H. B. Schioth (2005). "The repertoire of G-protein coupled receptors in fully sequenced genomes." Molecular pharmacology.
Fujii, N., M. Hamano, H. Hashimoto and F. Ono (1992). "Solubilization of a lipophilic compound in highly concentrated saccharide solutions containing protein." Bioscience, biotechnology, and biochemistry **56**(1): 118-121.
Gaddum, J. (1931). "An unidentified depressor substance in certain tissue extracts." The Journal of physiology **72**(1): 74-87.
Ganta, S., H. Devalapally, A. Shahiwala and M. Amiji (2008). "A review of stimuli-responsive nanocarriers for drug and gene delivery." Journal of Controlled Release **126**(3): 187-204.
Gao, W., J. M. Chan and O. C. Farokhzad (2010). "pH-responsive nanoparticles for drug delivery." Molecular pharmaceutics **7**(6): 1913-1920.
Gebhart, C. L., S. Sriadibhatla, S. Vinogradov, P. Lemieux, V. Alakhov and A. V. Kabanov (2002). "Design and formulation of polyplexes based on pluronic-polyethyleneimine conjugates for gene transfer." Bioconjugate chemistry **13**(5): 937-944.
Gerard, N. P., L. A. Garraway, R. L. Eddy Jr, T. B. Shows, H. Iijima, J. L. Paquet and C. Gerard (1991). "Human substance P receptor (NK-1): organization of the gene, chromosome localization and functional expression of cDNA clones." Biochemistry **30**(44): 10640-10646.
Ghadiali, J. E. and M. M. Stevens (2008). "Enzyme-responsive nanoparticle systems." Advanced Materials **20**(22): 4359-4363.
Godbole, A., S. Lyga, M. J. Lohse and D. Calebiro (2017). "Internalized TSH receptors en route to the TGN induce local G s-protein signaling and gene transcription." Nature communications **8**(1): 443.
Goldstein, D., O. Wang, J. Saper, R. Stoltz, S. Silberstein and N. Mathew (1997). "Ineffectiveness of neurokinin-1 antagonist in acute migraine: a crossover study." Cephalalgia **17**(7): 785-790.

Goode, T., J. O'connell, P. Anton, H. Wong, J. Reeve, G. O'sullivan, J. Collins and F. Shanahan (2000). "Neurokinin-1 receptor expression in inflammatory bowel disease: molecular quantitation and localisation." Gut **47**(3): 387-396.
Goodman Jr, O. B., J. G. Krupnick, F. Santini, V. V. Gurevich, R. B. Penn, A. W. Gagnon, J. H. Keen and J. L. Benovic (1996). "β-Arrestin acts as a clathrin adaptor in endocytosis of the β2-adrenergic receptor." Nature **383**: 447.
Grady, E. F., P. Baluk, S. Böhm, P. D. Gamp, H. Wong, D. G. Payan, J. Ansel, A. L. Portbury, J. B. Furness and D. M. McDonald (1996). "Characterization of antisera specific to NK1, NK2, and NK3 neurokinin receptors and their utilization to localize receptors in the rat gastrointestinal tract." Journal of Neuroscience **16**(21): 6975-6986.
Greeno, E. W., P. Mantyh, G. M. Vercellotti and C. F. Moldow (1993). "Functional neurokinin 1 receptors for substance P are expressed by human vascular endothelium." Journal of Experimental Medicine **177**(5): 1269-1276.
Gruenberg, J. (2001). "The endocytic pathway: a mosaic of domains." Nature reviews Molecular cell biology **2**(10): 721.
Gruenberg, J. (2003). "Lipids in endocytic membrane transport and sorting." Current opinion in cell biology **15**(4): 382-388.
Haensler, J. and F. C. Szoka Jr (1993). "Polyamidoamine cascade polymers mediate efficient transfection of cells in culture." Bioconjugate chemistry **4**(5): 372-379.
Halls, M. L., H. R. Yeatman, C. J. Nowell, G. L. Thompson, A. B. Gondin, S. Civciristov, N. W. Bunnett, N. A. Lambert, D. P. Poole and M. Canals (2016). "Plasma Membrane Localization of the μ-Opioid Receptor Controls Spatiotemporal Signaling." Science Signaling **9**: ra16-ra16.
Hamm, H. E. (1998). "The many faces of G protein signaling." Journal of Biological Chemistry **273**(2): 669-672.
Hanyaloglu, A. C. and M. v. Zastrow (2008). "Regulation of GPCRs by endocytic membrane trafficking and its potential implications." Annu. Rev. Pharmacol. Toxicol. **48**: 537-568.
Hargreaves, R. (2002). "Imaging substance P receptors (NK_1) in the living human brain positron emission tomography." The Journal of clinical psychiatry.
Harlan, R. E., M. M. Garcia and J. E. Krause (1989). "Cellular localization of substance P-and neurokinin A-encoding preprotachykinin mRNA in the female rat brain." Journal of Comparative Neurology **287**(2): 179-212.
Harrison, S. and P. Geppetti (2001). "Substance p." The international journal of biochemistry & cell biology **33**(6): 555-576.
He, C., Y. Hu, L. Yin, C. Tang and C. Yin (2010). "Effects of particle size and surface charge on cellular uptake and biodistribution of polymeric nanoparticles." Biomaterials **31**(13): 3657-3666.
He, H., S. Chen, J. Zhou, Y. Dou, L. Song, L. Che, X. Zhou, X. Chen, Y. Jia and J. Zhang (2013). "Cyclodextrin-derived pH-responsive nanoparticles for delivery of paclitaxel." Biomaterials **34**(21): 5344-5358.
Hershey, A. D., P. E. Dykema and J. Krause (1991). "Organization, structure, and expression of the gene encoding the rat substance P receptor." Journal of Biological Chemistry **266**(7): 4366-4374.
Hillaireau, H. and P. Couvreur (2009). "Nanocarriers' entry into the cell: relevance to drug delivery." Cellular and Molecular Life Sciences **66**(17): 2873-2896.
Hinshaw, J. (2000). "Dynamin and its role in membrane fission." Annual review of cell and developmental biology **16**(1): 483-519.
Hökfelt, T., B. Pernow and J. Wahren (2001). "Substance P: a pioneer amongst neuropeptides." Journal of internal medicine **249**(1): 27-40.
Holubarsch, C., R. Schneider, B. Pieske, T. Ruf, G. Hasenfuss, G. Fraedrich, H. Posival and H. Just (1995). "Positive and negative inotropic effects of DL-sotalol and D-sotalol in failing and nonfailing human myocardium under physiological experimental conditions." Circulation **92**(10): 2904-2910.
Horwitz, M. J., M. B. Tedesco, S. M. Sereika, B. W. Hollis, A. Garcia-Ocaña and A. F. Stewart (2003). "Direct comparison of sustained infusion of human parathyroid hormone-related protein-(1–

36)[hPTHrP-(1–36)] versus hPTH-(1–34) on serum calcium, plasma 1, 25-dihydroxyvitamin D concentrations, and fractional calcium excretion in healthy human volunteers." The Journal of Clinical Endocrinology & Metabolism **88**(4): 1603-1609.
Hu, Y., T. Litwin, A. R. Nagaraja, B. Kwong, J. Katz, N. Watson and D. J. Irvine (2007). "Cytosolic delivery of membrane-impermeable molecules in dendritic cells using pH-responsive core− shell nanoparticles." Nano letters **7**(10): 3056-3064.
Hu, Y. Q., M. S. Kim, B. S. Kim and D. S. Lee (2008). "RAFT synthesis of amphiphilic (A-ran-B)-b-C diblock copolymers with tunable pH-sensitivity." Journal of Polymer Science Part A: Polymer Chemistry **46**(11): 3740-3748.
Huang, B., T. D. Perroud and R. N. Zare (2004). "Photon Counting Histogram: One-Photon Excitation." ChemPhysChem **5**(10): 1523-1531.
Huang, R. R. C., H. Yu, C. D. Strader and T. M. Fong (1994). "Interaction of substance P with the second and seventh transmembrane domains of the neurokinin-1 receptor." Biochemistry **33**(10): 3007-3013.
Hunter, A. C. and S. M. Moghimi (2010). "Cationic carriers of genetic material and cell death: A mitochondrial tale." Biochimica et Biophysica Acta (BBA) - Bioenergetics **1797**(6): 1203-1209.
Huotari, J. and A. Helenius (2011). "Endosome maturation." The EMBO journal **30**(17): 3481-3500.
Irannejad, R., V. Pessino, D. Mika, B. Huang, P. B. Wedegaertner, M. Conti and M. von Zastrow (2017). "Functional Selectivity of GPCR-Directed Drug Action Through Location Bias." Nature Chemical Biology **13**(7): 799-806.
Irannejad, R., J. C. Tomshine, J. R. Tomshine, M. Chevalier, J. P. Mahoney, J. Steyaert, S. G. Rasmussen, R. K. Sunahara, H. El-Samad, B. Huang and M. von Zastrow (2013). "Conformational Biosensors Reveal GPCR Signalling from Endosomes." Nature **495**(7442): 534-538.
Irannejad, R. and M. von Zastrow (2014). "GPCR signaling along the endocytic pathway." Current opinion in cell biology **27**: 109-116.
J., G. K. and P. Charalabos (2007). "Role of neuropeptides in inflammatory bowel disease." Inflammatory Bowel Diseases **13**(7): 918-932.
Jafri, F., H. M. El-Shewy, M.-H. Lee, M. Kelly, D. K. Luttrell and L. M. Luttrell (2006). "Constitutive ERK1/2 Activation by a Chimeric Neurokinin 1 Receptor-β-Arrestin1 Fusion Protein: PROBING THE COMPOSITION AND FUNCTION OF THE G PROTEIN-COUPLED RECEPTOR "SIGNALSOME"." Journal of Biological Chemistry **281**(28): 19346-19357.
Jarcho, J. M., N. A. Feier, A. Bert, J. A. Labus, M. Lee, J. Stains, B. Ebrat, S. M. Groman, K. Tillisch and A. L. Brody (2013). "Diminished neurokinin-1 receptor availability in patients with two forms of chronic visceral pain." PAIN® **154**(7): 987-996.
Jarcho, J. M., N. A. Feier, A. Bert, J. A. Labus, M. Lee, J. Stains, B. Ebrat, S. M. Groman, K. Tillisch, A. L. Brody, E. D. London, M. A. Mandelkern and E. A. Mayer (2013). "Diminished Neurokinin-1 Receptor Availability in Patients with Two Forms of Chronic Visceral Pain." Pain **154**(7): 987-996.
Jensen, D. D., M. L. Halls, J. E. Murphy, M. Canals, F. Cattaruzza, D. P. Poole, T. Lieu, H.-W. Koon, C. Pothoulakis and N. W. Bunnett (2014). "Endothelin-Converting Enzyme 1 and β-Arrestins Exert Spatiotemporal Control of Substance P-induced Inflammatory Signals." The Journal of Biological Chemistry **289**: 20283-20294.
Jensen, D. D., T. Lieu, M. L. Halls, N. A. Veldhuis, W. L. Imlach, Q. N. Mai, D. P. Poole, T. Quach, L. Aurelio, J. Conner, C. K. Herenbrink, N. Barlow, J. S. Simpson, M. J. Scanlon, B. Graham, A. McCluskey, P. J. Robinson, V. Escriou, R. Nassini, S. Materazzi, P. Geppetti, G. A. Hicks, M. J. Christie, C. J. H. Porter, M. Canals and N. W. Bunnett (2017). "Neurokinin 1 Receptor Signaling in Endosomes Mediates Sustained Nociception and is a Viable Therapeutic Target for Prolonged Pain Relief." Science Translational Medicine **9**.
Ji, T. H., M. Grossmann and I. Ji (1998). "G Protein-coupled Receptors: I. DIVERSITY OF RECEPTOR-LIGAND INTERACTIONS." Journal of Biological Chemistry **273**(28): 17299-17302.
Jiang, W. and S. P. Schwendeman (2001). "Stabilization and controlled release of bovine serum albumin encapsulated in poly (D, L-lactide) and poly (ethylene glycol) microsphere blends." Pharmaceutical research **18**(6): 878-885.

Johannes, L., R. G. Parton, P. Bassereau and S. Mayor (2015). "Building endocytic pits without clathrin." Nature Reviews Molecular Cell Biology **16**: 311.
Johannessen, L., J. Remsberg, V. Gaponenko, K. M. Adams, J. J. Barchi, S. G. Tarasov, S. Jiang and N. I. Tarasova (2011). "Peptide Structure Stabilization by Membrane Anchoring and its General Applicability to the Development of Potent Cell-Permeable Inhibitors." Chembiochem **12**: 914-921.
Johnson, I. R., E. J. Parkinson-Lawrence, H. Keegan, C. D. Spillane, J. Barry-O'Crowley, W. R. Watson, S. Selemidis, L. M. Butler, J. J. O'Leary and D. A. Brooks (2015). "Endosomal gene expression: a new indicator for prostate cancer patient prognosis?" Oncotarget **6**(35): 37919.
Johnson, J., Y. Chen and J. D. Mueller (2010). "Characterization of brightness and stoichiometry of bright particles by flow-fluorescence fluctuation spectroscopy." Biophysical journal **99**(9): 3084-3092.
Johnson, P. and J. Bornstein (2004). "Neurokinin-1 and-3 receptor blockade inhibits slow excitatory synaptic transmission in myenteric neurons and reveals slow inhibitory input." Neuroscience **126**(1): 137-147.
Johnston, A. P., C. Cortez, A. S. Angelatos and F. Caruso (2006). "Layer-by-layer engineered capsules and their applications." Current Opinion in Colloid & Interface Science **11**(4): 203-209.
Joyal, J.-S., S. Nim, T. Zhu, N. Sitaras, J. C. Rivera, Z. Shao, P. Sapieha, D. Hamel, M. Sanchez and K. Zaniolo (2014). "Subcellular localization of coagulation factor II receptor-like 1 in neurons governs angiogenesis." Nature medicine **20**(10): 1165.
Kaczyńska, K., D. Zając, P. Wojciechowski, E. Kogut and M. Szereda-Przestaszewska (2018). "Neuropeptides and breathing in health and disease." Pulmonary pharmacology & therapeutics **48**: 217-224.
Katsube, N., M. Maruyama, T. Andoh and Y. Kuraishi (2001). "Involvement of Leukotriene B4 in Substance P-Induced Itch-Associated Response in Mice." Journal of Investigative Dermatology **117**(6): 1621-1626.
Kauppi, M., A. Simonsen, B. Bremnes, A. Vieira, J. Callaghan, H. Stenmark and V. M. Olkkonen (2002). "The small GTPase Rab22 interacts with EEA1 and controls endosomal membrane trafficking." Journal of cell science **115**(5): 899-911.
Khawaja, A. M. and D. F. Rogers (1996). "Tachykinins: receptor to effector." The International Journal of Biochemistry & Cell Biology **28**(7): 721-738.
Kilpatrick, L., S. Briddon, S. Hill and N. Holliday (2010). "Quantitative Analysis of Neuropeptide Y Receptor Association with β-arrestin2 Measured by Bimolecular Fluorescence Complementation." British Journal of Pharmacology **160**(4): 892-906.
Kilpatrick, L. E., S. J. Briddon and N. D. Holliday (2012). "Fluorescence Correlation Spectroscopy, Combined with Bimolecular Fluorescence Complementation, Reveals the Effects of β-arrestin Complexes and Endocytic Targeting on the Membrane Mobility of Neuropeptide Y Receptors." Biochimica et Biophysica Acta **1823**(6): 1068-1081.
Kilpatrick, L. E., S. J. Briddon and N. D. Holliday (2012). "Fluorescence correlation spectroscopy, combined with bimolecular fluorescence complementation, reveals the effects of β-arrestin complexes and endocytic targeting on the membrane mobility of neuropeptide Y receptors." Biochimica et Biophysica Acta (BBA) - Molecular Cell Research **1823**(6): 1068-1081.
Kim, B. J., I. Y. Chang, S. Choi, J. Y. Jun, J.-H. Jeon, W.-X. Xu, Y. K. Kwon, D. Ren and I. So (2012). "Involvement of Na+-leak channel in substance P-induced depolarization of pacemaking activity in interstitial cells of Cajal." Cellular Physiology and Biochemistry **29**(3-4): 501-510.
Kim, D., E. S. Lee, K. T. Oh, Z. G. Gao and Y. H. Bae (2008). "Doxorubicin-loaded polymeric micelle overcomes multidrug resistance of cancer by double-targeting folate receptor and early endosomal pH." Small **4**(11): 2043-2050.
Kim, J., A. Singh, M. DelPoeta, D. A. Brown and E. London (2017). "The effect of sterol structure upon clathrin-mediated and clathrin-independent endocytosis." J Cell Sci: jcs. 201731.
Kobayashi, T., A. Yamaji-Hasegawa and E. Kiyokawa (2001). Lipid domains in the endocytic pathway. Seminars in cell & developmental biology, Elsevier.

Kocan, M., M. Dalrymple, R. Seeber, B. Feldman and K. Pfleger (2011). "Enhanced BRET Technology for the Monitoring of Agonist-Induced and Agonist-Independent Interactions Between GPCRs and β-Arrestins." Frontiers in Endocrinology **1**: 12.
Koon, H. W. and C. Pothoulakis (2006). "Immunomodulatory properties of substance P." Annals of the New York Academy of Sciences **1088**(1): 23-40.
Kratz, F. (2008). "Albumin as a drug carrier: Design of prodrugs, drug conjugates and nanoparticles." Journal of Controlled Release **132**(3): 171-183.
Krupnick, J. G. and J. L. Benovic (1998). "The role of receptor kinases and arrestins in G protein–coupled receptor regulation." Annual review of pharmacology and toxicology **38**(1): 289-319.
Kunath, K., A. von Harpe, D. Fischer, H. Petersen, U. Bickel, K. Voigt and T. Kissel (2003). "Low-molecular-weight polyethylenimine as a non-viral vector for DNA delivery: comparison of physicochemical properties, transfection efficiency and in vivo distribution with high-molecular-weight polyethylenimine." Journal of Controlled Release **89**(1): 113-125.
Lagerström, M. C. and H. B. Schiöth (2008). "Structural diversity of G protein-coupled receptors and significance for drug discovery." Nature reviews Drug discovery **7**(4): 339.
Lai, J.-P., A. Cnaan, H. Zhao and S. D. Douglas (2008). "Detection of full-length and truncated neurokinin-1 receptor mRNA expression in human brain regions." Journal of Neuroscience Methods **168**(1): 127-133.
Lai, J.-P., S. Lai, F. Tuluc, M. F. Tansky, L. E. Kilpatrick, S. E. Leeman and S. D. Douglas (2008). "Differences in the Length of the Carboxyl Terminus Mediate Functional Properties of Neurokinin-1 Receptor." Proceedings of the National Academy of Sciences **105**(34): 12605-12610.
Lan, T. H., Q. Liu, C. Li, G. Wu and N. A. Lambert (2012). "Sensitive and High Resolution Localization and Tracking of Membrane Proteins in Live Cells with BRET." Traffic **13**(11): 1450-1456.
Lavin, S., B. Southwell, R. Murphy, K. Jenkinson and J. Furness (1998). "Activation of neurokinin 1 receptors on interstitial cells of Cajal of the guinea-pig small intestine by substance P." Histochemistry and cell biology **110**(3): 263-271.
Law, I. K. M., J. E. Murphy, K. Bakirtzi, N. W. Bunnett and C. Pothoulakis (2012). "Neurotensin-induced Proinflammatory Signaling in Human Colonocytes Is Regulated by β-Arrestins and Endothelin-converting Enzyme-1-dependent Endocytosis and Resensitization of Neurotensin Receptor 1." Journal of Biological Chemistry **287**(18): 15066-15075.
Lee, E. S., Z. Gao, D. Kim, K. Park, I. C. Kwon and Y. H. Bae (2008). "Super pH-sensitive multifunctional polymeric micelle for tumor pHe specific TAT exposure and multidrug resistance." Journal of Controlled Release **129**(3): 228-236.
Lee, E. S., H. J. Shin, K. Na and Y. H. Bae (2003). "Poly(l-histidine)–PEG block copolymer micelles and pH-induced destabilization." Journal of Controlled Release **90**(3): 363-374.
Leroy, D., N. Schmid, J.-P. Behr, O. Filhol, S. Pares, J. Garin, J.-J. Bourgarit, E. M. Chambaz and C. Cochet (1995). "Direct identification of a polyamine binding domain on the regulatory subunit of the protein kinase casein kinase 2 by photoaffinity labeling." Journal of Biological Chemistry **270**(29): 17400-17406.
Levental, I., M. Grzybek and K. Simons (2010). "Greasing Their Way: Lipid Modifications Determine Protein Association with Membrane Rafts." Biochemistry **49**: 6305-6316.
Levental, I., D. Lingwood, M. Grzybek, Ü. Coskun and K. Simons (2010). "Palmitoylation regulates raft affinity for the majority of integral raft proteins." Proceedings of the National Academy of Sciences **107**(51): 22050-22054.
Lingwood, D. and K. Simons (2010). "Lipid rafts as a membrane-organizing principle." science **327**(5961): 46-50.
Linning, P., U. Haussmann, I. Beyer, S. Weidlich, H. Schieb, J. Wiltfang, H.-W. Klafki and H.-J. Knölker (2012). "Optimisation of BACE1 Inhibition of Tripartite Structures by Modification of Membrane Anchors, Spacers and Pharmacophores–Development of Potential Agents for the Treatment of Alzheimer's Disease." Organic & Biomolecular Chemistry **10**(41): 8216-8235.

Lodish, H., A. Berk, S. L. Zipursky, P. Matsudaira, D. Baltimore and J. Darnell (1995). Molecular cell biology, WH Freeman New York.
Lomax, A., P. Bertrand and J. Furness (1998). "Identification of the populations of enteric neurons that have NK1 tachykinin receptors in the guinea-pig small intestine." Cell and tissue research **294**(1): 27-33.
Lombardi Borgia, S., M. Regehly, R. Sivaramakrishnan, W. Mehnert, H. C. Korting, K. Danker, B. Röder, K. D. Kramer and M. Schäfer-Korting (2005). "Lipid nanoparticles for skin penetration enhancement—correlation to drug localization within the particle matrix as determined by fluorescence and parelectric spectroscopy." Journal of Controlled Release **110**(1): 151-163.
Lu, B., M. Figini, C. Emanueli, P. Geppetti, E. F. Grady, N. P. Gerard, J. Ansell, D. G. Payan, C. Gerard and N. Bunnett (1997). "The control of microvascular permeability and blood pressure by neutral endopeptidase." Nature medicine **3**(8): 904.
Lu, S. M. and G. D. Fairn (2018). "Mesoscale organization of domains in the plasma membrane–beyond the lipid raft." Critical reviews in biochemistry and molecular biology **53**(2): 192-207.
Lungwitz, U., M. Breunig, T. Blunk and A. Göpferich (2005). "Polyethylenimine-based non-viral gene delivery systems." European Journal of Pharmaceutics and Biopharmaceutics **60**(2): 247-266.
Luo, X., M. Feng, S. Pan, Y. Wen, W. Zhang and C. Wu (2012). "Charge shielding effects on gene delivery of polyethylenimine/DNA complexes: PEGylation and phospholipid coating." Journal of Materials Science: Materials in Medicine **23**(7): 1685-1695.
Luo, Y., B. Bolon, S. Kahn, B. D. Bennett, S. Babu-Khan, P. Denis, W. Fan, H. Kha, J. Zhang and Y. Gong (2001). "Mice deficient in BACE1, the Alzheimer's β-secretase, have normal phenotype and abolished β-amyloid generation." Nature neuroscience **4**(3): 231.
Luttrell, L. M. (1999). "β-Arrestin-dependent formation of β2 adrenergic receptor-Src protein kinase complexes." Science **283**(5402): 655-661.
Lv, H., S. Zhang, B. Wang, S. Cui and J. Yan (2006). "Toxicity of cationic lipids and cationic polymers in gene delivery." Journal of Controlled Release **114**(1): 100-109.
Lynch, I., A. Salvati and K. A. Dawson (2009). "What does the cell see?" Nature Nanotechnology **4**: 546.
Lynd, N. A., A. J. Meuler and M. A. Hillmyer (2008). "Polydispersity and block copolymer self-assembly." Progress in Polymer Science **33**(9): 875-893.
M., W. S., S. K. M. and H. G. D. S. (2004). "Role of interstitial cells of Cajal in neural control of gastrointestinal smooth muscles." Neurogastroenterology & Motility **16**(s1): 112-117.
Ma, X., Y. Wang, T. Zhao, Y. Li, L.-C. Su, Z. Wang, G. Huang, B. D. Sumer and J. Gao (2014). "Ultra-pH-sensitive nanoprobe library with broad pH tunability and fluorescence emissions." Journal of the American Chemical Society **136**(31): 11085-11092.
Maeno, H., H. Kiyama and M. Tohyama (1993). "Distribution of the substance P receptor (NK-1 receptor) in the central nervous system." Molecular Brain Research **18**(1): 43-58.
Maggi, C. A. (1997). "The effects of tachykinins on inflammatory and immune cells." Regulatory peptides **70**(2-3): 75-90.
Mahon, E., A. Salvati, F. B. Bombelli, I. Lynch and K. A. Dawson (2012). "Designing the nanoparticle–biomolecule interface for "targeting and therapeutic delivery"." Journal of Controlled Release **161**(2): 164-174.
Mantyh, C. R., T. S. Gates, R. P. Zimmerman, M. L. Welton, E. P. Passaro, S. R. Vigna, J. E. Maggio, L. Kruger and P. W. Mantyh (1988). "Receptor binding sites for substance P, but not substance K or neuromedin K, are expressed in high concentrations by arterioles, venules, and lymph nodules in surgical specimens obtained from patients with ulcerative colitis and Crohn disease." Proceedings of the National Academy of Sciences **85**(9): 3235-3239.
Mantyh, C. R., J. E. Maggio, P. W. Mantyh, S. R. Vigna and T. N. Pappas (1996). "Increased substance P receptor expression by blood vessels and lymphoid aggregates inClostridium difficile-induced pseudomembranous colitis." Digestive diseases and sciences **41**(3): 614-620.
Mantyh, P. W., C. J. Allen, J. R. Ghilardi, S. D. Rogers, C. R. Mantyh, H. Liu, A. I. Basbaum, S. R. Vigna and J. E. Maggio (1995). "Rapid Endocytosis of a G protein-Coupled Receptor: Substance P Evoked

Internalization of its Receptor in the Rat Striatum in vivo." Proceedings of the National Academy of Sciences of the United States of America **92**(7): 2622-2626.
Mantyh, P. W., E. DeMaster, A. Malhotra, S. Rogers, C. Mantyh, H. Liu, A. Basbaum and J. Maggio (1995). "Receptor endocytosis and dendrite reshaping in spinal neurons after somatosensory stimulation." Science **268**(5217): 1629-1632.
Mantyh, P. W., T. Gates, C. R. Mantyh and J. E. Maggio (1989). "Autoradiographic localization and characterization of tachykinin receptor binding sites in the rat brain and peripheral tissues." Journal of Neuroscience **9**(1): 258-279.
Marchand, J. E., H. Shimonaka and R. M. Kream (1991). "Biochemical characterization and anatomical distribution of a major form of unamidated precursor of substance P in rat brain." Brain research **567**(2): 290-305.
Maria-Simonetta, F. P. (2006). "Relationships between neurokinin receptor-expressing interstitial cells of Cajal and tachykininergic nerves in the gut." Journal of Cellular and Molecular Medicine **10**(1): 20-32.
Marshansky, V. and M. Futai (2008). "The V-type H+-ATPase in vesicular trafficking: targeting, regulation and function." Current opinion in cell biology **20**(4): 415-426.
Marvizón, J. C. G., E. F. Grady, E. Stefani, N. W. Bunnett and E. A. Mayer (1999). "Substance P release in the dorsal horn assessed by receptor internalization: NMDA receptors counteract a tonic inhibition by GABAB receptors." European Journal of Neuroscience **11**(2): 417-426.
Marvizón, J. C. G., V. Martínez, E. F. Grady, N. W. Bunnett and E. A. Mayer (1997). "Neurokinin 1 Receptor Internalization in Spinal Cord Slices Induced by Dorsal Root Stimulation Is Mediated by NMDA Receptors." The Journal of Neuroscience **17**(21): 8129-8136.
Mashaghi, A., A. Marmalidou, M. Tehrani, P. M. Grace, C. Pothoulakis and R. Dana (2016). "Neuropeptide substance P and the immune response." Cellular and molecular life sciences **73**(22): 4249-4264.
Maurer, N., D. B. Fenske and P. R. Cullis (2001). "Developments in liposomal drug delivery systems." Expert opinion on biological therapy **1**(6): 923-947.
Mayor, S., R. G. Parton and J. G. Donaldson (2014). "Clathrin-independent pathways of endocytosis." Cold Spring Harbor perspectives in biology **6**(6): a016758.
Mayordomo, C., S. García-Recio, E. Ametller, P. Fernández-Nogueira, E. M. Pastor-Arroyo, L. Vinyals, I. Casas, P. Gascón and V. Almendro (2012). "Targeting of substance P induces cancer cell death and decreases the steady state of EGFR and Her2." Journal of cellular physiology **227**(4): 1358-1366.
McConalogue, K., O. Déry, M. Lovett, H. Wong, J. H. Walsh, E. F. Grady and N. W. Bunnett (1999). "Substance P-induced Trafficking of β-Arrestins: THE ROLE OF β-ARRESTINS IN ENDOCYTOSIS OF THE NEUROKININ-1 RECEPTOR." Journal of Biological Chemistry **274**(23): 16257-16268.
Mellman, I., R. Fuchs and A. Helenius (1986). "Acidification of the endocytic and exocytic pathways." Annual review of biochemistry **55**(1): 663-700.
Mellman, I. and Y. Yarden (2013). "Endocytosis and cancer." Cold Spring Harbor perspectives in biology **5**(12): a016949.
Meng, F., W. E. Hennink and Z. Zhong (2009). "Reduction-sensitive polymers and bioconjugates for biomedical applications." Biomaterials **30**(12): 2180-2198.
Mercer, J., M. Schelhaas and A. Helenius (2010). "Virus Entry by Endocytosis." Annual Review of Biochemistry **79**(1): 803-833.
Merriam, L. A., C. N. Baran, B. M. Girard, J. C. Hardwick, V. May and R. L. Parsons (2013). "Pituitary Adenylate Cyclase 1 Receptor Internalization and Endosomal Signaling Mediate the Pituitary Adenylate Cyclase Activating Polypeptide-Induced Increase in Guinea Pig Cardiac Neuron Excitability." The Journal of Neuroscience **33**(10): 4614-4622.
Meseth, U., T. Wohland, R. Rigler and H. Vogel (1999). "Resolution of fluorescence correlation measurements." Biophysical journal **76**(3): 1619-1631.

Meshki, J., S. D. Douglas, J.-P. Lai, L. Schwartz, L. E. Kilpatrick and F. Tuluc (2009). "Neurokinin 1 Receptor Mediates Membrane Blebbing in HEK293 Cells through a Rho/Rho-associated Coiled-coil Kinase-dependent Mechanism." Journal of Biological Chemistry **284**(14): 9280-9289.
Meyer, M., A. Philipp, R. Oskuee, C. Schmidt and E. Wagner (2008). "Breathing life into polycations: functionalization with pH-responsive endosomolytic peptides and polyethylene glycol enables siRNA delivery." Journal of the American Chemical Society **130**(11): 3272-3273.
Miriam, A., F. Steven, L. Baoxu, Z. Wei, Y. Peibin, B. Daniel, X. Wei, S. A. D., T. James, G. C. C. and G. P. T. (2011). "Artificially Induced Protein–Membrane Anchorage with Cholesterol-Based Recognition Agents as a New Therapeutic Concept." Angewandte Chemie International Edition **50**(28): 6248-6253.
Moghimi, S. M., P. Symonds, J. C. Murray, A. C. Hunter, G. Debska and A. Szewczyk (2005). "A two-stage poly(ethylenimine)-mediated cytotoxicity: implications for gene transfer/therapy." Molecular Therapy **11**(6): 990-995.
Mohrmann, K. and P. v. d. Sluijs (1999). "Regulation of membrane transport through the endocytic pathway by rabGTPases." Molecular membrane biology **16**(1): 81-87.
Muller, P. A., P. T. Caswell, B. Doyle, M. P. Iwanicki, E. H. Tan, S. Karim, N. Lukashchuk, D. A. Gillespie, R. L. Ludwig and P. Gosselin (2009). "Mutant p53 drives invasion by promoting integrin recycling." Cell **139**(7): 1327-1341.
Muñoz, M. and R. Coveñas (2014). "Involvement of substance P and the NK-1 receptor in human pathology." Amino acids **46**(7): 1727-1750.
Mura, S., J. Nicolas and P. Couvreur (2013). "Stimuli-responsive nanocarriers for drug delivery." Nature materials **12**(11): 991.
Murphy, J. E., B. E. Padilla, B. Hasdemir, G. S. Cottrell and N. W. Bunnett (2009). "Endosomes: A Legitimate Platform for the Signaling Train." Proceedings of the National Academy of Sciences of the United States of America **106**: 17615-17622.
Nakajima, Y., K. Tsuchida, M. Negishi, S. Ito and S. Nakanishi (1992). "Direct linkage of three tachykinin receptors to stimulation of both phosphatidylinositol hydrolysis and cyGMP cascades in transfected Chinese hamster ovary cells." Journal of Biological Chemistry **267**(4): 2437-2442.
Nakayama, M., T. Okano, T. Miyazaki, F. Kohori, K. Sakai and M. Yokoyama (2006). "Molecular design of biodegradable polymeric micelles for temperature-responsive drug release." Journal of Controlled Release **115**(1): 46-56.
Navratil, M., G. A. Mabbott and E. A. Arriaga (2006). "Chemical Microscopy Applied to Biological Systems." Analytical Chemistry **78**(12): 4005-4020.
Neer, E. J. (1995). "Heterotrimeric C proteins: Organizers of transmembrane signals." Cell **80**(2): 249-257.
Nel, A. E., L. Mädler, D. Velegol, T. Xia, E. M. Hoek, P. Somasundaran, F. Klaessig, V. Castranova and M. Thompson (2009). "Understanding biophysicochemical interactions at the nano–bio interface." Nature materials **8**(7): 543.
Neunlist, M., P. Aubert, C. Toquet, T. Oreshkova, J. Barouk, P. A. Lehur, M. Schemann and J. P. Galmiche (2003). "Changes in chemical coding of myenteric neurones in ulcerative colitis." Gut **52**(1): 84-90.
Nichols, M. L., B. J. Allen, S. D. Rogers, J. R. Ghilardi, P. Honore, N. M. Luger, M. P. Finke, J. Li, D. A. Lappi and D. A. Simone (1999). "Transmission of chronic nociception by spinal neurons expressing the substance P receptor." Science **286**(5444): 1558-1561.
Nikolaev, V. O., M. Bünemann, L. Hein, A. Hannawacker and M. J. Lohse (2004). "Novel Single Chain cAMP Sensors for Receptor-Induced Signal Propagation." Journal of Biological Chemistry **279**(36): 37215-37218.
Nikolaev, V. O., A. Moshkov, A. R. Lyon, M. Miragoli, P. Novak, H. Paur, M. J. Lohse, Y. E. Korchev, S. E. Harding and J. Gorelik (2010). "β2-Adrenergic Receptor Redistribution in Heart Failure Changes cAMP Compartmentation." Science **327**: 1653-1657.
Nixon, R. A. (2005). "Endosome function and dysfunction in Alzheimer's disease and other neurodegenerative diseases." Neurobiology of Aging **26**(3): 373-382.

Oakley, R. H., S. A. Laporte, J. A. Holt, L. S. Barak and M. G. Caron (1999). "Association of β-arrestin with G protein-coupled receptors during clathrin-mediated endocytosis dictates the profile of receptor resensitization." Journal of Biological Chemistry **274**(45): 32248-32257.
Osaki, F., T. Kanamori, S. Sando, T. Sera and Y. Aoyama (2004). "A quantum dot conjugated sugar ball and its cellular uptake. On the size effects of endocytosis in the subviral region." Journal of the American Chemical Society **126**(21): 6520-6521.
Otsuka, M. and K. Yoshioka (1993). "Neurotransmitter functions of mammalian tachykinins." Physiological reviews **73**(2): 229-308.
Parhamifar, L., A. K. Larsen, A. C. Hunter, T. L. Andresen and S. M. Moghimi (2010). "Polycation cytotoxicity: a delicate matter for nucleic acid therapy-focus on polyethylenimine." Soft Matter **6**(17): 4001-4009.
Park, M. R., K. O. Han, I. K. Han, M. H. Cho, J. W. Nah, Y. J. Choi and C. S. Cho (2005). "Degradable polyethylenimine-alt-poly (ethylene glycol) copolymers as novel gene carriers." Journal of Controlled Release **105**(3): 367-380.
Parton, R. G. and M. A. del Pozo (2013). "Caveolae as plasma membrane sensors, protectors and organizers." Nature Reviews Molecular Cell Biology **14**: 98.
Pelayo, J.-C., N. A. Veldhuis, E. M. Eriksson, N. W. Bunnett and D. P. Poole (2014). "Localisation and Activation of the Neurokinin 1 Receptor in the Enteric Nervous System of the Mouse Distal Colon." Cell and Tissue Research **356**(2): 319-332.
Pelayo, J. C., D. P. Poole, M. Steinhoff, G. S. Cottrell and N. W. Bunnett (2011). "Endothelin-converting Enzyme-1 Regulates Trafficking and Signalling of the Neurokinin 1 Receptor in Endosomes of Myenteric Neurones." Journal of Physiology **589**(Pt 21): 5213-5230.
Peng, Q., S. Zhang, Q. Yang, T. Zhang, X.-Q. Wei, L. Jiang, C.-L. Zhang, Q.-M. Chen, Z.-R. Zhang and Y.-F. Lin (2013). "Preformed albumin corona, a protective coating for nanoparticles based drug delivery system." Biomaterials **34**(33): 8521-8530.
Pennefather, J. N., A. Lecci, M. L. Candenas, E. Patak, F. M. Pinto and C. A. Maggi (2004). "Tachykinins and tachykinin receptors: a growing family." Life sciences **74**(12): 1445-1463.
Pereira-Leal, J. B. and M. C. Seabra (2001). "Evolution of the Rab family of small GTP-binding proteins." Journal of molecular biology **313**(4): 889-901.
Petersen, H., P. M. Fechner, A. L. Martin, K. Kunath, S. Stolnik, C. J. Roberts, D. Fischer, M. C. Davies and T. Kissel (2002). "Polyethylenimine-graft-poly (ethylene glycol) copolymers: influence of copolymer block structure on DNA complexation and biological activities as gene delivery system." Bioconjugate chemistry **13**(4): 845-854.
Petros, R. A. and J. M. DeSimone (2010). "Strategies in the design of nanoparticles for therapeutic applications." Nature reviews Drug discovery **9**(8): 615.
Pierce, K. L., R. T. Premont and R. J. Lefkowitz (2002). "Seven-Transmembrane Receptors." Nature Reviews. Molecular Cell Biology **3**(9): 639-650.
Pinto, F. M., T. A. Almeida, M. Hernandez, P. Devillier, C. Advenier and M. L. Candenas (2004). "mRNA expression of tachykinins and tachykinin receptors in different human tissues." European journal of pharmacology **494**(2-3): 233-239.
Pitcher, J. A., N. J. Freedman and R. J. Lefkowitz (1998). "G Protein–Coupled Receptor Kinases." Annual Review of Biochemistry **67**(1): 653-692.
Porther, N. and M. A. Barbieri (2015). "The role of endocytic Rab GTPases in regulation of growth factor signaling and the migration and invasion of tumor cells." Small GTPases **6**(3): 135-144.
Povsic, T. J., T. A. Kohout and R. J. Lefkowitz (2003). "β-Arrestin1 mediates insulin-like growth factor 1 (IGF-1) activation of phosphatidylinositol 3-kinase (PI3K) and anti-apoptosis." Journal of Biological Chemistry **278**(51): 51334-51339.
Poyner, D. and M. Wheatley (2009). G Protein-Coupled Receptors: Essential Methods, John Wiley & Sons.

Putnam, D., C. A. Gentry, D. W. Pack and R. Langer (2001). "Polymer-based gene delivery with low cytotoxicity by a unique balance of side-chain termini." Proceedings of the National Academy of Sciences **98**(3): 1200-1205.
Quartara, L. and C. a. Maggi (1997). "The Tachykinin NK1 Receptor. Part I: Ligands and Mechanisms of Cellular Activation." Neuropeptides **31**: 537-563.
Rajendran, L., H.-J. Knölker and K. Simons (2010). "Subcellular targeting strategies for drug design and delivery." Nature reviews Drug discovery **9**(1): 29.
Rajendran, L., A. Schneider, G. Schlechtingen, S. Weidlich, J. Ries, T. Braxmeier, P. Schwille, J. B. Schulz, C. Schroeder, M. Simons, G. Jennings, H.-J. Knölker and K. Simons (2008). "Efficient Inhibition of the Alzheimer's Disease beta-secretase by Membrane Targeting." Science **320**: 520-523.
Rajendran, L., V. Udayar and Z. V. Goodger (2012). "Lipid-Anchored Drugs for Delivery into Subcellular Compartments." Trends in Pharmacological Sciences **33**: 215-222.
Regoli, D., A. Boudon and J.-L. Fauchere (1994). "Receptors and antagonists for substance P and related peptides." Pharmacological reviews **46**(4): 551-599.
Reiner, J. E., A. Jahn, S. M. Stavis, M. J. Culbertson, W. N. Vreeland, D. L. Burden, J. Geist and M. Gaitan (2009). "Accurate optical analysis of single-molecule entrapment in nanoscale vesicles." Analytical chemistry **82**(1): 180-188.
Reitan, N. K., A. Juthajan, T. Lindmo and C. d. L. Davies (2008). Macromolecular diffusion in the extracellular matrix measured by fluorescence correlation spectroscopy, SPIE.
Rejman, J., V. Oberle, I. S. Zuhorn and D. Hoekstra (2004). "Size-dependent internalization of particles via the pathways of clathrin- and caveolae-mediated endocytosis." Biochemical Journal **377**(Pt 1): 159-169.
Renzi, D., B. Pellegrini, F. Tonelli, C. Surrenti and A. Calabro (2000). "Substance P (neurokinin-1) and neurokinin A (neurokinin-2) receptor gene and protein expression in the healthy and inflamed human intestine." The American journal of pathology **157**(5): 1511-1522.
Revankar, C. M., D. F. Cimino, L. A. Sklar, J. B. Arterburn and E. R. Prossnitz (2005). "A transmembrane intracellular estrogen receptor mediates rapid cell signaling." Science **307**(5715): 1625-1630.
Riss, T. L., R. A. Moravec, A. L. Niles, S. Duellman, H. A. Benink, T. J. Worzella and L. Minor (2016). "Cell viability assays."
Robertson, M. J., F. M. Deane, P. J. Robinson and A. McCluskey (2014). "Synthesis of Dynole 34-2, Dynole 2-24 and Dyngo 4a for investigating dynamin GTPase." Nat Protoc **9**(4): 851-870.
Röcker, C., M. Pötzl, F. Zhang, W. J. Parak and G. U. Nienhaus (2009). "A quantitative fluorescence study of protein monolayer formation on colloidal nanoparticles." Nature Nanotechnology **4**: 577.
Roosterman, D., G. S. Cottrell, B. E. Padilla, L. Muller, C. B. Eckman, N. W. Bunnett and M. Steinhoff (2007). "Endothelin-converting enzyme 1 degrades neuropeptides in endosomes to control receptor recycling." Proceedings of the National Academy of Sciences **104**(28): 11838-11843.
Rose, R. H., S. J. Briddon and S. J. Hill (2012). "A Novel Fluorescent Histamine H(1) Receptor Antagonist Demonstrates the Advantage of Using Fluorescence Correlation Spectroscopy to Study the Binding of Lipophilic Ligands." British Journal of Pharmacology **165**(6): 1789-1800.
Rosenbaum, D. M., S. G. Rasmussen and B. K. Kobilka (2009). "The structure and function of G-protein-coupled receptors." Nature **459**(7245): 356.
Rupniak, N. M., E. Perdona, C. Griffante, P. Cavallini, A. Sava, D. J. Ricca, K. B. Thor, E. C. Burgard and M. Corsi (2018). "Affinity, potency, efficacy, and selectivity of neurokinin A analogs at human recombinant NK2 and NK1 receptors." PloS one **13**(10): e0205894.
Saftig, P. and J. Klumperman (2009). "Lysosome biogenesis and lysosomal membrane proteins: trafficking meets function." Nature reviews Molecular cell biology **10**(9): 623.
Salmhofer, H., W. Neuhuber, P. Ruth, A. Huber, M. Russwurm and H. Allescher (2001). "Pivotal role of the interstitial cells of Cajal in the nitric oxide signaling pathway of rat small intestine." Cell and Tissue Research **305**(3): 331-340.

Sapsford, K. E., W. R. Algar, L. Berti, K. B. Gemmill, B. J. Casey, E. Oh, M. H. Stewart and I. L. Medintz (2013). "Functionalizing Nanoparticles with Biological Molecules: Developing Chemistries that Facilitate Nanotechnology." Chemical Reviews **113**(3): 1904-2074.
Schieb, H., S. Weidlich, G. Schlechtingen, P. Linning, G. Jennings, M. Gruner, J. Wiltfang, H. W. Klafki and H. J. Knölker (2010). "Structural Design, Solid-Phase Synthesis and Activity of Membrane-Anchored β-Secretase Inhibitors on Aβ Generation from Wild-Type and Swedish-Mutant APP." Chemistry-A European Journal **16**(48): 14412-14423.
Schmid, S. L. (2017). "Reciprocal regulation of signaling and endocytosis: Implications for the evolving cancer cell." The Journal of Cell Biology.
Schmidlin, F., D. Roosterman and N. W. Bunnett (2003). "The third intracellular loop and carboxyl tail of neurokinin 1 and 3 receptors determine interactions with β-arrestins." American Journal of Physiology-Cell Physiology **285**(4): C945-C958.
Schwille, P. (2001). "Fluorescence correlation spectroscopy and its potential for intracellular applications." Cell biochemistry and biophysics **34**(3): 383-408.
Schwille, P. (2005). Fluorescence correlation spectroscopy. Encyclopedic Reference of Genomics and Proteomics in Molecular Medicine, Springer**:** 576-578.
Schwille, P. (2006). Fluorescence Correlation Spectroscopy. Encyclopedic Reference of Genomics and Proteomics in Molecular Medicine. Berlin, Heidelberg, Springer Berlin Heidelberg**:** 576-578.
Schwille, P. and E. Haustein (2001). Fluorescence Correlation Spectroscopy - An Introduction to its Concepts and Applications.
Schwille, P., F. Oehlenschläger and N. G. Walter (1996). "Quantitative Hybridization Kinetics of DNA Probes to RNA in Solution Followed by Diffusional Fluorescence Correlation Analysis." Biochemistry **35**(31): 10182-10193.
Seipel, L. and H.-M. Hoffmeister (1993). "Inotropic and haemodynamic effects of d-and d, l-sotalol: comparison with other antiarrhythmics." European heart journal **14**(suppl_H): 36-40.
Sergin, I., Y.-J. I. Jong, S. K. Harmon, V. Kumar and K. L. O'Malley (2017). "Sequences within the C terminus of the metabotropic glutamate receptor 5 (mGluR5) are responsible for inner nuclear membrane localization." Journal of Biological Chemistry **292**(9): 3637-3655.
Sheng, R., Y. Chen, H. Y. Gee, E. Stec, H. R. Melowic, N. R. Blatner, M. P. Tun, Y. Kim, M. Källberg and T. K. Fujiwara (2012). "Cholesterol modulates cell signaling and protein networking by specifically interacting with PDZ domain-containing scaffold proteins." Nature communications **3**: 1249.
Shenoy, S. K., P. H. McDonald, T. A. Kohout and R. J. Lefkowitz (2001). "Regulation of receptor fate by ubiquitination of activated β2-adrenergic receptor and β-arrestin." Science **294**(5545): 1307-1313.
Shimizu, Y., H. Matsuyama, T. Shiina, T. Takewaki and J. Furness (2008). "Tachykinins and their functions in the gastrointestinal tract." Cellular and Molecular Life Sciences **65**(2): 295-311.
Shukla, A. K., K. Xiao and R. J. Lefkowitz (2011). "Emerging paradigms of β-arrestin-dependent seven transmembrane receptor signaling." Trends in biochemical sciences **36**(9): 457-469.
Simons, K. and J. Gruenberg (2000). "Jamming the endosomal system: lipid rafts and lysosomal storage diseases." Trends in Cell Biology **10**(11): 459-462.
Simons, K. and E. Ikonen (1997). "Functional rafts in cell membranes." Nature **387**(6633): 569.
Simons, K. and D. Toomre (2000). "Lipid rafts and signal transduction." Nature reviews Molecular cell biology **1**(1): 31.
Simons, K. and W. L. Vaz (2004). "Model systems, lipid rafts, and cell membranes." Annu. Rev. Biophys. Biomol. Struct. **33**: 269-295.
Sinha, B., D. Köster, R. Ruez, P. Gonnord, M. Bastiani, D. Abankwa, R. V. Stan, G. Butler-Browne, B. Vedie and L. Johannes (2011). "Cells respond to mechanical stress by rapid disassembly of caveolae." Cell **144**(3): 402-413.
Slessareva, J. E., S. M. Routt, B. Temple, V. A. Bankaitis and H. G. Dohlman (2006). "Activation of the phosphatidylinositol 3-kinase Vps34 by a G protein α subunit at the endosome." Cell **126**(1): 191-203.
Song, X., S. Coffa, H. Fu and V. V. Gurevich (2009). "How does arrestin assemble MAPKs into a signaling complex?" Journal of Biological Chemistry **284**(1): 685-695.

Song, Y., A. K. Kenworthy and C. R. Sanders (2014). "Cholesterol as a co-solvent and a ligand for membrane proteins." Protein Science **23**(1): 1-22.
Sorkin, A. and M. Von Zastrow (2009). "Endocytosis and signalling: intertwining molecular networks." Nature reviews Molecular cell biology **10**(9): 609.
Sorkin, A. and M. von Zastrow (2009). "Endocytosis and Signalling: Intertwining Molecular Networks." Nature Reviews. Molecular Cell Biology **10**: 609-622.
Sperling, R. A. and W. J. Parak (2010). "Surface modification, functionalization and bioconjugation of colloidal inorganic nanoparticles." Philosophical Transactions of the Royal Society of London A: Mathematical, Physical and Engineering Sciences **368**(1915): 1333-1383.
Steinhoff, M. S., B. von Mentzer, P. Geppetti, C. Pothoulakis and N. W. Bunnett (2014). "Tachykinins and their receptors: contributions to physiological control and the mechanisms of disease." Physiol Rev **94**(1): 265-301.
Steinhoff, M. S., B. von Mentzer, P. Geppetti, C. Pothoulakis and N. W. Bunnett (2014). "Tachykinins and Their Receptors: Contributions to Physiological Control and the Mechanisms of Disease." Physiological Reviews **94**(1): 265-301.
Stoddart, L. A., L. E. Kilpatrick, S. J. Briddon and S. J. Hill (2015). "Probing the Pharmacology of G Protein-Coupled Receptors with Fluorescent Ligands." Neuropharmacology **98**: 48-57.
Stoddart, L. A., A. J. Vernall, S. J. Briddon, B. Kellam and S. J. Hill (2015). "Direct Visualisation of Internalization of the Adenosine A3 Receptor and Localization with Arrestin3 Using a Fluorescent Agonist." Neuropharmacology **98**: 68-77.
Stoddart, L. A., A. J. Vernall, J. L. Denman, S. J. Briddon, B. Kellam and S. J. Hill (2012). "Fragment Screening at Adenosine-A3 Receptors in Living Cells Using a Fluorescence-Based Binding Assay." Chemistry & biology **19**(9): 1105-1115.
Stone, L. S. and D. C. Molliver (2009). "In search of analgesia: emerging poles of GPCRs in pain." Molecular interventions **9**(5): 234.
Sundelin, J. B., D. M. Provvedini, C. R. Wahlestedt, H. Laurell, J. S. Pohl and P. A. Peterson (1992). "Molecular cloning of the murine substance K and substance P receptor genes." The FEBS Journal **203**(3): 625-631.
Sweitzer, S. M. and J. E. Hinshaw (1998). "Dynamin undergoes a GTP-dependent conformational change causing vesiculation." Cell **93**(6): 1021-1029.
Symonds, P., J. C. Murray, A. C. Hunter, G. Debska, A. Szewczyk and S. M. Moghimi (2005). "Low and high molecular weight poly(l-lysine)s/poly(l-lysine)–DNA complexes initiate mitochondrial-mediated apoptosis differently." FEBS Letters **579**(27): 6191-6198.
Szallasi, A., C. Goso and S. Manzini (2017). Sensory Nerves and Tachykinins. Neuropeptides in Respiratory Medicine, Routledge**:** 173-196.
Takeda, Y., K. B. Chou, J. Takeda, B. Sachais and J. Krause (1991). "Molecular cloning, structural characterization and functional expression of the human substance P receptor." Biochemical and biophysical research communications **179**(3): 1232-1240.
Tatarkova, S. A., A. K. Verma, D. A. Berk and C. J. Lloyd (2005). "Quantitative fluorescence microscopy of macromolecules in gel and biological tissue." Physics in Medicine & Biology **50**(23): 5759.
Thomas, M. and A. M. Klibanov (2002). "Enhancing polyethylenimine's delivery of plasmid DNA into mammalian cells." Proceedings of the National Academy of Sciences **99**(23): 14640-14645.
Tohgo, A., K. L. Pierce, E. W. Choy, R. J. Lefkowitz and L. M. Luttrell (2002). "β-Arrestin Scaffolding of the ERK Cascade Enhances Cytosolic ERK Activity but Inhibits ERK-mediated Transcription following Angiotensin AT1a Receptor Stimulation." Journal of Biological Chemistry **277**(11): 9429-9436.
Torrens, Y., M. Montety, M. Etr, J. Beaujouan and J. Glowinski (1989). "Tachykinin receptors of the NK1 type (substance P) coupled positively to phospholipase C on cortical astrocytes from the newborn mouse in primary culture." Journal of neurochemistry **52**(6): 1913-1918.
Trejo, J. and S. R. Coughlin (1999). "The Cytoplasmic Tails of Protease-activated Receptor-1 and Substance P Receptor Specify Sorting to Lysosomes versusRecycling." Journal of Biological Chemistry **274**(4): 2216-2224.

Tseng, W.-C. and C.-M. Jong (2003). "Improved stability of polycationic vector by dextran-grafted branched polyethylenimine." Biomacromolecules **4**(5): 1277-1284.
Tsvetanova, N. G. and M. von Zastrow (2014). "Spatial Encoding of cyclic AMP Signaling Specificity by GPCR Endocytosis." Nature Chemical Biology **10**(12): 1061-1065.
Tyndall, J. D. and R. Sandilya (2005). "GPCR agonists and antagonists in the clinic." Medicinal chemistry **1**(4): 405-421.
Uhlén, M., L. Fagerberg, B. M. Hallström, C. Lindskog, P. Oksvold, A. Mardinoglu, Å. Sivertsson, C. Kampf, E. Sjöstedt and A. Asplund (2015). "Tissue-based map of the human proteome." Science **347**(6220): 1260419.
Ulbrich, K., K. Hola, V. Subr, A. Bakandritsos, J. Tucek and R. Zboril (2016). "Targeted drug delivery with polymers and magnetic nanoparticles: covalent and noncovalent approaches, release control, and clinical studies." Chemical reviews **116**(9): 5338-5431.
van Meer, G. (2005). "Cellular lipidomics." The EMBO journal **24**(18): 3159-3165.
Van Meer, G., D. R. Voelker and G. W. Feigenson (2008). "Membrane lipids: where they are and how they behave." Nature reviews Molecular cell biology **9**(2): 112.
Van Oss, C. J. (2006). Interfacial forces in aqueous media, CRC press.
Vannucchi, M.-G., L. Corsani and M.-S. Faussone-Pellegrini (1999). "Substance P immunoreactive nerves and interstitial cells of Cajal in the rat and guinea-pig ileum. A histochemical and quantitative study." Neuroscience letters **268**(1): 49-52.
Vassar, R., B. D. Bennett, S. Babu-Khan, S. Kahn, E. A. Mendiaz, P. Denis, D. B. Teplow, S. Ross, P. Amarante and R. Loeloff (1999). "β-Secretase cleavage of Alzheimer's amyloid precursor protein by the transmembrane aspartic protease BACE." science **286**(5440): 735-741.
Vauquelin, G. and S. J. Charlton (2010). "Long-Lasting Target Binding and Rebinding as Mechanisms to Prolong In Vivo Drug Action." British Journal of Pharmacology **161**(3): 488-508.
Vepa, S., W. Scribner and V. Natarajan (1997). "Activation of endothelial cell phospholipase D by polycations." American Journal of Physiology-Lung Cellular and Molecular Physiology **272**(4): L608-L613.
Wachten, S., N. Masada, L.-J. Ayling, A. Ciruela, V. O. Nikolaev, M. J. Lohse and D. M. F. Cooper (2010). "Distinct Pools of cAMP Centre on Different Isoforms of Adenylyl Cyclase in Pituitary-derived GH(3)B(6) cells." Journal of Cell Science **123**(1): 95-106.
Wang, W., Y. Qiao and Z. Li (2018). "New Insights into Modes of GPCR Activation." Trends in pharmacological sciences.
Webb, B. A., M. Chimenti, M. P. Jacobson and D. L. Barber (2011). "Dysregulated pH: a perfect storm for cancer progression." Nature Reviews Cancer **11**(9): 671.
Wike-Hooley, J., J. Haveman and H. Reinhold (1984). "The relevance of tumour pH to the treatment of malignant disease." Radiotherapy and Oncology **2**(4): 343-366.
Wiley, H. S. and P. M. Burke (2001). "Regulation of receptor tyrosine kinase signaling by endocytic trafficking." Traffic **2**(1): 12-18.
Won, Y.-Y., R. Sharma and S. F. Konieczny (2009). "Missing pieces in understanding the intracellular trafficking of polycation/DNA complexes." Journal of Controlled Release **139**(2): 88-93.
Wu, X. L., J. H. Kim, H. Koo, S. M. Bae, H. Shin, M. S. Kim, B.-H. Lee, R.-W. Park, I.-S. Kim and K. Choi (2010). "Tumor-targeting peptide conjugated pH-responsive micelles as a potential drug carrier for cancer therapy." Bioconjugate chemistry **21**(2): 208-213.
Yan, R., M. J. Bienkowski, M. E. Shuck, H. Miao, M. C. Tory, A. M. Pauley, J. R. Brashler, N. C. Stratman, W. R. Mathews and A. E. Buhl (1999). "Membrane-anchored aspartyl protease with Alzheimer's disease β-secretase activity." Nature **402**(6761): 533.
Yarwood, R. E., W. L. Imlach, T. Lieu, N. A. Veldhuis, D. D. Jensen, C. K. Herenbrink, L. Aurelio, Z. Cai, M. J. Christie and D. P. Poole (2017). "Endosomal signaling of the receptor for calcitonin gene-related peptide mediates pain transmission." Proceedings of the National Academy of Sciences **114**(46): 12309-12314.

Yokota, Y., Y. Sasai, K. Tanaka, T. Fujiwara, K. Tsuchida, R. Shigemoto, A. Kakizuka, H. Ohkubo and S. Nakanishi (1989). "Molecular characterization of a functional cDNA for rat substance P receptor." Journal of Biological Chemistry **264**(30): 17649-17652.
Yoshida, N., M. Tamura and M. Kinjo (2000). "Fluorescence correlation spectroscopy: a new tool for probing the microenvironment of the internal space of organelles." Single Molecules **1**(4): 279-283.
Yoshifumi, N., K. Takeshi, S. Ryuichi, N. Shigetada and M. Noboru (1994). "Immunohistochemical localization of substance P receptor in the central nervous system of the adult rat." Journal of Comparative Neurology **347**(2): 249-274.
You, J., G. Zhang and C. Li (2010). "Exceptionally high payload of doxorubicin in hollow gold nanospheres for near-infrared light-triggered drug release." ACS nano **4**(2): 1033-1041.
You, Y.-Z., K. K. Kalebaila, S. L. Brock and D. Oupicky (2008). "Temperature-controlled uptake and release in PNIPAM-modified porous silica nanoparticles." Chemistry of Materials **20**(10): 3354-3359.
Yu, J., D. A. Fischman and T. L. Steck (1973). "Selective solubilization of proteins and phospholipids from red blood cell membranes by nonionic detergents." Journal of supramolecular structure **1**(3): 233-248.
Zerial, M. and H. McBride (2001). "Rab proteins as membrane organizers." Nature reviews Molecular cell biology **2**(2): 107.
Zhang, L., F. Gu, J. Chan, A. Wang, R. Langer and O. Farokhzad (2008). "Nanoparticles in medicine: therapeutic applications and developments." Clinical pharmacology & therapeutics **83**(5): 761-769.
Zhang, M.-M., W. Ji, L.-Y. Pei, W. Wang, T. Chen, W. Wang, H. Li, T. Zhang, S.-X. Wu and Y.-Q. Li (2013). "Acute Colitis Induces Neurokinin 1 Receptor Internalization in the Rat Lumbosacral Spinal Cord." PLoS ONE **8**(3): e59234.
Zhang, S., H. Gao and G. Bao (2015). "Physical principles of nanoparticle cellular endocytosis." ACS nano **9**(9): 8655-8671.
Zhang, T., T. F. Sturgis and B.-B. C. Youan (2011). "pH-responsive nanoparticles releasing tenofovir intended for the prevention of HIV transmission." European Journal of Pharmaceutics and Biopharmaceutics **79**(3): 526-536.
Zhang, Y., X. Chen, C. Gueydan and J. Han (2017). "Plasma membrane changes during programmed cell deaths." Cell Research **28**: 9.
Zhao, D., X. Zhao, Y. Zu, J. Li, Y. Zhang, R. Jiang and Z. Zhang (2010). "Preparation, characterization, and in vitro targeted delivery of folate-decorated paclitaxel-loaded bovine serum albumin nanoparticles." International journal of nanomedicine **5**: 669.
Zhao, J. and M. H. Stenzel (2018). "Entry of nanoparticles into cells: the importance of nanoparticle properties." Polymer Chemistry.
Zhou, K., Y. Wang, X. Huang, K. Luby-Phelps, B. D. Sumer and J. Gao (2011). "Tunable, ultrasensitive pH-responsive nanoparticles targeting specific endocytic organelles in living cells." Angewandte Chemie **123**(27): 6233-6238.
Zwier, J. M., T. Roux, M. Cottet, T. Durroux, S. Douzon, S. Bdioui, N. Gregor, E. Bourrier, N. Oueslati and L. Nicolas (2010). "A fluorescent ligand-binding alternative using Tag-lite® technology." Journal of biomolecular screening **15**(10): 1248-1259.